DANMARKS OG GRØNLANDS GEOLOGISKE UNDERSØGELSE RAPPORT 2005/42

Greenstone belts in the central Godthåbsfjord region, southern West Greenland

Geochemistry, geochronology and petrography arising from 2004 field work, and digital map data

Julie A. Hollis (ed.)

GEOLOGICAL SURVEY OF DENMARK AND GREENLAND
MINISTRY OF THE ENVIRONMENT

GEUS

DANMARKS OG GRØNLANDS GEOLOGISKE UNDERSØGELSE RAPPORT 2005/42

Greenstone belts in the central Godthåbsfjord region, southern West Greenland

Geochemistry, geochronology and petrography arising from 2004 field work, and digital map data

Julie A. Hollis (ed.)

Contributions from Dirk Frei, Adam A. Garde, Julie A. Hollis, Hans Jepsen, Mac Persson, Ali Polat, Agnete Steenfelt, Jeroen van Gool, Mikkel Vognsen & Willy Weng

GEOLOGICAL SURVEY OF DENMARK AND GREENLAND
MINISTRY OF THE ENVIRONMENT

GEUS

Contents

Abstract

This report comprises extensive new geochronology and geochemistry data, petrographic studies, and new digital geological map data for the Nuuk region. The analytical data was obtained for samples collected during 2004 GEUS field mapping.

Both the mid-Archaean Bjørneøen-Qussuk and the late-Archaean Storø greenstone belts show geochemical variations consistent with both ocean floor and volcanic arc settings. The Storø belt also shows some contribution from a proximal continental source. On Qussuk, field and geochemical evidence point to a previously unrecognised mid-Archaean island arc, with gold occurrences related to either sea-floor hydrothermal activity or later amphibolite facies metamorphism in the mid-Archaean – distinct in timing from the late-Archaean gold occurrences on Storø.

More than 850 zircon grains in 41 samples were analysed for U-Pb isotopes via secondary ion and laser ablation mass spectrometry. The zircon age data indicate two distinct age groups of supracrustal rocks. The tectonically dismembered Qussuk–Bjørneøen greenstone belt (in the Akia terrane) is ≤ 3070 Ma and occurs on Store Malene, Sermitsiaq, Bjørneøen, part of Storø, and the Qussuk peninsula. This was affected by amphibolite facies metamorphism at c. 2980–2970 Ma – correlated with previously reported granulite facies metamorphism farther north-west in this terrane. The late Archaean Storø belt is also tectonically dismembered, cropping out on Storø, the Nuuk peninsula, Sermitsiaq, and Bjørneøen. Sedimentary rocks in this belt were deposited at c. 2800 Ma, mainly from a c. 2880 Ma source. An important volcanic component of the Storø belt was dated at c. 2830 Ma. The new age data show that the mid- and late Archaean supracrustal rocks are tectonically interleaved, in agreement with the new geochemical data. A panel of late Archaean supracrustal rocks, correlated with the Storø greenstone belt, structurally underlies the Bjørneøen greenstone belt from Sermitsiaq to Bjørneøen. The presence of late Archaean supracrustal rocks west of the previously established Ivinnguit fault terrane boundary, indicates more structural complexity in this region than previously recognised.

Chemical variations in rock samples from each of the belts suggest both syn-depositional and post-depositional alteration. Geochemical investigations indicate that the mafic metavolcanics of the mid-Archaean Ivisaartoq greenstone belt experienced seafloor hydrothermal alteration in a supra-subduction-zone setting, producing epidosites. Similar epidosites are observed also on the Qussuk peninsula.

Metamorphic and pegmatitic zircon age data indicate more than one episode, or a prolonged period, of thermal activity from 2700–2600 Ma. Amphibolite facies metamorphism of the Storø greenstone belt at c. 520–620°C and c. 4.5–6 kbar, was dated at c. 2700 and c. 2630 Ma. Abundant pegmatite emplacement during crustal–scale thrusting in the Storø shear zone occurred around 2630 Ma. Structural contraints show that this post-dates known gold mineralisation on Storø. 2700–2600 Ma metamorphic ages indicate that NE-striking shear zones on Bjørneøen may belong to the same phase of deformation as the Storø shear zone.

Introduction

In 2004 and 2005 GEUS has undertaken several related field and research projects with the overall aim of assessing whether a gold province exists in the Nuuk region. In this study we present new digital geological map data, geochronology, geochemistry, and petrographic results of studies of greenstone belts in the central Godthåbsfjord region, southern West Greenland.

This study was carried out by personnel from the Department of Geological Mapping and the Department of Ore Geology at the Geological Survey of Denmark and Greenland (GEUS), and by invited collaborators from several international research institutions including the University of Edinburgh (Scotland) and Windsor University and Memorial University (Canada).

Samples included in this study were collected in the 2004 summer as part of a GEUS field project financially supported by the Bureau of Minerals and Petroleum, Nuuk. Preliminary results of that field work were presented in Hollis et al. (2004). The reader is referred to that report for an overview of the regional geology of the central Godthåbsfjord region and description and interpretation of the field geology of mapped areas.

The enclosed DVD contains a PDF version of this report, a PDF version of Hollis et al. (2004) – for ease of reference – along with an ArcView© project file containing georeferenced analytical data including geochronological and geochemical data discussed in this report, along with new digital geological map data. The ArcView© project file also contains all field data reported on the DVD accompanying Hollis et al. (2004), i.e. localities, sample locations, structural data, and digital photographs. Instructions for accessing the DVD are given in Appendix 1.

Digital geological maps

Hans Jepsen
Geological Survey of Denmark and Greenland

Data sources

The geological mapping up to 1987 of the Ameralik – Godthåbsfjord – Fiskefjord area resulted in publishing, by the Geological Survey of Greenland, of three geological map sheet at scale 1:100 000 (see Fig. 1 and list below).

In order to establish a common geological reference map for this project the three map sheets have been compiled into a single digital map at a target scale of 1:100 000. The results of the geological mapping in the area since 1987 have been partly incorporated into the dataset, and the nomenclature of map units has been made consistent across the original map boundaries. The digital topographic base map for the compilation was established with the best possible precision prior to this project (joint BMP – GEUS project 69.40.01).

Map at target scale of 1:100 000

The three map sheets were originally produced as hand-drawn (scribed peel-coats) print originals; they thus had to be vectorised manually and transferred to GEUS's ESRI ArcInfo GIS database. During this process, line and polygon topology has been validated and attribute data added. The geometrical precision of the maps was very low, and vectorising has involved a great amount of adjustment with consequent loss of precision with respect to the positioning of geological boundaries and structures.

The project area including Qôrqut, Ivisaartoq and the eastern quarter of Fiskefjord map sheets (Fig. 1) is now covered by a seamless and homogeneous dataset which can be accessed as GIS-intelligent data. The amount of detail reflects the information on the published map sheets. Although concerted efforts have been made to quality-check the conversion from paper to digital form, errors are clearly unavoidable; we thus encourage the user to bring such potential problems to our attention so that ongoing refinement of this digital geological archive can be undertaken.

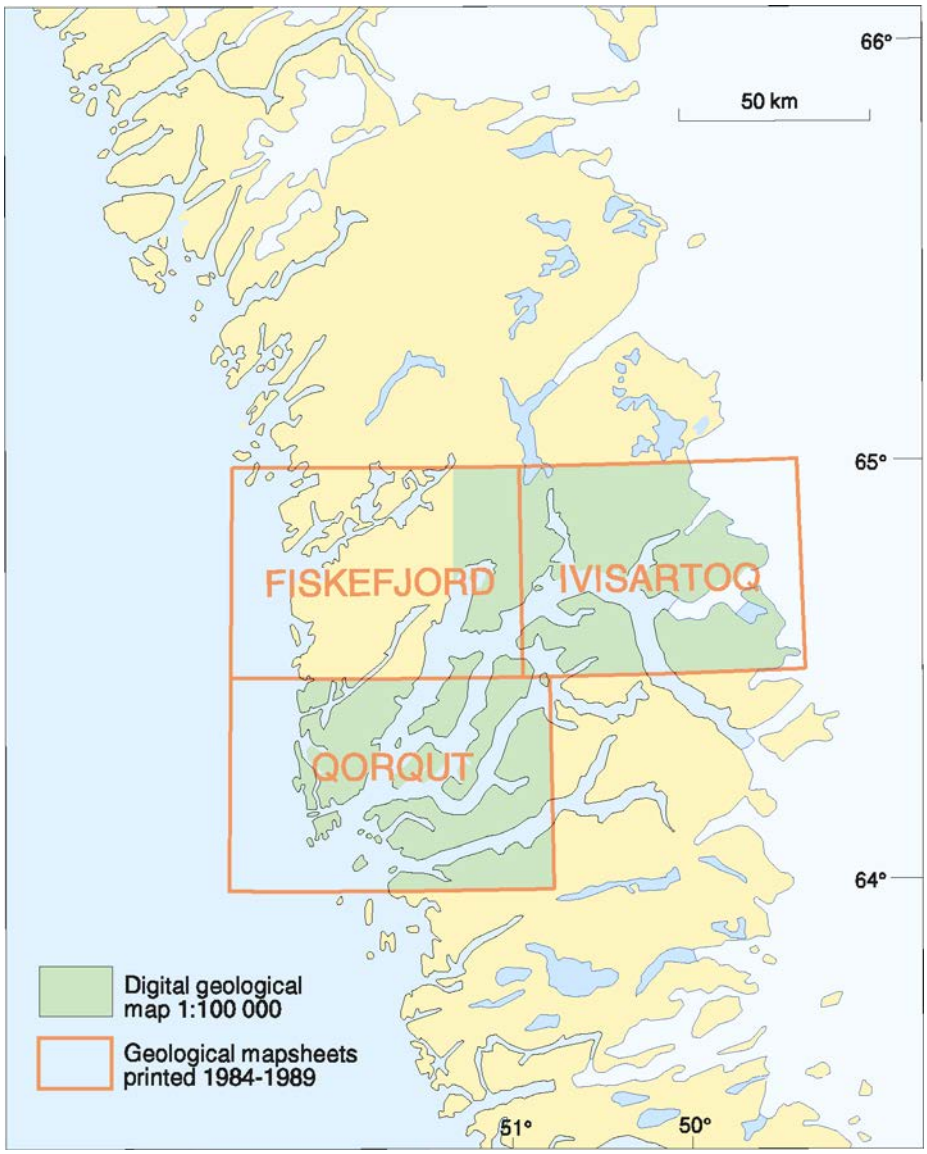

Figure 1. *Geological index map showing the areas digitised from 3 published geological map sheets at scale 1:100 000. Period of publication 1984–1989.*

Source maps

The following three 1:100 000 scale maps form the basis geological data source for the integrated digital geological dataset (Fig. 1):
McGregor, V.R. 1984: Geological map of Greenland, 1:100 000, Qôrqut, sheet 64 V.1 Syd. Copenhagen: Geological Survey of Greenland.
Chadwick, B. and Coe, K. 1988: Geological map of Greenland, 1:100 000, Ivisârtoq, sheet 64 V.2 Nord. Copenhagen: Geological Survey of Greenland.
Garde, A. A. 1989: Geological map of Greenland, 1:100 000, Fiskefjord, sheet 64 V.1 Nord. Copenhagen: Geological Survey of Greenland.

The Nordlandet area (Qôrqut map sheet) have been supplemented with data from:

McGregor, V. R., 1993: Qôrqut 74 V.1 Syd, Descriptive Text, Fig. 5. Geological map of Greenland 1:100 000. Copenhagen: Geological Survey of Greenland.
The northern part of Storø incorporates data from:
Steven Grimes, 2004: Preliminary bedrock geology map, north Storø, 1:20 000 (Hollis et al. 2004, Fig 30 and DVD).

Geochronology

Julie A. Hollis, Adam Garde, Dirk Frei, Jeroen van Gool
Geological Survey of Denmark and Greenland

Introduction

Over 100 structural constrained rock samples were collected in 2004 from the central Godthåbsfjord region for geochronology studies. Forty-one of the available samples were selected for inclusion in geochronology studies, specifically for the purposes of obtaining:

1. minimum depositional ages of sedimentary precursors to paragneiss units
2. age spectra of zircon populations from metasedimentary and metavolcanic rocks
3. crystallisation ages of orthogneiss of unknown affinity
4. crystallisation ages of cross-cutting dykes including pegmatites
5. metamorphic ages of a range of rock types

These ages were targeted to constrain:

1. age correlations between supracrustal rocks from different parts of the region
2. the provenance of supracrustal rocks in the region
3. the position of terrane boundary structures between distinct terranes
4. the timing of deformation – particularly the timing of deformation in the Storø shear zone
5. the timing of metamorphism across the region

Figure 2 is an overview of the locations of dated samples and the ages obtained. Age data were collected on zircon mineral separates via laser ablation – inductively coupled plasma – sector field mass spectrometry (LA-SF-ICPMS) and secondary ion mass spectrometry (SIMS).

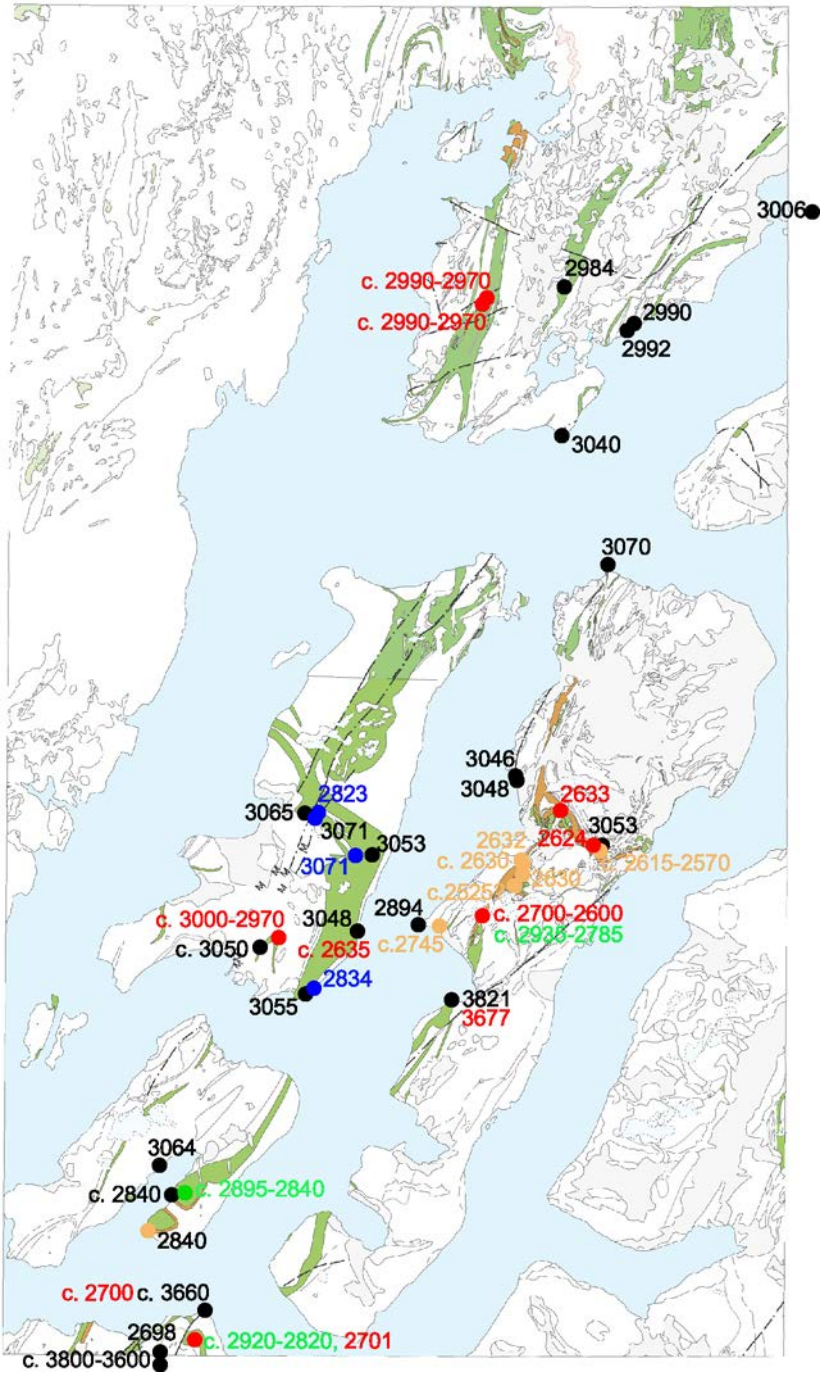

Figure 2. *Locations of dated samples and summary of zircon age data. Black dots and numbers refer to magmatic emplacement ages, blue dots and numbers refer to volcanic deposition ages, green dots and numbers refer to detrital zircon ages (sedimentary), red dots and numbers refer to metamorphic ages, and brown dots and numbers refer to pegmatite ages.*

Sample preparation

Rock samples were typically hammered into small, centimetre- to tens of centimetre-scale fragments on the outcrop. This was done to avoid potential contamination by breaking up the sample in the laboratory. The samples were jaw-crushed, crushed to a coarse powder in a steel ring mill, and sieved to obtain the < 400 μm fraction. The powders were separated using a shaking wash table, enabling pre-concentration of the heavy fraction and simultaneous removal of any very fine-grained material. Using the heavy fraction, magnetic minerals were separated out using a Frandz magnetic separator. The remaining non-magnetic fraction was further separated using heavy liquids to obtain the heaviest fraction, typically including phases such as zircon, titanite, rutile, and sulphide minerals.

Individual zircon grains were hand-picked from the heavy mineral fraction under an optical binocular microscope. These were mounted in rows on double-sided sticky tape. In the case of zircon samples mounted for SIMS work, a few grains of the 1065 Ma zircon standard 91500 (Wiedenbeck et al. 1995) were mounted along with the samples. The mounted zircons were then set in one inch diameter circular epoxy mounts, which were then ground to reveal the mid-sections of the zircon grains, and polished to one micron grade.

The polished zircons were imaged using back-scattered electrons (BSE) employing a Philips XL 40 scanning electron microscope at GEUS. BSE images were used to identify the internal morphology of the grains (influenced by, for example, growth, resorption, alteration, or metamorphism) to select areas of interest for analysis.

Secondary Ion mass spectrometry (SIMS) methodology

SIMS analysis was carried out using a CAMECA IMS 1270 secondary ion mass spectrometer at the NORDSIM laboratory, Swedish Museum of Natural History, Stockholm. The polished zircon mounts were coated with a c. 30 nm layer of gold. Analytical procedures and common lead corrections are similar to those described by Whitehouse et al. (1997). A primary O^{2-} ion beam is focussed into a 20 μm diameter spot that sputters material from the sample to form a flat-bottomed crater. Positive ions sputtered from the crater are extracted and mass-separated into the peaks of interest: $^{90}Zr_2{}^{16}O$, ^{204}Pb, ^{206}Pb, ^{207}Pb, ^{208}Pb, ^{238}U, $^{232}Th^{16}O$, and $^{238}U^{16}O$. Obtained isotopic data were corrected by matrix-matched external standardisation using the 1065 Ma 91500 zircon standard (Whitehouse et al. 1997). Age calculations for populations were carried out using the IsoPlot/Ex 3.0 excel add in (Ludwig 2003).

Laser ablation – inductively coupled plasma – sector field mass spectrometry (LA-SF-ICPMS) methodology

The LA-SF-ICPMS uses a focussed laser to ablate a small amount of a sample contained in an air-tight sample cell. The ablated material is transferred to a mass-spectrometer in a

carrier gas via plastic tubing for isotopic quantification. For the spot diameter (30 µm) and ablation times (55 s) used in this study, the ablated masses of zircon were approximately 200–500 ng.

The laser ablation system used at GEUS was a NewWave Research/Merchantek UP213 equipped with a frequency quintupled Nd-YAG laser emitting at a wavelength of 213 nm. The nominal pulse width of the laser is 5 ns with a pulse-to-pulse stability of 2 % RSD. The laser was operated at a repetition rate of 10 Hz and a nominal energy output of 44 %, corresponding to a laser fluency of 8 J cm^{-2}. All data were acquired with a single spot analysis on each individual zircon grain with a beam diameter of 30 µm. Samples and standards were held in the standard ablation cell delivered with the UP 213 system. He was used to flush the sample cell and was mixed downstream with the Ar sample gas of the mass-spectrometer. The washout time for this configuration is approximately 180 s. All sample mounts were rigorously cleaned before introduction into the sample cell to remove surface Pb contamination.

The ablated material was analysed with an Element2 (ThermoFinnigan, Bremen) single-collector double focusing magnetic sector ICPMS equipped with a fast field regulator for increased scanning speed. The total acquisition time for each analysis was 90 s with the first 35 s used to measure the gas blank. The instrument was tuned to give large, stable signals for the ^{206}Pb and ^{238}U peaks, low background count rates (typically around 300 counts per second for ^{207}Pb) and low oxide production rates ($^{238}U^{16}O/^{238}U$ generally below 2.5 %). All measurements were performed in low resolution mode using electrostatic scanning (E-scan) with the magnetic field resting at mass ^{202}Hg. The following masses were measured: ^{202}Hg, ^{204}(Pb + Hg), ^{206}Pb, ^{207}Pb, ^{208}Pb, ^{232}Th, ^{235}U, and ^{238}U. All data were acquired on four samples per peak with a sampling and a settling time of 1 ms for each isotope. Mass ^{202}Hg was measured to monitor the ^{204}Hg interference on ^{204}Pb (using a $^{202}Hg/^{204}Hg$-ratio of 4.36). Only if the net intensities for mass ^{204}Pb, corrected for ^{204}Hg, are significantly above the limit of detection a common Pb-correction was performed. The laser induced elemental fractionation and the instrumental mass bias on measured isotopic ratios were corrected by matrix-matched external standardisation using the GJ-1 zircon standard (Jackson et al. 2004). Samples were analysed in sequences where three standards are analysed initially, followed by ten samples, again three standards, and so on. The Plisovice zircon standard (338 ± 1 Ma, Jan Kosler, Charles University, Prague; Aftalion et al. 1989) was analysed as an unknown on a regular basis. The results are consistently concordant at 340 ± 2 Ma.

The raw data were exported in ASCII format and processed using in-house age data reduction spreadsheets. Age calculations for populations were carried out using the IsoPlot/Ex 3.0 excel add in (Ludwig 2003).

Comparison between SIMS and LA-SF-ICPMS data

Zircon populations from four samples were analysed using both methods – SIMS and LA-SF-ICPMS. Different sets of zircon grains in different epoxy mounts were used in the SIMS

compared with LA-SF-ICPMS analytical work. In general the results are in excellent agreement.

In the case of sample 481465 – a garnet-biotite-cordierite gneiss – LA-SF-ICPMS was used to analyse a large number of detrital cores whereas SIMS was used to target thin metamorphic rims. In each of the 3 other samples analyses were conducted using both methods to compare the results from the different analytical methods. Sample 479745 gave volcanic depositional ages of 2823 ± 2 (SIMS, MSWD 1.06, n = 10 of 16) and 2823 ± 5 Ma (LA-SF-ICP-MS, MSWD 0.51, n = 11 of 21). Sample 479049 gave magmatic emplacement ages of 3055 ± 3 (SIMS, MSWD 2.1, n = 13 of 15) and 3042 ± 4 Ma (LA-SF-ICP-MS, MSWD 0.60, n = 19 of 30). This sample shows some spread in ages and the slight discrepancy might be attributable to bias in sample selection, i.e. larger zircon grains were selected for the first (LA-SF-ICP-MS) analytical session leaving only smaller grains – possibly of a slightly different age – for the SIMS work. Sample 479014 gave magmatic emplacement ages of 2698 ± 4 (SIMS, MSWD 0.50, n = 9 of 19) and 2708 ± 5 Ma (LA-SF-ICP-MS, MSWD 1.04, n = 13 of 30).

Results

In the following pages SIMS and LA-SF-ICPMS U-Pb zircon dating results are given for each sample analysed. This data is subdivided into the main geological events recognised through the age data in the region. For samples where SIMS analyses were carried out BSE images of the grains analysed and the analysis locations are shown in a Supplementary data file on the DVD (Supplementary_data_zircon_images.pdf). For the samples analysed using LA-SF-ICPMS the images are not shown due to the very large number of grains analysed (> 500). $^{207}Pb/^{206}Pb$ weighted mean ages were calculated using the excel add-in Isoplot/Ex version 3.0 (Ludwig 2003). All ages in the text are quoted with two sigma uncertainties. Age data are presented on $^{206}Pb/^{238}U$-$^{207}Pb/^{235}U$ concordia diagrams and weighted mean age plots. Error ellipses on diagrams are shown with one sigma uncertainties and $^{207}Pb/^{206}Pb$ ages are shown on weighted mean age plots with two sigma uncertainty. Tabulated data are given in Appendixes 2 and 3 and are also stored on an excel spreadsheet on the DVD (Zircon_age_data.xls). The mean squared weighted deviates (MSWD) is used as a convenient measure of scatter in the data. An MSWD = 1 indicates that the scatter in the data is equal to that predicted from the analytical error. MSWD > 1 indicates greater scatter than would be predicted from analytical errors alone, whereas MSWD < 1 indicates less scatter than would be predicted from analytical errors alone. Thus MSWD significantly greater than 1 indicates that there is a real difference in ages of the grains analysed.

Early Archaean magmatic rocks (Færingehavn terrane)

479036
Collector: Julie Hollis
Lithology: Grey, homogeneous felsic orthogneiss with few felsic layers that may be transposed pegmatites.
Location: central west Storø
Locality: jho2004-197, 64 21.425°N, -51 09.474°W
Aim: age of orthogneiss of unknown affinity – specifically constraint on the location of the tectonic contact between early Archaean rocks of the Itsaq gneiss complex (E) and the Ikkattoq gneiss (W).
Method: LA-SF-ICPMS
Age of emplacement: 3821 ± 12 Ma (MSWD 1.6, n = 5 of 16)
Age of migmatisation: 3677 ± 11 Ma (MSWD 1.7, n = 7 of 16)

The zircons are typically 100–400 μm in length with aspect ratios 1:2 to 1:3, typically prismatic. Most have well-defined, closely spaced oscillatory zones, some with large homogeneous cores. A few have dark and/or metamict tips, probably indicative of high-U overgrowths.

Twenty spots in 20 grains were analysed. Four analyses with high common Pb were strongly discordant and were discarded. The zircons have 21–201 ppm U and Th/U typically 0.15 to 1.16. The 16 analyses give an age range of 3830 ± 17 to 3654 ± 20 Ma. Two age populations can be discerned but these cannot be linked to distinct zircon morphologies. The 7 youngest grains give a population of 3677 ± 11 Ma (MSWD 1.7). A second population of 5 grains gives 3821 ± 12 Ma (MSWD 1.6).

This grey, homogeneous orthogneiss with widely spaced transposed felsic layering lies just W of the Storø shear zone. It clearly belongs to the Itsaq gneiss complex, with its entirely early Archaean aged zircon populations. The two age groups at 3821 ± 12 and 3677 ± 11 Ma indicate significant thermal pulses at these times. These are interpreted as the ages of emplacement and migmatisation respectively.

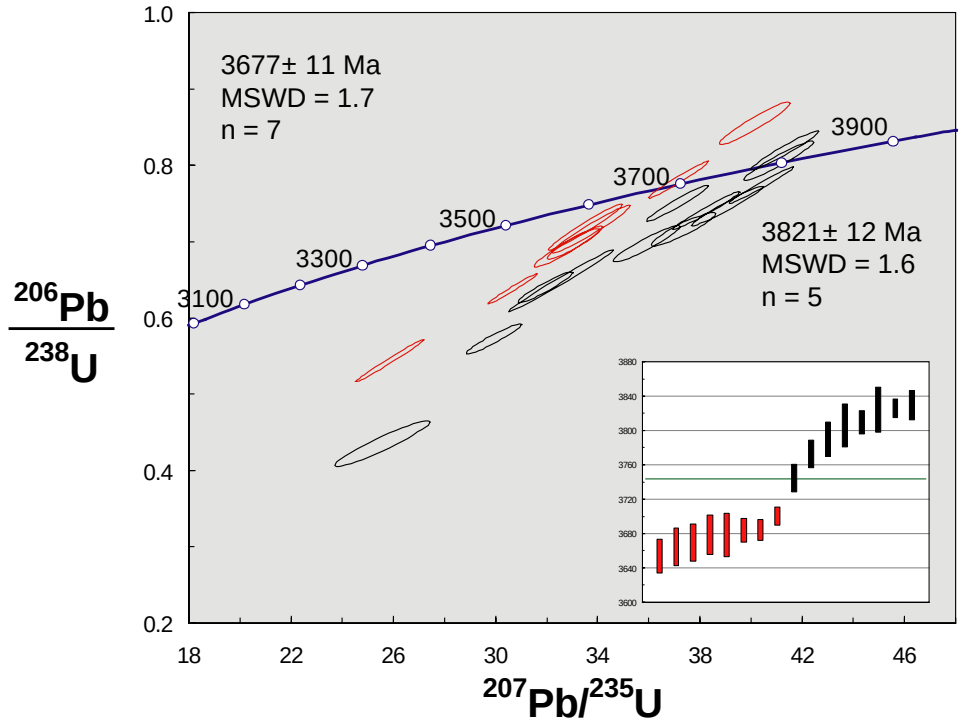

Figure 3. *479036 $^{206}Pb/^{238}U$-$^{207}Pb/^{235}U$ concordia diagram and inset $^{207}Pb/^{206}Pb$ age plot.*

481496
Collector: Julie Hollis
Lithology: High strain felsic orthogneiss with transposed felsic layers – light and dark homogeneous phases with finely dispersed biotite
Location: Nuuk peninsula S of Storø
Locality: jho2004-138, 64 11.655°N, -51 27.240°W
Aim: emplacement age of orthogneiss of unknown affinity and specifically constraint on Færingehavn–Tre Brødre terrane boundary
Method: LA-SF-ICPMS
Age of emplacement: c. 3800-3600 Ma (n = 20 of 20)

The zircons are typically 100–250 μm in length with aspect ratios of 1:2 to 1:4, typically 1:3, and commonly prismatic. Many show complex oscillatory zonation. A few grains are BSE bright and relatively homogeneous.

Twenty-two spots in 22 grains were analysed. Two analyses with high common Pb and which showed significant discordance were discarded. Ages range from 3847 ± 53 to 3491 ± 60 Ma. One older analysis at 3979 ± 74 Ma is dubious owing to significant discordance. These grains have 24–244 ppm U and Th/U of 0.13–0.76. There is no significant correlation between age, chemistry, and zircon morphology.

The sample was collected from a high strain felsic orthogneiss comprising light and dark homogeneous phases and transposed felsic layers. This lithology was targeted to establish the timing of emplacement of an orthogneiss of unknown affinity and specifically to constrain to location of the Færingehavn–Tre Brødre terrane boundary in this area. The 20 analyses ranging from 3847 ± 53 to 3491 ± 60 Ma place this within the Itsaq gneiss complex in the Færingehavn terrane. From the spread of ages it is not clear whether there are 2 or more age components and emplacement can be constrained only to c. 3800–3600 Ma.

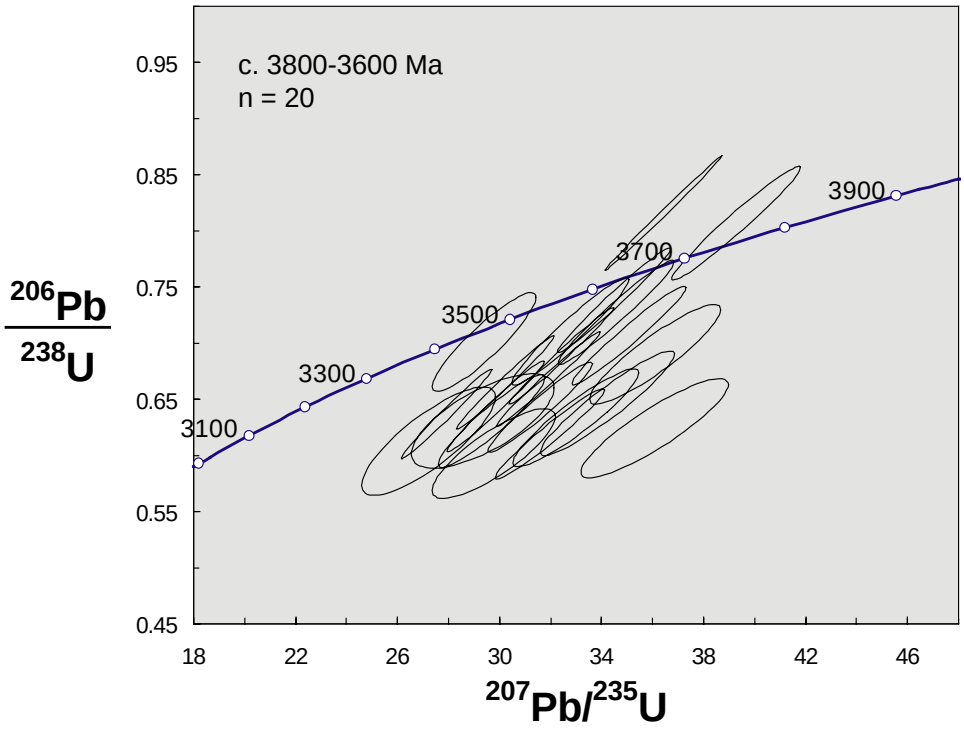

Figure 4. ***481496 $^{206}Pb/^{238}U$-$^{207}Pb/^{235}U$ concordia diagram.***

479704
Collector: Dirk Frei
Lithology: Medium-grained felsic augen gneiss of unknown affinity close to previously mapped contact between the Nûk gneiss and Itsaq gneiss complex.
Location: S of Storø on Nuuk peninsula
Locality: df2004-020, 64 13.118°N, -51 24.509°W
Aim: age of orthogneiss of unknown affinity – specifically constraint on the location of the tectonic contact between early Archaean rocks of the Itsaq gneiss complex (E) and the Nûk gneiss (W).
Method: LA-SF-ICPMS
Age of emplacement: c. 3660 Ma (n = 4 of 12)
Age of metamorphism: c. 2700 Ma (n = 8 of 12)

The zircons are typically 200–350 μm in length with aspect ratios 1:2 to 1:3, commonly prismatic. All show oscillatory zonation with very strong BSE contrasts between different zones. The majority have relatively dark cores with one or more very BSE bright internal zones (probably indicative of high U), and commonly dark zones on the rims.

Fifteen spots in 15 grains were analysed. Three analyses with high common Pb were strongly discordant and were discarded. The zircons have 47–124 ppm U. Four analyses of zircon cores gave the oldest ages: 3686 ± 26 to 3535 ± 14 Ma with relatively higher Th/U of 0.12–0.61. Eight analyses of rims gave ages of 2803 ± 35 to 2718 ± 31 Ma with lower Th/U of 0.09–0.11.

This medium-grained felsic augen gneiss was collected from close to the tectonic boundary between the Nûk gneiss and rocks belonging to the Itsaq gneiss complex south of Storø on Nuuk peninsula. At this locality metre-scale mafic amphibolite are boudinaged within the host augen gneiss and also metasomatically altered. The age data are consistent with emplacement at c. 3660 Ma, though an exact age cannot be defined from the limited number of core analyses. The spread of rim ages from 2803 ± 35 to 2718 ± 31 Ma indicates metamorphism in this period, which may correspond to the timing of alteration of the included amphibolite. The spread may derive in part from mixed core-rim ages as a result of drilling through zones of different ages. The exact age of metamorphism is not clear from this sample data, but probably falls close to 2700 Ma based on other data from the same area (e.g. sample 479010).

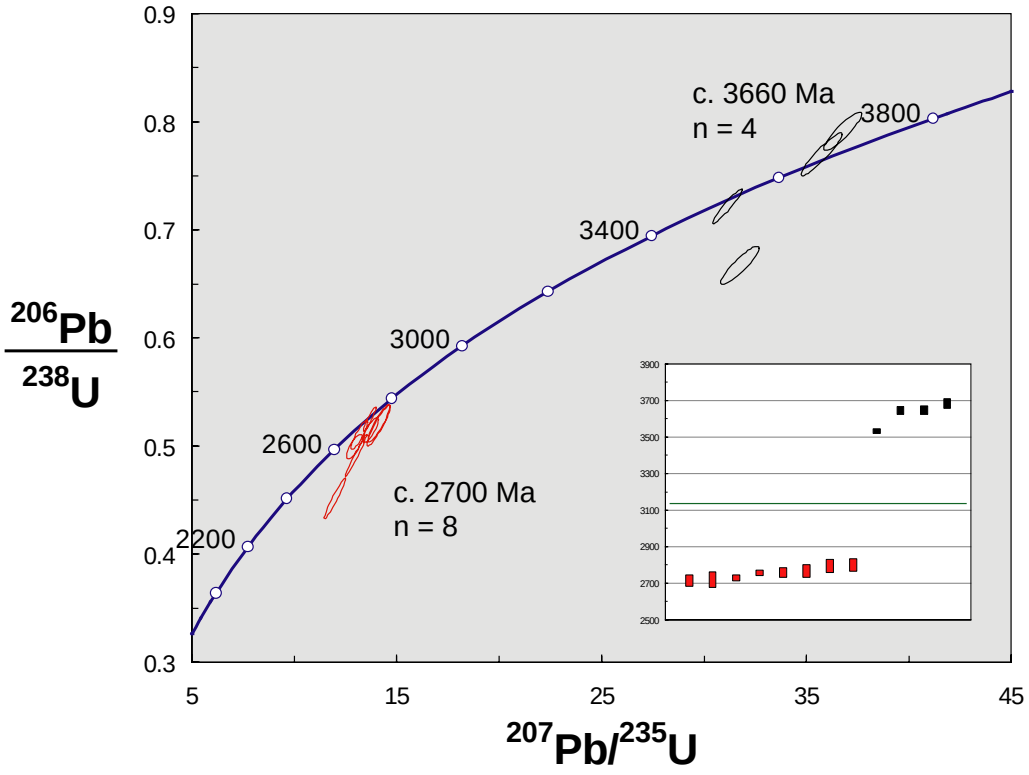

Figure 5. ***479704 $^{206}Pb/^{238}U$-$^{207}Pb/^{235}U$ concordia diagram and inset $^{207}Pb/^{206}Pb$ age plot.***

Mid-Archaean volcanics – Bjørneøen and Qussuk belt

479681
Collector: Nigel Kelly
Lithology: sheared biotite-schist with feldspar porphyroclasts
Location: central Bjørneøen
Locality: nmk2004-046, 64 25.263°N, -51 15.388°W
Aim: age of metamorphism associated with intense shearing
Method: LA-SF-ICPMS
Age of inferred volcanic precursor: 3071 ± 3 Ma (MSWD 1.1, n = 21 of 23)
Age of metamorphism: unknown – no record in the zircon population

The zircons are 100–300 μm with aspect ratios typically 1:2 to 1:3, commonly prismatic. All grains show well-defined oscillatory zonation. A few have relatively BSE dark cores with brighter rims.

Twenty-three spots in 19 grains were analysed. The data define a population at 3071 ± 3 (MSWD 1.1, n = 21 of 23) with significant discordance. The zircons have 113–210 ppm U with Th/U of 0.80–1.33. The analysed rims were relatively U-rich but no age difference between cores and rims was detected.

The sample was collected from a sheared biotite schist with feldspar porphyroclasts, inferred to be volcanic in origin. The 3071 ± 3 Ma age is interpreted as the age of a volcanic precursor. No information on the metamorphic history is preserved in these zircons. This age is identical to the depositional age of another intermediate metavolcanic from Bjørneøen – 479827 – of 3071 ± 1 Ma.

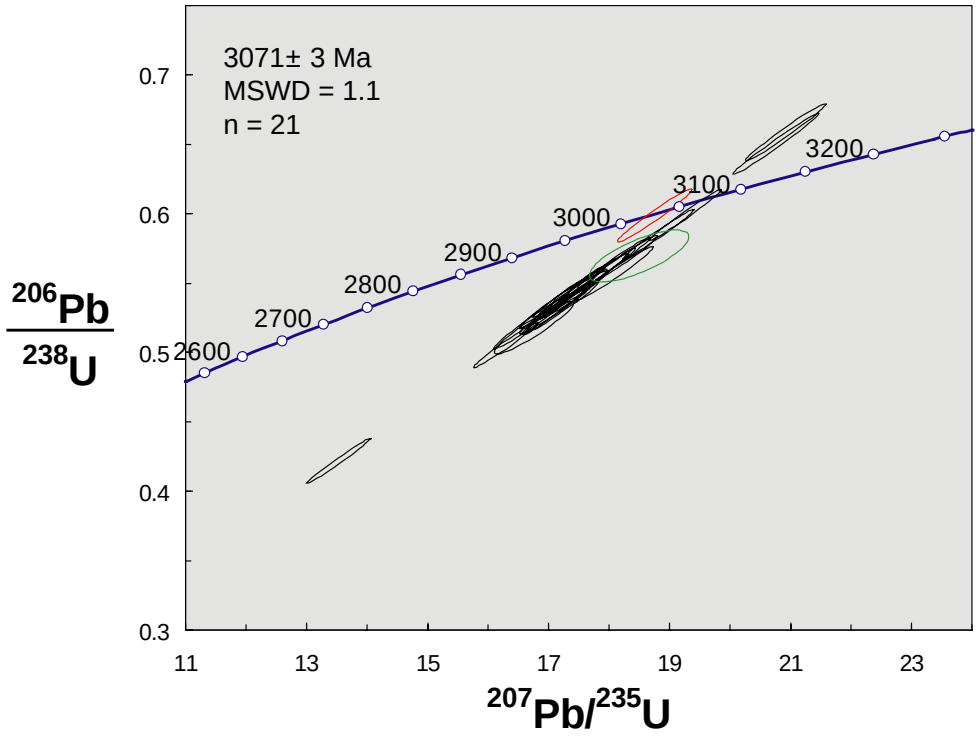

Figure 6. ***479681 $^{206}Pb/^{238}U$-$^{207}Pb/^{235}U$ concordia diagram.***

479827
Collector: Nigel Kelly
Lithology: Intermediate schist from intermediate volcanic map unit. Homogeneous, fine-grained layer within amphibolite near boundary with intermediate schists. Photo NMK2004-D153 (D141 in notebook) showing strain partitioning in layered intermediate schist; small tight folds are swept into a high strain zone at the base of the outcrop.
Location: central Bjørneøen
Locality: nmk2004-162, 64 26.251°N, -51 17.891°W
Aim: deposition age of intermediate amphibolite.
Method: SIMS

Age of deposition: 3071 ± 1 Ma (MSWD = 1.6, n = 16 of 21)

This sample contains a homogeneous population of very small (c. 100–150 μm), equant to stubby prismatic zircons with indistinct concentric zoning visible on BSE images, sometimes with relatively bright, prismatic cores and slightly darker rims. The zircons are generally somewhat pitted or cracked, especially the rims. Most grains have relatively high U and Th contents, around 850–2250 and 500–1500 ppm, respectively.

Twenty-one spots in 20 grains were analysed. Sixteen of these yield an age of 3071 ± 1 Ma, in accord with the field interpretation that this rock is of volcanoclastic origin and is largely derived from one volcanic source. Three other grains (5, 6 and 21) yield ages of 3059–3057 Ma. If these represent a second, well-defined source they would decrease the deposition age to 3057 Ma. The two remaining spots (8 from the rim of a large grain, and 17) with apparent ages of 3006 and 3021 Ma are unexplained but not considered sufficient evidence to propose a much lower age of deposition. An identical age of 3071 Ma was obtained from another schist from Bjørneøen (sample 479681), likewise interpreted to be of volcanic origin.

Assuming that the field identification as a volcanoclastic rock is correct, and assuming a direct correlation between the main metavolcanic belts on Bjørneøen and the Qussuk peninsula, there is a gap of 87 ± 2 Ma between the deposition of volcanics dated (479825, 479827) and emplacement of granitic sheets (477352).

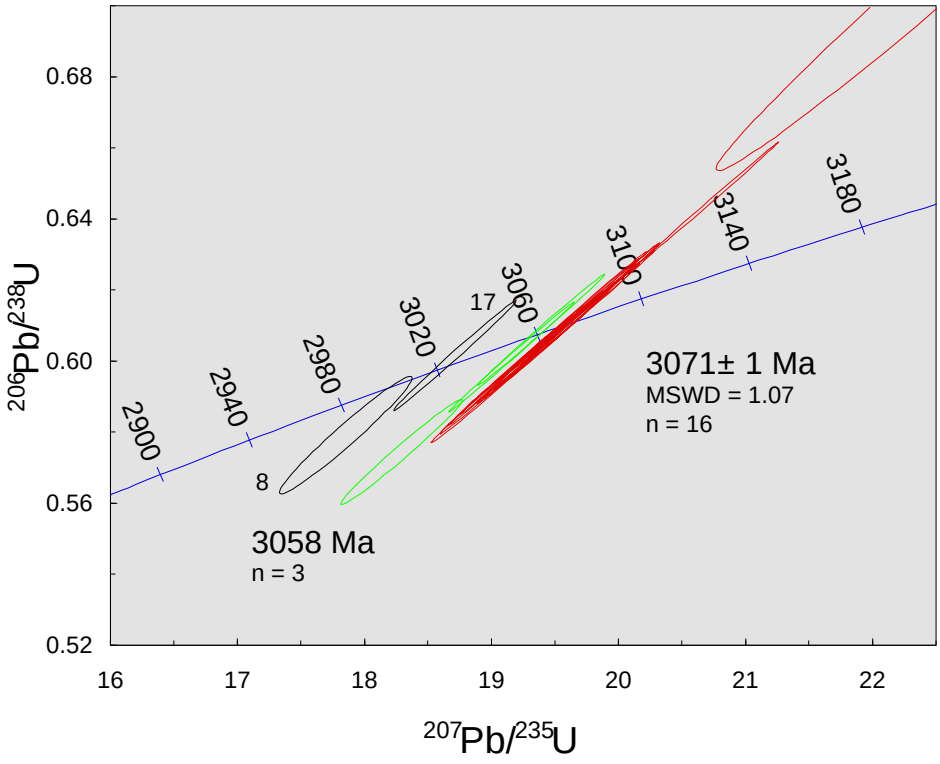

Figure 7. *479827 $^{206}Pb/^{238}U$-$^{207}Pb/^{235}U$ concordia diagram.*

477367
Collector: Adam A. Garde
Lithology: Fine-grained, garnet-bearing intermediate amphibolite
Location: Qussuk peninsula
Locality: aag2004-165, 64 39.987°N, -51 07.609°W
Aim: age spectra of detrital zircon populations from supracrustal package and minimum depositional ages of volcanic precursor
Method: SIMS
Age of volcanic precursor: c. 3040 Ma (n = 3 of 17)
Age of metamorphism: c. 3000–2940 Ma (n = 14 of 17)

The zircons are small – typically 50–150 μm in length – with aspect ratios typically 1:1 to 1:2, commonly rounded. The majority are homogeneous. A few contain relict darker cores, suggesting that homogeneous rims and whole grains are metamorphic.

Seventeen spots in 17 grains were analysed. Three analyses of dark cores with moderate U concentrations (267–521 ppm) give the oldest ages – 3068 ± 6, 3053 ± 8, and 3037 ± 6 Ma – and the highest Th/U of 0.24–0.47. These are interpreted as detrital zircon derived either from the volcanic precursor and/or from material included at the time of deposition. Fourteen analyses of homogeneous grains fall between 2995 and 2962 Ma with significant spread outside the error of individual analyses (i.e. a mean age of 2980 ± 12 Ma is probably meaningless and gives an MSWD of 134). These have high U concentrations of 631–1955 ppm and fairly low Th/U typically 0.05 to 0.16, consistent with a growth and/or recrystallisation during metamorphism. A single younger zircon at 2944 ± 6 Ma also has low Th/U (0.09) and probably also reflects metamorphic zircon growth or recrystallisation.

The sample was collected from a fragmental metavolcanic that forms part of the thin, dismembered supracrustal sequence on the Qussuk peninsula. The core analyses (n = 3) are within error of the age of Nûk gneiss ages from a number of localities and are consistent with derivation from the volcanic precursor (i.e. grown during magmatism and/or included from pre-existing mid-Archaean igneous precursors). Given the homogeneous nature of the remainder of the grains (n = 15), the low Th/U, and the spread in data, these are interpreted as zircon grown or recrystallised during amphibolite facies metamorphism in the period c. 3000–2940 Ma.

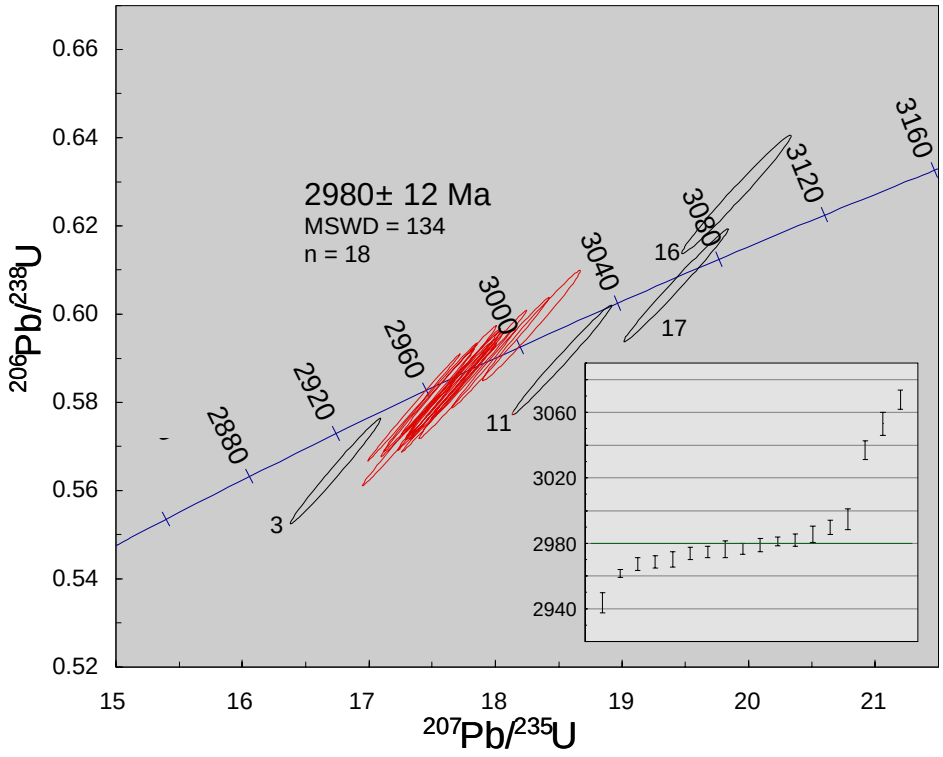

Figure 8. *477367 $^{206}Pb/^{238}U$-$^{207}Pb/^{235}U$ concordia diagram and inset $^{207}Pb/^{206}Pb$ age plot.*

477385
Collector: Adam A. Garde
Lithology: Fragmental metavolcanic rock, intensely deformed, with a strung-out, lensoid structure.
Location: Qussuk peninsula
Locality: aag2004-187, 64 40.163°N, -51 07.354°W
Aim: age spectra of detrital zircon populations from supracrustal package and minimum depositional ages of volcanic precursor
Method: SIMS
Age of old detrital grain: 3038 ± 12 Ma (n = 1 of 15)
Age of metamorphism: 2996 to 2951 Ma (n = 14 of 15)

The zircons are small – typically 50–100 μm in length – with aspect ratios of 1:1 to 1:2, commonly fairly rounded. The majority are homogeneous. A few contain relict darker cores, suggesting that homogeneous rims and whole grains are metamorphic.

Sixteen spots in 15 grains were analysed. One analysis of a dark core gives the oldest age – 3038 ± 12 Ma – and the highest Th/U of 0.37. This is interpreted as a zircon derived from a volcanic precursor and/or from material included at the time of deposition. Thirteen analyses of homogeneous grains and rims fall between 2996 and 2974 Ma with significant spread outside the error of individual analyses (i.e. a mean age of 2984 ± 4 Ma is probably meaningless and gives an MSWD of 19). These have high U concentrations of 640–2330 ppm and low Th/U typically 0.03 to 0.09, consistent with a growth and/or recrystallisation

during metamorphism. A single younger zircon at 2951 ± 6 Ma also has low Th/U (0.06) and probably also reflects metamorphic zircon growth or recrystallisation.

The sample was collected from a fragmental metavolcanic that forms part of the thin, dismembered supracrustal sequence on the Qussuk peninsula. The single core analysis is within error of the age of the Nûk gneiss from a number of localities (c. 3030 Ma) and is consistent with deposition of the volcanic precursor at the same, probably as part of the same genetic igneous association. Given the homogeneous nature of the remainder of the grains (n = 14), the very low Th/U, and the spread in data, these are interpreted as zircon grown or recrystallised during amphibolite facies metamorphism in the period c. 3000–2940 Ma.

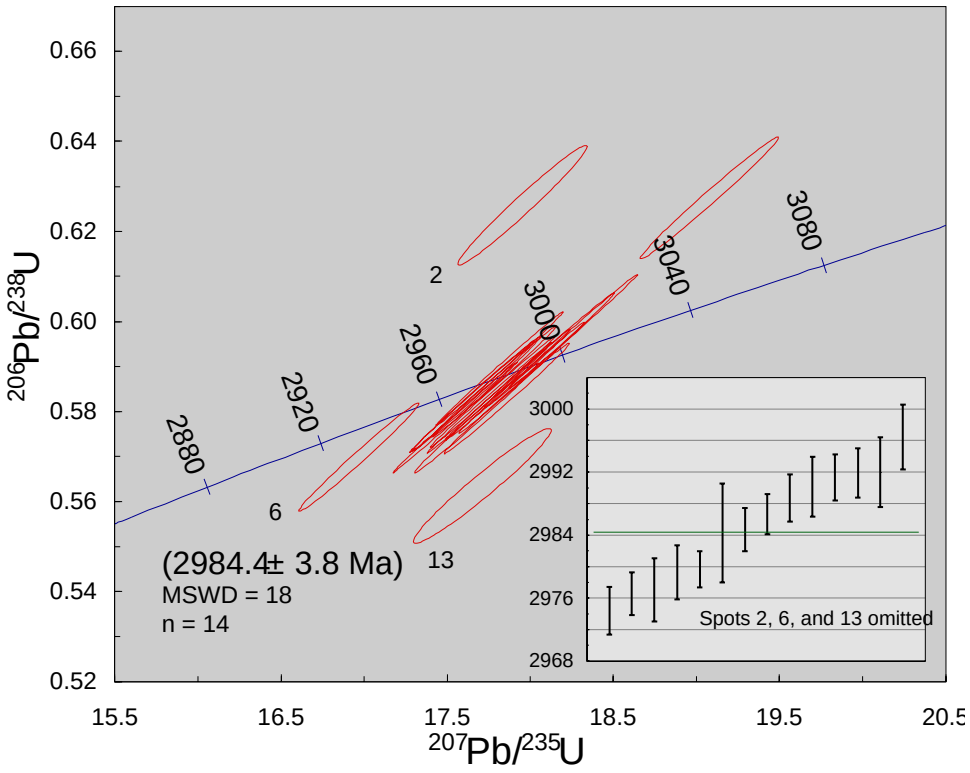

Figure 9. *477385 $^{206}Pb/^{238}U$-$^{207}Pb/^{235}U$ concordia diagram and inset $^{207}Pb/^{206}Pb$ age plot.*

479814
Collector: Nigel Kelly
Lithology: Intermediate schist
Location: central Bjørneøen
Locality: nmk2004-114, 64 23.074°N, -51 20.140°W
Aim: age spectra of volcanic precursor
Method: LA-SF-ICPMS
Age of emplacement: > 3000 Ma
Age of metamorphism: c. 3000–2970 Ma

The zircons are 80–150 μm in length with aspect ratios typically 1:1 to 1:2, and commonly rounded. The majority are homogeneous, a few with some poorly-defined oscillatory zonation and a few with wide BSE bright rims around darker cores.

Thirty spots in 29 grains were analysed. The main age population ranges from 3007 ± 25 to 2952 ± 20 Ma, with the spread outside the uncertainty on individual analyses. These grains have 163–549 ppm U and Th/U of 0.01–0.12. Two older grains are 3134 ± 68 and 3060 ± 40 Ma with 619 and 599 ppm U and Th/U of 0.01 and 0.04. The four youngest grains are 2870 ± 23, 2436 ± 153, 2416 ± 60, and 2023 ± 78 Ma. The 2870 ± 23 Ma grain has 487 ppm U and Th/U of 0.03. In contrast the 3 youngest grains have 21–95 ppm U and Th/U of 0.75–0.87.

The sample was collected from an intermediate schist near the structural base of the supracrustal sequence on central Bjørneøen. This lithology was targeted to investigate the timing of formation of the inferred volcanic precursor. Given the spread in ages outside the uncertainty on individual analyses, the typically very low Th/U ratios it seems likely that the isotopic system of the original zircon population has been variably reset during a later thermal event probably in the period 3000–2950 Ma. There is no plateau in the ages, making it difficult to estimate the age of formation of the volcanic precursor. The three oldest ages suggest the rock may have formed around the same time as much of the Nûk gneiss (> 3000 Ma). The significance of the youngest four ages is not clear as these do not correspond to known ages of thermal activity in the region.

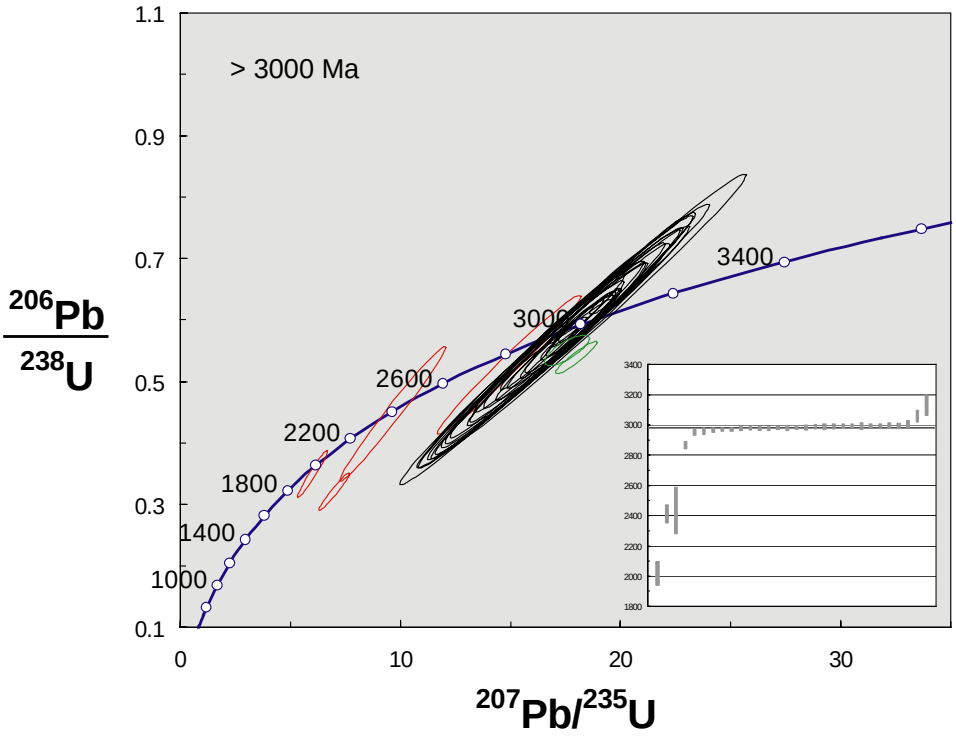

Figure 10. *479814 $^{206}Pb/^{238}U$-$^{207}Pb/^{235}U$ concordia diagram and inset $^{207}Pb/^{206}Pb$ age plot.*

Mid-Archaean magmatic rocks (Akia terrane)

481201
Collector: Jeroen van Gool
Lithology: Granodioritic gneiss from high strain zone at the contact with amphibolite to the E
Location: NW Storø
Locality: jvg2004-007, 64 33.062°N, -50 59.829°W
Aim: age spectra of emplacement and thus position of terrane boundary along this coast
Method: LA-SF-ICPMS
Age of emplacement: 3072 ± 4 Ma (MSWD 0.90, n = 24 of 28)
Age of metamorphism: c. 2970 Ma or later (n = 3 of 28)

The zircons are 200–250 μm in length with aspect ratios typically 1:2 to 1:3, and commonly prismatic. All grains show well-defined oscillatory zonation.

Thirty spots in 30 grains were analysed. Two analyses with high common Pb were discarded. Twenty-four grains define a population at 3072 ± 4 Ma (MSWD 0.90). These have 16–68 ppm U and Th/U of 0.43–1.25. One older grain is 3147 ± 37 Ma with 32 ppm U and Th/U of 0.73. The 3 youngest grains are 3042 ± 25, 3012 ± 15, and 2973 ± 21 Ma with 40–

62 ppm U and Th/U of 0.70–0.72. There is no distinction between these age groups that can be made on the basis of zircon morphology.

The sample was collected from an intensely sheared granodioritic gneiss from a high strain zone on the north-west coast of Storø, with the purpose of investigating the position of the terrane boundary along this coast. The main population at 3072 ± 4 Ma (MSWD 0.90, n = 24) is interpreted as the emplacement age and is consistent with similar Nûk gneiss ages from across the Akia terrane. This places the eastern limit of the Akia terrane to the E of this locality. The single older age indicates a small component of older mid Archaean inheritance. The 3 younger ages suggest some partial resetting of the isotopic system as a result of a thermal event in the late Archaean (c. 2970 Ma or later).

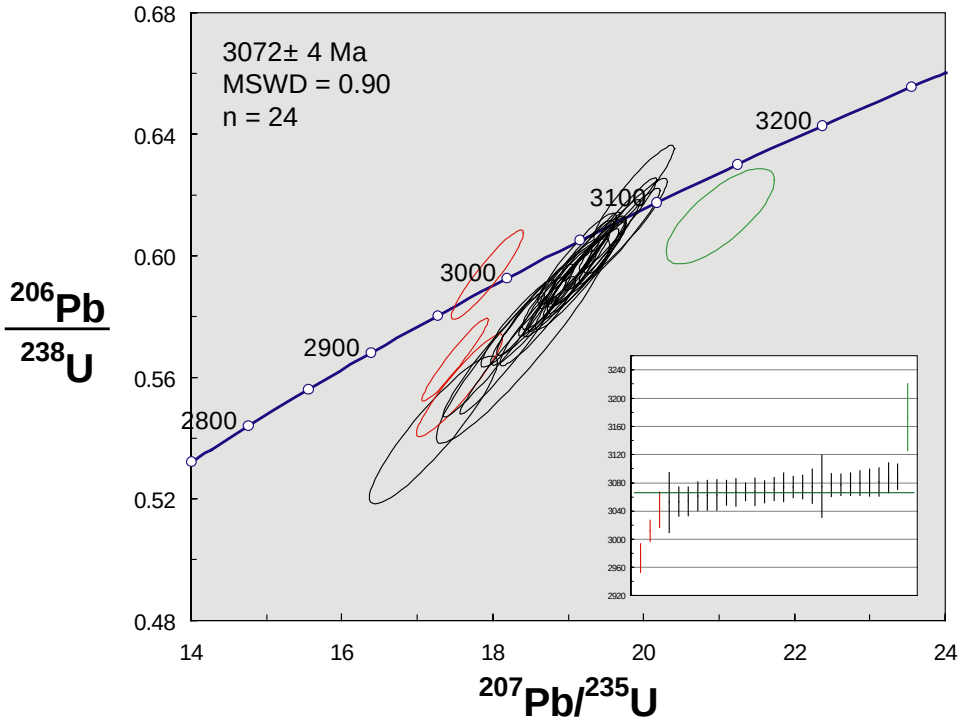

Figure 11. *481201 $^{206}Pb/^{238}U$-$^{207}Pb/^{235}U$ concordia diagram and inset $^{207}Pb/^{206}Pb$ age plot.*

479825
Collector: Nigel Kelly
Lithology: Plagioclase-quartz-biotite orthogneiss
Location: interior of Bjørneøen, west of banded amphibolite.
Locality: nmk2004-153, 64 26.388°N, -51 18.534°W
Aim: emplacement age of orthogneiss of unknown affinity and metamorphic age.
Method: SIMS
Age of emplacement: 3065 ± 5 Ma (MSWD =1.3, n = 8 of 15)
Age of emplacement: 2999 ± 3 Ma (MSWD = 1.3, n = 5 of 15)

The zircons in this sample are all morphologically similar. They are short prismatic crystals up to c. 350 μm long, with relatively distinct, broad oscillatory zoning. A few grains have brighter cores, and some areas are almost completely homogeneous on BSE images.

The sample contains two distinct age populations of 3065 ± 5 Ma (MSWD =1.3, n = 8) and 2999 ± 3 Ma (MSWD = 1.3, n = 5), with no morphological difference. One other grain yielded an age intermediate between the two age populations, and one grain yielded a still lower age. We interpret this data set as indicating that the sample is composed of two different rock components, an orthogneiss host and a subordinate younger phase.

Both age populations are typical for the eastern part of the Akia terrane. The 3065 Ma population is just a few million years younger than the quartzo-feldspathic schists of volcanoclastic origin from central Bjørneøen which are intruded by tonalitic gneiss, and the young component (2999 Ma) is roughly comparable with the ages of granitic veins such as 477318 and 477320 east of Qussuk dated at around 2990 Ma.

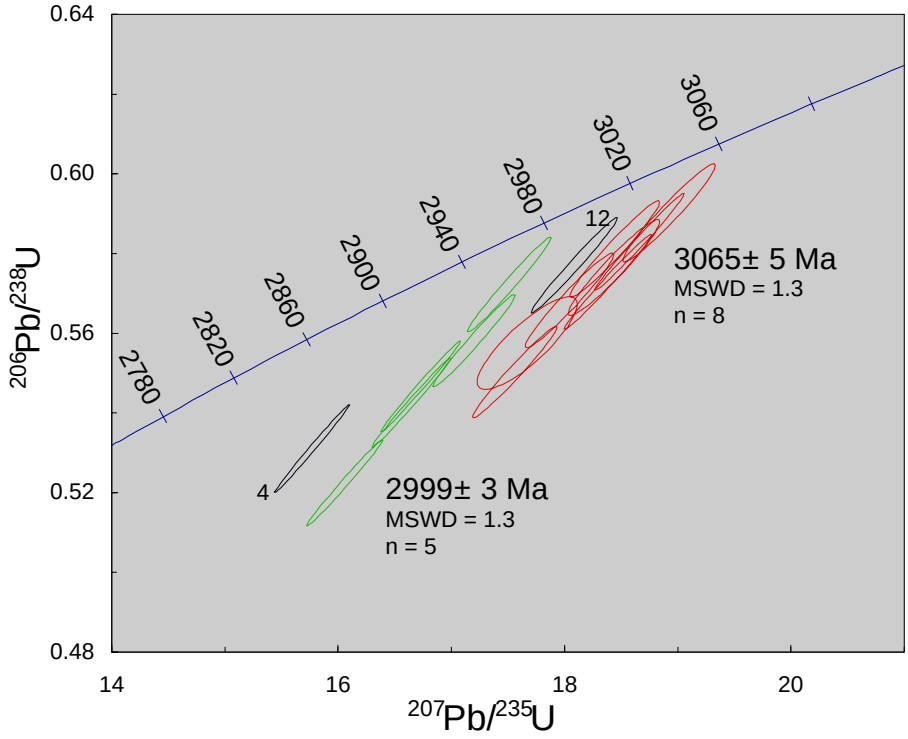

Figure 12. *479825 $^{206}Pb/^{238}U$-$^{207}Pb/^{235}U$ concordia diagram.*

479606
Collector: Nigel Kelly
Lithology: Garnet-biotite felsic gneiss boudinaged and folded within amphibolite within the Nûk gneiss
Location: Sermitsiaq
Locality: nmk2004-004, 64 16.975°N, -51 27.370°W
Aim: age of garnet-bearing component of felsic gneiss and possibly age of metamorphism
Method: LA-SF-ICPMS
Age of emplacement: 3064 ± 3 (MSWD 1.02, n = 28 of 28)
Age of metamorphism: no metamorphic zircon

The zircons are 150–400 μm in length with aspect ratios 1:2 to 1:4 (typically 1:3), and commonly prismatic. The majority show well-defined oscillatory zonation and only a few are homogeneous. There is no development of BSE bright rims.

Twenty-eight spots in 28 grains were analysed. The data define a single population at 3064 ± 3 (MSWD 1.02, n = 28). The zircons have 16–323 ppm U with a tendency toward higher U concentrations at lower ages, and Th/U of 0.39–0.73.

The sample was collected from a thin garnet-bearing component of a felsic gneiss boudinaged and folded within amphibolite within the Nûk gneiss. It was thought that the zircon fraction might preserve some evidence of the metamorphic age of these rocks, though this was not the case. The well-defined 3064 ± 3 Ma age is interpreted as the emplacement age of the felsic gniess and is consistent with the age of emplacement of Nûk gneiss from other parts of the Akia terrane.

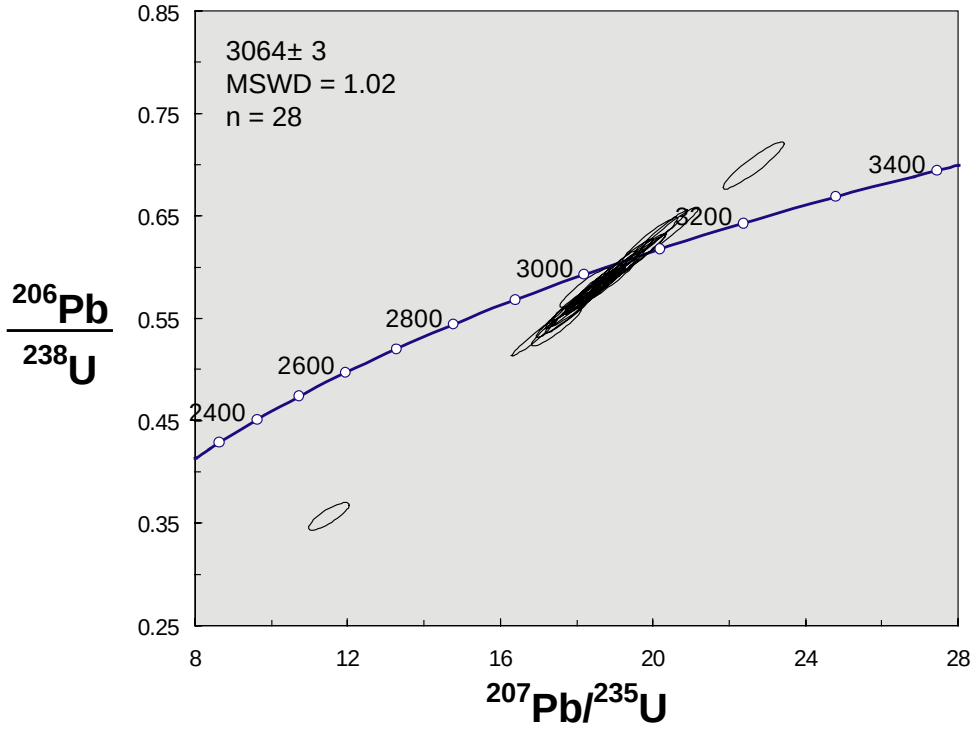

Figure 13. *479606 $^{206}Pb/^{238}U$-$^{207}Pb/^{235}U$ concordia diagram.*

479049
Collector: Julie Hollis
Lithology: Foliated granitic sheet (1m side) cross-cutting foliation in amphibolite that forms part of Bjørneøen supracrustal sequence.
Location: SE Bjørneøen
Locality: jho2004-211, 64 21.567°N, -51 18.435°W
Aim: crystallisation age of cross-cutting granitic sheet and thus minimum age of formation and deformation in host supracrustal amphibolite on Bjørneøen.
Method: SIMS and LA-SF-ICPMS
Age of inheritance (LA-SF-ICPMS): 3079 ± 26, 3069 ± 19, and 3063 ± 18 Ma (n = 3 of 30)
Age of emplacement (SIMS): 3055 ± 3 Ma (MSWD 2.1, n = 13 of 15)

The zircons are 100–200 μm in length with aspect ratios typically 1:2 to 1:3, and commonly prismatic. The majority have broad oscillatory zones, often with a darker, more homogeneous core.

Fifteen spots in 15 grains were analysed via SIMS. Thirteen grains give a fairly well-defined and concordant population at 3055 ± 3 Ma (MSWD 2.1) with 157–452 ppm U and Th/U 0.28–0.53. Two younger grains are 3021 ± 12 and 3016 ± 8 Ma and with similar U concentrations and Th/U.

These results compare fairly well with a main population defined via LA-SF-ICPMS analysis of 19 (of 30) different grains of 3042 ± 4 Ma (MSWD 0.60). Three older grains analysed via LA-SF-ICPMS are 3079 ± 26, 3069 ± 19, and 3063 ± 18 Ma. The 3 youngest grains are 2956 ± 42, 2915 ± 26, and 2880 ± 15 Ma.

The sample was collected from a deformed granitic dyke (c. 1m diameter) cross-cutting the thick amphibolite package on south-east Bjørneøen. The main population at 3055 ± 3 Ma (SIMS) is interpreted as the age of crystallisation of the granitic dyke, thus giving a minimum age of formation of the host mafic amphibolite that the dyke cross-cuts. This is consistent with similar minimum ages of formation of metavolcanic rocks from the Akia terrane (this volume) inferred from their detrital zircon populations. The slightly younger grains may have been partially influenced by later thermal activity – indeed the main population also show some spread toward slightly younger ages.

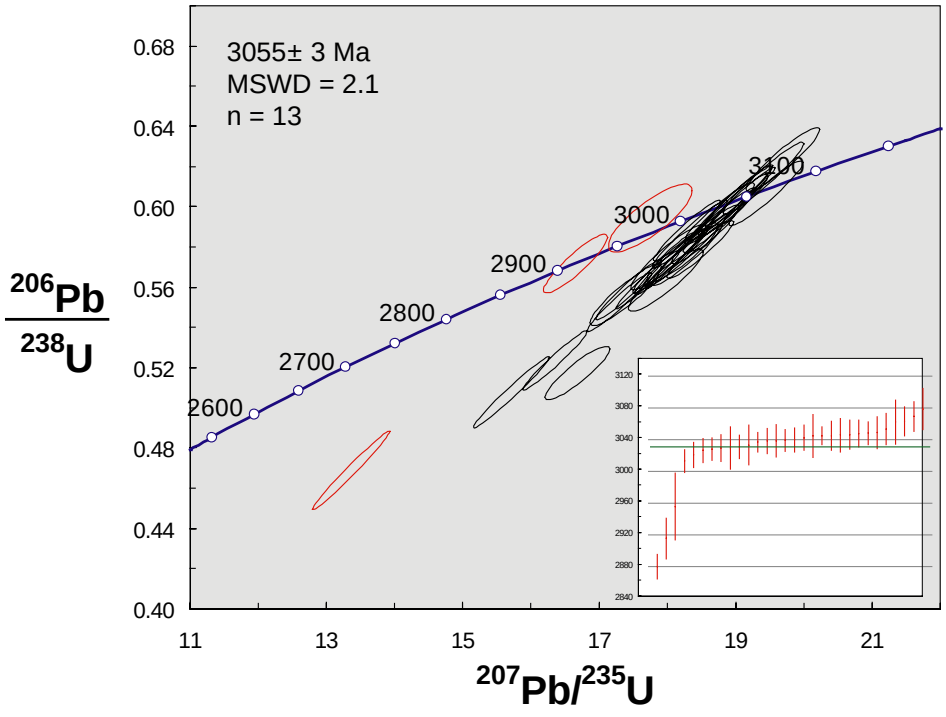

Figure 14. *479049 $^{206}Pb/^{238}U$-$^{207}Pb/^{235}U$ concordia diagram and inset $^{207}Pb/^{206}Pb$ age plot.*

479665
Collector: Nigel Kelly
Lithology: intensely deformed intermediate gneiss cross-cutting felsic orthogneiss
Location: central Bjørneøen
Locality: nmk2004-040, 64 25.282°N, -51 14.363°W
Aim: age of emplacement and minimum age of host felsic orthogneiss
Method: LA-SF-ICPMS
Age of emplacement: 3053 ± 6 (MSWD 1.9, n = 13 of 13)

The zircons are 150–300 μm with aspect ratios typically 1:2 to 1:3, commonly prismatic. All grains show well-defined oscillatory zonation with no distinct cores or rims.

Thirteen spots in 13 grains were analysed. The data define a single population at 3053 ± 6 (MSWD 1.9, n = 13) with significant normal discordance. The zircons have 30–197 ppm U (1 outlier at 393 ppm) with Th/U of 0.11–0.64 (outlier at 0.67). The oldest grain at 3074 ± 15 Ma is the most discordant grain and has the highest U (393 ppm) and Th/U (0.67).

The sample was collected from an intensely deformed intermediate gneiss cross-cutting the host felsic orthogneiss, inferred to be a part of the Nûk gneiss. The emplacement age of 3053 ± 6 Ma gives a minimum age of the host felsic orthogneiss and gives a maximum constraint on the timing of the intense deformation.

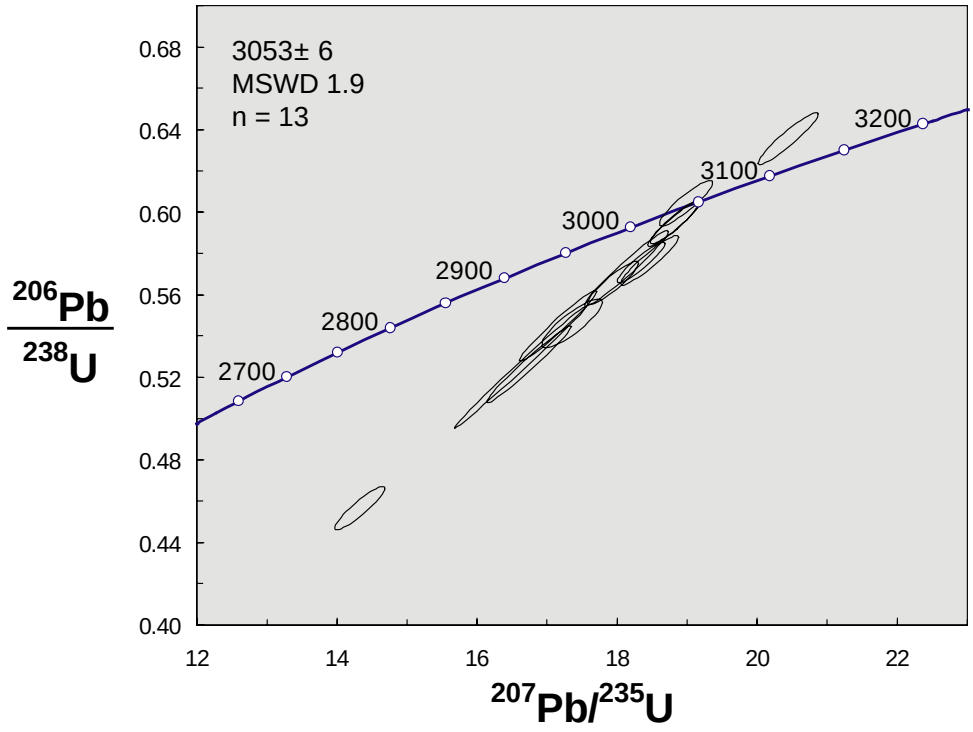

Figure 15. *479665 $^{206}Pb/^{238}U$-$^{207}Pb/^{235}U$ concordia diagram and inset $^{207}Pb/^{206}Pb$ age plot.*

481271
Collector: Jeroen van Gool
Lithology: Homogeneous grey tonalitic gneiss cutting metagabbro-anorthosite sequence
Location: Eastern part of central Storø.
Locality: jvg2004-111, 64 25.546°N, -51 00.191°W
Aim: emplacement age tonalitic gneiss cutting metagabbro-anorthosite, which in turn cuts amphibolites at the base of the supracrustal sequence, thus giving minimum constraint on age of the supracrustal rocks
Method: SIMS
Age: 3053 ± 4 Ma (MSWD = 1.9, n = 9 of 9)

The zircons in 481271 are mainly stubby prismatic, euhedral grains up to 400 microns long, with very distinct oscillatory zoning displayed on BSE images, and almost no recrystallisation features. A few of the grains are pitted, but most are well preserved. They contain less than 300 ppm U and 200 ppm Th.

The nine analysed points in 8 crystals form a near-concordant, overlapping linear array yielding an age of 3053 ± 4 Ma (MSWD = 1.9).

The implication of this age is that the metagabbro-anorthosite, and hence part of the supracrustal package on Storø, is much older than previously assumed. Either the greenstone belt is part of the Akia or Kapisillik terrane, or it represents a panel of older rocks within the Tre Brødre terrane.

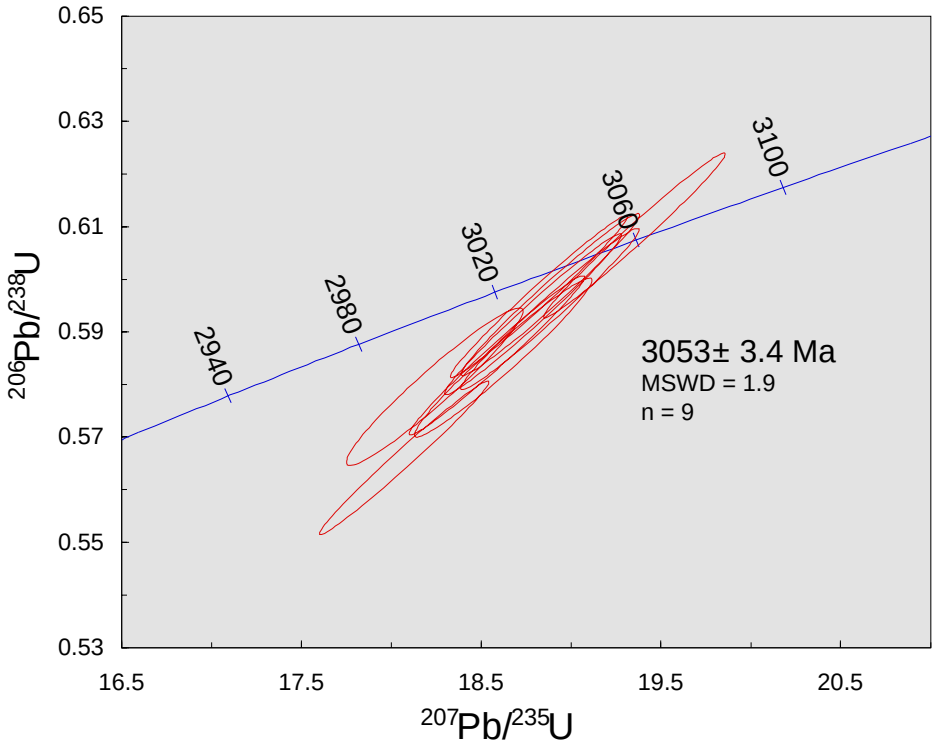

Figure 16. *481271 $^{206}Pb/^{238}U$-$^{207}Pb/^{235}U$ concordia diagram and inset $^{207}Pb/^{206}Pb$ age plot.*

479813
Collector: Nigel Kelly
Lithology: intensely sheared layered intermediate and felsic orthogneiss
Location: central Bjørneøen
Locality: nmk2004-103, 64 22.804°N, -51 21.264°W
Aim: age spectra of metamorphism associated with intense shearing
Method: LA-SF-ICPMS
Age of emplacement: c. 3050 Ma
Age of metamorphism: c. 2980 Ma

The zircons are 100–200 μm in length with aspect ratios typically 1:1 to 1:3, and commonly prismatic. The majority are fairly homogeneous with some poorly-defined sector or oscillatory zonation. A few grains have BSE bright homogeneous rims.

Twenty-five spots in 24 grains were analysed. The data show a considerable spread in ages from 3052 ± 33 to 2980 ± 13 Ma (n = 25). The age spread is outside the uncertainty on individual analyses with no identifiable populations. The zircons have 140–491 ppm U (with 1 outlier at 775 ppm) and generally very low Th/U of 0.03–0.16 with a tendency toward higher Th/U of 0.6–0.31 for the older grains (> 3011 ± 14 Ma). There is no clear distinction in ages that can be made on the basis of zircon morphology, although sector-zoned grains tend to fall in the younger range (< c. 3000 Ma).

The sample was collected from an intensely sheared layered intermediate and felsic orthogneiss on central Bjørneøen. This lithology was targeted to investigate the age of metamorphism associated with the strong shear fabric in this area. Unfortunately only a few BSE bright rims were found and these did not show an age signature distinct from analyses of cores and grains without bright rims. The spread in ages from 3052 ± 33 to 2980 ± 13 Ma (n = 25) is interpreted as the product of variable recrystallisation of an igneous zircon population (probably c. 3050 Ma) during a later thermal event. This is supported by the generally very low Th/U of most grains, particularly the younger ones. The exact timing of this thermal event is not clear but probably falls close to the minimum age – 2980 ± 13 Ma. The same metamorphic age is represented in analyses of samples from the Qussuk area.

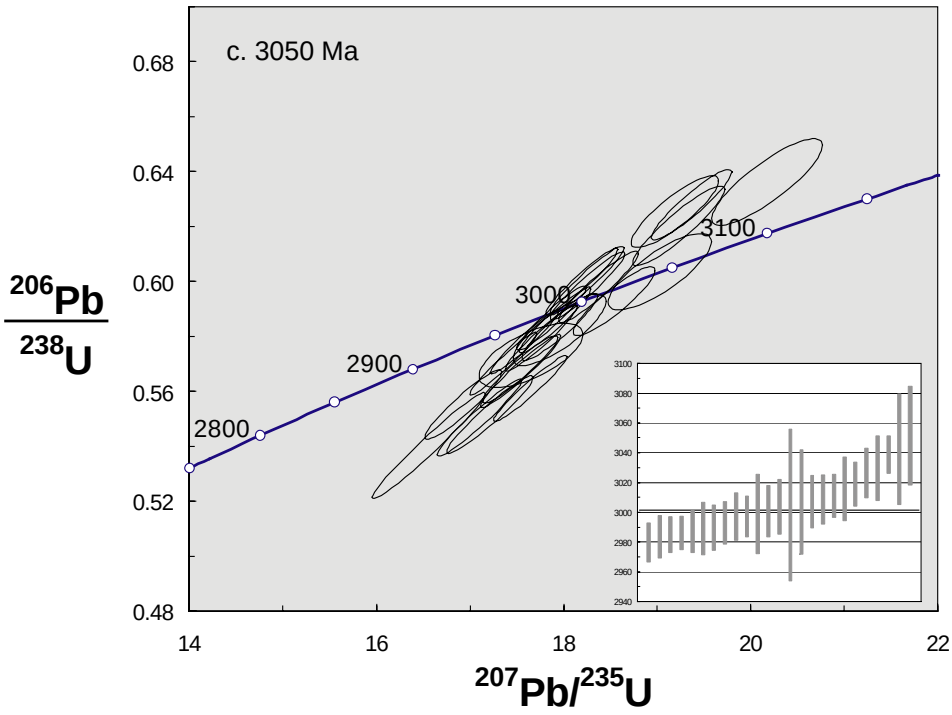

Figure 17. *479813 $^{206}Pb/^{238}U$-$^{207}Pb/^{235}U$ concordia diagram and inset $^{207}Pb/^{206}Pb$ age plot.*

481311
Collector: Steven Grimes
Lithology: Well lineated protomylonitic tonalitic gneiss from the south-east margin of the Storø shear zone.
Location: central W Storø
Locality: swg2004-025, 64 27.283°N, -51 05.449°W
Aim: age of emplacement of protomylonitic tonalitic gneiss and thus constraint on the position of the eastern-most extent of the Akia terrane
Method: LA-SF-ICPMS
Age of emplacement: 3048 ± 6 Ma (MSWD 1.9, n = 19 of 26)

The zircons are 150–300 μm in length with aspect ratios typically 1:3 to 1:4, and commonly prismatic. Most grains show well-defined oscillatory zonation with no development of rims. Twenty-six spots in 26 grains were analysed. The data show considerable spread in ages outside the uncertainty of the individual analyses and with no correlation with zircon morphologies. The oldest 19 grains define a rough population ranging from 3077 ± 30 to 3027 ± 20 Ma, which give an age of 3048 ± 6 Ma (MSWD 1.9). These have 37–241 ppm U and Th/U of 0.17–0.56. Seven younger grains range in age from 3013 ± 46 to 2823 ± 22 Ma with 56–163 ppm U and Th/U of 0.16–0.52.

The sample was collected from well lineated protomylonitic tonalitic gneiss from the south-east extent of the Storø shear zone. An emplacement age of 3048 ± 6 Ma (MSWD 1.9, n = 19 of 26) indicates that the gneiss belongs to the Nûk gneiss suite and thus that the Akia terrane extends some way E of the Storø shear zone in this area. The 7 younger ages ranging from 3013 ± 46 to 2823 ± 22 Ma indicate some resetting due to thermal activity in the late Archaean. The exact timing of this is not clear.

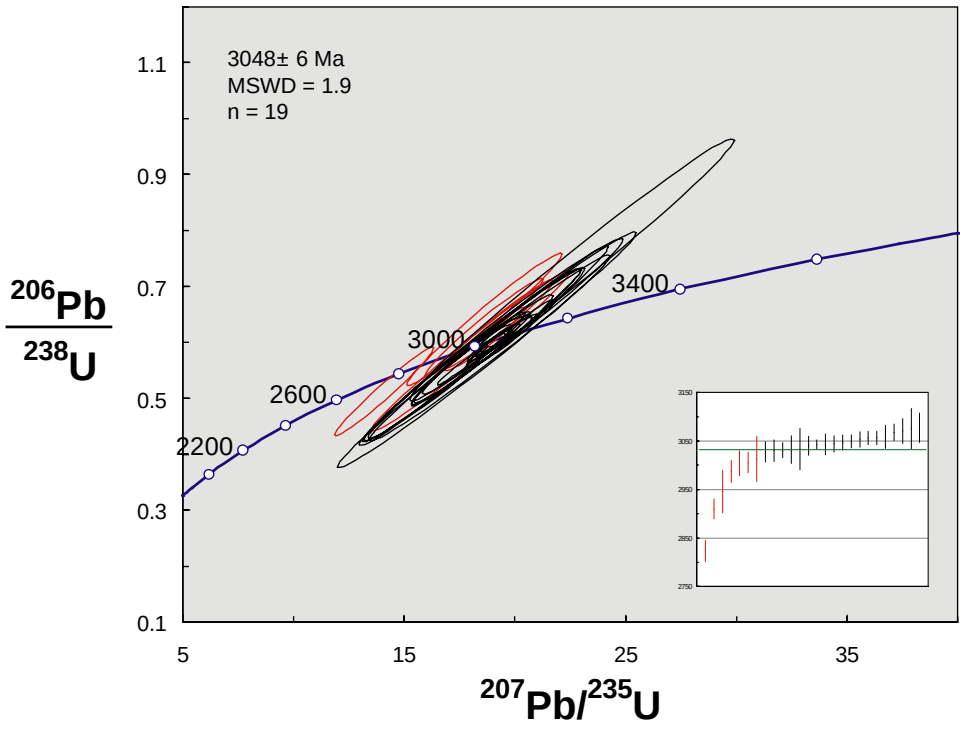

Figure 18. *481311 $^{206}Pb/^{238}U$-$^{207}Pb/^{235}U$ concordia diagram and inset $^{207}Pb/^{206}Pb$ age plot.*

479060
Collector: Julie Hollis
Lithology: Coarse grained, strongly lineated felsic orthogneiss inferred to be the Nûk gneiss.
Location: SE Bjørneøen
Locality: jho2004-217, 64 23.245°N, -51 15.262°W
Aim: crystallisation and metamorphic age of orthogneiss
Method: SIMS
Age of emplacement: 3048 ± 4 Ma (n = 6 of 15)
Age of metamorphism: c. 2635 Ma (n = 3 of 15)

The zircons are 100–200 μm in length with aspect ratios of 1:1 to 1:2, commonly prismatic. The majority have broad oscillatory zones, sometimes with a homogeneous core. Many have metamict tips, indicative of high U in these zones. A few give a bright homogeneous BSE response and a few have distinct bright homogeneous rims that may be metamorphic.

Sixteen spots in 15 grains were analysed and the resulting age signature is fairly complex. Six analyses of oscillatory zoned grains give a mean age of 3048 ± 4 Ma (MSWD 1.4). These have moderate U concentrations of 280–501 ppm and Th/U 0.15–0.35. Six younger grains give ages spread from 2973 ± 8 to 2630 ± 4 Ma. Two are >5% discordant. The youngest three form a cluster at c. 2635 Ma and also have very low Th/U of 0.003 to 0.008. Of these three one is from a homogeneous rim and another from a homogeneous grain. This is consistent with a metamorphic origin for these youngest grains.

The sample was collected from a strongly lineated felsic orthogneiss from the E coast of Bjørneøen. The oldest 6 grains fall within the known age range of the Nûk gneiss suite. Some spread in the larger population probably reflects variable resetting during later metamorphism, probably related to the development of the shear zone along the E coast of Bjørneøen and Sermitsiaq. This is supported by the spread of younger ages, down to c. 2635 Ma. The three youngest ages may be representative of the timing of the main thermal pulse resulting in lower amphibolite facies metamorphism and deformation of these rocks.

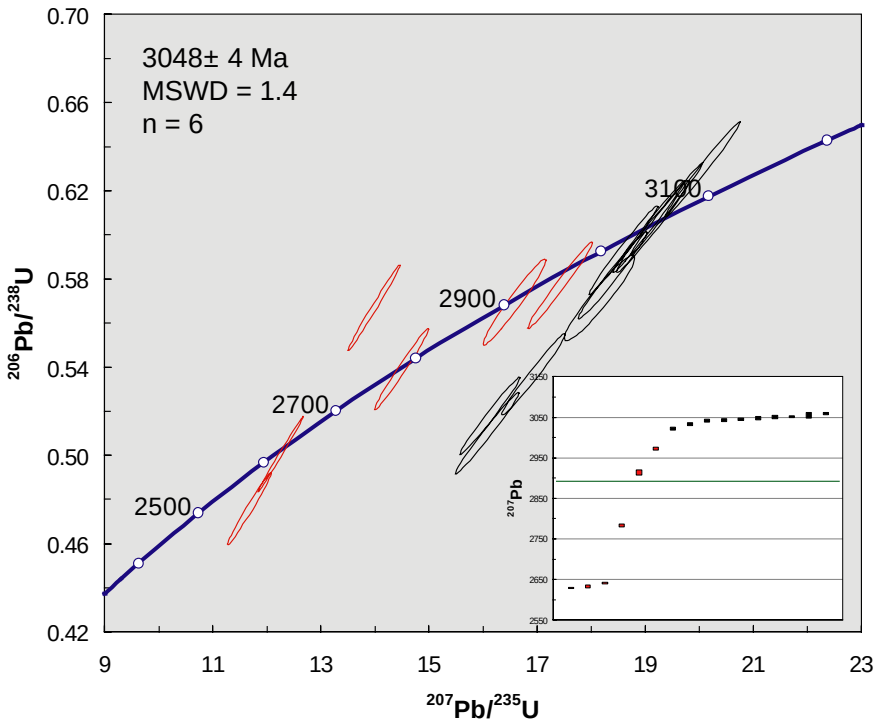

Figure 19. *479060 $^{206}Pb/^{238}U$-$^{207}Pb/^{235}U$ concordia diagram and inset $^{207}Pb/^{206}Pb$ age plot.*

481227
Collector: Jeroen van Gool
Lithology: tonalitic spotted gneiss with relatively low strain fabric.

Locality: jvg2004-033C, 64 27.401°N, -51 05.536°W
Location: central W Storø
Aim: age of emplacement of tonalitic gneiss and thus constraint on the position of the eastern-most extent of the Akia terrane
Method: LA-SF-ICPMS
Age of emplacement: 3046 ± 5 Ma (MSWD 1.3, n = 15 of 24)

The zircons are 100–300 μm in length with aspect ratios typically 1:3 to 1:4, and commonly prismatic. Most grains show oscillatory zonation, often with a large relatively homogeneous core. Some show patchy BSE bright zones often but not always along the rims, consistent with partial recrystallisation.

Twenty-four spots in 24 grains were analysed. The data show considerable spread in ages outside the uncertainty of the individual analyses. The oldest 20 grains define a rough population ranging from 3067 ± 24 to 3019 ± 18 Ma, and 15 of these define a population at 3046 ± 5 Ma (MSWD 1.3). These have 53–169 ppm U and Th/U of 0.31–0.55. Nine younger grains range in age from 3029 ± 9 to 2943 ± 13 Ma with 64–139 ppm U and Th/U of 0.25–0.43. There is no distinction between these age groups that can be made on the basis of zircon morphology.

The sample was collected from a tonalitic spotted gneiss with relatively low strain fabric close to the inferred eastern-most extent of the Akia terrane. The emplacement of this pegmatite is inferred to have occurred prior to or during development of the shear zone. The main population at 3046 ± 5 Ma indicates that this belongs to the Nûk gneiss suite. Some spread in the data may be a consequence of either two or more populations of igneous zircon (i.e. multiple magma pulses) or partial resetting of the ages during a later Archaean thermal event. The latter is suggested by the occurrence of 9 younger ages in the range 3029 ± 9 to 2943 ± 13 Ma.

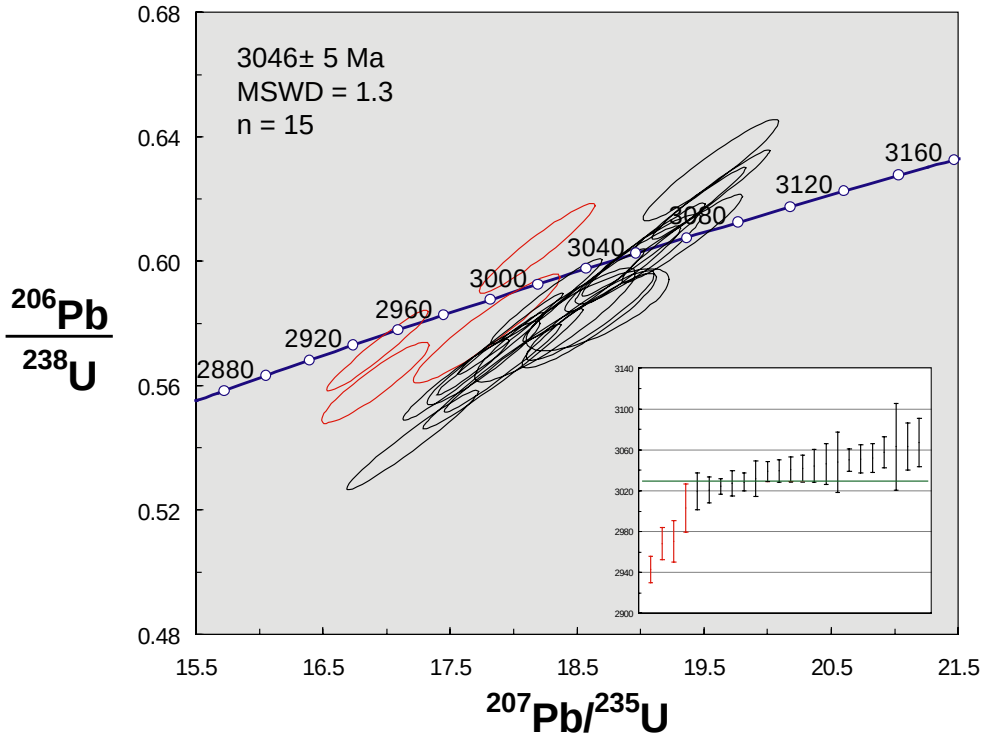

Figure 20. *481227 $^{206}Pb/^{238}U$-$^{207}Pb/^{235}U$ concordia diagram and inset $^{207}Pb/^{206}Pb$ age plot.*

477321
Collector: Adam A. Garde
Lithology: Leucocratic orthogneiss
Location: SE tip of Qussuk peninsula
Locality: aag2004-103, 64 36.490°N, -51 02.696°W
Aim: emplacement age of orthogneiss of unknown affinity
Method: SIMS
Age of 5 inherited grains: 3057 ± 4 Ma (MSWD = 0.14, n = 5 of 16)
Age of emplacement: 3040 ± 2 Ma (MSWD = 1.08, n = 10 of 16)

The zircons are small, prismatic and stubby grains (shape ratios up to 4:1) around 150 μm in length, with variable oscillatory zoning. In some grains cores and rims as well as partial recrystallisation are visible on BSE images. The crystals are frequently somewhat cracked. The U and Th contents are very variable but generally normal for orthogneisses, except one grain with c. 6500 ppm U and 2200 ppm Th.

Sixteen spots in 15 grains were analysed and define two distinct age groups, which could not be distinguished by morphology. Five spots yield 3057 ± 4 Ma (MSWD = 0.14) and are interpreted as inherited, and 10 spots mostly with higher U and Th contents yield 3040 ± 2 Ma (MSWD = 1.08), which is interpreted as the magmatic emplacement age of the or-

thogneiss precursor. Spot 2 appears visually problematic, as it belongs to the older age group, whereas spot 1 nearby in the same grain is part of the younger age group. Maybe the visible section of this grain is so superficial that the older core is not clearly recognised on the picture. Grain no. 8 with very high U and Th contents and an apparent age of 3014 Ma was discarded.

The small area of orthogneisses that form a promontory on the south-eastern coast of the Qussuk peninsula is separated from the Taserssuaq tonalite by a high-strain zone along the flank of an isoclinal fold. The age data presented here demonstrates that this orthogneiss is either part of the Akia terrane (but clearly older than the adjacent Taserssuaq complex) or perhaps belongs to the newly discovered Kapisillik terrane in the east, but has nothing to do with the Tre Brødre or Færingehavn terranes.

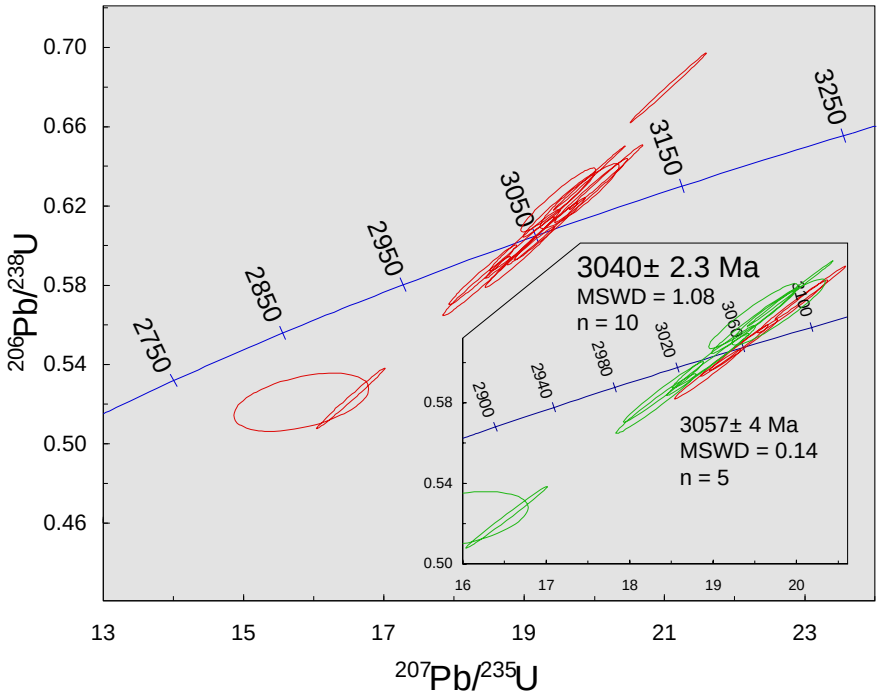

Figure 21. *477321 $^{206}Pb/^{238}U$-$^{207}Pb/^{235}U$ concordia diagram.*

477307
Collector: Adam A. Garde
Lithology: Leucogabbro/diorite
Location: Innajuattup Qeqertaa, eastern Qussuk peninsula. At the Ivinnguit fault on the south-eastern boundary of the Akia terrane.
Locality: aag2004-092, 64 42.448°N, -50 47.069°W
Aim: emplacement age of leucogabbro of unknown affinity
Method: SIMS
Age of emplacement: 3006 ± 6 Ma (MSWD = 0.82, n = 8 of 9)

The zircons are very uniform and relatively large (300–600 μm). Most are short stubby, euhedral prisms with typical length/width aspects of 3:1, but a few more slender crystals also occur. BSE images display a weak concentric zoning in almost all grains, which gen-

erally appear fresh, unaltered, and not recrystallised. The U and Th contents are c. 25–125 and 10–60 ppm, respectively, with uniform Th/U ratios of around 0.4.

Nine grains were analysed and give almost identical results, despite large counting errors due to the low U content. Eight of them yield a concordant age of 3006 ± 6 Ma (MSWD = 0.82). If grain 8 with a slightly lower 207Pb/206Pb ratio is included, the age is 3005 ±6 Ma, and the MSWD increases to 1.4.

This sample was collected at the Ivinnguit fault, and it was expected that the age might be around 2835 Ma (Tre Brødre terrane). Instead, the age indicates that the leucogabbro or hornblende diorite is related to the Taserssuaq tonalite complex.

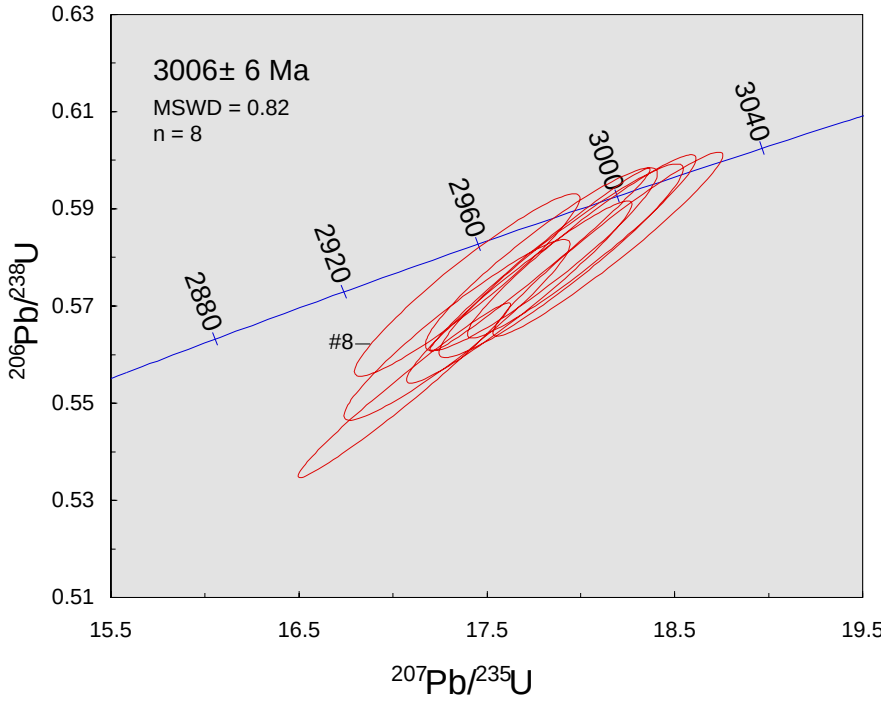

Figure 22. *477307 $^{206}Pb/^{238}U$-$^{207}Pb/^{235}U$ concordia diagram.*

477320
Collector: Adam A. Garde
Lithology: Deformed granite vein in high-strain zone that intrudes intensely deformed host
Location: Qussuk peninsula
Locality: aag2004-100, 64 39.301°N, -50 58.643°W
Aim: syn- or lower age limit of the high-strain zone
Method: SIMS
Age of emplacement: 2992 ± 3 Ma (MSWD = 0.92, n = 6 of 10)
Age of inherited grains: 3005 ± 3 Ma (MSWD = 1.5, n = 4 of 10)

The zircons in sample 477320 are all small, equant to stubby prismatic, and around 150 microns large. A weak concentric zonation is just visible on BSE images, besides metamict rims only a few microns wide. In some grains a small core is visible. The zircons contain c. 400–800 ppm U and 200–500 ppm Th and are quite well preserved.

The 10 analysed spots all yield concordant results in a cluster around 3000 Ma, but two different, well-defined, concordant age populations can be detected without excluding any analyses. Grains 2, 4, 6, and 10 yield 3005 ± 3 Ma (MSWD = 1.5), and the remaining six grains 2992 ± 3 Ma (MSWD = 0.92). The latter age is interpreted as the emplacement age of the granite vein.

As for sample 477318, sample 477320 shows that a major part of the intense deformation in the south-eastern part of the Qussuk peninsula occurred close to (or even before) 3000 Ma, and there is no evidence of post-Akia magmatic activity in the area. See also sample 477321.

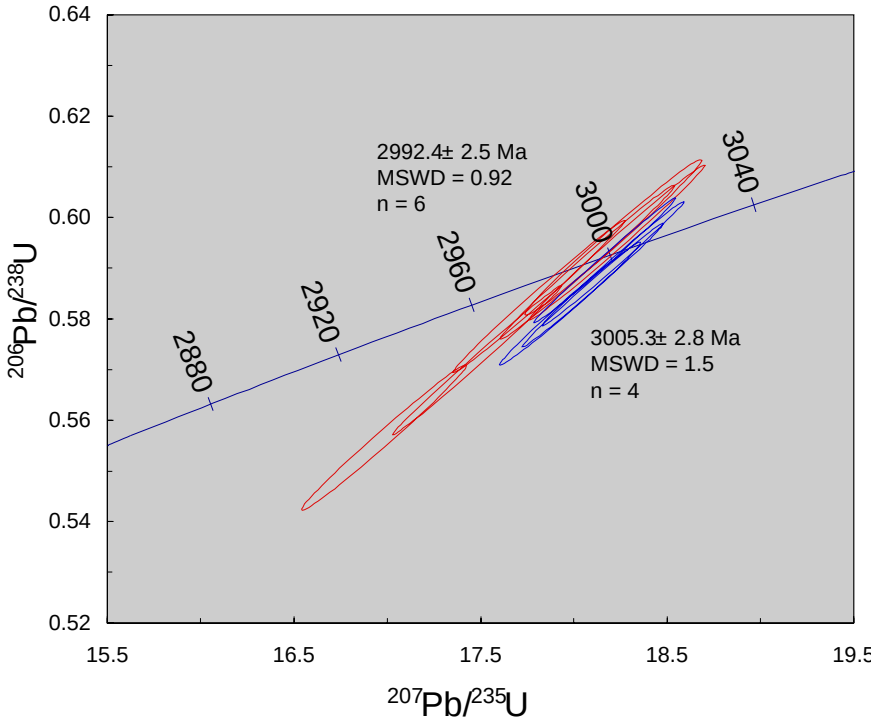

Figure 23. *477320 $^{206}Pb/^{238}U$-$^{207}Pb/^{235}U$ concordia diagram.*

477318
Collector: Adam A. Garde
Lithology: Granite vein, Cuts an intense LS fabric in metagabbro of the Taserssuaq complex and itself weakly deformed.
Location: eastern Qussuk peninsula
Locality: aag2004-099, 64 39.485°N, -50 58.176°W
Method: SIMS
Aim: Constrains the age of a high-strain zone in the south-eastern boundary region of the Akia terrane.
Age of emplacement: 2990 ± 4 Ma (MSWD = 5.3, n = 10 of 15)

The zircons are pale pinkish, stubby prisms 200–500 μm long, most of which display wide indistinct concentric zones on BSE images. A few grains have well-defined cores surrounded by rims c. 25 microns wide. Other grains appear homogeneous, or have large homogeneous parts, occasionally with outer rims only a few microns wide, suggesting partial recrystallisation. The U and Th contents are very variable, from c. 70–3080 and 10–3300 ppm, respectively. Many of the BSE-bright, U-rich grains are internally pitted and cracked, and a few are heavily altered.

Fifteen spots in 14 different grains were analysed. Ten of these yield an age of 2990 ± 4 Ma (MSWD = 5.3). This is believed to be the emplacement age of the granite; the relatively high MSWD-value may suggest that the apparent analytical precision is overestimated in this sample, or the apparent age is lowered by metamorphic recrystallisation soon after the magmatic emplacement. Five analyses in five grains are omitted: one low-U grain of 3016 Ma (spot 5) which is presumably inherited, three high-U grains with lower ages (spots 8, 9, 13, 2970–2930 Ma, early Pb loss?), as well as spot 15 with an apparent age of only 2536 Ma.

The age constrains most of the deformation in the NE-trending high-strain zones on the Qussuk peninsula to be older than 2990 Ma. These zones are parallel to the Palaeoproterozoic Ataneq fault, and the position of the latter was probably controlled by the mid-Archaean high-strain zones.

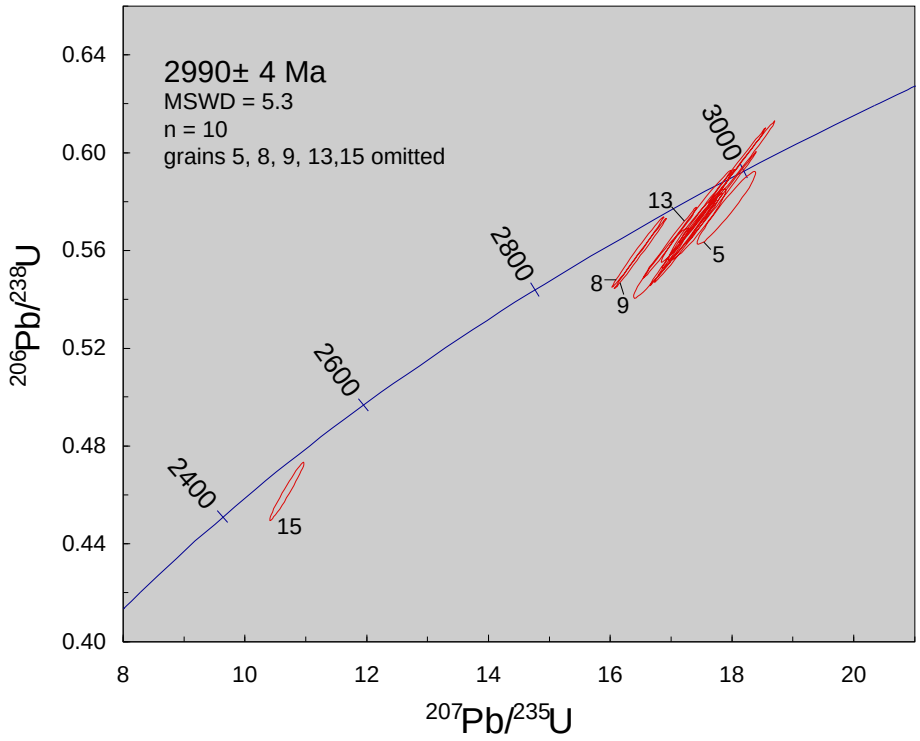

Figure 24. *477318 $^{206}Pb/^{238}U$-$^{207}Pb/^{235}U$ concordia diagram.*

477352
Collector: Adam A. Garde
Lithology: Granite vein cutting intermediate amphibolite
Location: Qussuk peninsula.
Locality: aag2004-147, 64 40.456°N, -51 02.540°W
Aim: minimum age of intermediate amphibolite.
Method: SIMS
Age of emplacement: 2984 ± 2 Ma (MSWD = 0.83, n = 6 of 21), with four inherited zircons (c. 3000 Ma) and a tail of younger apparent ages from 11 high-U grains

Two different zircon populations with different shapes and very different U contents are present in this granite. The first group is stubby grains 250–350 μm long with low U contents (40–95 ppm) and narrow, metamict, high-U rims. The second group consists of smaller, slender prismatic zircons 150–250 microns long with U contents above 1250 ppm; both groups contain less than 100 ppm Th. Most zircons in the second group have strongly pitted cores with occasional small, BSE-bright inclusions (probably monazite), and up to 40 microns long, more homogeneous growth zones at their tips, in which fine oscillatory zoning may be visible.

21 spots in 19 grains were analysed. Four grains in the first, low-U group (no. 1, 12, 13, 21) yield a poorly defined common age of 3000 ± 22 Ma (MSWD = 2.8). These zircons are interpreted as inherited. In the second group of 15 grains, most spots were placed in the well-preserved broad tips with fine oscillatory zoning, but also dark cores with weak oscillatory zoning and a few brighter, less homogeneous cores were analysed. Six of the broad,

high-U tips yield a very precise age of 2984 ± 1 Ma (MSWD = 0.83), while the remaining 11 spots in high-U, pitted cores and homogeneous tips yield younger ages ranging between 2978–2810 Ma. Given that all of these younger ages are from high-U zircons and that some of them were obtained from cores, they are interpreted as due to metamorphic re-crystallisation or, perhaps more likely, early lead loss, and are discarded.

The age of 2984 ± 2 Ma obtained from six broad, oscillatory zoned tips of high-U zircons (commonly with pitted cores) is considered to represent final magmatic crystallisation of the granite. The dated sample is part of a system of granite veins that cuts strongly deformed panels of leucocratic amphibolite and is itself folded in the main, steeply S-plunging fold system. However, the granite veins are less tightly folded than their amphibolite hosts, and the age of the granite dates the main event of folding on the Qussuk peninsula that affects both the amphibolite, its orthogneiss host, and, in part, the still younger granite sheets.

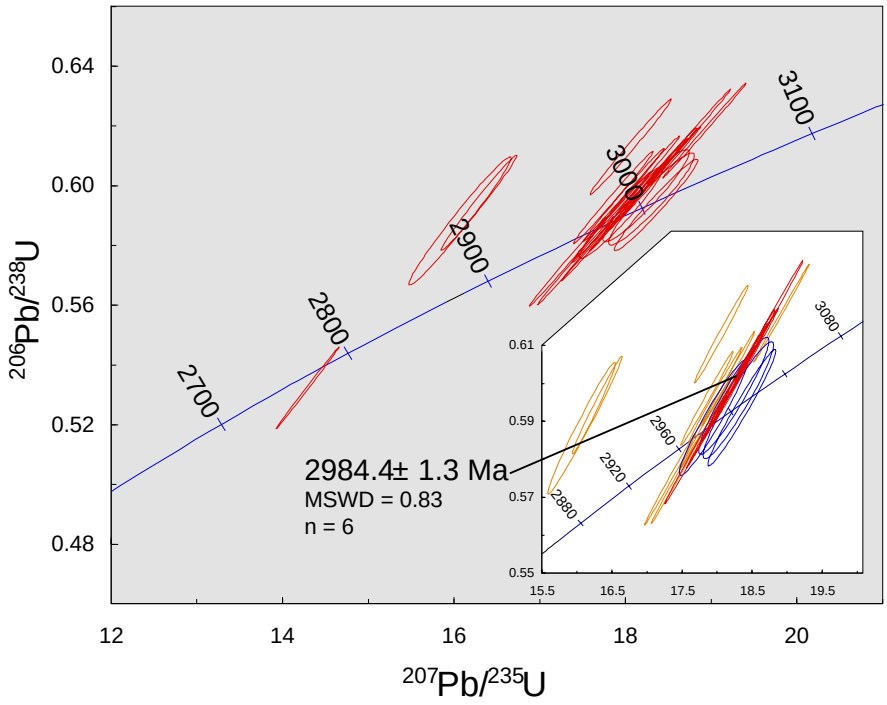

Figure 25. *477352 $^{206}Pb/^{238}U$-$^{207}Pb/^{235}U$ concordia diagram.*

Late Archaean magmatic rocks

479040
Collector: Julie Hollis
Lithology: Sugary felsic gneiss with rare garnet-bearing felsic layers
Location: W coast of Storø.
Locality: jho2004-203, 64 23.433°N, -51 11.503°W
Aim: emplacement age of package of banded orthogneisses of unknown affinity
Method: SIMS
Age: 2894 ± 3 Ma (MSWD = 2.6, n = 8 of 10)

The zircons are 100–200 μm long and stubby prismatic grains. Most possess a weak concentric zoning visible on BSE images, and narrow, commonly cracked rims. The U and Th contents are generally a few hundred ppm. However, some areas in some crystals are homogeneous and contain up to around 3000 ppm U and 2000 ppm Th, and are clearly recrystallised.

Eight out of 10 analysed points yield a concordant age of 2894 ± 3 Ma (MSWD = 2.6), besides one significantly older and one younger grain, which are both discordant. There is no age difference between the oscillatory zoned, low-U and recrystallised, high-U parts.

The robust and precise age of this gneiss is remarkable, since it is far younger than any hitherto recognised member of the Akia terrane (>2975 Ma), and far too old to be a member of the Ikkattoq gneiss of the Tre Brødre terrane (c. 2830 Ma). However, the age suggests that this orthogneiss may represent a previously unknown source of detrital zircons in the metasedimentary samples 479008 and 479326.

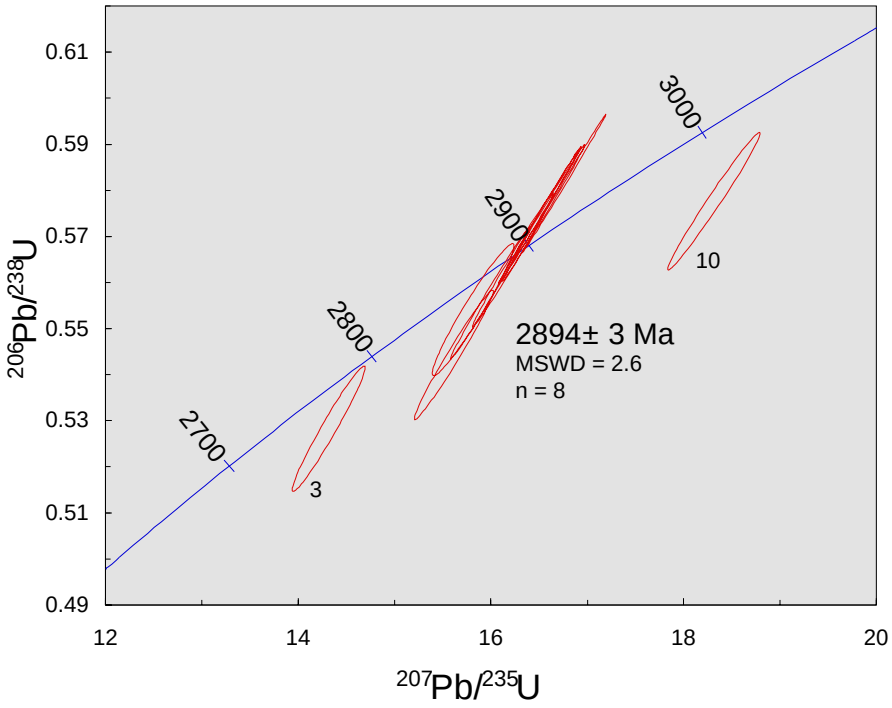

Figure 26. *479040 $^{206}Pb/^{238}U$-$^{207}Pb/^{235}U$ concordia diagram and inset $^{207}Pb/^{206}Pb$ age plot.*

479703
Collector: Dirk Frei
Lithology: medium-grained felsic augen gneiss of unknown affinity
Location: central Bjørneøen
Locality: df2004-018, 64 16.186°N, -51 26.622°W
Aim: emplacement age of orthogneiss of unknown affinity
Method: LA-SF-ICPMS
Age of emplacement: c. 2840 Ma (n = 22 of 29)
Age of metamorphism: unknown – partial resetting but no distinct age

The zircons are 200–400 μm with aspect ratios typically 1:2 to 1:3, commonly blocky and prismatic. Grains are oscillatory and sector zoned. Some show restricted BSE bright areas (typically < 30 μm diameter and not necessarily rims) suggestive of partial recrystallisation. Twenty-nine spots in 29 grains were analysed. The data show a spread in ages from 2855 ± 18 to 2796 ± 19 Ma, with the spread in ages outside the uncertainty on individual analyses. U concentrations range from 29–201 ppm with Th/U 0.21–0.98. An indistinct plateau in ages at 2840 ± 4 Ma (MSWD = 1.6, n = 22 of 29) may reflect a real event at this time. The range in ages cannot be linked to specific zircon morphologies.

The sample was collected from a medium-grained felsic augen gneiss of unknown affinity, and which was dated to test the extent of the Ikkattoq cf. Nûk gneiss in this region. The 2840 ± 4 Ma age may reflect emplacement, roughly consistent with belonging to the Ikkattoq gneiss suite. However the spread toward lower ages makes it difficult to categorically define the emplacement age. The age spread is interpreted as indicative of partial resetting

during later thermal activity. Unfortunately no clear metamorphic rims are present so it is not possible to establish the exact timing of metamorphism in this sample. It may be that some of this spread is derived from mixed ages resulting from sampling of zones of slightly different ages.

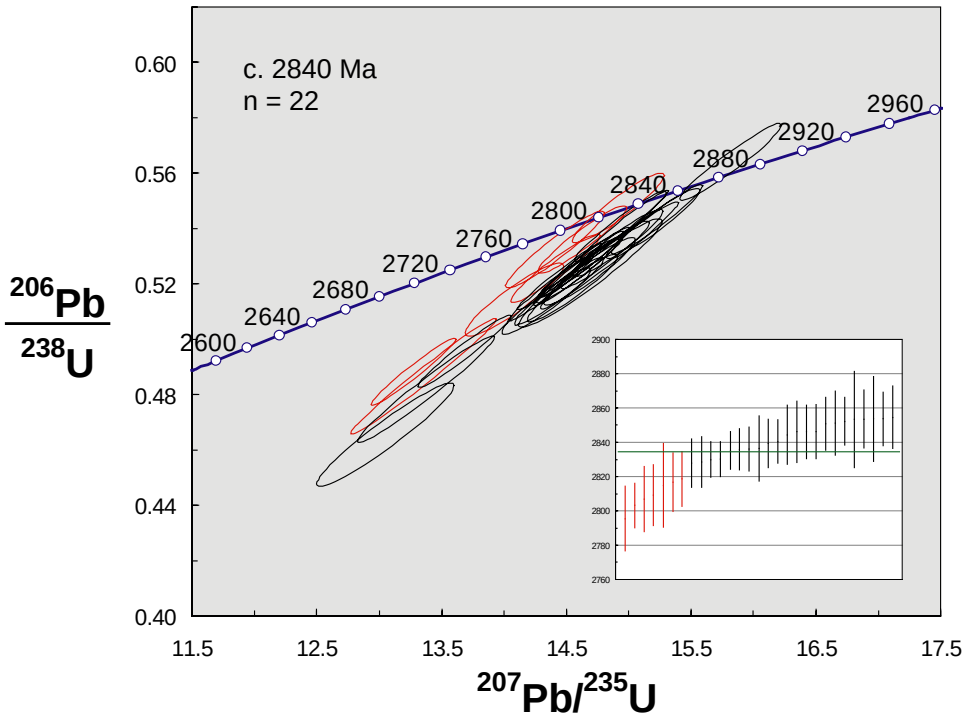

Figure 27. *479703 $^{206}Pb/^{238}U$-$^{207}Pb/^{235}U$ concordia diagram and inset $^{207}Pb/^{206}Pb$ age plot.*

479301
Collector: Mikkel Vognsen
Lithology: Garnet-bearing granitic pegmatite intruded along contact between supracrustal rocks (NW) and the structurally underlying Ikkattoq gneiss (SE)
Location: S Sermitsiaq
Locality: mvo2004-007, 64 15.238°N, -51 28.061°W
Aim: age of abundant pegmatites (thermal activity) along the base of the Bjørneøen supracrustal belt
Method: LA-SF-ICPMS
Age of emplacement: 2840 ± 5 (MSWD 1.8, n = 22 of 22)

The zircons are prismatic, typically 100–300 μm in length with aspect ratios of 1:3, and show distinct oscillatory zonation.

Twenty-nine spots in 29 grains were analysed. Seven analyses of grains with relatively high U had high common Pb and were discarded. The remaining 22 grains form a single population at 2840 ± 5 (MSWD 1.8). The zircons have 75–227 ppm U and Th/U of 0.31 to 0.57.

The boundary zone between the supracrustal package and the structurally underlying Ikkattoq gneiss on south Sermitsiaq is swamped with abundant granitic pegmatites, some of them garnet-bearing. This sample was taken from a garnet-bearing pegmatite cutting the Ikkattoq gneiss just metres below the contact with the supracrustal sequence. The late Archaean age is interpreted as that of emplacement of the pegmatite and is most likely related to the thermal pulse associated with formation of the Ikkattoq gneiss. Notably, the age is exactly the same as gneiss sample 479703, also close to this tectonic contact on Sermitsiaq.

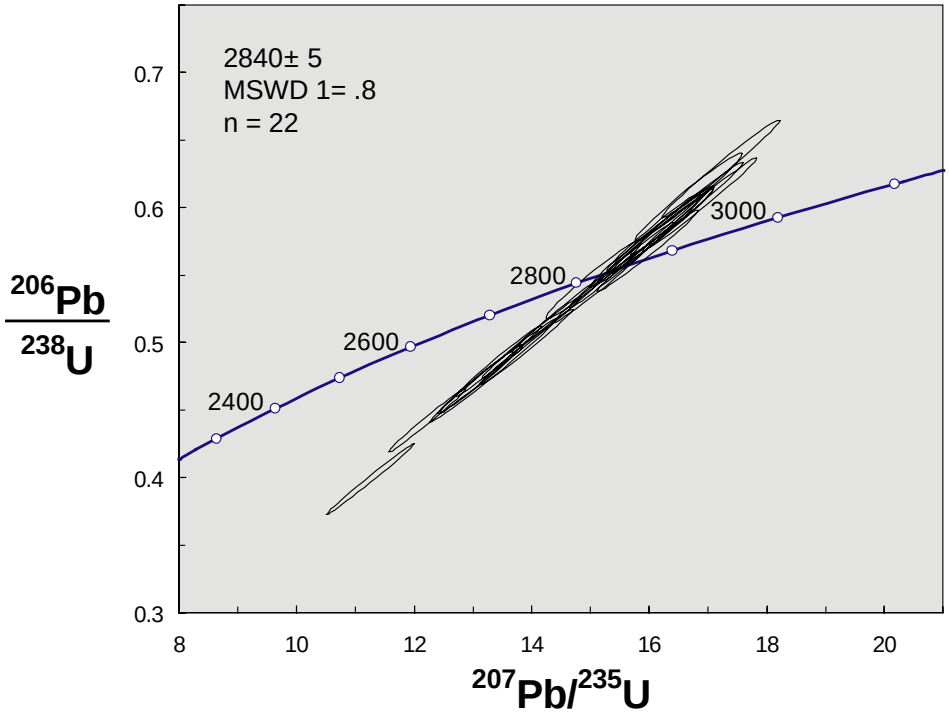

Figure 28. *479301 $^{206}Pb/^{238}U$-$^{207}Pb/^{235}U$ concordia diagram and inset $^{207}Pb/^{206}Pb$ age plot.*

479014

Collector: Julie Hollis

Lithology: Medium to coarse grained banded heterogeneous felsic orthogneiss with isoclinal folding of compositional layers and a low abundance of transposed pegmatites.

Location: S of Storø on Nuuk peninsula

Locality: jho2004-136, 64 11.999°N, -51 27.259°W

Aim: age of orthogneiss of unknown affinity – specifically constraint on the location of the tectonic contact between early Archaean rocks of the Itsaq gneiss complex (E) and the Nûk gneiss (W). Note this sample also investigated using LA-SF-ICPMS for comparison.

Age of inherited grain: 2994 ± 16 Ma (n = 1 of 19)

Method: SIMS and LA-SF-ICPMS

Age of inherited grains (LA-SF-ICPMS): 3551 ± 11, 3504 ± 24, 3037 ± 17, and 3036 ± 59 Ma (n = 4 of 21)

Age of emplacement (SIMS): 2698 ± 4 Ma (MSWD 0.5, n = 9 of 19)
Age of metamorphism: c. 2700–2600 Ma (SIMS and LA-SF-ICPMS)

The zircons are typically 80–200 μm in length with aspect ratios 1:2 to 1:3, commonly prismatic. Roughly one third of the grains show a distinct morphology characterised by a large core that is either homogeneous, has broad sector zonation, or has broad diffuse oscillatory zonation, with elongate tips that show distinct, closely spaced bright and dark alternating oscillatory zones. In many cases very dark rims are present, likely indicating very U-rich zones. The morphology of other grains varies from homogeneous to diffuse oscillatory zoned and/or sector zoned to patchy zoned. A few have bright rims possibly indicative of partial recrystallisation.

Nineteen spots in 19 grains were analysed via SIMS. Four grains give very strongly discordant ages and another three give ages that are > 5% discordant. Of these, the most strongly discordant grain is also very high in U (3785 ppm). The main population of 18 analyses give a spread in ages from 2709 ± 14 to 2604 ± 8 Ma with the spread falling outside the uncertainty on individual analyses. However a plateau at 2698 ± 4 Ma (MSWD 0.5, n = 9 of 19) is interpreted as the timing of emplacement. This population has 60–330 ppm U and Th/U 0.43–0.84. Of the 9 younger grains with ages that spread from 2687 ± 5 to 2604 ± 8 Ma, most have higher U and similar Th/U, however 2 analyses of homogeneous rims (2632 ± 8 and 2604 ± 8 Ma) have very low Th/U of 0.02, consistent with a metamorphic origin. A single older grain is 2994 ± 34 Ma with 190 ppm U and Th/U of 0.51.

Thirty spots in 30 grains were analysed via LA-SF-ICPMS. Nine analyses of generally U-rich grains with high common Pb component are strongly discordant and were discarded. The zircons have 46–380 ppm U and Th/U typically 0.22–0.93 (with 1 outlier at 1.50). Most grains are rather strongly discordant. The main group of 13 grains defines a population at 2708 ± 5 Ma (MSWD 1.04), with 2 older grains at 2783 ± 27 and 2721 ± 12 Ma excluded. This compares excellently with the 2698 ± 4 Ma SIMS age. Four older grains are 3551 ± 11 Ma, 3504 ± 24, 3037 ± 17, and 3036 ± 59 Ma. A single strongly discordant bright recrystallised rim is 2659 ± 15 Ma with Th/U 0.28 and may be metamorphic.

This heterogeneous compositionally banded felsic orthogneiss lies just W of the mapped tectonic boundary with rocks belonging to the Itsaq gneiss complex. The age data are consistent with emplacement at 2708 ± 5 Ma (SIMS) with minor mid and early Archaean inheritance. The spread of ages and the presence of metamorphic rims indicates metamorphism in the period c. 2700–2600 Ma.

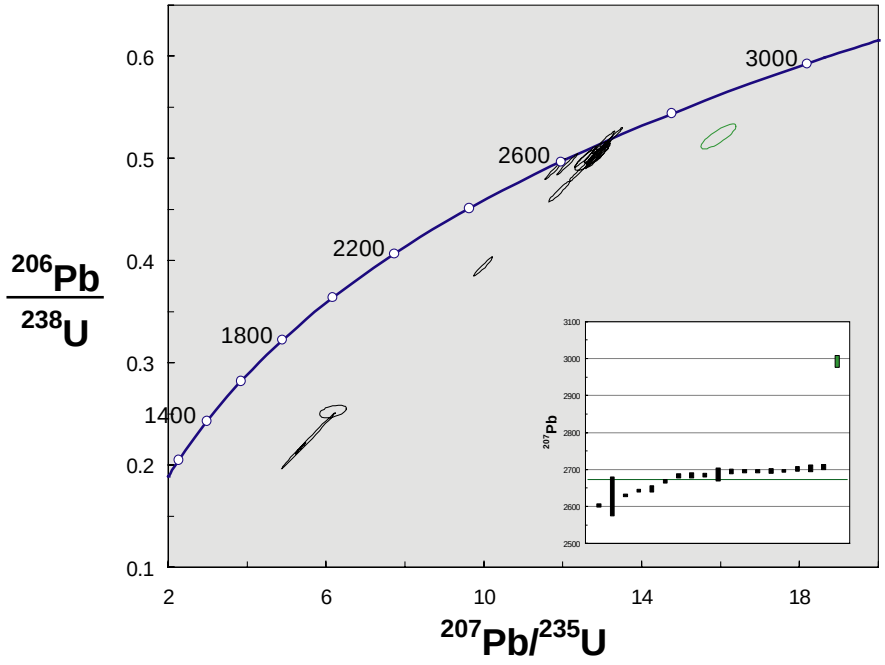

Figure 29. *479014 $^{206}Pb/^{238}U$-$^{207}Pb/^{235}U$ concordia diagram and inset $^{207}Pb/^{206}Pb$ age plot for SIMS data.*

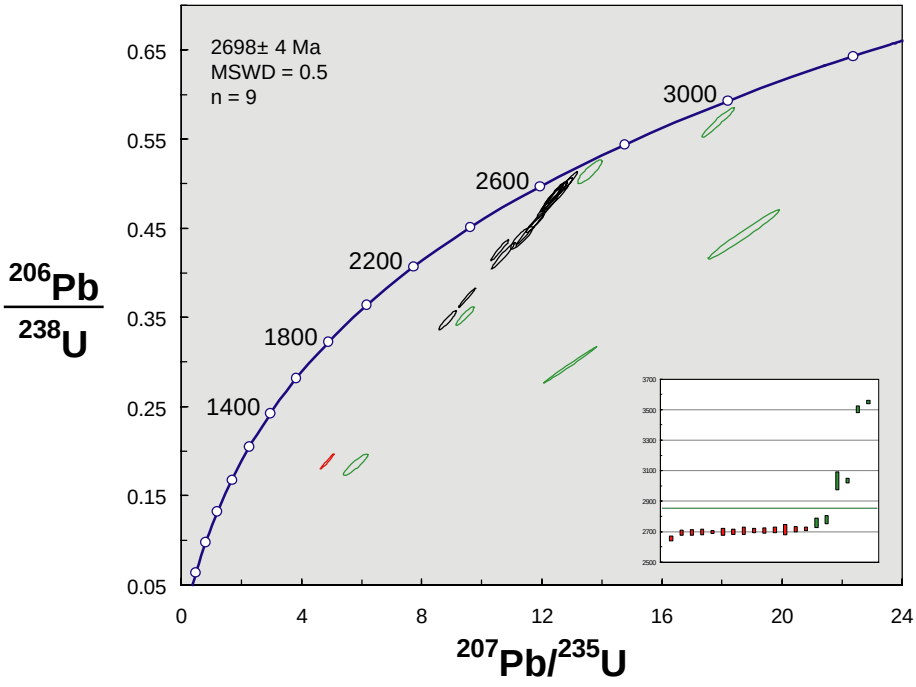

Figure 30. *479014 $^{206}Pb/^{238}U$-$^{207}Pb/^{235}U$ concordia diagram and inset $^{207}Pb/^{206}Pb$ age plot for LA-SF.ICPMS data.*

Late Archaean volcanics - Storø belt

479052
Collector: Julie Hollis
Lithology: Pale garnet-bearing quartzo-feldspathic rock of probable volcanic origin, with refolded, strong S fabric
Location: SE point of Bjørneøen.
Locality: jho2004-212, 64 21.723°N, -51 17.921°W
Aim: age of deposition of inferred volcanic precursor
Method: SIMS
Age: 2834 ± 3 Ma (MSWD = 1.8, n = 10 of 10)

The zircon population is very homogeneous, consisting of small (c. 150 μm), pale, stubby, prismatic to slightly rounded grains with occasional, small BSE-bright inner cores and oscillatory zoning. The small, stubby zircons with oscillatory zoning of presumed magmatic origin are typical of felsic volcanic rocks. The U and Th contents are uniform, ranging between c. 120–420 ppm U and 65–250 ppm Th.

10 grains were analysed and yielded an age of 2834 ± 3 Ma, no data excluded. The age is interpreted as the depositional age of the volcanic precursor to the volcano-sedimentary rock and confirms the previously supposed terrane boundary at the south-east point of Bjørneøen. However, other age data presented in this report suggest this tectonic model is an over-simplification.

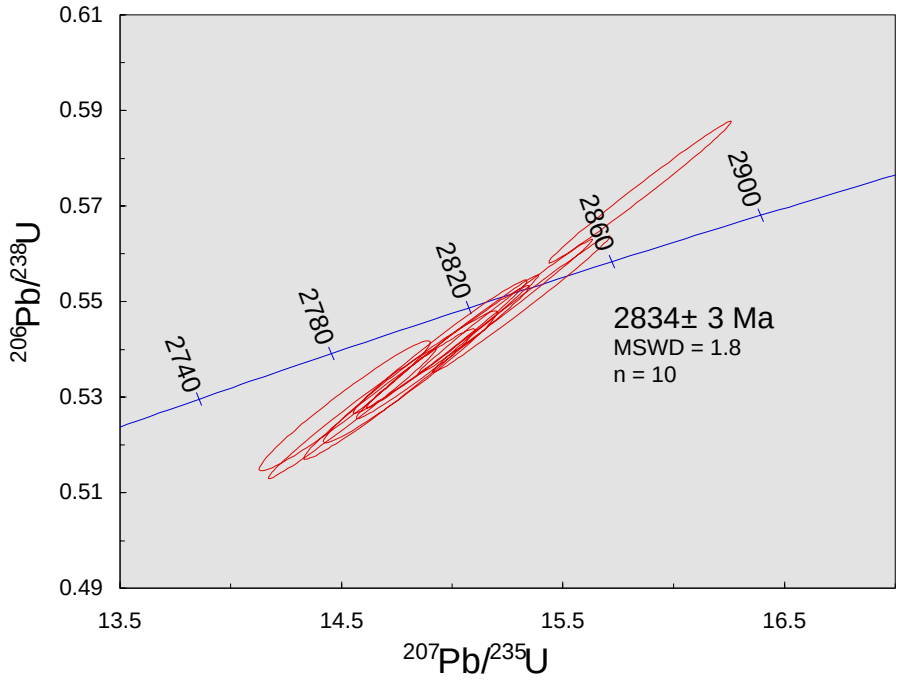

Figure 31. *479052 $^{206}Pb/^{238}U$-$^{207}Pb/^{235}U$ concordia diagram.*

479745
Collector: Dirk Frei
Lithology: Typical heterogeneous, intermediate schist of inferred metavolcanic origin
Location: central Bjørneøen
Locality: df2004-079, 64 26.398°N, -51 17.719°W
Aim: age spectra of detrital zircon populations from supracrustal package and minimum depositional ages of volcanic precursor
Method: SIMS and LA-SF-ICPMS
Age of volcanic precursor (SIMS): 2823 ± 2 Ma (MSWD 1.06, n = 10 of 16)

The zircons are 100–250 μm in length with aspect ratios typically 1:2 to 1:3, and commonly prismatic. The majority have broad oscillatory zones.

Sixteen spots in 16 grains were analysed via SIMS. Fourteen give a spread population from at 2828 ± 6 to 2806 ± 12 Ma with 232–695 ppm U and Th/U 0.23–0.51, aside from one strongly discordant grain (2811 ± 10 Ma), which is U rich (1885 ppm). Ten of these grains define a population at 2823 ± 2 Ma (MSWD 1.06). Two younger grains are also discordant: 2791 ± 10 and 2742 ± 10 Ma. The oldest of these has similar U and Th/U to the main population, while the other is relatively U-rich (1594 ppm) with low Th/U (0.10).

Twenty-four spots in 21 grains were analysed via LA-SF-ICPMS. The data show considerable spread in ages outside the uncertainty on individual analyses. The main population at 2823 ± 5 Ma (MSWD 0.51, n = 11) has 101–353 ppm U and Th/U of 0.15–0.52. An older group ranges from 2908 ± 39 to 2845 ± 15 Ma (n = 11) with 8–330 ppm U and Th/U of 0.14–0.61. The two youngest grains are 2774 ± 10 and 2743 ± 33 Ma with 240 and 105 ppm U and Th/U of 0.03 and 0.18. No distinctions can be made between the different age groups based on zircon morphology.

The sample was collected from an intermediate composition schist of inferred volcanic origin on central Bjørneøen. This lithology forms part of the supracrustal package on central Bjørneøen. The main population at 2823 ± 2 Ma given by the SIMS analyses compares excellently with the 2823 ± 5 Ma LA-SF-ICPMS age. This is interpreted as zircon derived from the volcanic precursor and gives an age of deposition. The older age range (LA-SF-ICPMS) is consistent with the detrital age spectra of metasedimentary rocks from the structural base of the supracrustal sequence on Sermitsiaq and from metasedimentary rocks from Storø and the Nuuk peninsula, suggesting some contribution from these same sources. The absence of these older ages in the SIMS data may be a product of sampling bias, i.e. the larger grains, which are generally older, were selected for the first analysis session on LA-SF-ICPMS, whereas smaller grains were left for later SIMS analysis. Of the younger grains, low Th/U suggests a metamorphic origin. However, these are discordant and so their significance is difficult to establish.

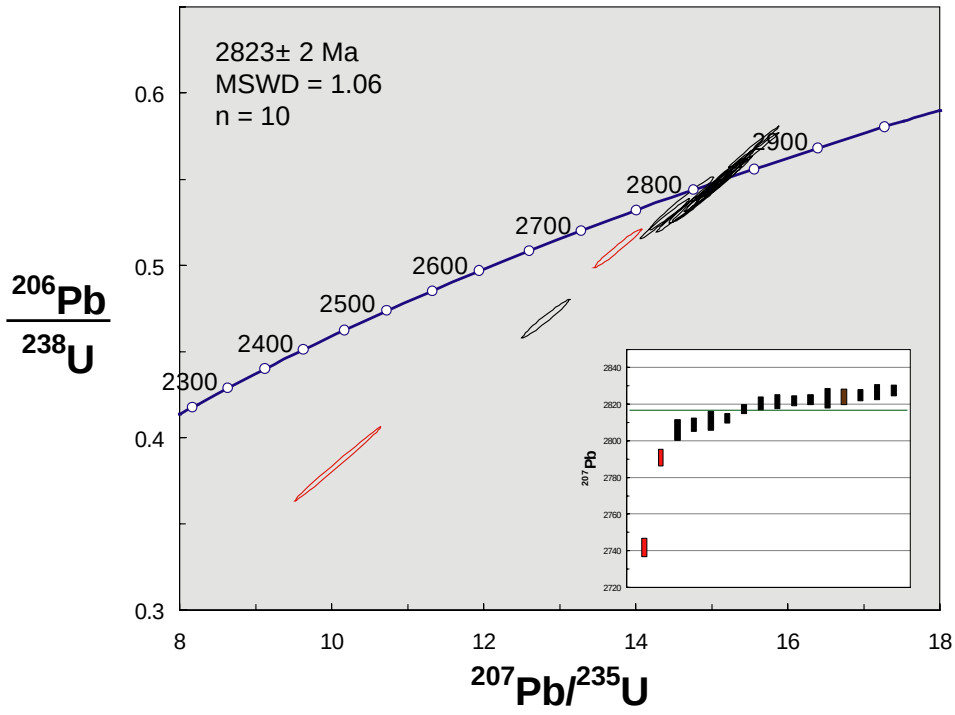

Figure 32. *479745 $^{206}Pb/^{238}U$-$^{207}Pb/^{235}U$ concordia diagram and inset $^{207}Pb/^{206}Pb$ age.*

Late Archaean metasedimentary rocks - Storø belt

481465
Collector: Julie Hollis
Lithology: Medium to coarse grained garnet-biotite-sillimanite-cordierite-quartz gneiss with foliation parallel cordierite-bearing felsic layers
Location: central Storø
Locality: jho2004-112, 64 23.672°N, -51 07.557°W
Aim: age of metamorphism
Method: SIMS and LA-SF-ICPMS
Age of detrital population (LA-SF-ICPMS): c. 2935–2785 Ma (n = 49 of 59) with minor older inheritance at 3083 ± 19, 2987 ± 18, and 2970 ± 27 Ma
Age of metamorphism (SIMS): c. 2700–2630 (n = 10 of 12)

The zircons are typically 150–300 μm in length with aspect ratios of 1:2 to 1:3 and commonly rounded. The majority show oscillatory zonation and often have thin (up to 50 μm) BSE bright homogeneous rims. A few grains are BSE bright and completely homogeneous. The oscillatory zoned cores (detrital in origin) were targeted with LA-SF-ICPMS work.

Twelve spots in 12 grains were analysed via SIMS, targeting bright rims and homogeneous grains. Of the two oldest analyses (2878 ± 4 and 2781 ± 5 Ma), the oldest has the highest

Th/U (0.41) and is strongly discordant. The youngest also has a relatively high Th/U of 0.09 and may be a mixed core-rim age. The remaining 10 analyses of homogeneous grains and rims give a spectrum of ages between 2699 ± 4 and 2631 ± 8 Ma. A mean age of these analyses is considered to be meaningless as the spread in ages is significantly larger than the error on individual analyses. All 10 have moderate to high U concentrations of 504–1198 ppm and very low Th/U of 0.002–0.005, consistent with a growth and/or recrystallisation during metamorphism.

Fifty-nine spots in 58 grains were analysed via LA-SF-ICPMS targeting cores. Fifty-two analyses of oscillatory zoned cores range in age from 3083 ± 19 to 2785 ± 34 Ma with the vast majority falling between 2940 and 2800 Ma. These have 15–269 ppm U and Th/U of 0.12–0.86. The remaining 7 younger analyses of BSE bright homogeneous grains and rims (plus 1 darker core) fall between 2706 ± 35 and 2607 ± 30 Ma with 178–716 ppm U and Th/U of 0.01–0.04.

The sample was collected from an amphibolite facies garnet-sillimanite-cordierite gneiss from within the supracrustal sequence on central Storø, within the Storø shear zone. The lithology has a strong shear zone fabric at this locality. The 52 LA-SF-ICPMS analyses of oscillatory zoned cores ranging from 3083 ± 19 to 2785 ± 34 Ma are interpreted as detrital in origin, giving a maximum depositional age of c. 2785 Ma. The 10 youngest SIMS ages and 7 youngest LA-SF-ICPMS analyses of homogeneous grains and bright rims – all with very low Th/U – are interpreted as metamorphic. The spread in ages from c. 2700–2600 Ma may be indicative of prolonged or episodic thermal activity over this period.

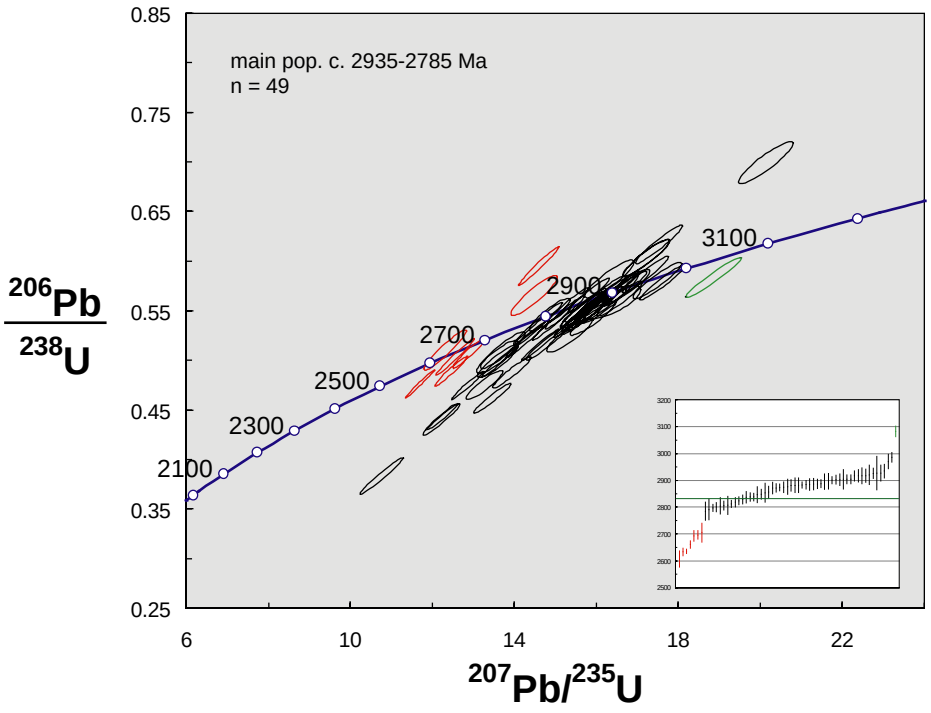

Figure 33. *481465 $^{206}Pb/^{238}U$-$^{207}Pb/^{235}U$ concordia diagram and inset $^{207}Pb/^{206}Pb$ age for LA-SF-ICPMS data.*

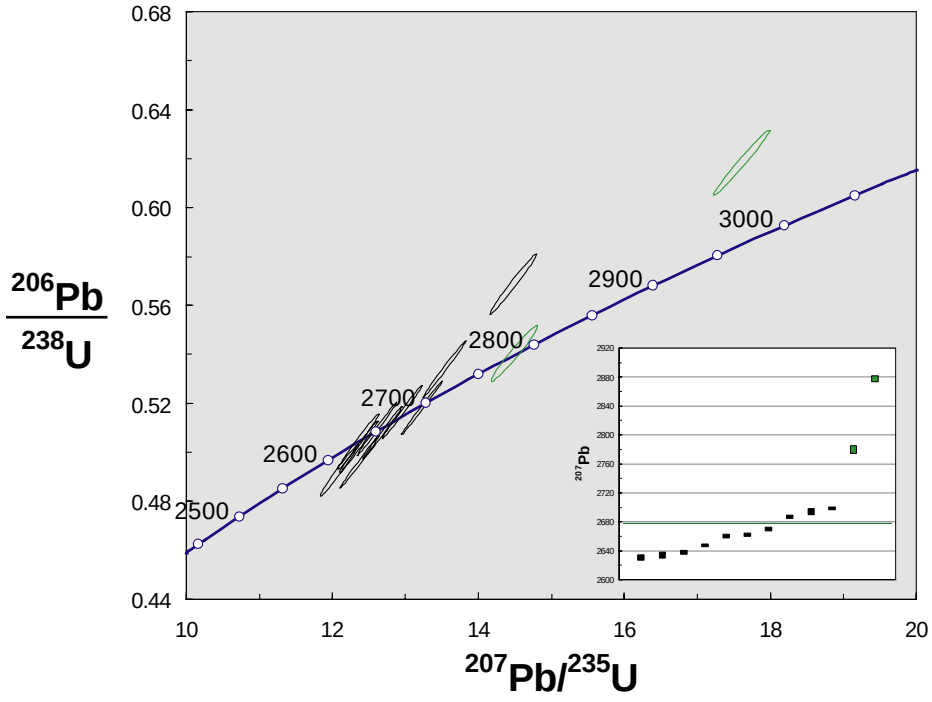

Figure 34. *481465 $^{206}Pb/^{238}U$-$^{207}Pb/^{235}U$ concordia diagram and inset $^{207}Pb/^{206}Pb$ age for SIMS data.*

479008
Collector: Julie Hollis
Lithology: Rusty weathered garnet-sillimanite-biotite-quartz gneiss from thin metasedimentary package at structural top of a thick amphibolite sequence
Location: Nuuk peninsula S of Storø
Locality: jho2004-149, 64 12.33°N, -51 25.148°W
Aim: age spectra of detrital zircon populations from paragneiss at the structural top of the supracrustal package and minimum depositional ages of sedimentary precursor
Method: LA-SF-ICPMS
Age of old detrital grains: 3622 ± 25, 3619 ± 20, and 3253 ± 14 Ma (n = 3 of 27)
Age of main detrital population: c. 2920 to 2820 Ma (n = 23 of 27) with main population at 2892 ± 5 Ma (MSWD 0.74, n = 16 of 27)

The zircons are 150–350 μm in length with aspect ratios 1:1 to 1:3 (typically 1:2), and commonly rounded. The majority show clear oscillatory zonation, though a few are sector zoned. Very few have thin BSE bright rims inferred to be metamorphic.

Twenty-nine spots in 29 grains were analysed. Two analyses of grains with high common Pb were strongly discordant and were discarded. The data fall into three age groups that are not morphologically distinct. The largest group of 24 analyses defines a population spread from 2919 ± 26 to 2801 ± 36 Ma typically with 25–100 ppm U and Th/U of 0.3–1.4. The spread in ages falls outside the error on individual analyses in the range c. 2880–2800 Ma, though a plateau in ages occurs at 2892 ± 5 Ma (MSWD 0.74, n = 16). Three older grains are 3622 ± 25, 3619 ± 20, and 3253 ± 14 Ma. These have similar U concentrations and Th/U to the main population. One younger grain is 2710 ± 13 Ma, with 228 ppm U and a very low Th/U of 0.02, and is probably metamorphic.

The sample was collected from a thin garnet-sillimanite-cordierite-bearing metasedimentary gniess with foliation-parallel felsic layers interpreted as melt formed during upper amphibolite facies metamorphism. This lithology forms the structural top to a thick amphibolite on the Nuuk peninsula. All but the youngest analysis are interpreted as detrital zircon ages (the youngest being metamorphic). The spread of ages from 2919 ± 26 to 2801 ± 36 Ma forms the main detrital population and a plateau of ages at 2892 ± 5 Ma is consistent with a distinct source of this age. This is consistent with derivation from sources such as the late Archaean tonalitic orthogneiss from central west Storø – sample 479040. Three older grains are 3622 ± 25, 3619 ± 20, and 3253 ± 14 Ma indicate small but significant early and mid Archaean sources.

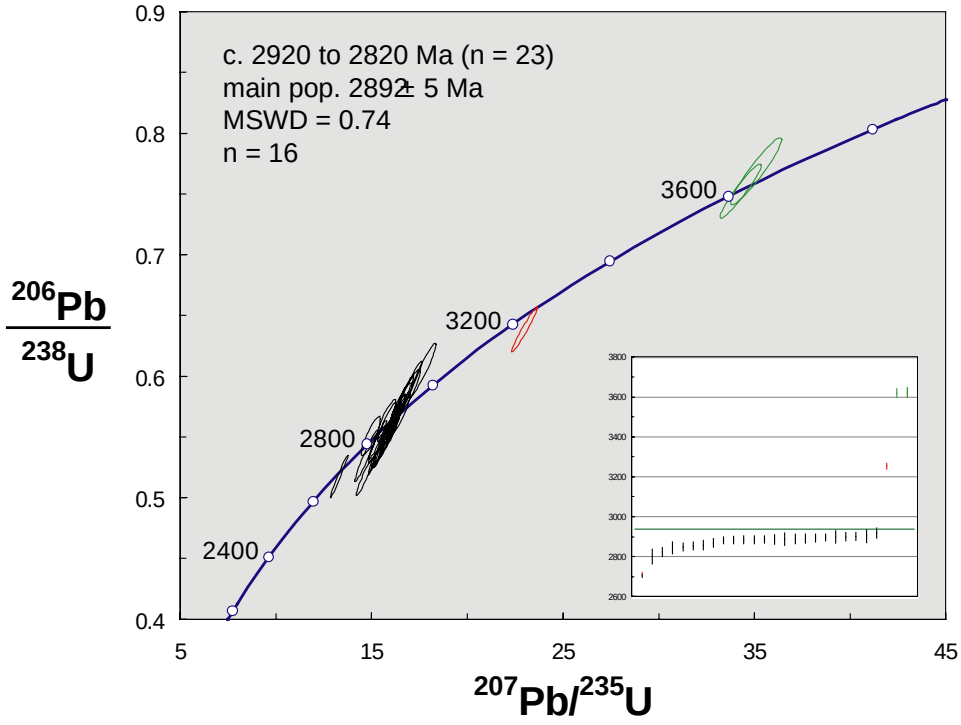

Figure 35. *479008 $^{206}Pb/^{238}U$-$^{207}Pb/^{235}U$ concordia diagram and inset $^{207}Pb/^{206}Pb$ age.*

479326
Collector: Mikkel Vognsen
Lithology: Quartz-rich laminated biotite-bearing metasedimentary rock
Location: SE Sermitsiaq
Locality: mvo2004-016, 64 16.251°N, -51 25.772°W
Aim: age spectra of detrital zircon populations from paragneiss at the structural base of the supracrustal package and minimum depositional ages of sedimentary precursor
Method: LA-SF-ICPMS
Age of main detrital population: 2894–2844 Ma (n = 28 of 30)
Minimum age of deposition: 2844 ± 31 Ma (youngest zircon)

The zircons are typically 300–400μm in length with aspect ratios 1:1 to 1:3. They are commonly rounded, though many also retain a more prismatic shape. All show the same well-defined and simple closely-spaced oscillatory zonation. Only a very few have thin bright BSE overgrowths (< 30 μm).

Thirty spots in 30 grains were analysed. No obvious morphological differences were noted between grains with different ages. The zircons typically have only 10–30 ppm U and Th/U typically 0.2–0.8. The vast majority of grains (26) fall in the age range 2894–2844 Ma with a weighted mean age of 2879 ± 4 Ma (MSWD 1.07). Two older grains give are 2926 ± 42 and 2940 ± 21 Ma and two younger grains are 2747 ± 26 and 2606 ± 38 Ma. The youngest 2 have relatively low Th/U of 0.19 and 0.08 and may be metamorphic in origin.

This quartz-rich metasedimentary rock was collected from close to the structural base of the supracrustal package on Sermitsiaq. The rounded grains suggest a detrital origin and the tightly clustered main population and consistently low U contents are consistent with derivation from a single source. The 2 youngest grains at 2747 ± 26 Ma and 2606 ± 38 Ma grain may be metamorphic in origin. A conservative estimate of the minimum age of deposition of the sedimentary precursor to this rock is c. 2844 Ma (the youngest detrital grain). This is consistent with derivation from sources such as the late Archaean tonalitic orthogneiss from central west Storø – sample 479040.

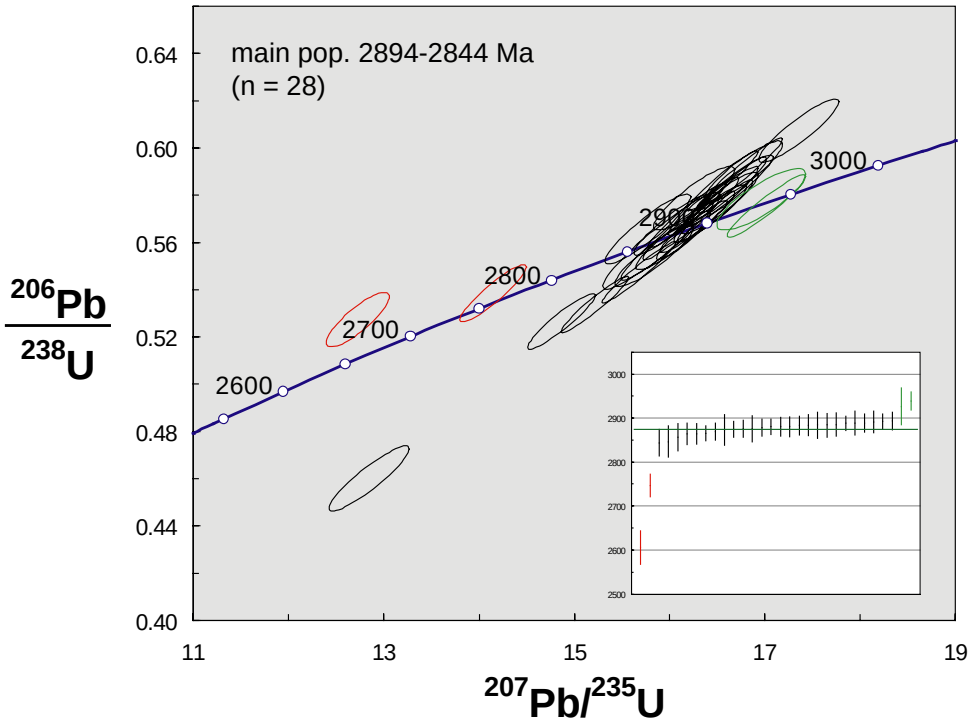

Figure 36. *479326 $^{206}Pb/^{238}U$-$^{207}Pb/^{235}U$ concordia diagram and inset $^{207}Pb/^{206}Pb$ age.*

Late Archaean thermal event: metamorphic zircon and pegmatites

481217
Collector: Jeroen van Gool
Lithology: coarse-grained pegmatite, deformed within the Storø shear zone fabric and concordant with foliation. Intruded prior to or during deformation.
Location: central W Storø
Locality: jvg2004-021A, 64 23.390°N, -51 10.197°W
Aim: age spectra of emplacement of pegmatite and thus maximum age of deformation in the Storø shear zone
Method: LA-SF-ICPMS
Age of emplacement/ max. age of Storø shear zone: c.2745 Ma (n = 13 of 20)

The zircons are 200–500 μm in length with aspect ratios typically 1:3 to 1:4, and commonly prismatic. Most grains are strongly metamict either throughout or in restricted zones – usually in the cores – and are commonly very BSE bright, consistent with high U concentrations. Some grains show relict oscillatory zonation.

Thirty spots in 30 grains were analysed. Ten analyses with high common Pb and which showed significant discordance were discarded. Thirteen grains define a rough population with considerable spread at c. 2745 Ma. These have 314–707 ppm U and Th/U of 0.03–0.06. Five older grains range in age from 2856 ± 13 to 2779 ± 17 Ma with 467–2295 ppm U and Th/U of 0.04–0.05. The 2 youngest grains are 2690 ± 12 and 2684 ± 8 Ma with 2613 and 1750 ppm U and Th/U of 0.04 and 0.05 respectively. There is no distinction between these age groups that can be made on the basis of zircon morphology.

The sample was collected from a coarse-grained pegmatite that is deformed within the Storø shear zone fabric and which is concordant within the shear foliation. The emplacement of this pegmatite is inferred to have occurred prior to or during development of the shear zone. The main population falls between 2760 ± 5 and 2736 ± 8 Ma. This is interpreted as the approximate timing of emplacement but gives only a poorly defined age of c. 2745 Ma (n = 13). The 5 older grains at 2856 ± 13 to 2779 ± 17 Ma are probably inherited. The 2 younger ages at 2690 ± 12 and 2684 ± 8 Ma likely relate to a later thermal event, possibly development of the shear zone.

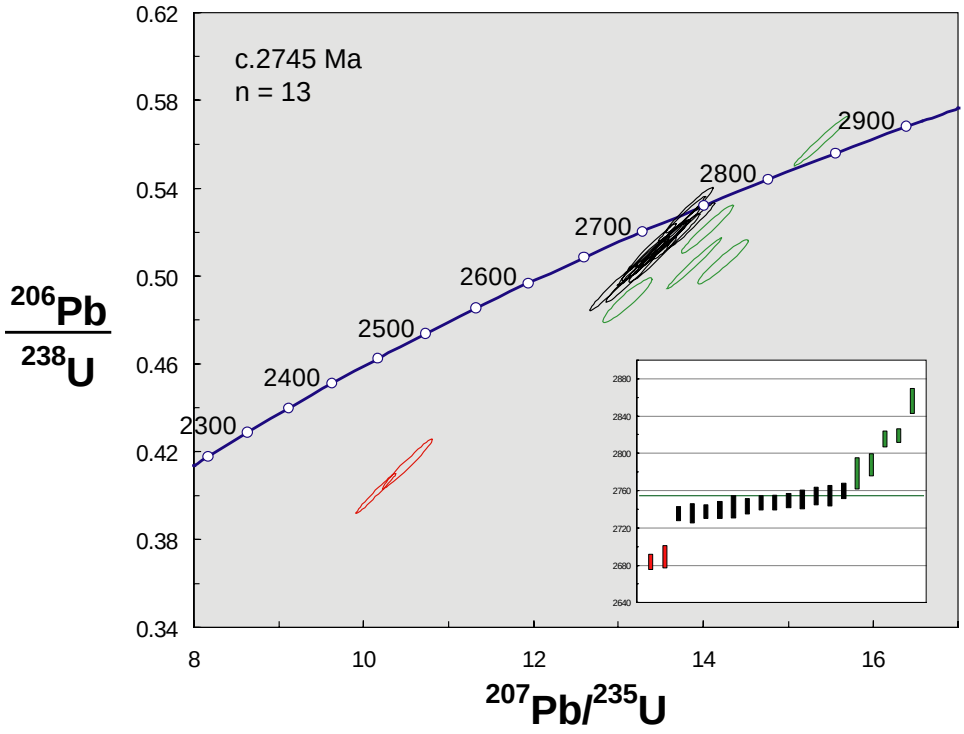

Figure 37. *481217 $^{206}Pb/^{238}U$-$^{207}Pb/^{235}U$ concordia diagram and inset $^{207}Pb/^{206}Pb$ age.*

479010
Collector: Julie Hollis
Lithology: Cordierite-bearing melt fraction in metasedimentary rock
Location: Mainland NE of Nuuk
Locality: jho2004-149, 64 12.33°N, -51 25.148°W
Aim: age of melt generation and thus amphibolite facies metamorphism of host gneiss.
Method: SIMS
Age: 2701 ± 3 Ma (MSWD = 2.1, n = 11 of 12)

Large (>500 μm), stubby, subhedral to euhedral, dark brown zircons, which commonly have distinct, dark brown outer rims about 10–20 μm wide surrounding equant or rounded cores of possible detrital origin. Concentric zoning is visible on BSE images of many grains. Other grains appear to be homogeneous on BSE images or display sector zoning. Many grains possess finely pitted internal growth zones (pointing to high U contents), where analysis was not attempted. The U and Th contents are mostly around 500 and 25 ppm, respectively. Two grains have higher U contents, c. 800–1700 ppm.

Twelve spots in 11 grains were analysed. The data are concordant, and no age difference between concentric zoned, homogeneous (?recrystallised), or partly recrystallised sites of analysis was detected, except in spot 10, a rim analysis which yields a slightly younger age (2678 ± 8 Ma) than the rest. The weighted mean $^{207}Pb/^{206}Pb$ age is 2701 ± 3 Ma, omitting

spot 10. The latter may represent early lead loss or an episode of overgrowth not observed in the rim of spot 11.

The zircon geochronology of this neosome in an amphibolite facies metasedimentary rock points to a regional thermal event at around the time of terrane assembly. The uniformity of the ages obtained, compared to the concentric zoning and dark rims observed in several of the analysed grains, suggests that the zircons are not detrital but were formed during thermal activity close to 2700 Ma.

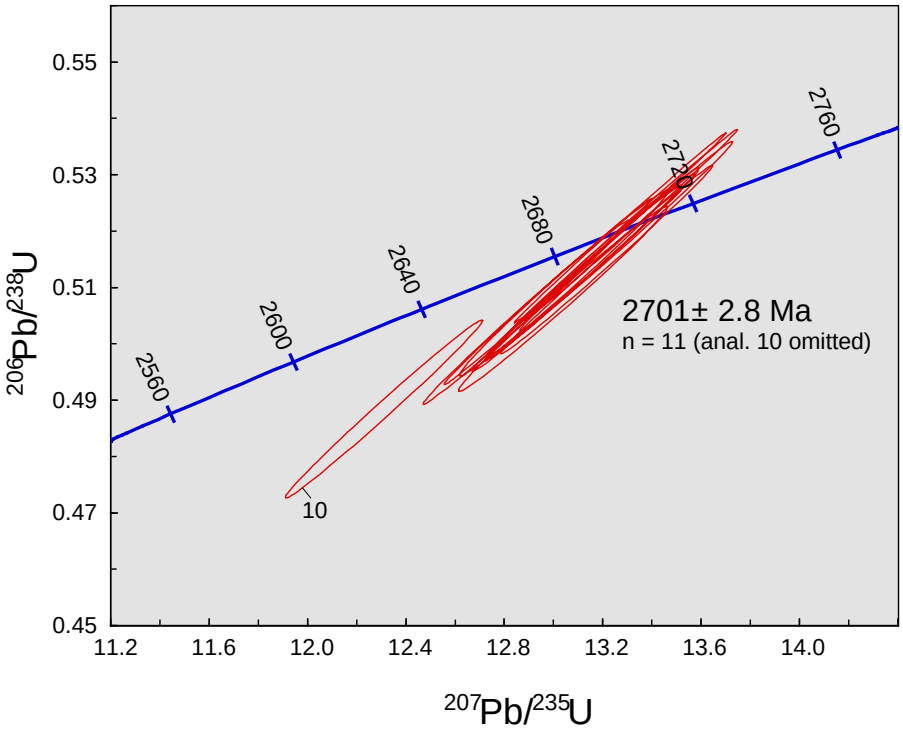

Figure 38. *479010 $^{206}Pb/^{238}U$-$^{207}Pb/^{235}U$ concordia diagram and inset $^{207}Pb/^{206}Pb$ age.*

481461
Collector: Julie Hollis
Lithology: Very coarse-grained cordierite-bearing discontinuous felsic layers, discordant to foliation but also deformed.
Location: central Storø
Locality: jho2004-110, 64 26.476°N, -51 02.763°W
Aim: age of metamorphism
Method: SIMS
Age of crystallisation and metamorphism: 2633 ± 2 Ma (MSWD 0.5, n = 7 of 14)

The zircons are 150–300 μm in length with aspect ratios typically 1:3, commonly prismatic. The majority have dark oscillatory zoned or homogeneous cores with broad BSE bright homogeneous rims (up to 100μm). A few grains are BSE bright and completely homogeneous. Bright rims and homogeneous grains were targeted in the SIMS work. This sample was investigated via SIMS and LA-SF-ICPMS for comparison.

Fourteen spots in 14 grains were analysed. The oldest age has the highest Th/U (0.19) and a large associated uncertainty – 2688 ± 48 Ma. The remaining 13 analyses of homogeneous rims and grains give a spread of ages from 2635 ± 4 to 2613 ± 4 Ma with fairly high U of 631–1281 ppm and very low and consistent Th/U of 0.003 to 0.004, consistent with a metamorphic origin. Six of these define a population at 2633 ± 2 Ma (MSWD 0.5).

The sample was collected from cordierite-bearing felsic layers from within a garnet-sillimanite-cordierite-quartz gniess from central Storø. These felsic layers are interpreted as melt formed during upper amphibolite facies metamorphism of the Storø supracrustal belt. This locality is structurally just above the Storø shear zone and the lithology here does not hold the shear zone fabric, unlike outcrops of the same lithology further west (e.g. sample 481465 above). The oldest analysis (2688 ± 48 Ma), which is significantly older than the main group, may reflect a real age of thermal activity or a mixed core-rim age. A population of homogeneous rims and grains at 2633 ± 2 Ma (n = 6) is interpreted as the timing of crystallisation of the melt and thus upper amphibolite facies metamorphism of this lithology.

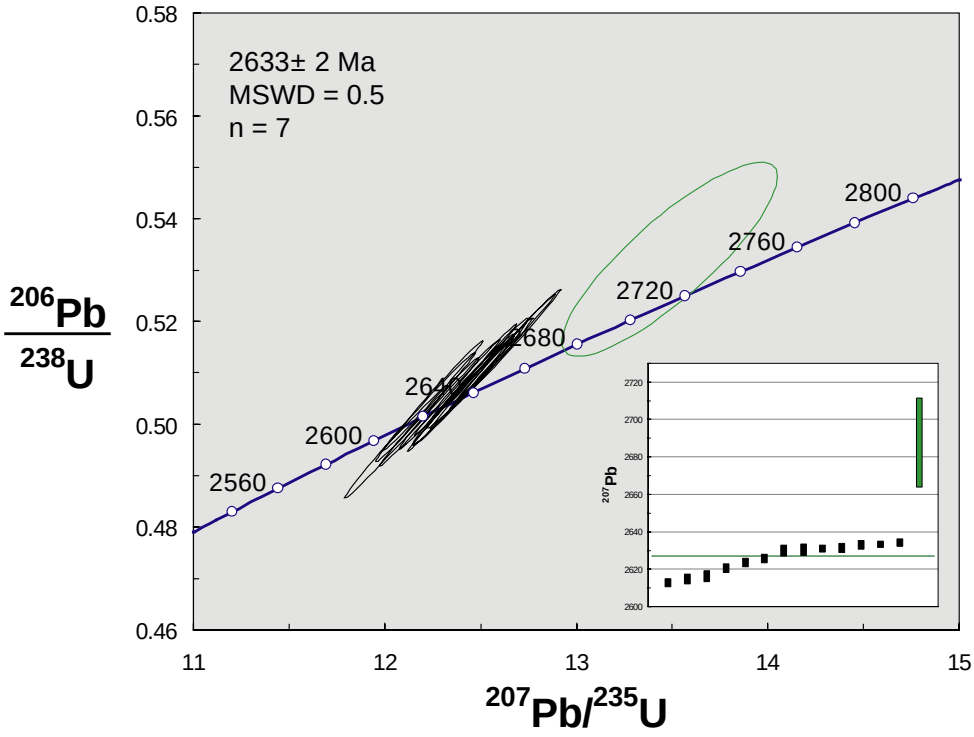

Figure 39. *481461 $^{206}Pb/^{238}U$-$^{207}Pb/^{235}U$ concordia diagram and inset $^{207}Pb/^{206}Pb$ age.*

465048
Collector: Mac Persson
Lithology: Coarse-grained, highly deformed pegmatite parallel to the main foliation in the Storø shear zone
Location: central Storø.
Locality: mpe2004-126, 64 25.158°N, -51 05.142°W
Aim: emplacement age of pegmatite giving max. age of deformation in the Storø shear zone
Method: SIMS
Age: 2632 ± 2 Ma (MSWD = 22, n = 24 of 32)

The zircons are about 150–400 μm long, slender prismatic and pale. They commonly have roundish, corroded cores that are relatively bright on BSE images, surrounded by large, commonly weakly oscillatory zoned bodies and up to c. 50 μm long terminations, likewise commonly with weak oscillatory zoning. The U and Th contents are high to very high, 2000–12000 and 60–12000 ppm, respectively.

Thirty-two spots in 27 grains were analysed in 2 sessions. Omitting seven spots with lower ages due to likely early lead loss and one older age, the remaining 24 spots yield an age of 2632 ± 2 Ma (MSWD = 22). The very high MSWD value is probably due to the high U contents (1921–11880 ppm), which result in good counting statistics combined with likely disturbance and lead loss after the zircons crystallised – 16 analyses show > 5% discordance. There are no systematic age differences between the inner cores, main bodies or terminations of the zircons. It therefore seems that all parts of the zircons were formed (or the inner cores recrystallised) together with the pegmatite.

The sample was collected from a strongly deformed granitic pegmatite parallel to foliation in the Storø shear zone. The poorly defined 2632 ± 2 Ma age is interpreted as the age of emplacement of the pegmatite. Accordingly, the high-strain zone through central Storø must have been active at or after c. 2630 Ma.

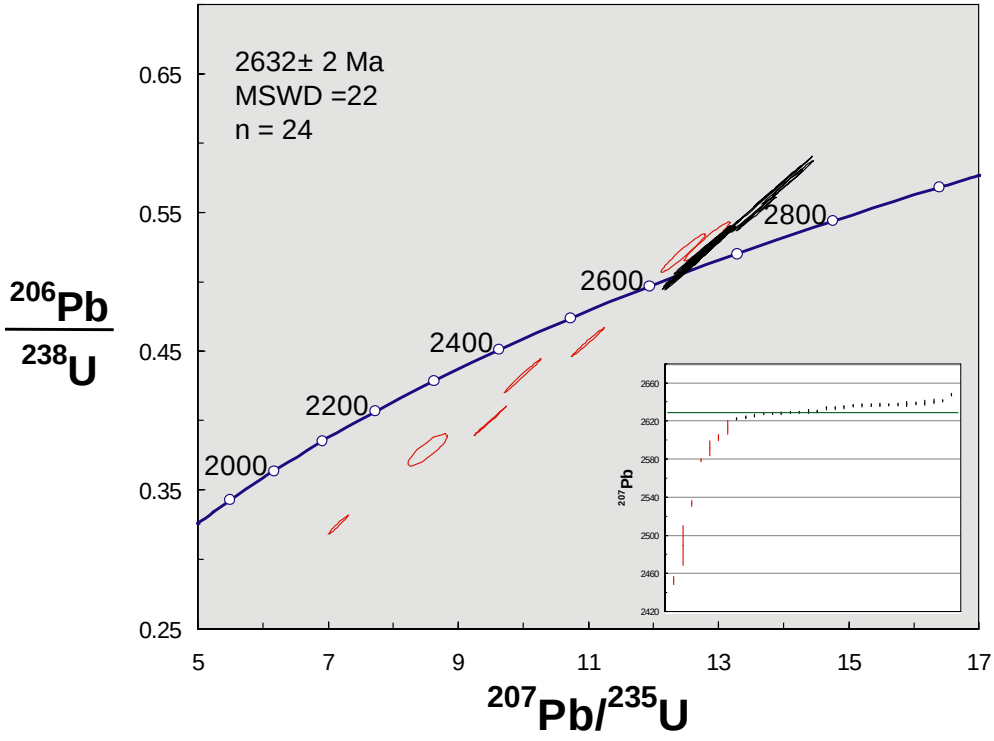

Figure 40. *465048 $^{206}Pb/^{238}U$-$^{207}Pb/^{235}U$ concordia diagram and inset $^{207}Pb/^{206}Pb$ age.*

465054
Collector: Mac Persson
Lithology: Deformed pegmatite with cross cutting relations to host supracrustal amphibolite deformed within Storø shear zone
Locality: mpe2004-129, 64 24.758°N, -51 05.086°W
Aim: emplacement age of pegmatite, minimum age of amphibolite and maximum age Storø shear zone
Method: SIMS
Age of emplacement: 2630 ± 5 Ma (MSWD 7.6, n = 5 of 14)

The zircons are 250–500 μm in length with aspect ratios typically 1:3 to 1:5, and commonly prismatic. The majority are very BSE bright and metamict, indicative of high U contents, typical of pegmatitic zircon. In a few grains relict oscillatory zonation is still discernible.

Fourteen spots in 14 grains were analysed. Six analyses are strongly discordant, 2 being reverse discordant. All are very high in U (2150–9489 ppm) and all have quite low Th/U (0.04–0.08 with one outlier at 0.38). Five grains form a rough population spread at 2630 ± 5 Ma (MSWD 7.6). The spread falls outside the uncertainty on individual analyses. Two younger grains (2490 ± 6 and 2435 ± 22 Ma) are discordant and may or may not reflect the timing of geologically meaningful events. Two older grains (2776 ± 2 and 2685 ± 14 Ma) are strongly reverse discordant and are probably not geologically meaningful.

The sample was collected from a deformed granitic pegmatite cross-cutting foliation in an amphibolite from within the supracrustal sequence on central Storø, within the Storø shear zone. The spread population at 2630 ± 5 Ma is interpreted as the timing of emplacement of the pegmatite. Thus the amphibolite is necessarily older and the Storø shear zone was formed during or after this period.

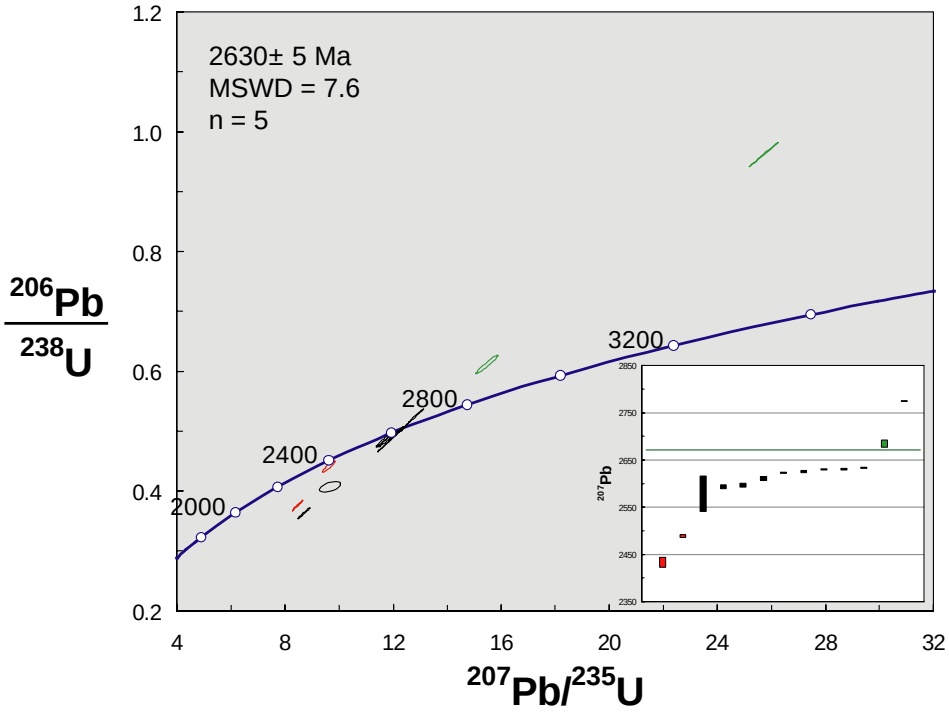

Figure 41. *465054 $^{206}Pb/^{238}U$-$^{207}Pb/^{235}U$ concordia diagram and inset $^{207}Pb/^{206}Pb$ age.*

465049
Collector: Mac Persson
Lithology: Coarse-grained pegmatite with discordant relationship to its host amphibolite
Location: central Storø, from the Storø shear zone.
Locality: mpe2004-127, 64 25.055°N, -51 05.029°W
Aim: emplacement age of pegmatite giving max. age of deformation in the Storø shear zone
Method: SIMS
Age: c. 2630 Ma? (n = 9 of 9)

The zircons are mostly slender prismatic with shape ratios commonly more than 4:1, and pale. They are mostly strongly cracked, have relict oscillatory zoning visible on BSE images, and display patchy recrystallisation in places. Their U contents range between c. 2000–16000 ppm; Th is c. 40–740 ppm.

Nine partially metamict grains were analysed in this sample. Due to their very high U contents they yield strongly reversely discordant ages, which range between 2568–2732 Ma. In

the concordia diagram they form a long, reversely discordant linear array. Excluding the oldest grain (7), the mean age for eight grains is 2630 ± 29 Ma, with an extremely high MSWD value (1293). This age, although not well defined, is close to the age of 2631 Ma obtained from better preserved zircons in sample 465048, likewise from a pegmatite on central Storø.

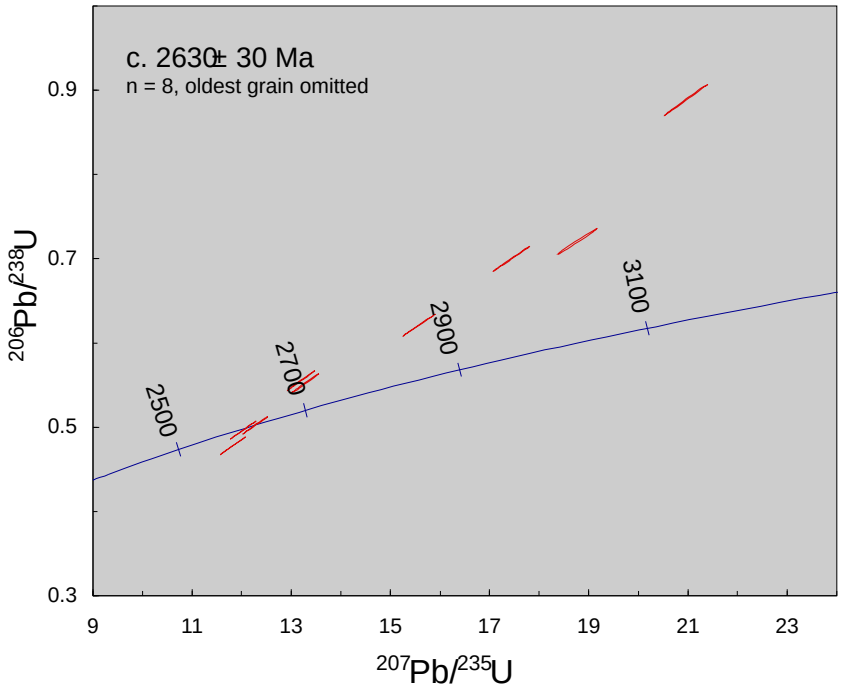

Figure 42. *465049 $^{206}Pb/^{238}U$-$^{207}Pb/^{235}U$ concordia diagram and inset $^{207}Pb/^{206}Pb$ age.*

461526
Collector: Jeroen van Gool
Lithology: light-grey homogeneous amphibolite, locally with L fabric, which forms an integral part of the amphibolite sequence
Location: central Storø
Locality: jvg2004-254, 64 25.543°N, -51 00.749°W
Aim: age of inferred volcanic precursor
Method: LA-SF-ICPMS
Age of volcanic precursor: unknown – no record in the zircon population
Age of metamorphism: at 2624 ± 3 (MSWD 0.82, n = 20 of 22)

The zircons are 100–250 μm with aspect ratios typically 1:1 and irregular to rounded. All grains show broad sector and patchy zonation, indicative of a metamorphic origin. No relict cores were observed.

Twenty-two spots in 22 grains were analysed. The data define a population at 2624 ± 3 (MSWD 0.82, n = 20) with significant normal discordance. The zircons have 45–198 ppm U with very low Th/U of 0.01–0.05. A single older grain at 2703 ± 23 Ma is the most discordant grain and has the highest U concentration (335 ppm). Thus, this is not regarded as a reliable age.

The sample was collected from a light-grey homogeneous amphibolite that forms an integral part of the base of the supracrustal sequence on central Storø and is inferred to be volcanic in origin. The 2624 ± 3 Ma population is interpreted as a metamorphic age, based on the morphology of the zircons, the very low Th/U contents and the age itself, which is coincident with abundant pegmatite emplacement at this time.

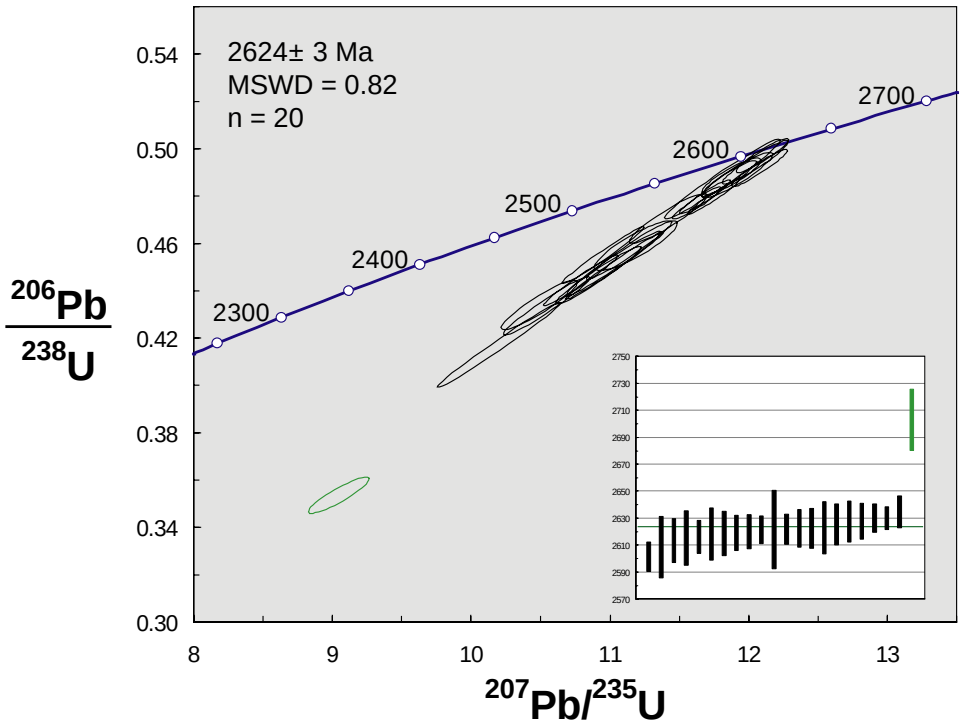

Figure 43. *461526 $^{206}Pb/^{238}U$-$^{207}Pb/^{235}U$ concordia diagram and inset $^{207}Pb/^{206}Pb$ age.*

481293
Collector: Jeroen van Gool
Lithology: Pegmatite truncating high-grade deformation in amphibolite and itself deformed
Location: central Storø.
Locality: jvg2004-164D, 64 25.391°N, -51 00.287°W
Aim: maximum age of the youngest phase of deformation.
Method: SIMS
Age around 2570 Ma? (2568 ± 2.2 Ma, MSWD = 0.92, n = 7 of 16) or around 2615 Ma? (2617 ± 4 Ma, n = 3 of 16)

Most zircons are euhedral and stubby, with 3:1 to 4:1 length/width ratios, and better preserved than in sample 481246. U and Th contents range between c. 250–4400 and 15–420 ppm, respectively. BSE images show broad concentric zoning and bright, variably metamict rims up to c. 30 microns wide. These have higher U contents than most of the cores and probably represent a distinct geological event. Homogeneous areas of apparent replacement with irregular boundaries towards older and zoned areas occur in a few grains, e.g. at spot 11.

16 spots were analysed in 9 different grains. Spot 3 in a core at 2923 ± 17 Ma (2s) is clearly inherited. Three cores (spots 7, 10 and 13) yield ages around 2617 ± 4 Ma and may either be inherited or represent the emplacement age of the pegmatite. Several other cores as well as some high-U rims yield an age of 2568 ± 2.2 Ma (n = 7), which may alternatively

be the emplacement age or reflect a subsequent thermal episode. Other high-U rims yield scattered ages below 2500 Ma, interpreted as due to early lead loss.

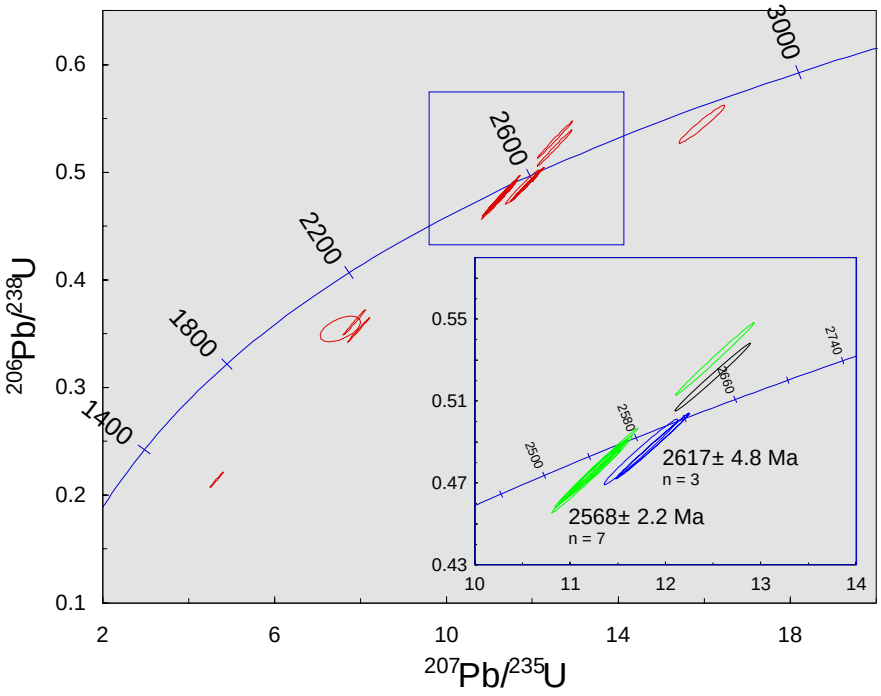

Figure 44. *481293 $^{206}Pb/^{238}U$-$^{207}Pb/^{235}U$ concordia diagram.*

481246
Collector: Jeroen van Gool
Lithology: Coarse-grained pegmatite, central Storø.
Location: Triangular zone at Qingaq, central Storø, beneath which 3 mineralised zones are inferred to meet.
Locality: jvg2004-056, 64 24.478°N, -51 05.616°W
Aim: emplacement age of pegmatite giving max. age of deformation in the Storø shear zone
Method: SIMS
Age c. 2525 Ma? (n = 11 of 11)

The zircons are up to c. 500 μm long and heavily metamict, and crystal fragments are common. Also many monazites are present in the heavy mineral fraction. Zoning is only rarely observed on BSE images, maybe due to the pitted, heavily metamict status of most grains.

Eleven spots in seven crystals were analysed. The spots for analysis were selected in rare, least metamict areas, which were only found in a handful of grains, and several analyses were performed as pairs next to each other in the same grain. The uranium content of the zircons reaches 25500 ppm, and the analytical data from these high-U grains are awfully reversely discordant due to improper correction of element fractionation. Besides, the very high measured precision of the individual $^{207}Pb/^{206}Pb$ ratios is not geologically meaningful in view of the poor condition of the zircons.

It is difficult to estimate the real age of the pegmatite. The highest ages, 2778 and 2590 Ma, were obtained from spots 7 and 8 in a relatively un-metamict grain, with respectively c. 4000 and 20 000 ppm U. Other high-U grains (17000–25500 ppm U) yield apparent ages of 2430–2260 Ma. However, based on the morphology, disturbed internal structure of the zircons, and inconsistent twin analyses, these are likely variably affected by early lead loss and hence unreliable.

An age of 2524 ± 11 Ma (MSWD = 3.1) was calculated from spots 5, 6, and 9 in two not so U-rich crystals (c. 1800–3750 ppm). This might represent an approximation to the real age, suggesting that the pegmatite is part of the Qôrqut granite complex. It is also possible that the pegmatite is somewhat older.

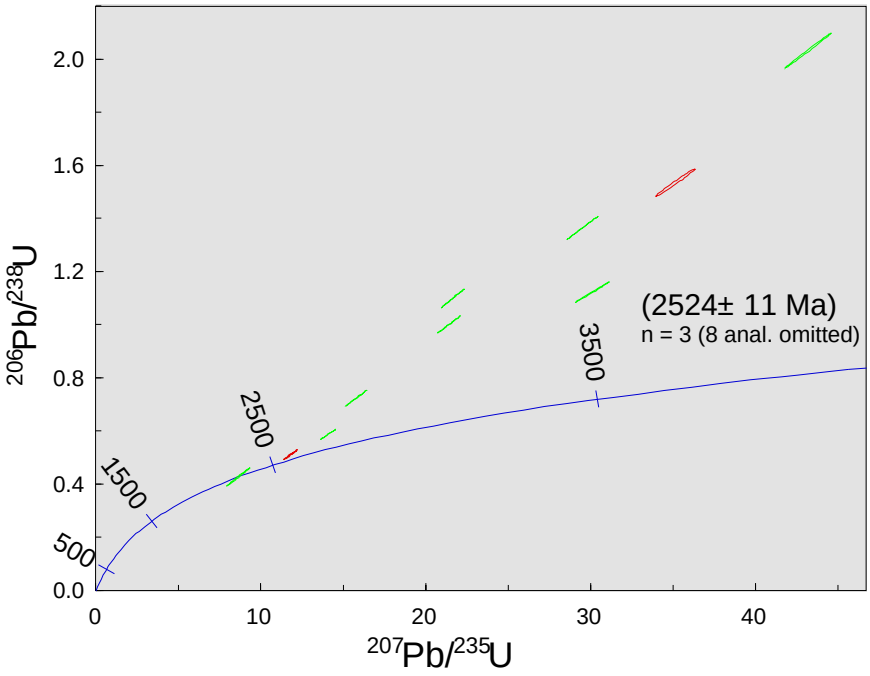

Figure 45. 481246 $^{206}Pb/^{238}U$-$^{207}Pb/^{235}U$ concordia diagram and inset $^{207}Pb/^{206}Pb$ age.

Main Findings

Age correlations between supracrustal rocks and their provenance

The new zircon age data and lithological and geochemical correlation confirm the field-based interpretation, along with existing age and map data in the region, that there are two tectonically dismembered greenstone belts of distinct ages in the central Godthåbsfjord region – the Bjørneøen-Qussuk belt and the Storø belt.

The Bjørneøen-Qussuk greenstone belt

Volcanic precursors to schists of intermediate composition of the Bjørneøen-Qussuk greenstone belts are c. 3071 ± 3 Ma (samples 479827 and 479681, Bjørneøen). This is the first direct dating of supracrustal rocks in the Akia terrane. A deformed granitic dyke on south-eastern Bjørneøen was emplaced into host mafic amphibolites at 3055 ±3 Ma, giving a consistent minimum constraint on the depositional age of the volcanic precursors to the amphibolite.

The timing of deposition of intermediate volcanics in the Bjørneøen and Qussuk belts is broadly synchronous with emplacement ages of felsic Nûk gneiss in these regions – i.e. 3070 ± 4, 3053 ± 4, 3048 ± 6, 3046 ± 5 Ma (Storø: 481201, 481271, 481311, 481227), 3065 ± 5, 3064 ± 3, 3053 ± 6, 3048 ± 4, 3048 ± 4 Ma (Bjørneøen: 479825, 479606, 479665, 479060), and 3040 ± 6 Ma (Qussuk: 477321).

These internally consistent age data, along with andesitic geochemical signatures indicative of arc-magmatism from amphibolites on both Bjørneøen and the Qussuk peninsula (see Appendix 5), suggest a genetic link between the Bjørneøen and Qussuk greenstone belts.

A tonalitic gneiss intrusive into leucogabbro-anorthosite on central Storø – in turn intrusive into the base of the greenstone belt– was emplaced at 3053 ± 4 Ma (481271). This unexpected result indicates that at least part of the structurally lowermost supracrustal rocks on Storø are mid-Archaean (or older) and may be correlative with the Kapisillik or the Akia terrane.

The Storø greenstone belt

One of the main findings relating to the Storø greenstone belt is that a tectonic panel of the same age as the Storø belt are present at the structural base of the Bjørneøen greenstone belt. The presence of late Archaean metasedimentary and metavolcanic rocks at the structural base of this belt on Store Malene and Sermitsiaq has previously been proposed by several workers (e.g. Nutman et al. 1989; McGregor et al. 1991). Our data show that metasedimentary and metavolcanic rocks of this age also exist on south-east Bjørneøen and extend further north into central Bjørneøen, requiring revision of the terrane boundary between the Akia terrane and Archaean rocks of distinct ages on Bjørneøen. It is likely that the metasedimentary rocks along the base of the supracrustal package on Sermitsiaq and south-eastern Bjørneøen are genetically distinct from the mid-Archaean Bjørneøen greenstone belt itself, and instead can be correlated with the Storø greenstone belt. This is also supported by metamorphic data (see later section). Notably this suggests that the tourmaline- and scheelite-rich rocks at the structural base of the greenstone belt on Bjørneøen, Sermitsiaq and Store Malene may be late Archaean and not a part of the Akia terrane. However, this does not preclude the possibility that mid Archaean tourmaline and scheelite-rich rocks also exist in the region, as indeed they do on parts of the Qussuk peninsula (Hollis et al. 2004) and Ivisaartoq (Nutman et al. 2004; Polat, this volume).

Metasedimentary samples from central Storø (481465), the Nuuk peninsula (479008), and from structurally below the Bjørneøen greenstone belt on Sermitsiaq (479326) show similar detrital zircon populations: 2935–2785, 2920–2820, and 2895–2840 Ma respectively, all with a dominant peaks at c. 2880 Ma, consistent with a common source of this age. Nutman et al. (2004) suggested that zircons of this age from metasedimentary rocks from outer Ameralik fjord may have been sourced from the Tasiusarsuaq terrane to the south. In this context it is worth noting that we have obtained an age of 2894 ± 3 Ma for a felsic orthogneiss from the western tip of central Storø – an age which is otherwise unknown in central Godthåbsfjord. Contacts with surrounding early to late Archaean rocks of quite different ages are tectonised, making it difficult to determine the significance of the presence of rocks of this age here. However this is a potential source rock for the detrital zircon of this age in the late Archaean metasedimentary rocks of the Storø greenstone belt. Notably both samples 481465 (Storø) and 479008 (Nuuk peninsula) also have a very small mid-Archaean population, and sample 479008 has a small early Archaean population. This is consistent with existing zircon data (Schiøtte et al. 1988; Nutman et al. 2004) from Rypeø

and Simiutâ south-east of Nuuk and from outer Ameralik, where late Archaean metasedimentary samples also contain small populations of mid and early Archaean detrital zircon. These data indicate that mid and early Archaean crust formed a minor source to these – probably once contiguous – late Archaean supracrustal rocks. Owing to tectonised contacts, it is unclear what formed the basement to the sedimentary and volcanic precursors to this belt.

Two metavolcanic samples from the Storø greenstone belt– both from the structural base of the Bjørneøen greenstone belt on Bjørneøen – were also dated. These samples (479052 and 479745) give inferred volcanic deposition ages of 2834 ± 3 and 2823 ± 2 Ma respectively. These ages are consistent with those reported by Schiøtte et al. (1988) and Nutman et al. (2004) for four samples of metasedimentary rocks in contact with the Færingehavn terrane in outer Ameralik. Nutman et al. (2004) interpreted a dominant mean age of 2831 ± 6 Ma as that of an A-type volcanic component within these metasedimentary rocks. Sample 479745 from central Bjørneøen, collected several kilometres west of the mapped Ivinnguit fault, indicates the presence of a previously unrecognised panel of late Archaean supracrustal rocks in this area. This also questions whether the Ivinnguit fault, as previously believed, defines the eastern margin of the Akia terrane on Bjørneøen. This is further discussed below with reference to the timing of metamorphism in the region.

Timing of metamorphism across the region

In all parts of the Akia terrane studied (on Bjørneøen, Storø, Qussuk peninsula) both metavolcanic rocks and orthogneiss zircon populations typically show a significant spread in ages down toward c. 2970 Ma, often outside the uncertainty on individual analyses. This is interpreted as partial to complete resetting of the isotopic system due to a metamorphic event around this time. On the Qussuk peninsula the resetting is most prevalent in samples collected in the most north-westerly areas (e.g. 477367, 477385). This may be the result of higher temperature conditions experienced in these areas. Indeed this corresponds with the known age of granulite facies metamorphism in the Akia terrane on Nordlandet (e.g. Garde et al. 2000). The same thermal event – at amphibolite facies – also appears to have had a widespread effect on U-Pb systematics further south on the Qussuk peninsula, Bjørneøen and Storø, where almost all the Nûk gneiss samples we have dated show some significant younger spread toward c. 2970 Ma, often with associated decreasing Th/U in zircon, consistent with a metamorphic origin (477318, 477320, 481201, 481227, 481311).

Metamorphism is also recorded in the period 2700–2600 Ma on Storø, the Nuuk peninsula south-west of Storø and west to the base of the greenstone belt on Sermitsiaq and Bjørneøen. This may relate to a prolonged period of thermal activity in the period 2700–2600 Ma, though the data suggest that there may have been distinct thermal events at c. 2700 and c. 2630 Ma. Samples of cordierite-bearing melt from garnet-sillimanite-cordierite gneiss, from central Storø and from the Nuuk peninsula south-west of Storø give metamorphic ages of 2700–2600 and 2632 ± 2 Ma (Storø: 481465, 481461) and 2701 ± 3 Ma (Nuuk peninsula: 479010). Similarly an amphibolite of intermediate composition at the base of the greenstone belt on Storø gives a wholly metamorphic zircon population at 2624 ± 3 Ma

(461526). This is consistent with the age of new igneous zircon growth in early Archaean orthogneiss on the Nuuk peninsula at c. 2700 Ma (479704) and emplacement of felsic orthogneiss in this region at 2698 ± 4 Ma (479014). Pegmatites that predate, or are synchronous with the Storø shear zone, were emplaced at c. 2630 Ma (see below). Likewise a Nûk gneiss from close to a NE-striking high strain zone on south-east Bjørneøen shows a strong disturbance in its age population with spread down to c. 2600 Ma (479060), possibly associated with movement on this shear zone.

These data are consistent with previous data of Nutman et al. (1989) who found c. 2700 Ma metamorphic ages corresponding to regional amphibolite facies metamorphism and minimum ages of terrane amalgamation from cross-cutting dyke relationships. However our data also point to metamorphism at c. 2630 Ma, associated with shear zone formation (see also below).

Major tectonic structures and timing of deformation

The eastern tectonic boundary structure to the Akia terrane

The Ivinnguit fault has been defined as the eastern tectonic boundary of the mid Archaean Akia terrane with early and late Archaean rocks to the west (McGregor et al. 1991) and has been mapped over tens of kilometres on Store Malene, eastern Sermitsiaq, south-eastern Bjørneøen and cutting the north-west coast of Storø. In our study we find that the understanding of the eastern margin of the Akia terrane, and also the Ivinnguit fault, requires some revision.

Several samples from Sermitsiaq and Bjørneøen (479326, 479052, 479060, 479745) shed new light on the eastern tectonic margin of the Akia terrane in these areas. We have identified a panel of late Archaean rocks on Sermitsiaq, which continue north-east to south-eastern and central Bjørneøen. These late Archaean rocks include the previously mapped Ikkattoq gneiss and structurally overlying metasedimentary and metavolcanic rocks immediately under the Bjørneøen greenstone belt. This supports the idea – postulated in Hollis et al. (2004) – that the kilometre-wide shear zone on Sermitsiaq and south-east Bjørneøen does not separate rocks of distinct age along its entire length but may be a reactivated or a relatively late structure post-dating tectonic juxtaposition of different terranes. On south-east Bjørneøen the high strain zone separates mid-Archaean amphibolites of the Bjørneøen greenstone belt from a panel of late Archaean metasedimentary and metavolcanic rocks and Ikkattoq gneiss. These late Archaean supracrustal rocks continue north and west structurally beneath the Bjørneøen greenstone belt into central Bjørneøen, swinging away from the high strain zone north-west of the mapped Ivinnguit fault. Along with the recognition of mid-Archaean supracrustal rocks (from 3053 ± 4 Ma cross-cutting tonalitic gneiss, 481271) at the structural base of the greenstone belt on central Storø, this indicates that one or more tectonic panels of interleaved mid and late Archaean orthogneiss and supracrustal rocks exist on both Bjørneøen and Storø (and possibly also elsewhere) that are not structurally controlled by the Ivinnguit fault as currently known.

This lends support to the idea, proposed in Hollis et al. (2004), that the high strain zone on Sermitsiaq and south-east Bjørneøen, and possibly also similar high strain zones mapped on central Bjørneøen (but not on south-eastern Qussuk – 477318, 477320), may represent relatively late structures unrelated to terrane assembly.

In the northern part of the study area the eastern tectonic margin of the Akia terrane lies to the east of the Qussuk peninsula in Godthåbsfjord, as confirmed by samples dated from the Qussuk peninsula in this study, which all give mid-Archaean emplacement ages.

The Storø shear zone

The Storø shear zone formed during or after an amphibolite facies metamorphism that resulted in garnet-sillimanite-cordierite-bearing mineral assemblages in metasedimentary rocks on Storø. This is evidenced by associated cordierite-bearing leucosome in this lithology, which is undeformed outside the shear zone and deformed within it. One sample of a cordierite-bearing leucosome (481461) from outside the shear zone on central Storø, and interpreted as a former syn-metamorphic melt fraction, has a metamorphic age of 2633 ± 2 Ma, giving a maximum age of formation of the Storø shear zone. The shear zone is also constrained by age data from pegmatites. These are generally quite discordant or spread out ages, largely owing to Pb loss from high-U and metamict zircon. Five pegmatites from the Storø shear zone are all deformed by it and were hence emplaced prior to or during shearing. They yield ages of c. 2745, 2632 ± 2, 2630 ± 5, c. 2630, and 2615–2570 Ma (481217, 465048, 465054, 465049, 481293), consistent with formation of the Storø shear zone during or after the thermal event at c. 2630 Ma.

It is possible that the parallel NE-striking high strain zones on Bjørneøen belong to the same structural generation as the Storø shear zone. This is supported by a general trend toward metamorphic ages of 2700–2600 Ma and low Th/U zircon in rocks with proximity to these shear zones, including samples 479825, 479827, 479681, 479060, 479814, and 479813 (all from Bjørneøen), and 479326 and 479703 (Sermitsiaq).

Implications for mineral occurrences – specifically gold

Field mapping, geochemistry and geochronology have established that the Bjørneøen greenstone belt was formed at c. 3070 Ma. It is likely that greenstones on Qussuk peninsula are of the same age, though this is poorly defined by the age data owing to variable metamorphic recrystallisation of zircon at c. 2980–2970 Ma. There is no zircon geochronological evidence for significant thermal activity after c. 2980–2970 Ma granulite and amphibolite facies metamorphism in the north and the south of the Akia terrane respectively. Although no direct dating has been carried out on sulphides related to gold mineralisation in the Akia terrane as part of this study, it is possible that Au mineralisation occurred in the mid-Archaean, either during deposition of the volcanics (see Appendix 5), or during subsequent amphibolite facies metamorphism.

Structural analysis of the Storø shear zone based on 2004 field mapping was reported in Appel et al. (2005). Here Coller and Coller report evidence for Au mineralisation during an early phase of ductile thrusting predating formation of the Storø shear zone. This is supported by Pb-Pb age data of sulphides associated with Au mineralisation at c. 2850 ± 100 Ma (Frei, pers. comm.). Given detrital age data from metasedimentary rocks from the Storø greenstone belt, which indicate a minimum depositional age of c. 2800 Ma, this is consistent with Au mineralisation soon after deposition. However, this does not preclude the possibility of remobilisation later in the tectonometamorphic history. The source of the Au on Storø is poorly defined with the existing data. However Pb-Pb sulfide data point to a mid-Archaean or older source (Frei, pers. comm.), which would be consistent with its derivation either from mid-Archaean supracrustal rocks (which have now been identified locally) or from an older source.

There are no indications from regional geochemistry, mapping, structural constraints, or geochronology that Au occurrences are associated with a regional-scale structural boundary between the Akia terrane and early and late Archaean terranes to the south-east. Au occurrences in the Akia terrane probably pre-date the formation of the structure/s that form this tectonic break. Furthermore, Au occurrences on Storø probably pre-date amalgamation of the distinct early, mid and late Archaean blocks at c. 2700 Ma (though they may have been later remobilised). These occurrences certainly pre-date development of the Storø shear zone. On the basis of this study it appears that Au mineralisation in the region may be linked with the depositional setting of the supracrustal sequences, rather than later crustal-scale structures. In this study we have seen that the Au-bearing late Archaean Storø greenstone belt is tectonically dismembered, with fragments cropping out on Sermitsiaq, Bjørneøen, and Storø, and probably also Store Malene. It may be that the known Au occurrences on Bjørneøen in fact occur within late Archaean amphibolites, though further work is required to establish the thickness of late Archaean greenstones on central Bjørneøen. Other parts of this dismembered greenstone belt in the region should also be targeted for exploration. Greenstone belts further north-east in the inner Godthåbsfjord region are poorly understood, and their ages and correlation with better studied belts in outer Godthåbsfjord should be investigated. This is the subject of a GEUS study in 2005, financially supported by the BMP.

Geochemical and petrographic characteristics of the Ivisaartoq and Storø greenstone belts, southern West Greenland: progress report

Ali Polat
Department of Earth Sciences, University of Windsor, Windsor, ON, Canada
N9B 3P4

Introduction

Archaean greenstone belts represent the integrated product of multiple geological processes such as magmatism, sedimentation, tectonism, and metamorphism operating over different spatial and temporal scales (de Wit 1998; Polat et al. 1998). In the following sections, major geological, petrographic, and geochemical characteristics of the mid-to-late Archaean Ivisaartoq and Storø greenstone belts, southern West Greenland (Fig. 46), are presented, to provide an understanding of the origin and geodynamic setting of these belts. Field investigation was conducted during a four-week field period in 2004. The main objective of this progress report is contribute to a better understanding of the geodynamic evolution of these greenstone belts, with a view to understand the geochemical characteristics of these belts. Geochemistry of these belts may be used to provide significant new information with other exploration tools, on the geological and geochemical phenomena that control mineral deposit (e.g., gold, massive sulphide) prospectivity of the belts.

Metavolcanic and metasedimentary rocks analysed for this report are divided into compositionally distinct groups. This subdivision is based on: (1) field characteristics, (2) thin section observations, (3) major element compositions, and (4) chondrite-normalised REE and primitive mantle-normalised trace element patterns. Each rock group is interpreted to be result of different geological processes. The geochemical characteristics of these groups are used to interpret their petrogenesis and geodynamic settings. Tabulated geochemical data are given in Appendix 4.

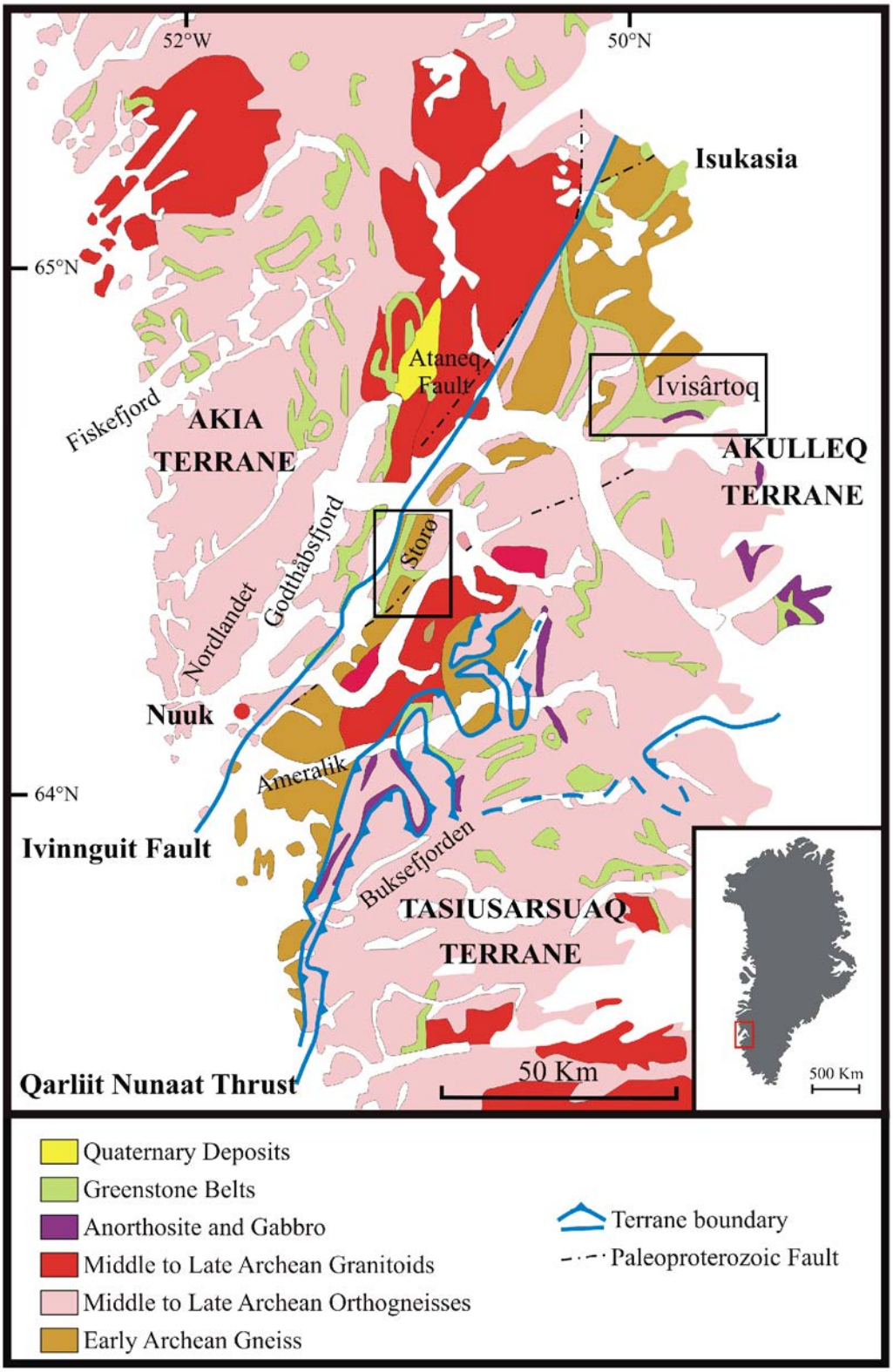

Figure 46. *Simplified geological map of the Nuuk region, showing the locations of the Ivisaartoq and Storø greenstone belts, modified from Escher & Pulvertaft (1995).*

Sampling, analytical methods, and data presentation

Approximately 90 samples were collected from the Ivisaartoq greenstone belt. Seventy-five of these samples have been analysed for major and some trace elements (Ba, Sr, Zr, Y, V, Sc). Fifty samples were additionally analysed for trace elements, including rare earth elements (REE), high field strength elements (HFSE), large ion lithophile elements (LILE), and transition metals (Ni, Co, Cr, V, Sc). About thirty-five samples were collected from the Storø greenstone belt. Twenty-seven of these samples have been analysed for major and trace elements. All samples were examined using an ordinary petrographic microscope

All samples were powdered using an agate mill in the Department of Earth Sciences, University of Windsor, Canada. Major and several trace (Ba, Sr, Y, Zr, Sc, V) elements were determined by Thermo Jarrel-Ash ENVIRO II ICP at ActLabs in Ancaster, Canada. Samples were mixed with a flux of lithium metaborate and lithium tetraborate, and fused in an induction furnace. Molten melt was immediately poured into a solution of 5% nitric acid containing an internal standard, and mixed continuously until completely dissolved. Calibration was performed using seven prepared USGS and CANMET certified reference materials. Results of standard analyses are given in Table A4.1. Totals of major element oxides are 100 $\pm$ 1 wt.% and the analytical precisions are 1 to 2 % (Table A4.1).

Samples were analysed for REE, HFSE, LILE, and transition metals (Ni, Co, Cr, and V) by a high-sensitivity Thermo Elemental X7 ICP-MS at the Great Lakes Institute for Environmental Research (GLIER), University of Windsor, Canada, using the protocols of Jenner et al. (1990). Wet chemical procedures were conducted under clean lab conditions, and all acids were distilled twice. All samples were analysed twice, using the HF-HNO_3 and Na_2O_2 sinter techniques to circumvent potential problems associated with HFSE (e.g., Zr, Hf, Nb, Ta) and REE in refractory minerals. Approximately 100–150 mg of sample powder was used for dissolution and sintering. Samples were dissolved in a concentrated HF-HNO_3 mixture at a temperature of ~120°C for four days, and then further attacked with concentrated HNO_3 until no residue was visible. BHVO-1, BHVO-2, and AGV-2 were used as international reference materials to estimate precision and accuracy (Table A4.2). Analytical precisions are estimated as follows: 1 to 10 % for REE, Rb, Li, Cs, Sr, Ba, Y, Cu, Zn, and Pb; 10 to 20 % for Zr, V, Cr, Ni, Co, Nb, and U; and 20 to 30 % for Ta and Th (Table A4.2).

Selected elements are normalised to primitive mantle (pm) (Hofmann 1988) and chondrite (cn) (Sun and McDonough 1989). Nb/Nb*, Zr/Zr* and Eu/Eu* ratios, representing anomalies, were calculated with respect to the neighbouring immobile elements, following the method of Taylor & McLennan (1985). Samples were recalculated to 100 % anhydrous for inter-comparisons. Mg-numbers were calculated as the molecular ratio of $Mg/(Mg+Fe^{2+})$, where Fe^{2+} is assumed to be 90 % of total Fe.

Ivisaartoq greenstone belt

Geological and petrographic characteristics

The Ivisaartoq greenstone belt is the largest Mesoarchaean (~3075 Ma) supracrustal assemblage in southern West Greenland (Figs 46, 47; Brewer et al. 1984; Chadwick 1986, 1990; Friend & Nutman, 2005). The belt is composed mainly of mafic to ultramafic volcanic rocks, gabbros, and serpentinites (Figs 48, 49; Hall 1981; Chadwick 1985, 1986, 1990). Sedimentary rocks constitute volumetrically a minor component of the belt (Fig. 49). All samples analysed for this report were collected from the southern limb of the asymmetric syncline in the greenstone belt (Fig. 47; Friend et al. 1981; Chadwick 1986). Volcanic rocks consist dominantly of foliated amphibolites and deformed pillow basalts (Figs 48, 50; Chadwick 1985, 1986, 1990; this study). The volcano-sedimentary sequence in the belt is subdivided into younger (upper amphibolite) and older (lower amphibolite) groups by a thin layer (up to 50 m thick) of chlorite- and magnetite-rich calc-silicate formation, called “magnetic marker” (Fig. 48; Chadwick 1986). This marker is exposed discontinuously over a distance of seven km. Hydrothermal alteration of mafic to ultramafic volcanic rocks in the vicinity of the “magnetic marker” resulted in the formation of strata-bound scheelite mineralisation in a calc-silicate formation (Appel 1994, 1997). The intensity of deformation appears to increase towards the contact between the two groups. The contact between the two groups appears to be tectonised (Fig. 51a). In addition to calc-silicate formation, the boundary between the two groups underwent silica alteration. Absolute ages of the volcanic rocks are unknown. Siliceous volcano-sedimentary rocks have yielded an average U-Pb zircon age of 3075 Ma (Friend & Nutman, 2005). The belt is intruded by 2963 ± 12 Ma old granites, constraining the minimum age of the belt (Friend & Nutman, 2005).

Volcanic rocks in the lower group are more intensely deformed than those in the upper group. They display well-developed foliation characterised by hornblende rich domains (Fig. 51b). Relict pillow structures are rare. Mineralogically, they are composed mainly of hornblende + plagioclase + quartz ± diopside ± epidote ± titanite (sphene) ± sulphide (Fig. 52). Compositional layering is also common in the group. The foliation is cut by one to ten-cm-thick deformed (folded) quartz veins. Up to 50 m wide and 5 km long a rusty layer of weathered sulphide deposit (pyrite) is exposed discontinuously in the lower amphibolite group. Discordant to concordant, relative to dominant foliation, calc-silicate formation of diopside-hedenbergite + garnet (grossularite-andradite) + hornblende + plagioclase + quartz ± vesuvianite ± epidote ± scheelite assemblage occurs mainly towards the top of the lower amphibolite sequence (Figs 53, 54). The thickness of these calc-silicate formation ranges from several centimetres to several metres.

The upper sequence is composed mainly of deformed pillow basalts, foliated amphibolites, gabbros, actinolite schist, and serpentinites (Figs 48, 49, 50). The serpentinites are exposed discontinuously as three major sheets throughout the sequence (Chadwick 1986, 1990). They form boudins up to 600 m long separated by pegmatites or deformed pillow basalts (Chadwick 1986). Chadwick (1986) reports the presence of olivine in these ultramafic bodies. They locally grade up into gabbro with a spotty texture of hornblendes set

in a plagioclase matrix. According to Chadwick (1986), the protoliths of the serpentinites intruded as sills.

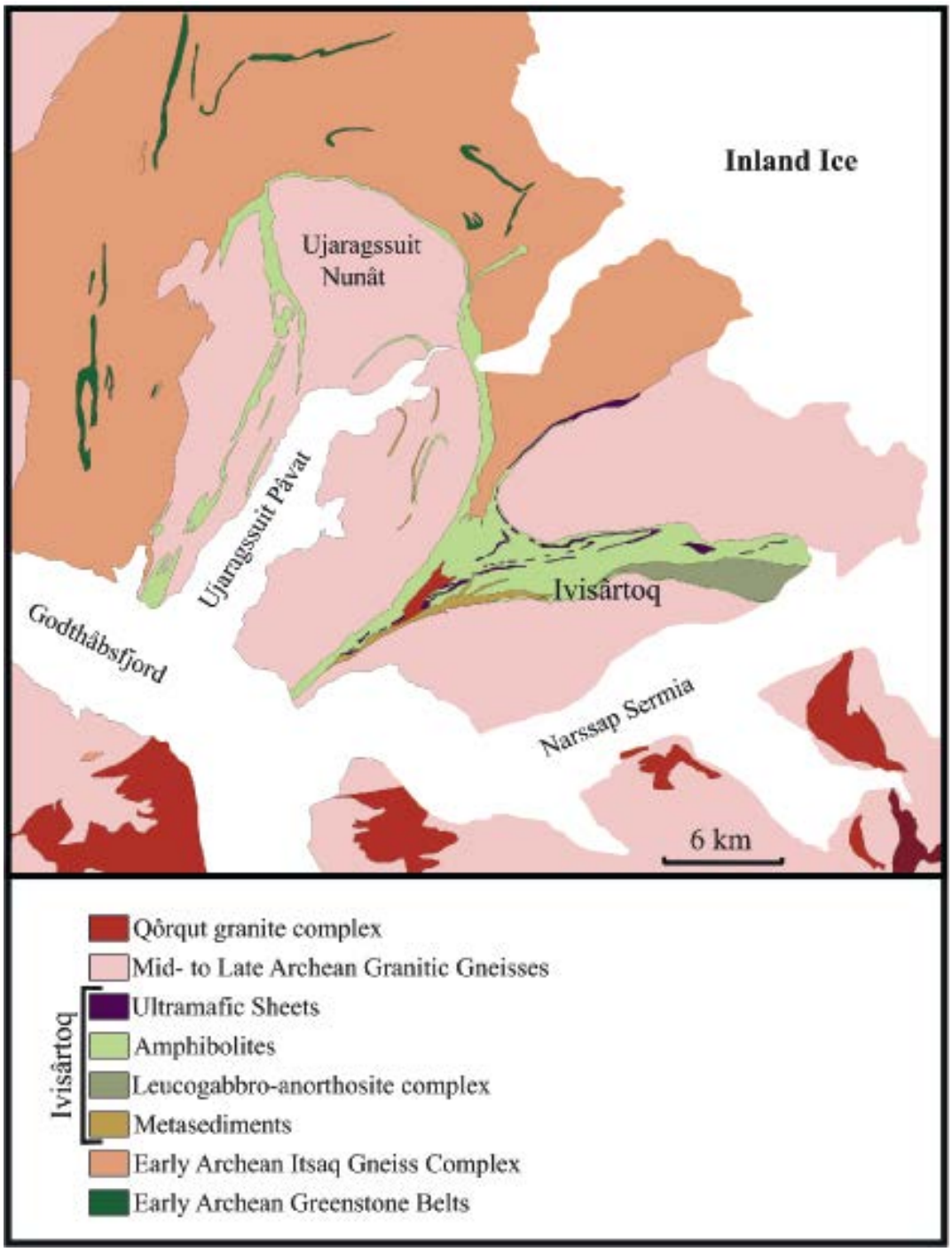

Figure 47. *Simplified geological map of the Ivisaartoq region. Modified from Chadwick & Coe (1988).*

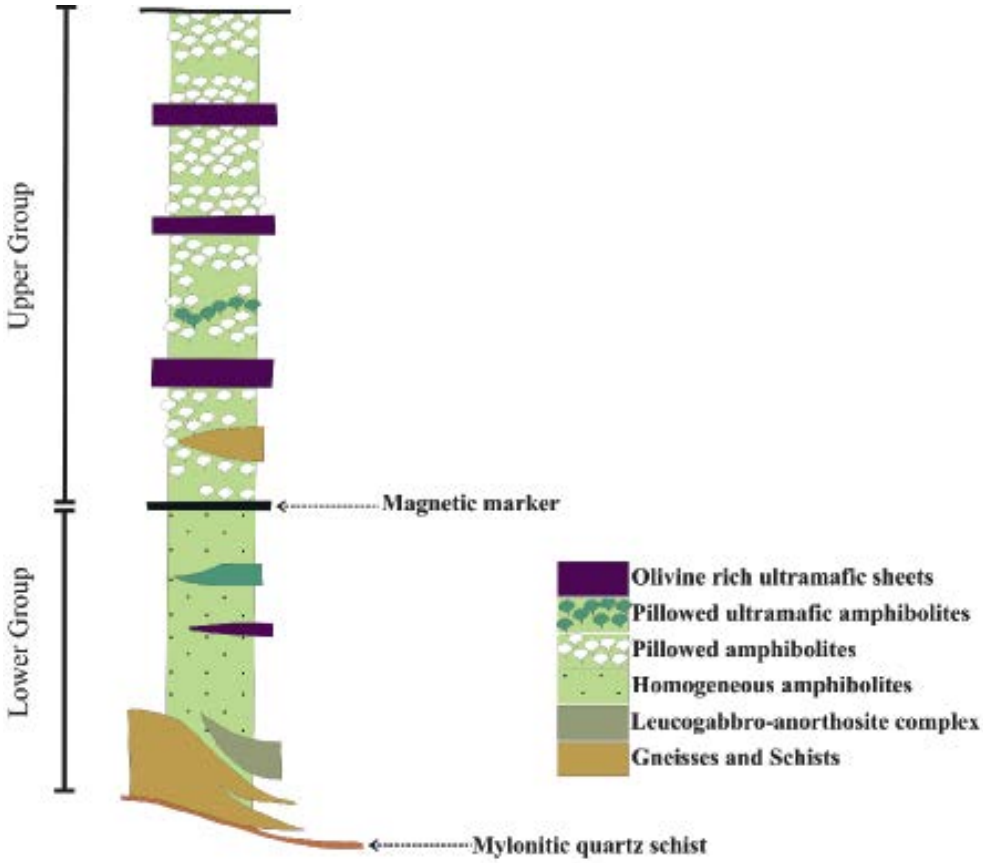

Figure 48. *Tectonostratigraphic section of the Ivisaartoq greenstone belt. Modified after Chadwick (1990).*

Pillow basalts are characterised by well-preserved core and rim structures (Fig. 50). The pillows range from 10 to over 100 cm in size. Many pillow cores display cavities at the centre, which are filled mainly with diopside + epidote + quartz (Fig. 50). They are probably of a seafloor hydrothermal origin (cf. Alt 1999; Humphris et al. 1998; and references therein). Some pillow cores are mineralogically and chemically zoned (Fig. 50). For descriptive purposes, the pillow cores are divided into inner and outer parts (Fig. 50b). The inner cores are composed dominantly of diopside (30–40 %) + epidote (20–30%) + quartz (20–30 %) + plagioclase (10–20 %) + amphibole (0–10 %) metasomatic alteration assemblage (Fig. 50, 52). Epidote is significantly replaced by diopside. The amount of epidote reaches up to 50 % in some pillow cores.

The outer pillow cores are characterised by white ellipsoidal ocelli structures (Fig. 52b, 55a, b). The ocelli structures are dispersed in a mafic matrix and their long axes ranges from a few millimetres to several centimetres (Fig. 55). They consist mainly of quartz (30–40 %) and plagioclase (30–50 %) + amphibole (10–20 %) ± epidote (0–5 %). The matrix surrounding the ocelli is made of hornblende (50–60 %) + plagioclase (20–30) + quartz (10–20 %) + epidote (0–5%) + titanite (0–5 %). In only one sample a relict grain of clinopyroxene was observed, indicating that amphibole resulted from the alteration of clinopyroxene.

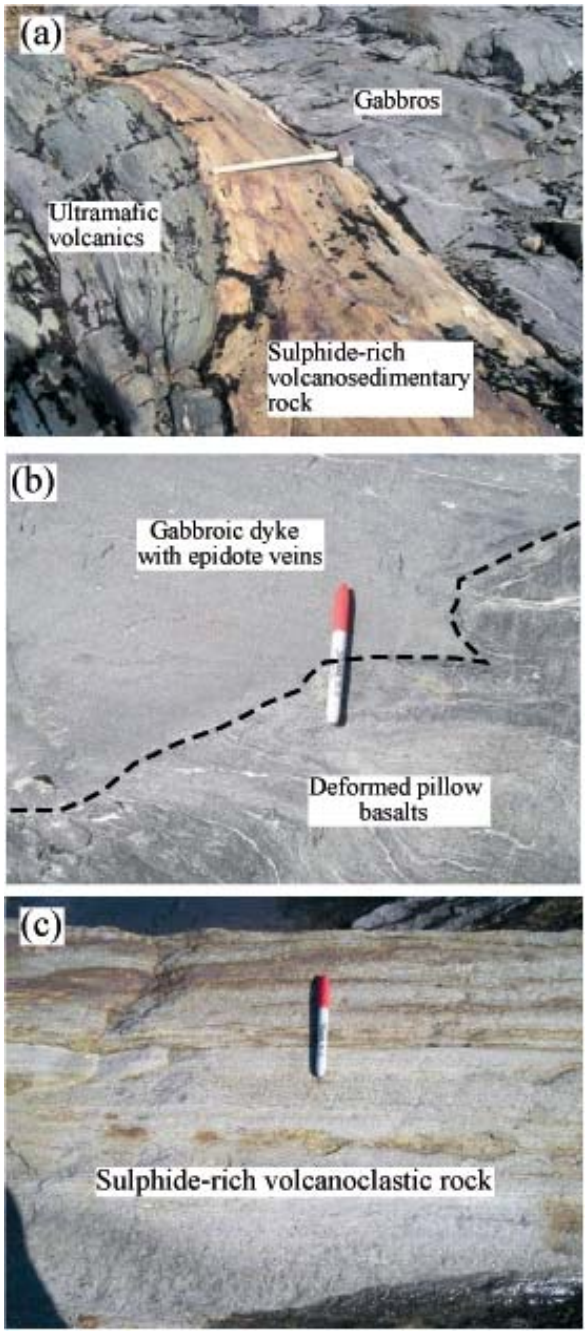

Figure 49. *Metavolcanic, metasedimentary, and gabbroic rocks in the Ivisaartoq greenstone belt.*

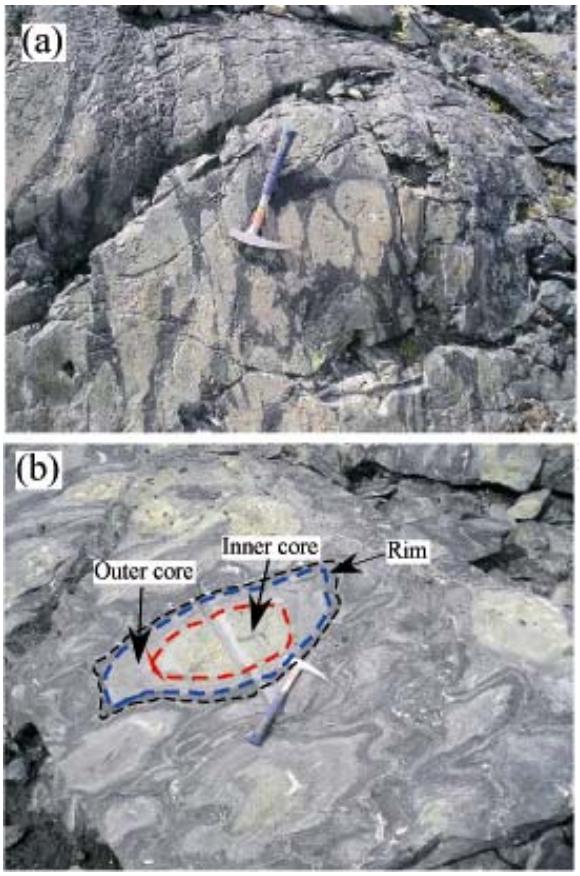

Figure 50. *Metasomatised pillow basalts (epidosites) in the Ivisaartoq greenstone belt.*

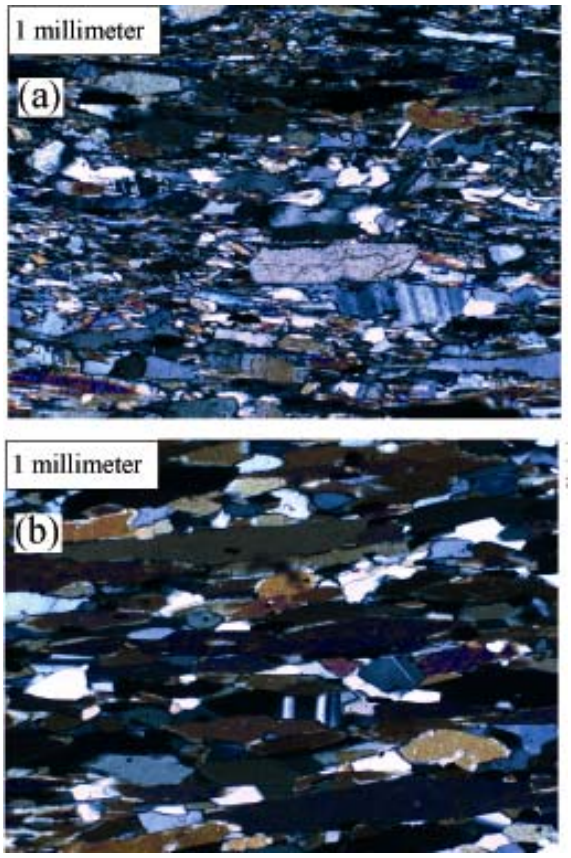

Figure 51. *Photomicrographs of amphibolites in the Ivisaartoq greenstone belt. (a) Sheared (tectonised) amphibolite at the contact between upper and lower amphibolites. (b) Hornblende-plagioclase-quartz-titanite schist in the lower amphibolite.*

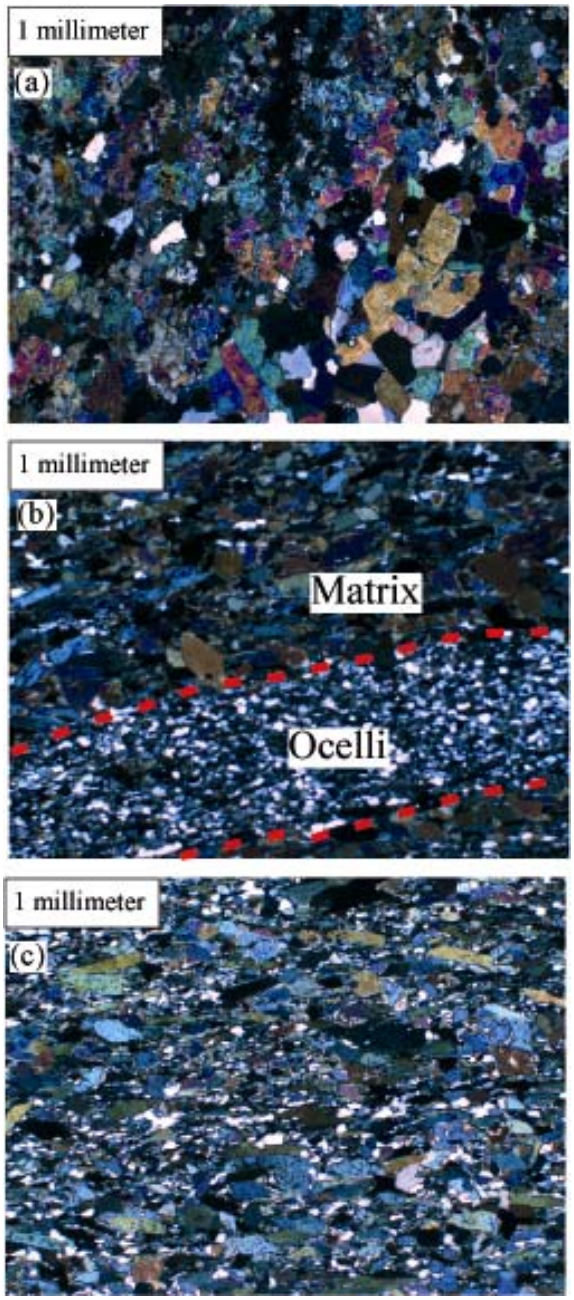

Figure 52. *Photomicrographs of pillow basalts in the Ivisaartoq greenstone belt. (a) Epidosite in the inner pillow core composed dominantly of diopside, epidote, quartz. (b) Ocelli structure in the outer pillow core consisting of quartz and plagioclase. The matrix is composed mainly of amphibole with minor quartz. (c) Pillow rim composed dominantly of amphibole with minor plagioclase and quartz.*

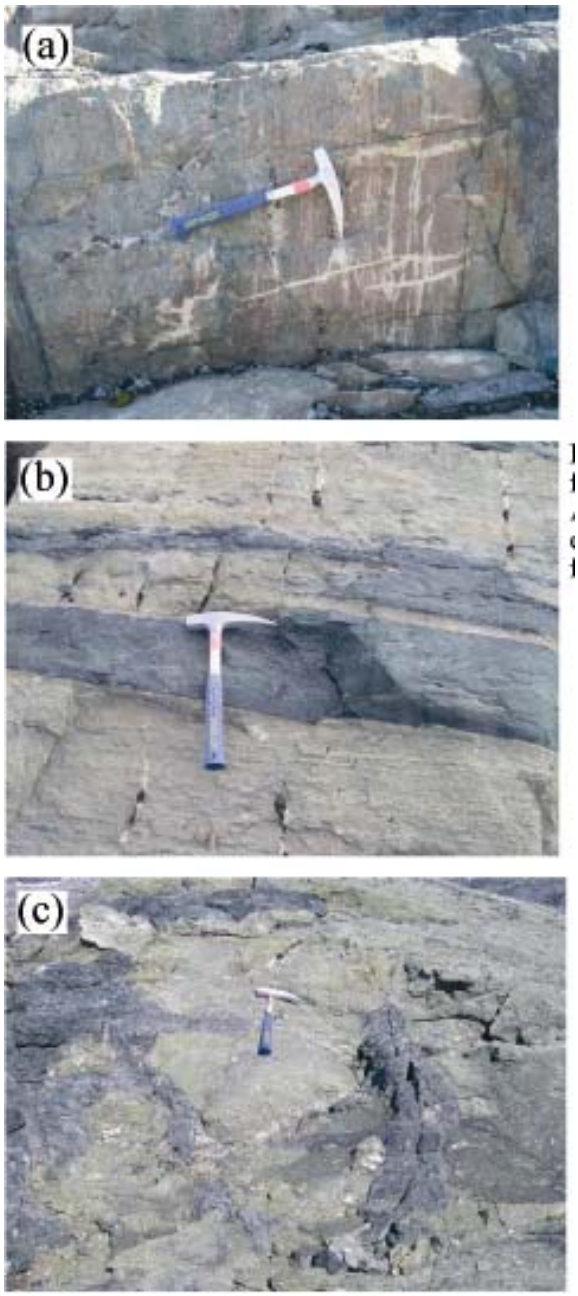

Figure 53. *Photographs of calc-silicate formation in the Ivisaartoq greenstone belt. (a) Garnet-diopside-epidote-quartz-vesuvianite calc-silicate occurring within shear zones and cutting previously formed epidote-rich calc-silicates. (b) Epidote-diopside-garnet calc-silicate formation within an ultramafic flow. Actinolite is replaced dominantly by epidote. Replacement follows the foliation plane. (c) Patches of epidote-diopside calc-silicate formation within mafic flow. Hornblende is replaced dominantly by epidote.*

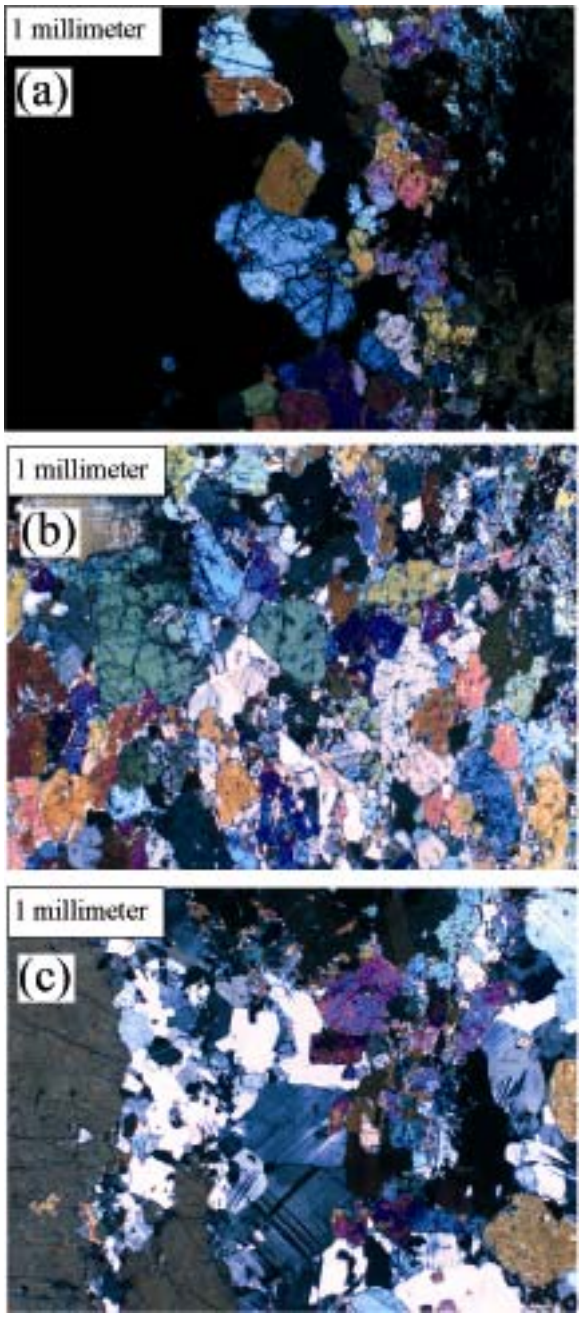

Figure 54. *Photomicrographs of calc-silicate formation in the Ivisaartoq greenstone belt. (a) Garnet-diopside-epidote calc-silicate. (b) Diopside-vesuvianite (idocrase) epidote-quartz calc-silicate. (c) Vesuvianite (idocrase)-plagioclase-diopside-epidote-quartz-garnet calc-silicate.*

Pillow cores that do not show any diopside-epidote-quartz metasomatic assemblage are composed predominantly of ocelli-matrix texture, indicating that the epidote-quartz metasomatic assemblage replaced the ocelli texture (Fig. 55). It appears that epidote (diopside)-quartz metasomatic assemblage grew outward from the pillow centres towards the rims. Epidote (diopside)-quartz metasomatic assemblage also occurs in pillow interstitial space (triple junctions), suggesting that the metasomatic assemblage was produced by fluids flowing through pillow pipes and interstitial voids. No ocelli structures have been observed

in the pillow rims (Fig. 55b). The rims are composed of 1-4-cm-thick hornblende + quartz + plagioclase. They are probably alteration product of volcanic glass. In some places, they have been replaced by quartz (Fig. 55c).

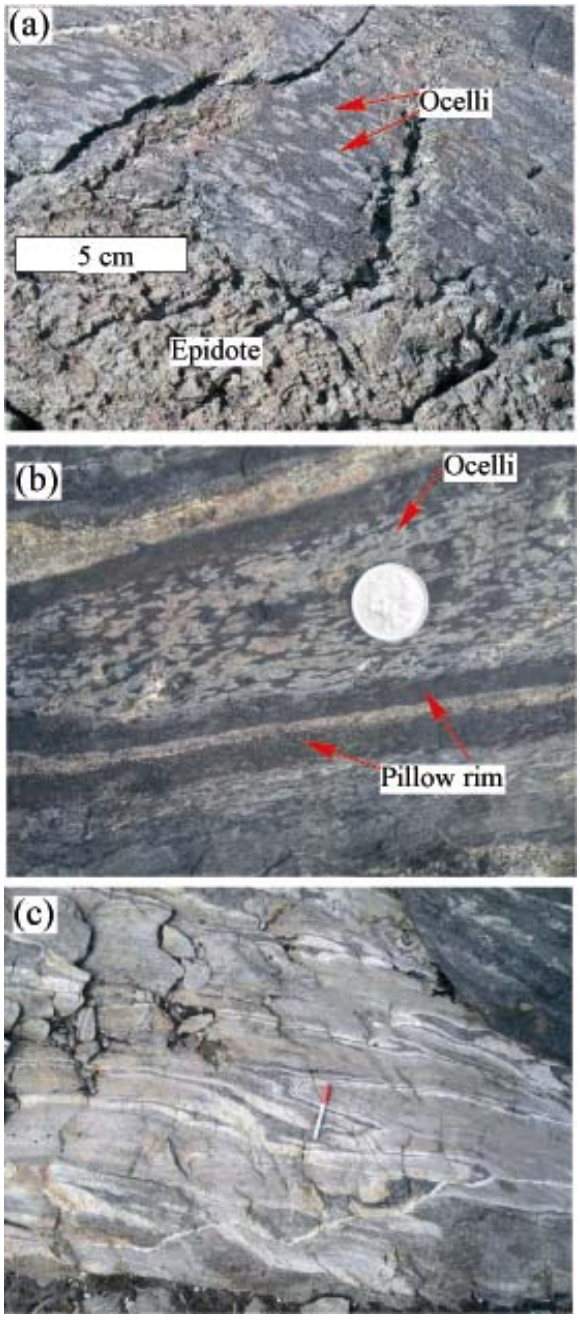

Figure 55. *Pillow basalts with ocelli structures (a-b), and silicified pillow rims.*

All known ocelli structures have Archaean ages. The ocelli structures occurring in the Ivisaartoq belt are morphologically and mineralogically similar to those found in other Archaean belts (see Gélinas et al. 1976; de Wit et al. 1992). They have been interpreted to represent immiscible liquids (cf. Gélinas et al. 1976; Cawthorn et al. 1979; Coltorti et al. 1987). The geochemical characteristics of the Ivisaartoq ocelli structures are currently under investigation.

Pillow basalts replaced by metasomatic assemblage have been folded by an early phase of deformation, suggesting that metasomatism took place prior to early deformation of the Ivisaartoq belt. Formation of calc-silicate assemblage that contain garnet + diopside pair is consistent with medium- to upper-amphibolite facies metamorphic conditions (Appel 1997). Given the petrographic observations that epidote in pillow cores is replaced by diopside, we suggest that epidote + quartz ± plagioclase ± amphibole metasomatic assemblage formed as epidosites under upper-greenschist to lower-amphibolite facies metamorphic conditions during hydrothermal alteration of the oceanic crust. Accordingly, epidote (diopside)-dominated pillow basalt cores and veins in the Ivisaartoq belt are defined as relict epidosites in this study. Early seafloor hydrothermal metamorphism was later overprinted by medium- to upper-amphibolite facies regional metamorphism.

Epidosites have been identified in six Phanerozoic supra-subduction zone ophiolites and Tonga forearc (see Banerjee et al. 2000; Gillis & Banerjee, 2000). The epidote-dominated alteration assemblage, except for diopside replacement, in the Ivisaartoq belt is mineralogically and texturally similar to epidosites found in Phanerozoic ophiolites (see Richardson et al. 1987; Harper et al. 1988; Gillis & Robinson, 1990; Nehling et al. 1994; Banerjee et al. 2000).

The origin of Phanerozoic epidosites is attributed to high-temperature seafloor hydrothermal alteration (see Nehling et al. 1994; Banerjee et al. 2000). The degree of alteration is more pervasive in sheeted dyke complexes than in volcanic and intrusive sequences. Phanerozoic ophiolites are interpreted to have formed during or shortly after dyke swarms intruded. All supra-subduction zone ophiolites show evidence for high-temperature hydrothermal discharge in the form of poly-metallic sulphide deposits and/or metalliferous sedimentary rocks. They form at temperatures of up to 450°C and high cumulative fluid/rock ratios. Exhalative massive sulphide deposits occur at all depths within volcanic sequences, from the sheeted dyke-volcanic sequence transition up to the volcanic sequence sedimentary rock interface; therefore, hydrothermal systems were active during all stages of crustal accretion. Compelling evidence for the high-temperature alteration in the Ivisaartoq belt comes from the presence of massive sulphide deposit in both the lower and upper amphibolite groups (Fig. 49a; Chadwick 1990; Appel 1988). According to the best knowledge of the author, the Ivisaartoq epidosites represent the oldest known example.

Gabbros occur as several metres to several tens of metre-thick (5–30 m) lenticular sills or dykes. In some places they alternate with pillow basalts and ultramafic flows. Chill margins are observed in several locations, indicating that they intruded into the pillow basalt sequence. Like pillow basalts, gabbros also underwent epidote-quartz alteration mainly along the margins, indicating that they intruded prior to, or during, seafloor hydrothermal alteration. They are composed mainly of hornblende + plagioclase ± epidote ± quartz. Magmatic layering and cumulus textures are locally preserved in gabbros (Fig. 56a, b). Primary igneous textures, minerals, and magmatic layering are locally preserved in low-strain domains (Fig. 56b). Only two samples contain relict clinopyroxene and plagioclase (Fig. 57a).

Some pillow basalt layers are composed predominantly of actinolites, and interlayered with ultramafic flows (actinolite schists). Primary magmatic textures, such as cumulates, are

locally preserved in low-strain domains (Figs 56c, 57b). Cumulates are composed primarily of altered clinopyroxene phenocrysts (Fig. 57b).

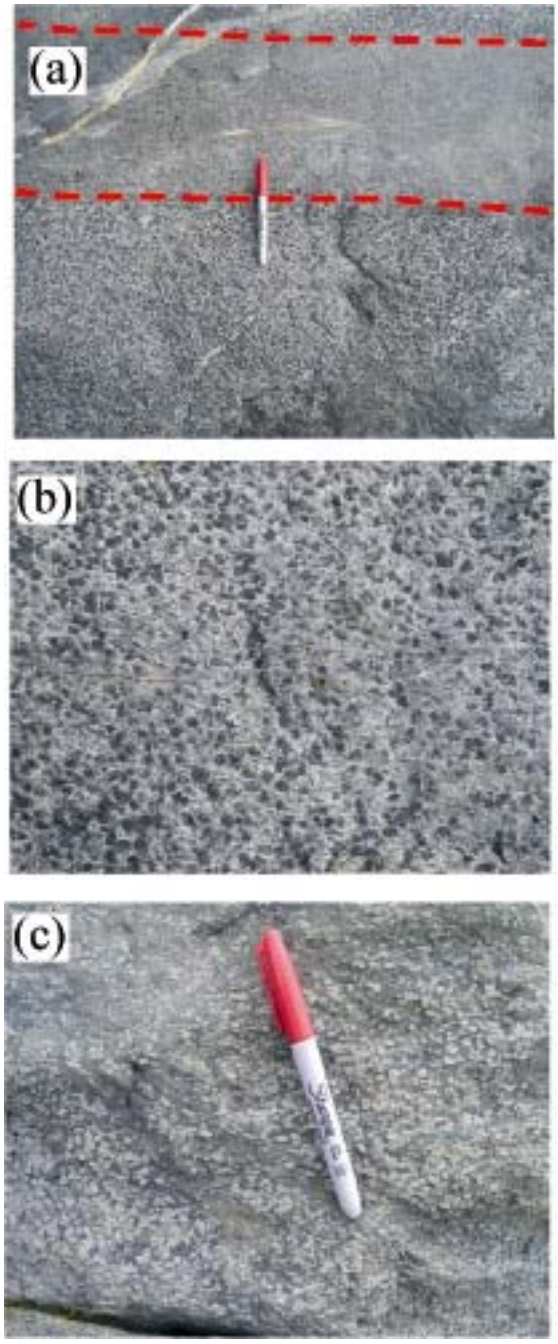

Figure 56. *Cumulates in gabbros and ultramafic flows in the Ivisaartoq belt. (a) Relict magmatic layering and cumulus texture in the gabbroic sills. (b) Relict cumulus texture. Clinopyroxene is replaced by amphibole. (c) Deformed clinopyroxene cumulates in the ultramafic flows.*

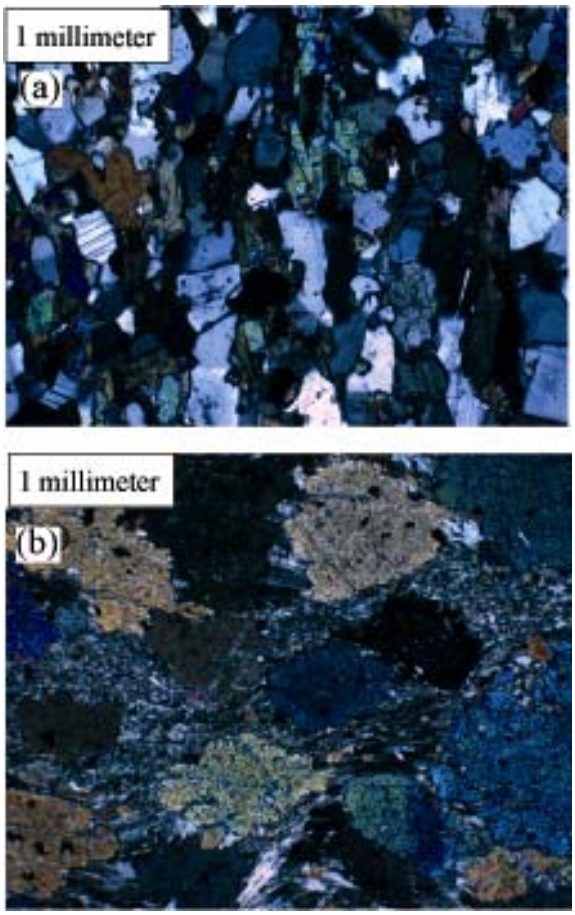

Figure 57. *Photomicrographs of cumulate sections of ultramafic flows, and gabbroic dykes and sills, with relict clinopyroxene. (a) Gabbro with relict clinopyroxene and plagioclase. (b) Relict clinopyroxene phenocrysts in the cumulate section of the ultramafic flow. The matrix is composed of actinolite.*

Geochemical characteristics

Lower amphibolites

Amphibolites in the lower sequence are geochemically divided into four groups (Table A4.3). Group 1 amphibolites have lower SiO_2 (43–48 wt.%) and Na_2O (0.9–1.8 wt.%) but higher CaO (12.9–14.5 wt.%) contents than the other three groups (Table A4.3). They are characterised by convex-upward REE patterns (La/Smcn=0.2–0.4; Gd/Ybcn=1.0–1.3) and variably negative Eu (Eu/Eu*=0.4–0.6), Nb (Nb/Nb*=0.2–0.4), Ti (Ti/Ti*=0.4–0.8), and Zr (Zr//Zr*=0.8–0.9) anomalies (Figs 58, 59).

Group 2 amphibolites display U-shaped (concave upward) REE patterns with strong positive Eu anomalies (La/Smcn=2.6–3.1; Gd/Ybcn=0.30–0.45; Eu/Eu*=1.9–2.3; Fig. 58). In contrast to Group 1 amphibolites, they have positive Nb anomalies (Nb/Nb*=1.3–1.4; Fig. 59).

Group 3 amphibolites have flat to slightly depleted LREE patterns (La/Smcn=0.78–1.06) and minor negative to positive Eu (Eu/Eu*= 0.93–1.04) anomalies (Fig. 58). They have moderately negative Nb (Nb/Nb*=0.45–0.74) and negative to positive Zr (Zr/Zr*=0.83–1.19) anomalies (Fig. 58). Group 4 amphibolites display LREE enriched patterns (La/Smcn=2.05–4.74; Gd/Ybcn=1.55–15.47) and negative Eu (0.82–0.89) and Nb (Nb/Nb*=0.17–0.20) anomalies (Figs 58, 59).

Diverse REE patterns in the Ivisaartoq amphibolites likely reflect mobility of these elements during calc-silicate alteration rather than primary geochemical signature, because these patterns do not correlate with relatively immobile elements Zr, Ti, and Al. For example, the U-shaped REE patterns of Group 2 amphibolites are comparable to those of Phanerozoic and Archaean boninites. However, their low Al_2O_3/TiO_2 ratios and low MgO, Ni, and Cr contents, compared to those of boninites, are inconsistent with a boninitic composition (Polat et al. 2002). Similarly, Eu anomalies do not correlate with Sr and CaO contents (Table A4.3).

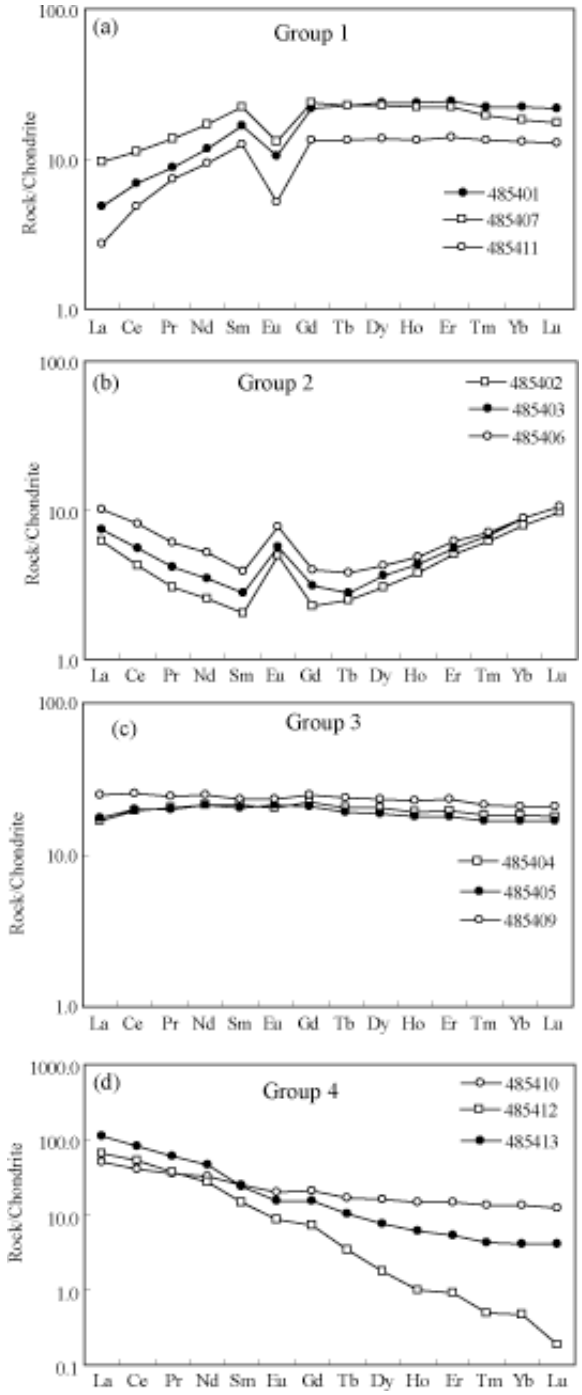

Figure 58. *Chondrite-normalised REE patterns of lower amphibolites in the Ivisaartoq greenstone belt.*

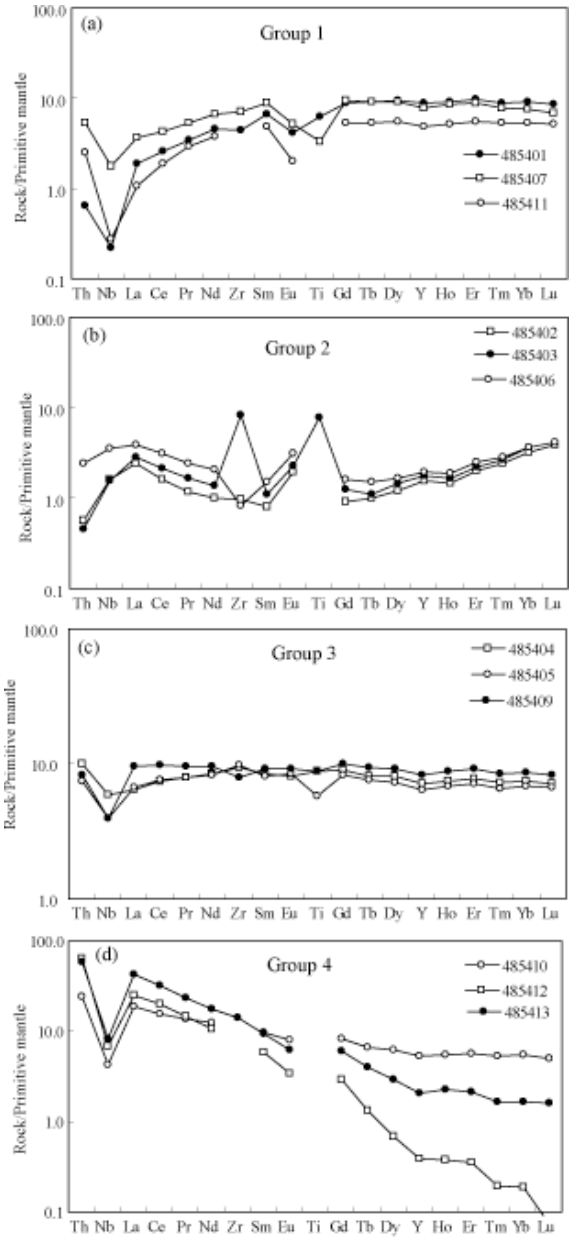

Figure 59. *Primitive mantle-normalised trace element patterns of lower amphibolites in the Ivisaartoq greenstone belt.*

Pillow basalts in the upper amphibolite group

The inner pillow cores have relatively low MgO (4.0–5.9 wt.%), Fe_2O_3 (6.9–10.0 wt.%), K_2O (0.01–0.03 wt.%), TiO_2 (0.47–0.57 wt.%), Zr (27–32 ppm), and Nb (1.2–2.2 ppm), but high CaO (17.4–20.8 wt.%), SiO_2 (49.2–55.7 wt.%) contents (Table A4.4) compared to average modern mid-ocean ridge basalts (MORB; see Hofmann 1988). Mg-numbers range from 0.47–0.57 (Table A4.4). They display consistently higher Ni (267–403 ppm), Cr (546–735 ppm), and Co (41–70 ppm) concentrations than average MORB (see Hofmann 1988). Al_2O_3/TiO_2 ratios (26–28 vs 22) are slightly super-chondritic, whereas Zr/Y (1.8–2.3 versus 2.4) and Ti/Zr (97–104 versus 115) ratios tend to be sub-chondritic (see Sun & McDonough 1989). On chondrite- and primitive mantle-normalised diagrams, they have the following

geochemical features: (1) moderately fractionated LREE patterns (La/Smcn=1.5–1.9; La/Ybcn=1.2–2.0), near flat HREE patterns (Gd/Ybcn=0.9–1.2); and (3) variably negative Nb (Nb/Nb*=0.3–0.6), Ti (Ti/Ti*=0.7–0.8), and Zr (Zr/Zr*=0.8–0.9) anomalies (Figs 60, 61).

Outer pillow cores have higher MgO (5.3–8.4 wt.%), SiO_2 (51.3–58.4 wt.%), K_2O (0.10–0.18 wt.%), and Na_2O (0.81–2.5 wt.%), but lower CaO (11.4–14.2 wt.%) contents than the inner counterparts (Table A4.4). Mg-numbers are consistently higher in the outer than inner cores (0.56–0.65 versus 0.46–0.57). Al_2O_3, TiO_2, Cr, Ni, Co, Zr, and V contents, and Al_2O_3/TiO_2, Ti/Zr, and Zr/Y ratios in the outer cores are similar to those in the inner cores (Table A4.4). Similarly, the chondrite-normalised and primitive mantle patters are comparable to those of inner cores (Figs 60, 61).

The pillow rims are compositionally uniform at 8.1–10.3 wt.% MgO, 47.4–51.1 wt.% SiO_2, 11.7–13.2 wt.% CaO, 0.53–0.57 wt.% TiO_2, 10.7–12.9 wt.% Fe_2O_3, 592–670 ppm Cr, and Mg-number = 0.59–0.62 (Table A4.4). Ratios of Al_2O_3/TiO_2 (22–27) are super-chondritic, whereas Ti/Zr (96–102) and Zr/Y (1.8–2.3) ratios are consistently sub-chondritic (see Sun and McDonough, 1989). In addition, they have the following geochemical features: (1) depleted to slightly enriched LREE patterns (La/Smcn=0.87–1.17); (2) flat HREE patterns (Gd/Ybcn=1.0–1.1); (3) negative Nb (Nb/Nb*=0.40–0.62) and Ti (Ti/Ti*=0.75–0.85) anomalies; and (4) depletion of Zr relative to Nd and Sm, generating negative Zr anomalies (Zr/Zr*=0.82–0.99; Figs 60, 61).

Given the presence of primary ocelli structures in the outer cores, they likely represent the least altered (metasomatised) part of the pillow basalts. High CaO and SiO_2 contents in the inner cores likely have resulted from the formation of metasomatic epidote and quartz (epidosites). Lower La/Sm ratios in the rims, compared to outer cores, are consistent with the loss of these elements during seafloor hydrothermal alteration. LREE enriched but HFSE depleted trace element patterns in the outer cores are consistent with a subduction zone geochemical signature (cf. Saunders et al. 1991; Hawkesworth et al. 1993; Pearce & Peate 1995). The presence of similar REE and HFSE characteristics in both the least metasomatised outer cores and the most metasomatised inner cores (Figs 60, 61) suggests that subduction zone geochemical signature was not obliterated by seafloor hydrothermal alteration and subsequent regional metamorphism.

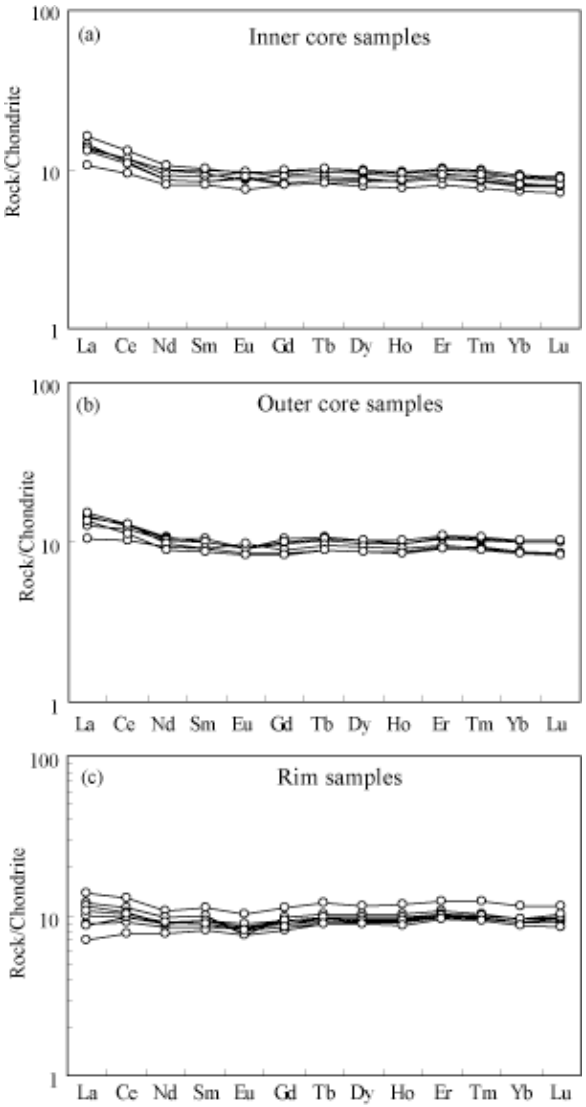

Figure 60. *Chondrite-normalised REE patterns of pillow basalts in the Ivisaartoq greenstone belt*

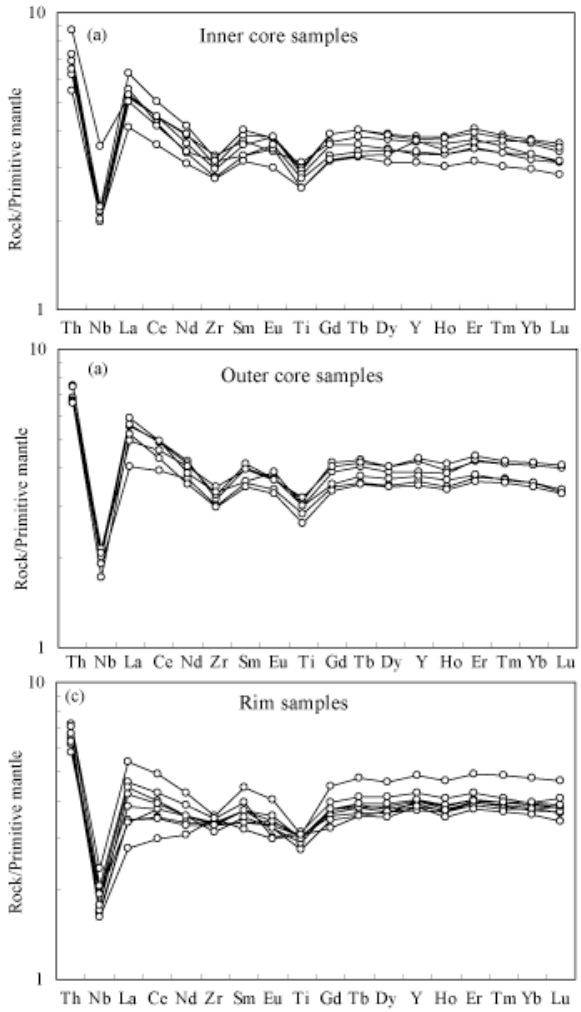

Figure 61. *Primitive mantle-normalised trace element patterns of pillow basalts in the Ivisaartoq greenstone belt.*

Storø greenstone belt

Geological and petrographic characteristics

The Storø greenstone belt (Fig. 46) is composed of interlayered metavolcanic and metasedimentary rocks. In addition to these supracrustal rocks, the belt contains lenses of ultramafic rocks composed mainly of actinolite and serpentine. Given the intensity of metamorphism and deformation, the origin of the ultramafic rocks is not clear. Both metavolcanic and metasedimentary rocks have been intensively sheared and folded at various scales (Figs 62, 63). The thickness of both lithologies varies laterally, indicating structural truncation and transposition. They display a well-developed foliation. Most of the contacts between different lithologies are sheared (Fig. 63). They are cut by deformed (sheared, folded) mafic to felsic (pegmatite) dykes, and intruded by late Archaean anorthosites and granites (Fig. 62). Field observations indicate that intrusion of the anorthosites took place

after development of major foliation, folding, and shearing (Fig. 63). The metavolcanic rocks are mainly mafic amphibolites. Some of the intermediate to felsic schists may have derived from volcano-clastic sedimentary rocks.

The amphibolites are composed mainly of hornblende + plagioclase + quartz ± biotite ± garnet ± titanite ± sulphide (pyrite) ± kyanite ± chlorite (Fig. 64). There are at least three sets of quartz veins in the amphibolites. The oldest quartz veins occur along the foliation planes and have been folded and boudinaged. Younger dilatational net works of veins cross cut the foliation and associated calc-silicate formation (Figs 65, 66a). These calc-silicates are composed of quartz + garnet + diopside + plagioclase + amphibole (Fig. 66a). The calc-silicate formation displays a corona texture in that amphibolite form between plagioclase and clinopyroxene (diopside), consistent with retrograde metamorphism.

Metasedimentary rocks are compositionally more diverse than their metavolcanic counterparts. The following mineral assemblages have been recognised (Figs 62–66):

(1) Quartz + biotite + microcline + plagioclase + garnet ± muscovite ± sillimanite
(2) Quartz + magnetite + garnet + kyanite ± biotite
(3) Quartz + kyanite + biotite + hornblende + plagioclase
(4) Quartz + biotite + muscovite + microcline
(5) Quartz + garnet + biotite + plagioclase + staurolite
(6) Biotite + muscovite + garnet + quartz + plagioclase
(7) Hornblende + kyanite + biotite + quartz
(8) Garnet + hornblende + biotite + quartz + plagioclase + chlorite
(9) Garnet + biotite + kyanite + sillimanite + quartz
(10) Quartz + fuchsite

In assemblage (2) magnetite and kyanite occurs as inclusions, indicating that they pre-date the garnet growth. Similarly, magnetite occurs as inclusion in kyanite and quartz, suggesting that it is one of the earliest minerals to crystallise. The presence of kyanite is consistent with high-pressure metamorphic conditions. In some samples kyanite has been replaced by biotite and hornblende, indicating a retrograde metamorphic overprint. Biotite is locally altered to chlorite, consistent with a retrograde metamorphic event.

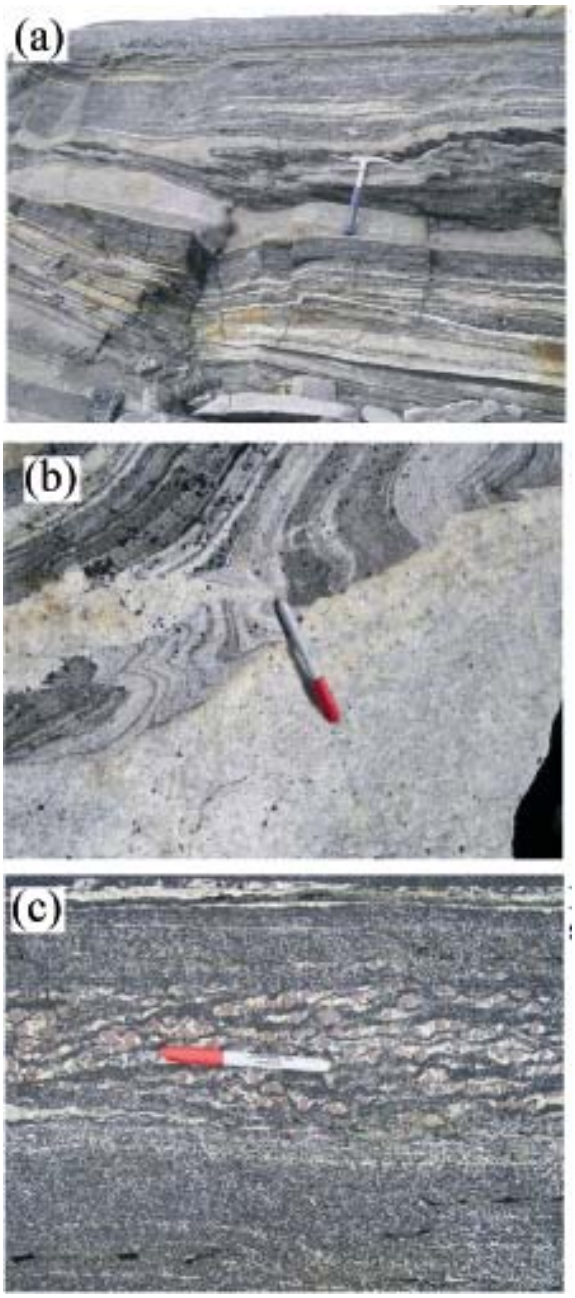

Figure 62. *Volcano-sedimentary rocks and their field characteristics, Storø greenstone belt. (a) Deformed volcano-sedimentary rocks. (b) Deformed volcano-sedimentary rocks are cut by late-Archaean anorthosite. (c) Porphyroblastic garnet in the volcano-sedimentary rocks.*

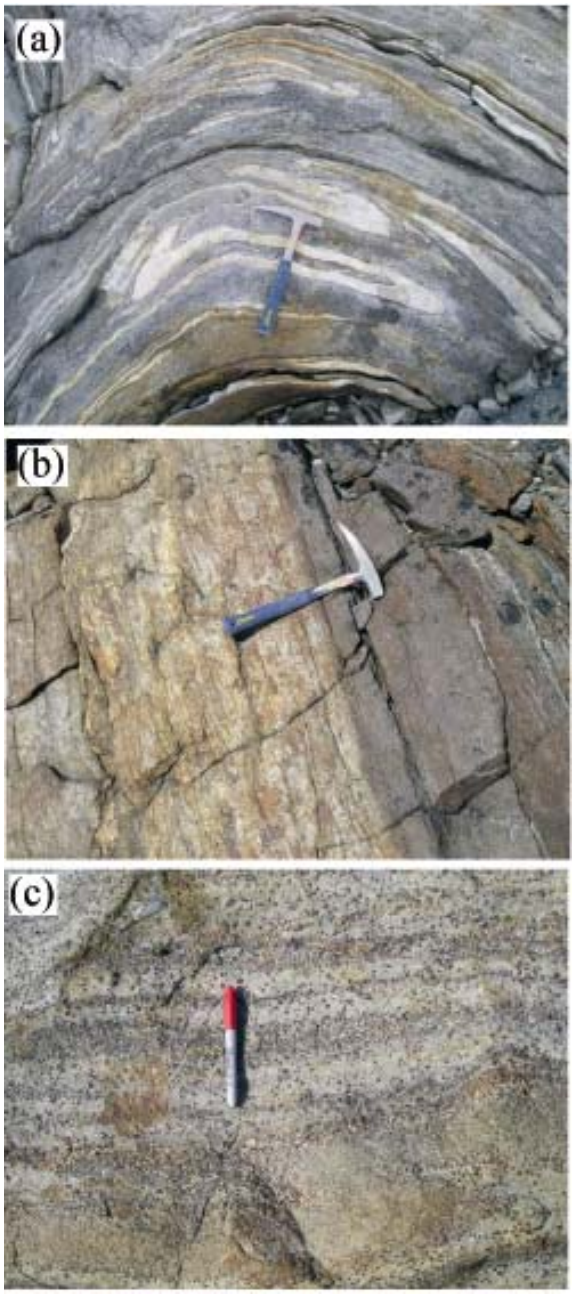

Figure 63. *Field characteristics of volcano-sedimentary and metasedimentary rocks in the Storø greenstone belt. (a) Folded and re-folded volcano-sedimentary rocks. (b) sheared quartz- and magnetite-rich metasedimentary rocks. (c) Garnet-rich metasedimentary rocks.*

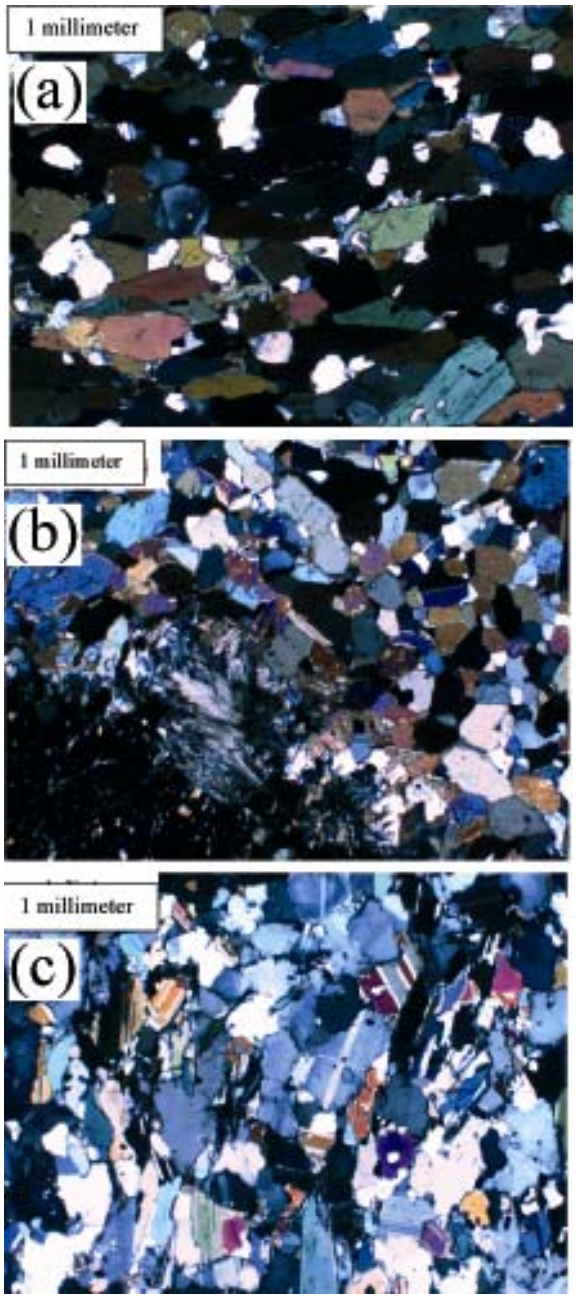

Figure 64. *Photomicrographs of metamorphic rocks in the Storø greenstone belt. (a) Amphibolite schist composed dominantly of hornblende, plagioclase, and quartz, likely derived from a mafic volcanic (basalt) protolith. (b) Garnet-hornblende-biotite-quartz-plagioclase-chlorite-titanite schist. Chlorite occurs between garnet and biotite in reaction rims. This rock is likely derived from a mafic sedimentary or volcano-sedimentary protolith. (c) Quartz-kyanite-biotite-plagioclase schist, likely derived from a sedimentary protolith.*

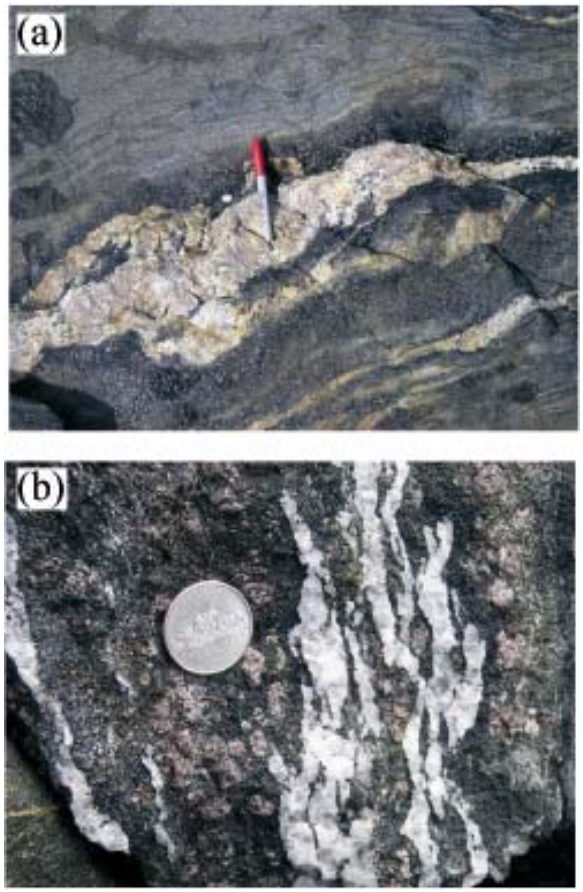

Figure 65. *Quartz veins within the amphibolites and garnet amphibolites.*

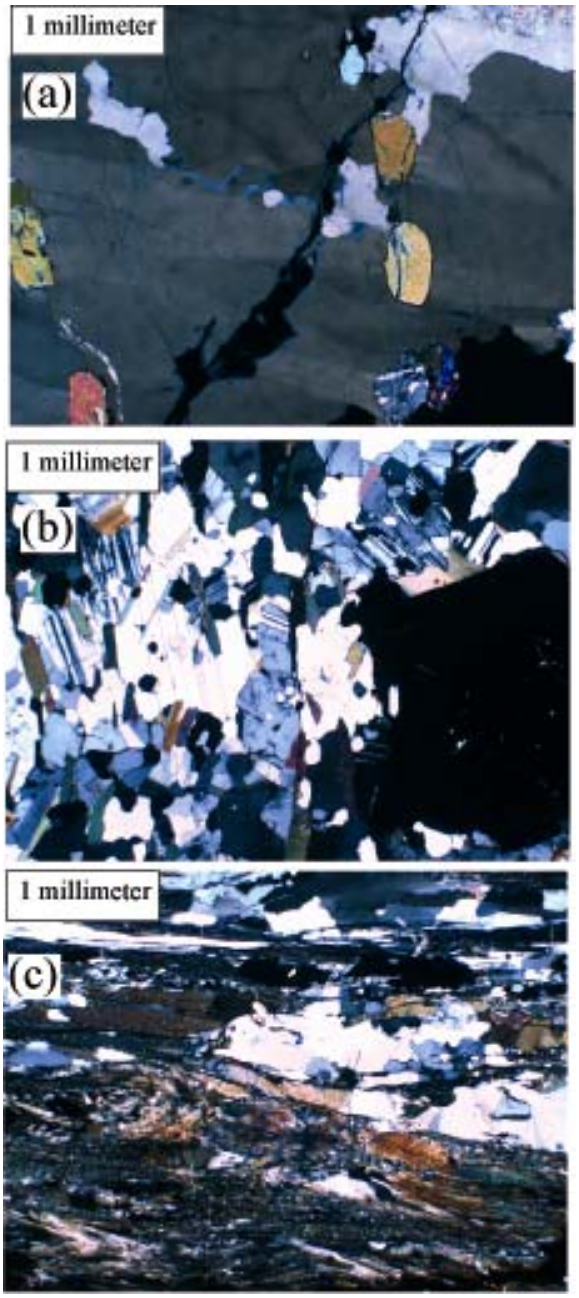

Figure 66. *Photomicrographs of calc-silicate and metasedimentary rocks in the Storø greenstone belt. (a) Calc-silicate composed predominantly of quartz-diopside-garnet, occurring as veins in metavolcanic amphibolites. (b) Kyanite-plagioclase-garnet-quartz-biotite-amphibole schist, likely with a sedimentary protolith. Some biotites appear to replace kyanite, indicating retrograde metamorphism. (c) Quartz-plagioclase-kyanite-sillimanite-biotite schist, likely with a sedimentary protolith.*

Geochemical characteristics

Metavolcanic amphibolites

Amphibolites have large variations in MgO (4.7–14.4 wt.%), TiO_2 (0.59–2.52 wt.%), Fe_2O_3 (12.0–17.8 wt.%), Na_2O (0.62–2.88 wt.%), Ni (48–217 ppm), and Cr (53–490 ppm), and moderate variations in SiO_2 (47.6–52.5 wt.%), CaO (8.7–11.8 wt.%), and Al_2O_3 (9.85–16.08 wt.%; Fig. 67; Table A4.5). On the basis of their trace element patterns, amphibolites are divided into three groups.

Group 1 is characterised by strongly to moderately depleted LREE patterns (La/Smcn=0.49–0.73), and negative Eu (Eu/Eu*=0.55–0.89), Nb (Nb/Nb*=0.43–0.85), and Ti (Ti/Ti*=0.45–1.00) anomalies (Figs 68, 69). Zr/Y (1.7–3.8), Ti/Zr (81–118), and Al_2O_3/TiO_2 (7.8–23.0) ratios are in the range of sub-chondritic to chondritic values. Nb/Ta ratios (15–17) are lower than the chondritic value (18).

Group 2 amphibolites have near-flat REE patterns (La/Smcn=0.93–1.03) and minor negative to positive Eu (Eu/Eu*=0.95–1.17) anomalies (Table A4.5; Figs 68, 69). In addition, on a primitive mantle-normalised trace element diagram, they display negative Nb (Nb/Nb=0.14–0.60) anomalies. Nb/Ta (15.1–16.0), Ti/Zr (89–108), and Al_2O_3/TiO_2 (7–20) ratios are systematically sub-chondritic, whereas Zr/Y ratios range from chondritic to super-chondritic (2.4–3.9).

Group 3 amphibolites have the largest population (Table A4.5). On chondrite- and primitive mantle-normalised trace element diagrams they have the following significant features: (1) enriched LREE patterns (La/Smcn=1.15–2.72; La/Ybcn=1.32–7.74); (2) positively fractionated HREE patterns (1.15–2.07); (3) negative Nb (Nb/Nb*=0.30–0.90) and Ti (Ti/Ti*=0.8–1.0) anomalies, and (4) negative to positive Zr (Zr/Zr*=0.75–1.27) and Eu (Eu/Eu*=0.67–1.48) anomalies. Al_2O_3/TiO_2 ratios are sub-chondritic (6.2–13.5), whereas Zr/Y ratios are super-chondritic (2.4–4.0). Collectively, the geochemical characteristics of the Storø metavolcanic rocks are consistent with a subduction zone geochemical signature.

Metasedimentary rocks

Diverse lithological and mineralogical characteristics of the Storø metasedimentary rocks are reflected in their geochemical compositions (Table A4.6). They have large variations in SiO_2 (43.12–87.10 wt.%), TiO_2 (0.22–2.52 wt.%), MgO (0.68–8.15 wt.%), CaO (0.85–8.15 wt.%), Fe_2O_3 (2.45–49.46 wt.%), Na_2O (0.01–4.16 wt.%), Al_2O_3 (4.61–21.77 wt.%), Cr (5–194 ppm), and Ni (8–120 ppm; Table A4.6; Fig. 70). Magnetite-rich rocks are enriched in Fe_2O_3 (e.g. 493103) and quartz-rich rocks (e.g., 485499) have higher silica contents. Samples having large amount of garnet and mica (e.g., 493105, 493106) have high Al_2O_3 contents. Mg-numbers range from 0.08 to 0.45. Al_2O_3/TiO_2 ratios are dominantly sub-chondritic, whereas Zr/Y ratios are superchondritic (Table A4.6). Garnet, mica, kyanite, and feldspar-rich rocks have LREE-enriched patterns (La/Ybcn=4.0–26.6), with negative to positive Eu (Eu/Eu*=0.54–1.18) anomalies (Fig. 70; Table A4.6). On a primitive mantle-normalised diagram, these samples have negative Nb (Nb/Nb=0.20–0.42), Ti (Ti/Ti*=0.20–0.49), and minor negative to positive Zr (Zr/Zr*= 0.94–1.38) anomalies (Fig. 70). Mineralogical and geochemical compositions indicate that they were derived from quartz- and feldspar-rich protoliths, such as quartz sandstones and greywacke sandstones. Quartz rich sediments in modern Earth form mainly in passive continental margins. LREE-enriched

REE patterns and negative Nb and Ti anomalies indicate a magmatic arc, or continental source area. The lower Al_2O_3/TiO_2 (8–27) ratios and variably high TiO_2 (up to 2.54), are however, inconsistent with a typical continental source area (see Taylor & McLennan, 1995). High Ni and Cr contents in some samples are consistent with a mafic source region.

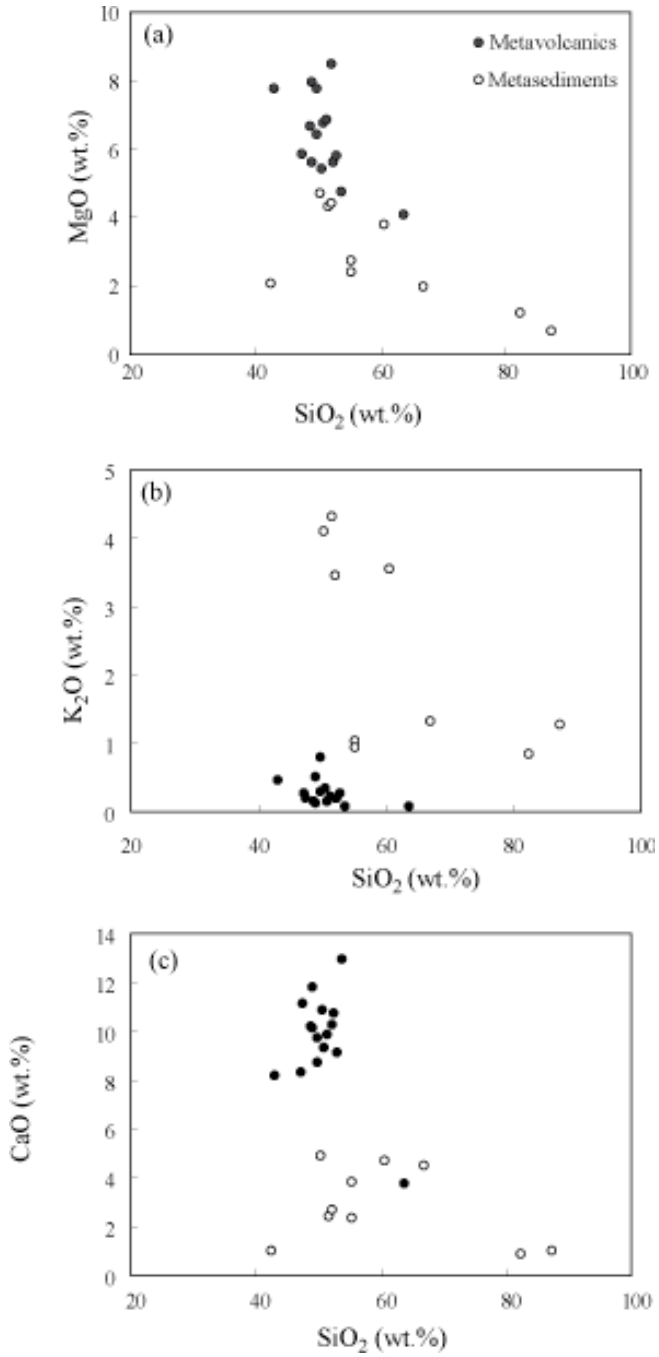

Figure 67. *Major element plots for metavolcanic and metasedimentary rocks of the Storø greenstone belt.*

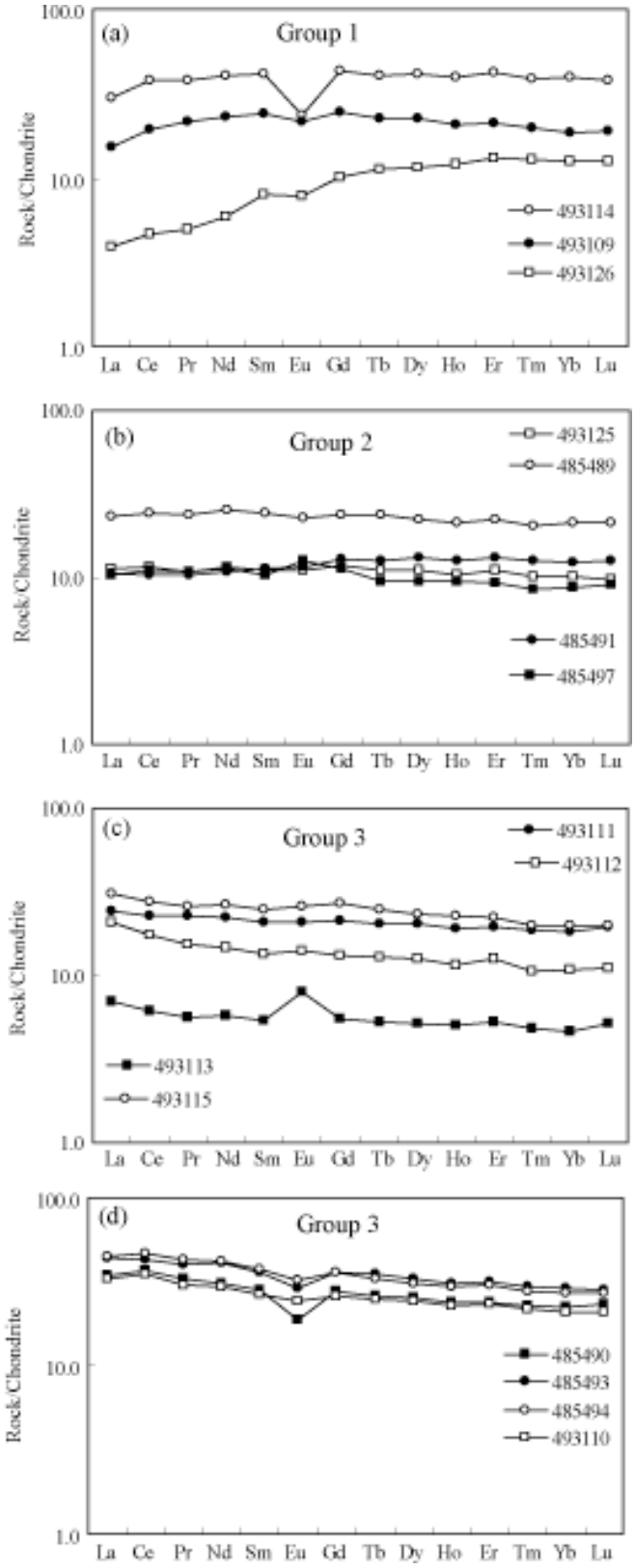

Figure 68. *Chondrite-normalised REE patterns of metavolcanic amphibolites in the Storø greenstone belt.*

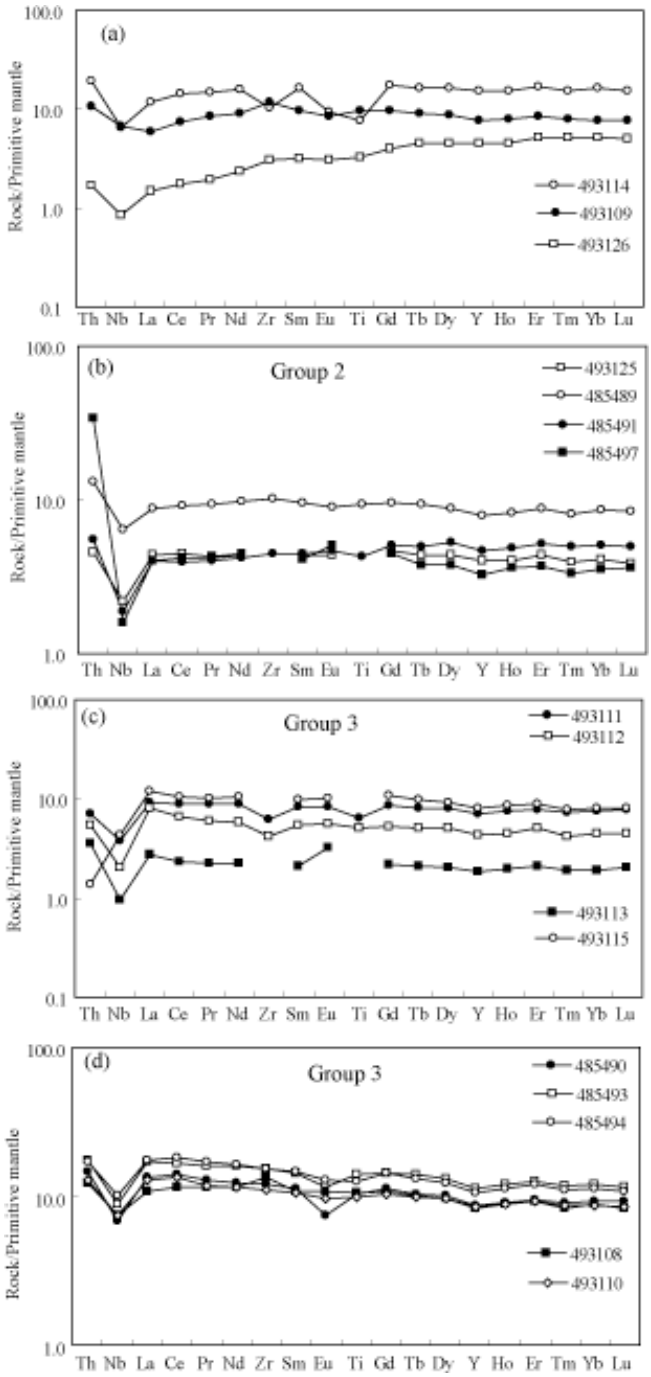

Figure 69. *Primitive mantle-normalised trace element patterns of metavolcanic amphibolites in the Storø greenstone belt.*

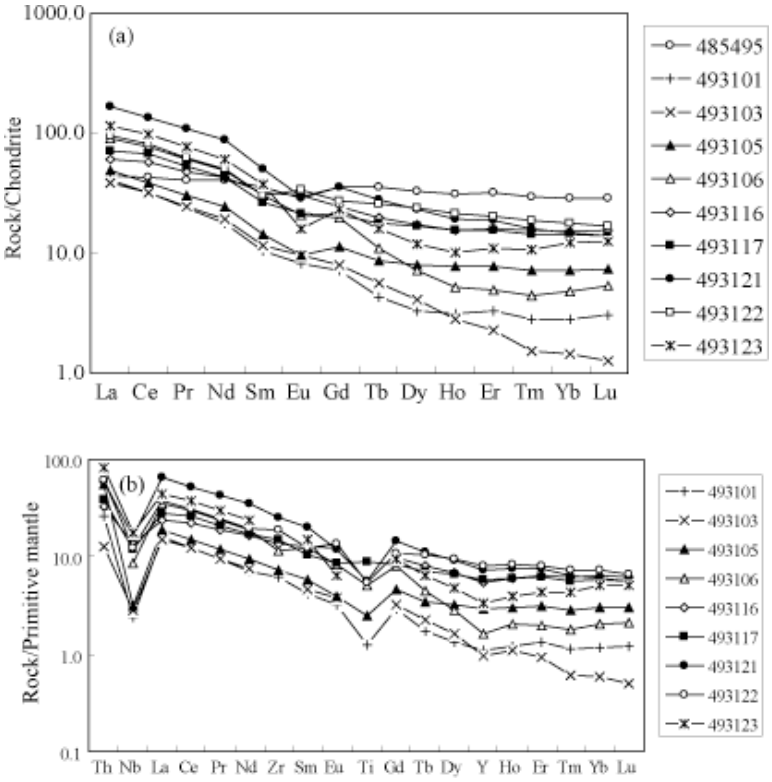

Figure 70. *Chondrite- and primitive mantle-normalised REE and trace element patterns (respectively) of metasedimentary rocks in the Storø greenstone belt.*

Preliminary interpretation of the mineral deposits

Epidosites are well documented in Phanerozoic supra-subduction zone ophiolites (Richardson et al. 1987; Schiffman et al. 1987; Harper et al. 1988; Nehling et al. 1994). Field and petrologic studies of epidosite-bearing Phanerozoic ophiolites suggest that epidosites form in upflow zones at the base of ore-forming hydrothermal system. Accordingly, epidosites represent the pathways of discharging hydrothermal fluids that ultimately resulted in massive sulphide deposition at the seawater/seafloor interface. As a result, the identification of epidosites can be a useful exploration tool for the location of massive sulphide deposits in the Ivisaartoq belt.

The Storø greenstone belt contains gold mineralisation (Appel 1990; Appel et al. 2000). Analyses of metavolcanic and metasedimentary rocks indicate that gold is concentrated in amphibolites, with a subduction zone geochemical signature, above the garnet-feldspar-mica-quartz-schists (Table A4.7). Foliation in amphibolites is cut by quartz veins, suggesting gold was precipitated after the development of major foliation. Most samples record evidence of retrograde metamorphism. Kyanite has been replaced by biotite and hornblende, suggesting that pressure of the metamorphism decreased during retrogression. The lower pressure metamorphic conditions may have resulted from uplifting and unroofing of the belt during terrane accretion in the late Archaean. Formation of dilatational quartz veins and gold mineralisation may have associated with this tectonic event.

Geochemistry

Agnete Steenfelt
Geological Survey of Denmark and Greenland

This section describes and discusses chemical analytical data for rock samples collected during the fieldwork in 2004. Results of preliminary analyses of a total of 258 rock samples were presented in the report by Hollis et al. (2004). New analytical data have been obtained in the first half of year 2005, and they are all included in the tables of the ArcView© project stored on the DVD accompanying the present report. The data acquired and compiled during the project represents a considerable increase in available chemical data for the Godthåbsfjord region, which is useful to future investigations. Presently, the new data are used to recognise geochemical signatures related to the origin and alteration of metavolcanic units within the greenstone belts.

Acquisition of new analytical data

The previously obtained analytical data (Hollis et al. 2004) did not include major element oxide compositions. Such analyses have now been performed at Rock Geochemical Laboratory, GEUS, using X-ray fluorescence spectrometry (XRF) on glass discs (sodium borate flux) and atomic absorption spectrometry (AAS) for Na. In total, 221 samples collected in various parts of the greenstone belts of the Godthåbsfjord region were analysed. In addition, 21 samples from the greenstone belt east of Qussuk (Qussuk peninsula) have been analysed at GEUS for trace elements by inductively coupled plasma mass spectrometry (ICPMS) upon dissolution of fused discs, and 110 samples from Ivisaartoq and Storø have been analysed for major and trace elements at Windsor University Canada and Activation Laboratories Ltd. using ICPMS upon dissolution of fused samples (see report by Ali Polat, this volume, for more details about analytical methods). Figure 71 shows the location of the samples analysed for this report, and Table 1 lists the elements and components determined. As a result of the application of several methods of analysis, some elements have been determined by more than one method with slightly different results, but no serious bias was discovered. The quality varies, see Table 1.

Data available on the DVD

Three datafiles are included in the ArcView©-project on the DVD. The file '2005GEUS_data' contains the new XRF and AAS data for the 221 samples together with the 2004-data for the same samples derived from instrumental neutron activation (INA) and inductively coupled plasma emission spectrometry (ICPES) at Activation Laboratories Ltd. The present compilation also involves data on samples from Storø, that were obtained by GEUS in 2004. The file '2005Windsor_data' contains major and trace element data from Windsor University Canada, and '2005Qussuk_data' both major and trace elements deter-

mined in 2005. Thus, major element data for the 21 selected samples from Qussuk peninsula occur in both '2005GEUS_data' and '2005Qussuk_data'. Trace element data from samples collected by Bjørn Thomassen and Henrik Stendal (both GEUS) were included in the files presented in 2004, but these samples have not been analysed further and their data are not included in the view named '2005Geochemistry'.

In the data file '2005geus_data' on the DVD, concentrations that are below the lower limit of detection for the analytical method are given in two ways, depending on the data source. In data supplied by GEUS, not detected is given as '0'. In data from Activation Laboratories Ltd. they are given as negative numbers, the numbers indicating the detection limit.

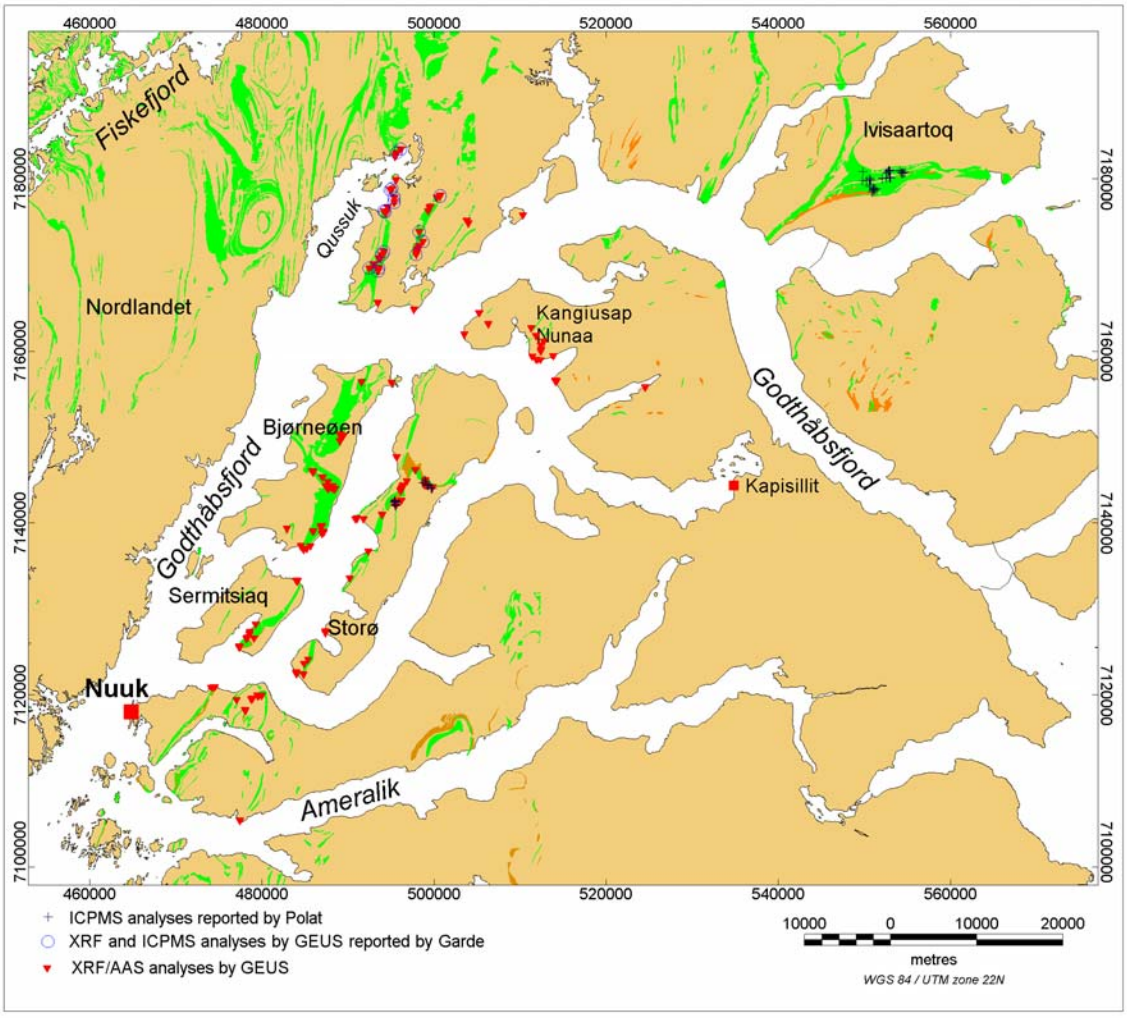

Figure 71. *Location of rock samples analysed in 2005 on map showing amphibolites in green and metasedimentary schists in brown.*

Significance and treatment of the new analytical data

The determination of the major element composition of the rock samples allows a general petrogenetic classification, which is important for the comparison of the rock assemblages of the greenstone belts in the Nuuk region with rock assemblages in present and past plate-tectonic environments. The separate reports by Ali Polat and Adam Garde illustrate the use of major and trace element data together with field observations to distinguish rocks formed at oceanic spreading ridges from those formed in volcanic island arcs. Whereas the major element data define the rock types, specific trace element characteristics, particularly rare earth element data, are used to recognise the plate-tectonic environment.

The major element data also reveal the character and degree of alteration that has affected many parts of the volcano-sedimentary sequences during and after their deposition. This aspect is also discussed in the reports mentioned above.

Chemical alteration

Two major types of alteration are recognised in the chemical data. The first, syn-depositional calc-silicate alteration, is also easily recognisable in the field and has been observed in variable intensity in all greenstone belts (Hollis et al. 2004; Polat this report). Mineralogically, it leads to formation of epidote and diopside at the expense of plagioclase, pyroxene and olivine, and chemically the alteration is reflected in high CaO relative to SiO_2 and MgO (Fig. 72). The regional distribution of samples with calc-silicate alteration is illustrated in Figure 73. Syn-depositional alteration also comprised introduction of sulphur leading to the formation of iron sulphides (now metamorphosed to pyrrhotite), but locally also Cu and Zn bearing sulphides (Fig. 74; see also Hollis et al. 2004). As remarked by Polat (this volume), syn-depositional alteration is typically developed in connection with the formation of volcanogenic massive sulphide deposits.

Post-depositional hydrothermal alteration may be related to granitic magmatism in which case the supracrustal units affected are enriched in K_2O (together with one or more of Ba, Rb, Th, U, La, Ce, Zr, Hf, Nb). Chemically, this alteration may be difficult to distinguish from enrichment in the same elements due to magmatic crystal fractionation, but increased concentration of any of those elements that occur uncorrelated with an increase in SiO_2 or decrease in MgO are likely to reflect alteration. Another kind of post-depositional alteration is related to hydrothermal percolation of shear and fracture zones and can lead to enrichment in silica, alkali feldspars, sulphides and/or calcium carbonate (enrichment in SiO_2, CaO, Na_2O, K_2O and/or S) and to deposition of elements such as Au, As, Sb, Bi, Cu, Sr, Ba. Figure 73 illustrates the distribution of granitic components in metavolcanic rocks.

2005geus data				**2005qussuk data**			**2005windsor data**		
Component	Unit	Method	Quality	Component	Unit	Method	Component	Unit	Method
SiO_2	%	XRF	very good	**SiO_2**	%	XRF	**SiO_2**	%	ICP-MS
TiO_2	%	XRF	very good	**TiO_2**	%	XRF	**TiO_2**	%	ICP-MS
Al_2O_3	%	XRF	very good	**Al_2O_3**	%	XRF	**Al_2O_3**	%	ICP-MS
Fe_2O_3	%	XRF	very good	**Fe_2O_3**	%	XRF	**Fe_2O_3**	%	ICP-MS
FeO	%	XRF	very good	**FeO**	%	XRF	**MnO**	%	ICP-MS
MnO	%	XRF	very good	**MnO**	%	XRF	**MgO**	%	ICP-MS
MgO	%	XRF	very good	**MgO**	%	XRF	**CaO**	%	ICP-MS
CaO	%	XRF	very good	**CaO**	%	XRF	**Na_2O**	%	ICP-MS
Na_2O	%	AAS	very good	**Na_2O**	%	AAS	**K_2O**	%	ICP-MS
K_2O	%	XRF	very good	**K_2O**	%	XRF	**P_2O_5**	%	ICP-MS
P_2O_5	%	XRF	very good	**P_2O_5**	%	XRF	**Volatiles**	%	LOI
Volatiles	%	LOI	very good	**Volatiles**	%	LOI	**Cr**	ppm	ICP-MS
V	ppm	XRF	acceptable	**Sc**	ppm	ICP-MS	**Co**	ppm	ICP-MS
Cr	ppm	XRF	acceptable	**V**	ppm	ICP-MS	**Ni**	ppm	ICP-MS
Ni	ppm	XRF	acceptable	**Cr**	ppm	ICP-MS	**Rb**	ppm	ICP-MS
Cu	ppm	AAS	very good	**Co**	ppm	ICP-MS	**Sr**	ppm	ICP-MS
Zn	ppm	XRF	acceptable	**Ni**	ppm	ICP-MS	**Cs**	ppm	ICP-MS
Rb	ppm	XRF	acceptable	**Zn**	ppm	ICP-MS	**Ba**	ppm	ICP-MS
Sr	ppm	XRF	acceptable	**Ga**	ppm	ICP-MS	**Sc**	ppm	ICP-MS
Y	ppm	XRF	poor	**Rb**	ppm	ICP-MS	**V**	ppm	ICP-MS
Zr	ppm	XRF	acceptable	**Sr**	ppm	ICP-MS	**Ta**	ppm	ICP-MS
Ba	ppm	XRF	acceptable	**Y**	ppm	ICP-MS	**Nb**	ppm	ICP-MS
Au	ppb	INA	acceptable	**Zr**	ppm	ICP-MS	**Zr**	ppm	ICP-MS
As	ppm	INA	acceptable	**Nb**	ppm	ICP-MS	**Hf**	ppm	ICP-MS
Ba	ppm	INA	poor precision	**Cs**	ppm	ICP-MS	**Th**	ppm	ICP-MS
Br	ppm	INA	acceptable	**Ba**	ppm	ICP-MS	**U**	ppm	ICP-MS
Co	ppm	INA	acceptable	**Hf**	ppm	ICP-MS	**Y**	ppm	ICP-MS
Cr	ppm	INA	acceptable	**Ta**	ppm	ICP-MS	**Cu**	ppm	ICP-MS
Cs	ppm	INA	acceptable	**Pb**	ppm	ICP-MS	**Zn**	ppm	ICP-MS
Hf	ppm	INA	acceptable	**Th**	ppm	ICP-MS	**Mo**	ppm	ICP-MS
Rb	ppm	INA	poor	**U**	ppm	ICP-MS	**Ga**	ppm	ICP-MS
Sb	ppm	INA	acceptable	**La**	ppm	ICP-MS	**Pb**	ppm	ICP-MS
Sc	ppm	INA	acceptable	**Ce**	ppm	ICP-MS	**La**	ppm	ICP-MS
Ta	ppm	INA	acceptable	**Pr**	ppm	ICP-MS	**Ce**	ppm	ICP-MS
Th	ppm	INA	acceptable	**Nd**	ppm	ICP-MS	**Pr**	ppm	ICP-MS
U	ppm	INA	acceptable	**Sm**	ppm	ICP-MS	**Nd**	ppm	ICP-MS
W	ppm	INA	poor	**Eu**	ppm	ICP-MS	**Sm**	ppm	ICP-MS
Zn	ppm	INA	poor	**Gd**	ppm	ICP-MS	**Eu**	ppm	ICP-MS
La	ppm	INA	acceptable	**Tb**	ppm	ICP-MS	**Gd**	ppm	ICP-MS
Ce	ppm	INA	acceptable	**Dy**	ppm	ICP-MS	**Tb**	ppm	ICP-MS
Nd	ppm	INA	acceptable	**Ho**	ppm	ICP-MS	**Dy**	ppm	ICP-MS
Sm	ppm	INA	acceptable	**Er**	ppm	ICP-MS	**Ho**	ppm	ICP-MS
Eu	ppm	INA	acceptable	**Tm**	ppm	ICP-MS	**Er**	ppm	ICP-MS
Tb	ppm	INA	mostly < d.l.	**Yb**	ppm	ICP-MS	**Tm**	ppm	ICP-MS
Yb	ppm	INA	acceptable	**Lu**	ppm	ICP-MS	**Yb**	ppm	ICP-MS
Lu	ppm	INA	acceptable				**Lu**	ppm	ICP-MS
Ag	ppm	ICP-ES	mostly < d.l.						
Be	ppm	ICP-ES	mostly < d.l.						
Bi	ppm	ICP-ES	mostly < d.l.						
Cd	ppm	ICP-ES	mostly < d.l.						
Cu	ppm	ICP-ES	good						
Mn	ppm	ICP-ES	good						
Mo	ppm	ICP-ES	good						
Ni	ppm	ICP-ES	good						
Pb	ppm	ICP-ES	good						
Zn	ppm	ICP-ES	good						
Sr	ppm	ICP-ES	good						
V	ppm	ICP-ES	good						
Y	ppm	ICP-ES	good						
S	%	ICP-ES	good						

Table 1. *Chemical components and elements determined in rock samples, units of concentration and analytical methods. LOI: loss on ignition. XRF: X-ray fluorescence spectrometry by GEUS. AAS: atomic absorption spectrometry by GEUS. INA: instrumental neutron activation by Activation Laboratories Ltd. ICP-ES: inductively coupled plasma emission spectrometry upon 4-acid solution of powder by Activation Laboratories Ltd. ICP-MS: inductively coupled plasma mass spectrometry upon acid solution of fused powder, see Polat (this volume) for details on source. d.l.: detection limit.*

Grouping of metavolcanic rocks

The major element data for metavolcanic and volcanogenic metasediments have been screened to exclude samples with obvious signs of alteration. The screened data comprise rocks of ultrabasic to dacitic compositions. Samples with ultrabasic compositions have been collected in all parts of the greenstone belts rocks, but their chemistry is not treated further in this section. The rocks of basic to intermediate compositions have been divided into two groups, basaltic metavolcanics and andesitic-dacitic metavolcanics on chemical criteria in combination with the field descriptions. Basic metavolcanics have SiO_2 between 46 and 56 %, and MgO between 3.5 and 10 %. In the group of more SiO_2-rich metavolcanic rocks (comprising the fragmental grey amphibolites of Qussuk peninsula), SiO_2 is between 54 and 65 %, and MgO between 6 and 1.5 %. Samples with Al_2O_3 above 18 % are excluded from both groups, as they are likely to include a high proportion of non-volcanogenic material. The regional distribution of grouped samples (Fig. 75) shows that rocks with andesitic composition have been identified in all parts of the greenstone belts except at Ivisaartoq.

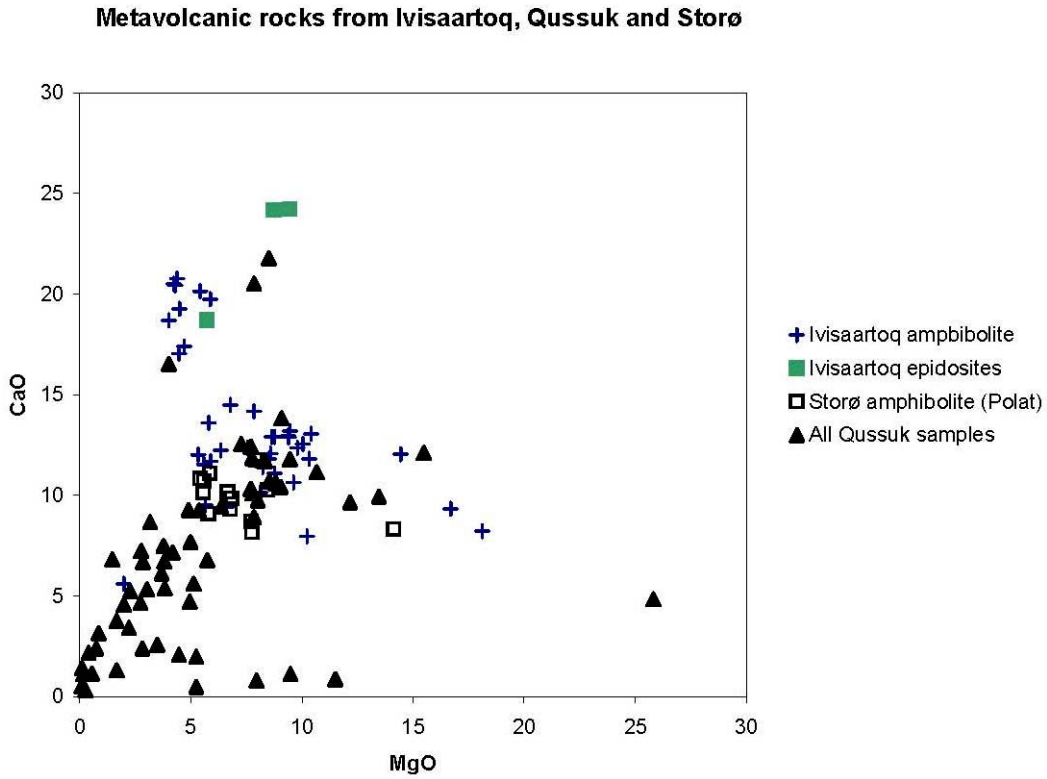

Figure 72. *Diagram of MgO-CaO variation with samples of metavolcanic rocks from Ivisaartoq, Storø and Qussuk peninsula (see Polat, this volume, and Garde, this volume). Normal volcanic rocks exhibit correlated MgO-CaO variation. Samples selectively enriched in CaO have suffered calc-silicate alteration. Samples with high MgO are ultramafic, and samples from Qussuk with very low CaO and variable MgO are enriched in sulphide and/or garnet and quartz, and they are considered by Garde (this volume) to be volcanogenic-exhalative or hydrothermally altered rocks.*

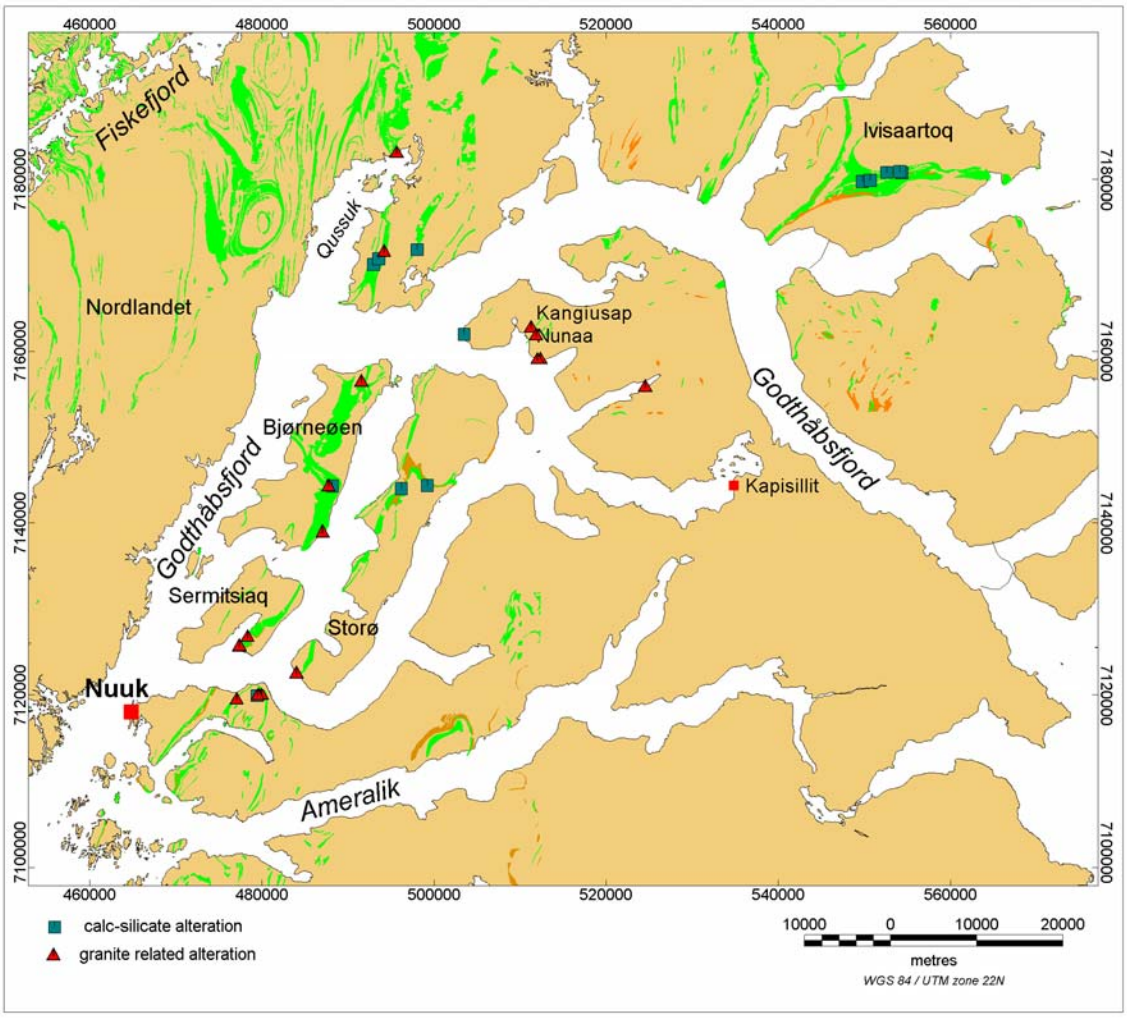

Figure 73. *Location of samples showing chemical alteration suggesting either syn-depositional calc-silicate alteration or alteration associated with granitic magmatism.*

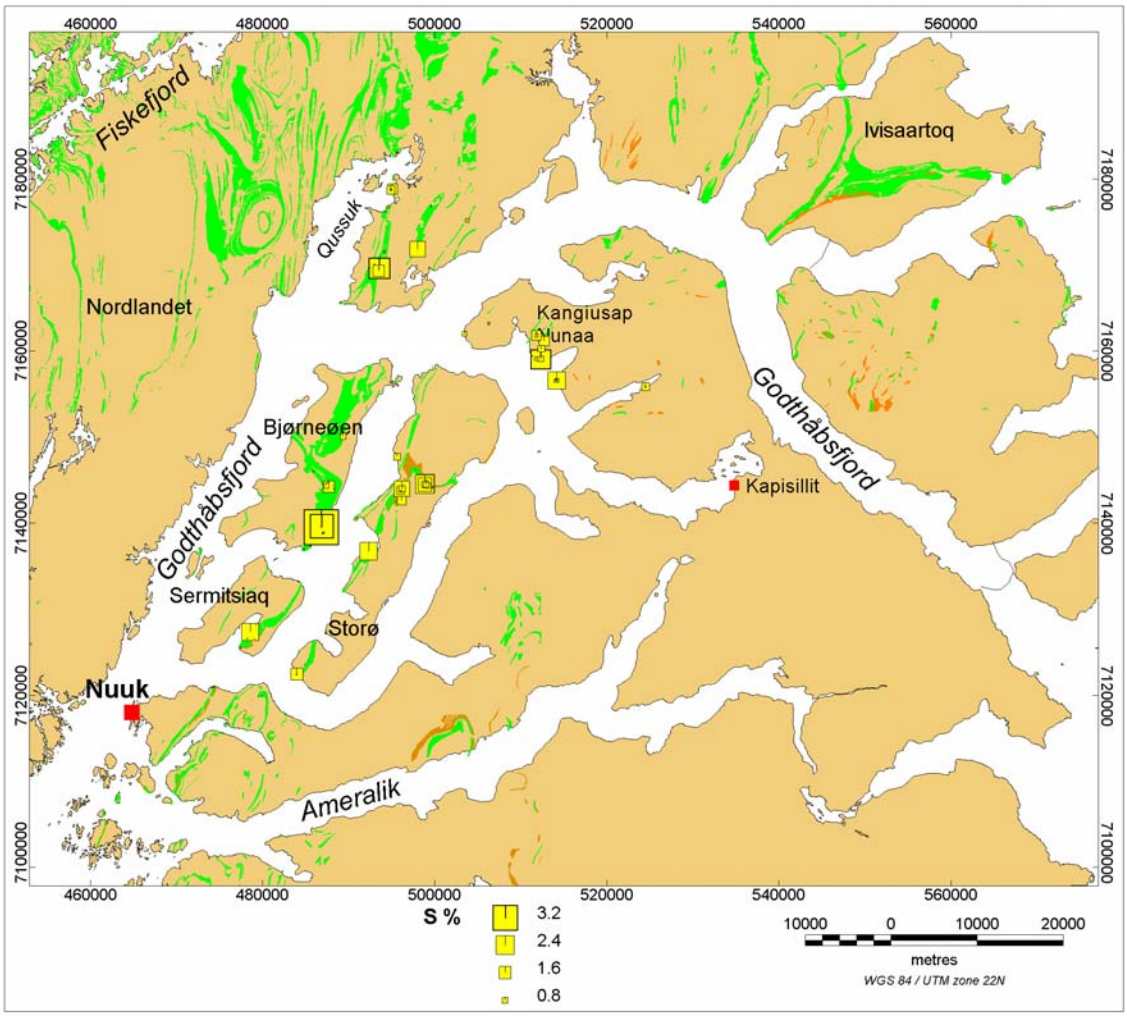

Figure 74. *Distribution of sulphur in rock samples. Samples from Ivisaartoq have not been analysed for sulphur, but sulphide mineralisation is also known from that area (Appel et al. 2003).*

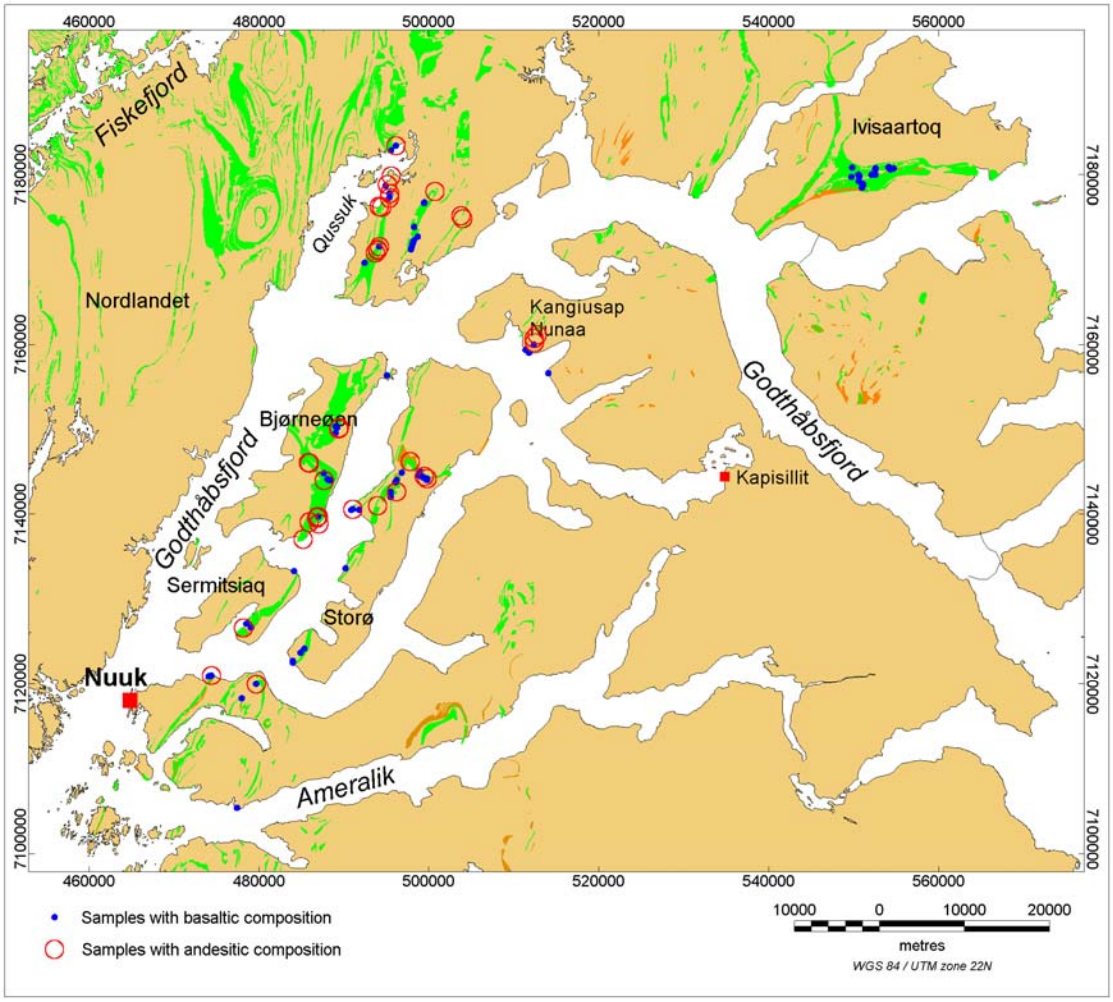

Figure 75. *Distribution of metavolcanic rock samples chemically divided into basaltic and andesitic-dacitic compositions.*

Rare earth element characterisation of metavolcanic rocks

In the interpretation of trace element data for metavolcanic rocks, Polat and Garde use the widely accepted notion that the shape of the chondrite normalised REE spectra is very important in recognising the petrogenetic setting of the volcanic rocks. Simply stated, flat spectra characterise ocean floor and spreading ridge environments and steeper spectra suggest volcanic arc environments. As demonstrated in the section on geochemistry in Hollis et al. (2004), the previously obtained REE data by INA, although giving useful indications, were not entirely satisfactory to define reliable REE spectra. Therefore, it is very valuable to have the improved REE data for the samples from Ivisaartoq, Storø and Qussuk peninsula. A plot of data for La and Yb, respectively, shows good correlation between the INA data obtained in 2004 and ICPMS data obtained in 2005 (Fig. 76). Although the limited number of REE determined by INA and the problems of determining very low concentrations do not allow the construction of full chondrite normalised spectra for most of the samples, it is now justified to use at least La and Yb data. These data will provide informa-

tion on the slope of the spectra or the degree of fractionation between light REE and heavy REE.

Figure 77 shows La-Yb scatter diagrams for rocks discussed by Garde (this report) and Polat (this report) and metavolcanic rocks from Bjørneøen and Storø. Based on chondrite and primitive mantle normalised trace and REE spectra many Ivisaartoq and some Qussuk amphibolites were shown to have ocean floor and oceanic spreading ridge characteristics. These samples (Ivisaartoq and Qussuk amphibolites in Fig. 77) plot in the low La – low Yb part of the upper diagram. Trace and REE variations for andesitic rocks from Qussuk and basaltic rocks from Storø suggest they were generated in island arc settings. The La-Yb diagrams show that samples from Storø exhibit correlated La-Yb variation, while the andesitic rocks from Qussuk exhibit preferential La-enrichment. The lower diagram comprises samples of metavolcanic rocks and volcanogenic metasediments from Bjørneøen and Storø analysed for La and Yb in 2004. The general La-Yb variation in the lower diagram resembles that of the upper diagram, which is taken to indicate that both greenstone belts comprise rocks from different plate-tectonic settings. The implication is that volcanic rock assemblages of different origin have been intercalated tectonically either during plate convergence and/or during the later continent assembly.

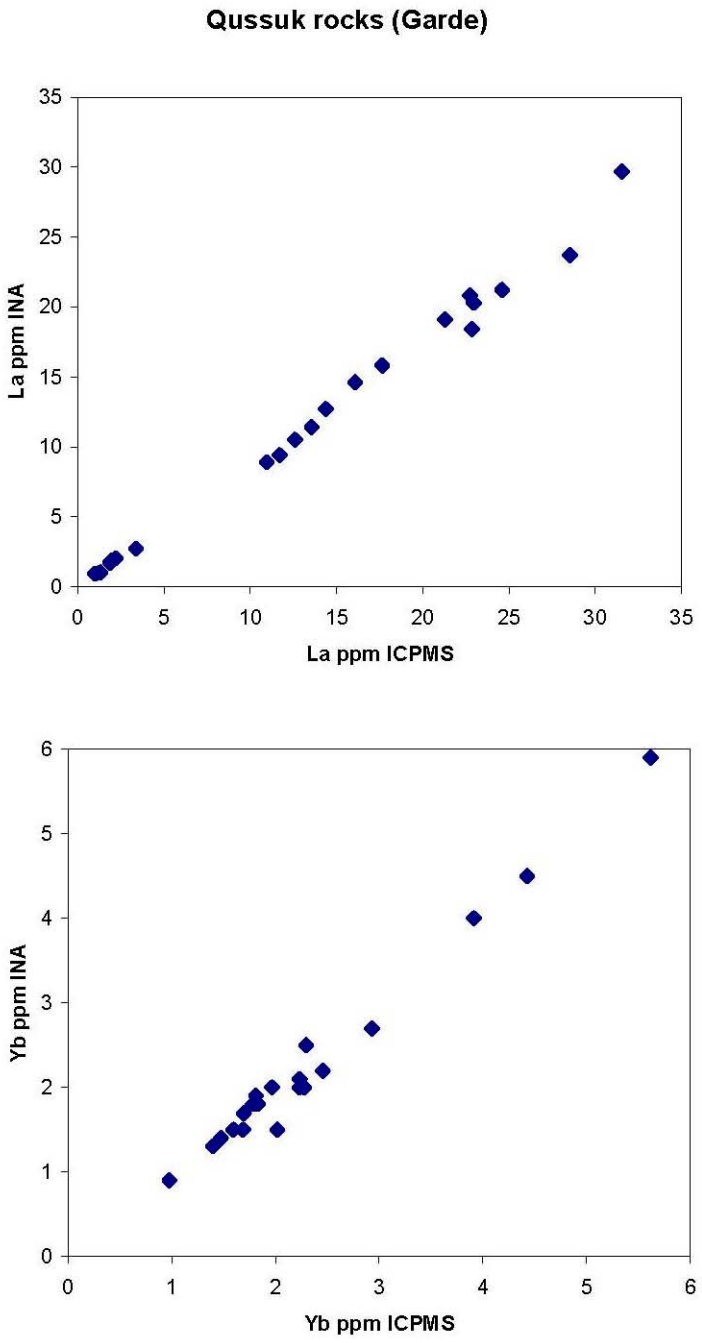

Figure 76. *Correlation of La (upper diagram) and Yb (lower diagram) values determined by two different analytical methods, inductively coupled plasma mass spectrometry on dissolved fused samples (ICPMS) and instrumental neutron activation (INA). The samples are 21 metavolcanic rocks from Qussuk peninsula, see Garde this report.*

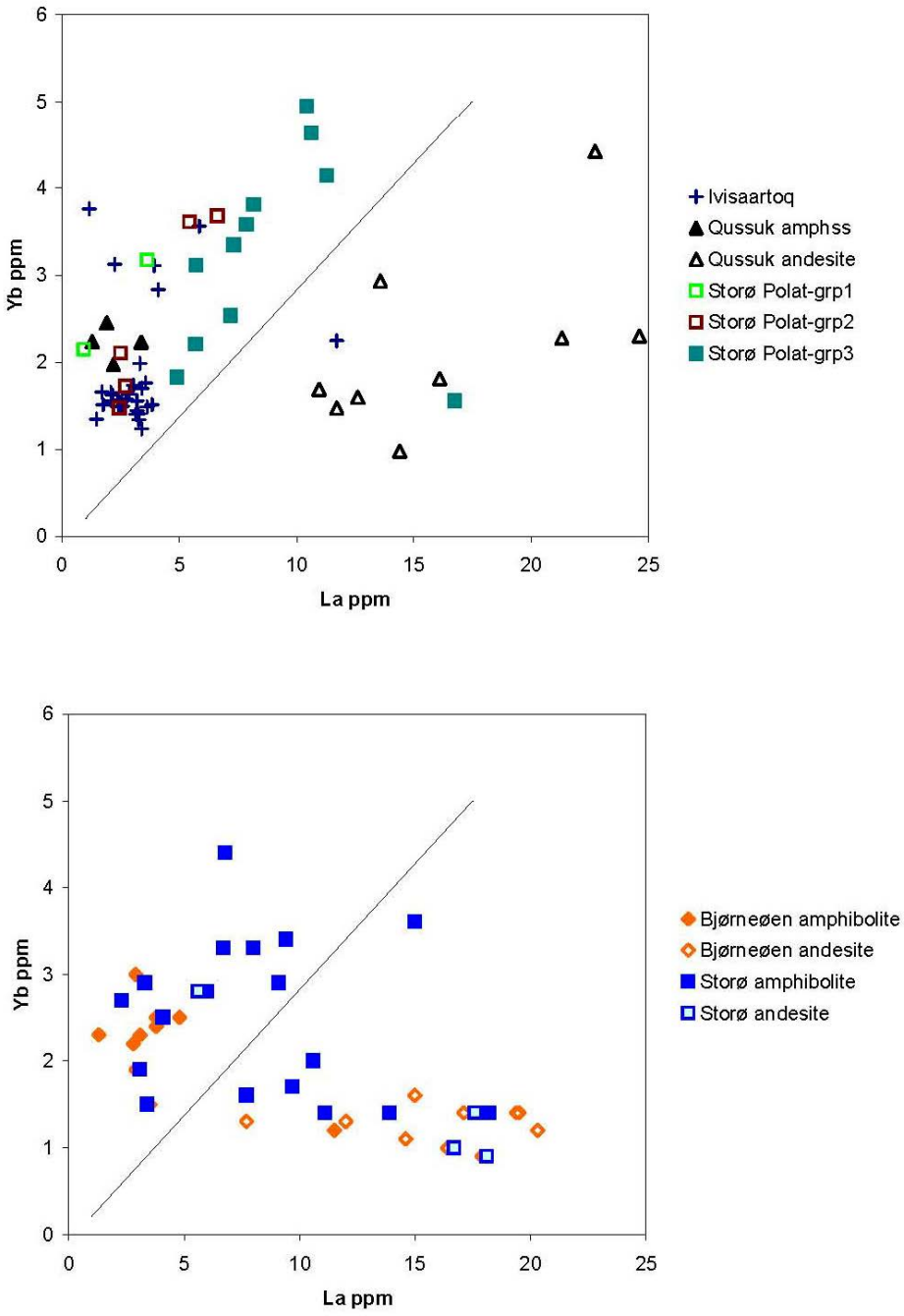

Figure 77. *La-Yb variation diagrams for metavolcanic rocks from the central Godthåbsfjord region. The upper diagram shows the position of rocks interpreted to have formed in different plate-tectonic environments. Samples from Ivisaartoq and amphibolites (s.s.) from Qussuk peninsula (Qussuk amphibolites) are from ocean floor or oceanic spreading ridge environments. Amphibolites from Storø, divided into three groups by Polat (this volume), as well as andesitic rocks (fragmental metavolcanic rocks, see Garde this volume) from Qussuk are interpreted to have formed in volcanic island arc environments. The lower diagram displays data from metavolcanic rocks on Bjørneøen and Storø divided into basaltic (amphibolite) and andesitic compositions. Amphibolites and andesitic rocks from Bjørneøen plot in the same parts of the diagram as the corresponding rocks from Qussuk.*

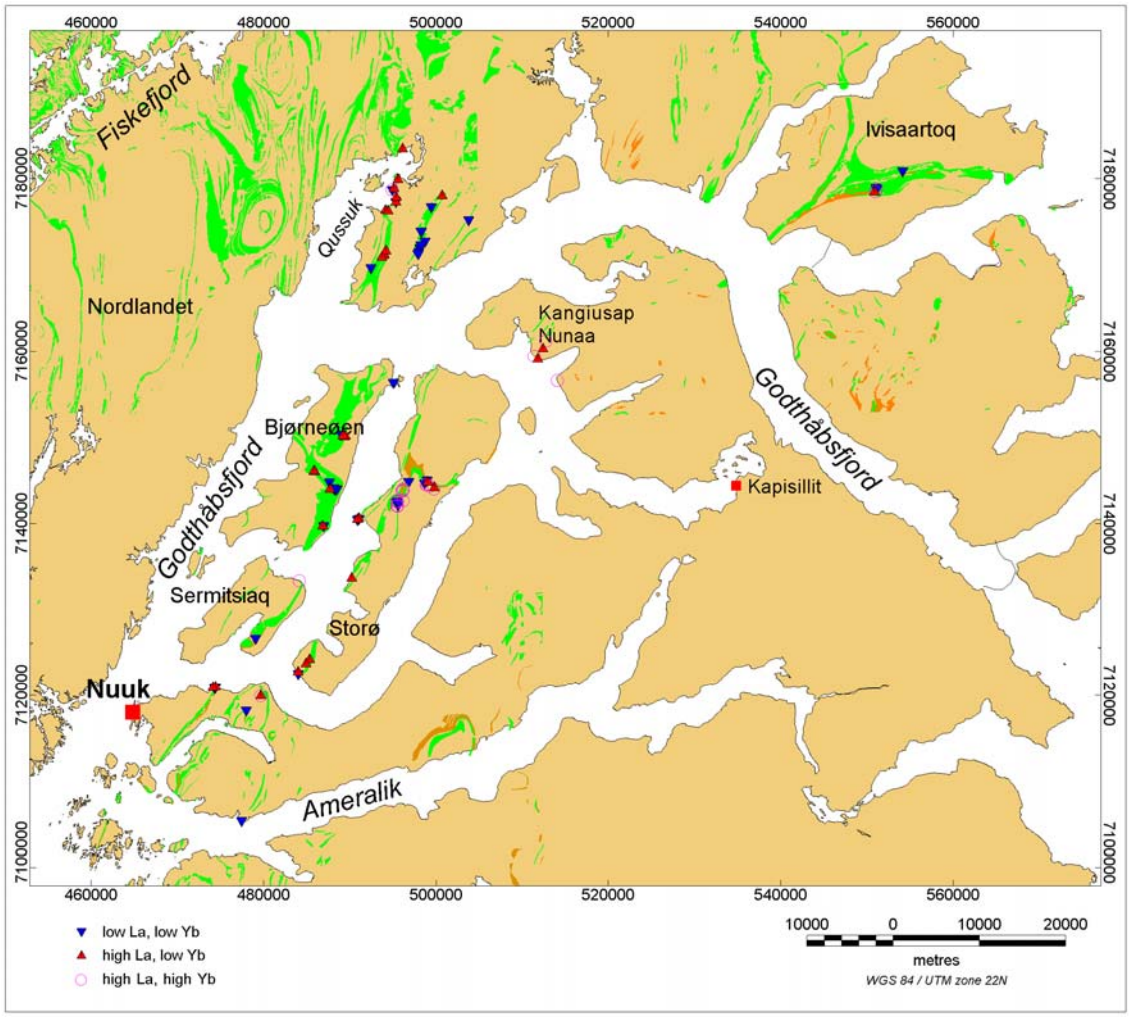

Figure 78. *Regional distribution of metavolcanic rocks with different La-Yb characteristics (see Figure 77). The first group (low La, low Yb) probably represents rocks from oceanic environments, while the other two groups likely formed in volcanic island arc environments. All parts of the greenstone belts, although probably of different ages, seem to host volcanic rocks formed in island arc environments.*

Conclusion

The chemical data resulting from analytical work of the present project have increased the geochemical data base for the Godthåbsfjord region considerably, and have provided important evidence for the origin of volcanic members of the greenstone belts. The chemistry of samples of metavolcanic and volcanogenic metasediments from the greenstone belts of the central Godthåbsfjord region show that basaltic and ultrabasic compositions are found in samples from all parts of the belts, while andesitic compositions are not registered in Ivisaartoq. Rock samples from the each of the greenstone belts exhibit chemical variations that may be assigned to both syn-depositional and post-depositional alteration. La-Yb variation in metavolcanic rocks of basaltic and andesitic compositions compared to more elaborate REE and trace element data from Qussuk peninsula and Ivisaartoq and Storø suggest that the Bjørneøen-Sermitsiaq belt hosts volcanic rocks of both ocean floor and

island arc origin, thereby resembling the situation in the Qussuk belts. The Storø belt, likewise, hosts volcanic rocks derived from oceanic floor and arc setting, although this belt differs from the Bjørneøen-Sermitsiaq belt in age and general lithology.

Metamorphic petrology

Garnet amphibolites and garnet-mica schists: petrography, mineral chemistry and thermobarometry

[1]Julie A. Hollis and [2]Mac Persson
[1]Geological Survey of Denmark and Greenland
[2]University of Copenhagen

Hollis et al. (2004) gave an overview of the field geology of the main supracrustal lithologies in the central Godthåbsfjord region including a brief discussion of their mineralogy and metamorphic facies. On the basis of field observations and previous work in the region, amphibolites facies metamorphism is though to have affected the southern part of the Akia terrane in the mid Archaean (c. 2970–2970 Ma). Late Archaean amphibolite facies metamorphism of the Storø greenstone belt and surrounding early and late Archaean orthogneiss is likely occurred during amalgamation of different crustal terranes at c. 2700 Ma (eg. Nutman et al. 1989). Amphibolite facies metmorphism and emplacement of abundant granitic pegmatites in the central Godthåbsfjord region is also recorded at c. 2630 (Hollis et al., this volume).

Here we present data from a selection of metavolcanic and metasedimentary samples from Sermitsiaq, Bjørneøen, the Nuuk peninsula, and Storø, for the purpose of investigating the metamorphic history of supracrustal rocks in the central Godthåbsfjord region. The locations of sample discussed are shown in Figure 79. Descriptions of samples analysed along with thermobarometry results are given in Table 2. Representative mineral chemical analyses are given in Table 3.

Figure 79. *Locations of petrology samples discussed in this section.*

Sample settings and lithologies

Bjørneøen greenstone belt

The Bjørneøen greenstone belt is dominantly comprised of compositionally layered amphibolite interpreted as former basaltic flows (in some cases relict pillows are preserved in low strain domains). They also comprise widespread fragmental heterogeneous intermediate composition amphibolite interpreted as deformed and metamorphosed pyroclastic and volcanoclastic rocks. The amphibolites of the Bjørneøen greenstone belt typically hold schistose fabrics defined by hornblende ± biotite with plagioclase-quartz-titanite ± garnet ± epidote ± diopside ± calcite. These include locally preserved early layer-parallel foliations with associated mineral lineations (typically defined by hornblende) and early isoclines. These are deformed by broad NE-striking high strain zones with associated NW-plunging mineral

lineations, tight folds, and NW-directed thrusts. Locally retrogression to greenschist facies has occurred. In some cases early fabrics are overprinted by greenschist facies NE-striking, E-dipping mylonites.

Storø greenstone belt

The Storø greenstone belt is a tectonically dismembered belt of mafic amphibolite, intermediate amphibolite, ultrabasic rocks, garnet-mica schists or gneiss and quartzite. A thin sequence of heterogeneous layered felsic metavolcanics and metasedimentary rocks at the structural base of the Bjørneøen greenstone belt is now know to be late Archaean and likely correlates with the late Archaean greenstone sequence on Storø and the Nuuk peninsula. The main gneissic fabric in the Storø greenstone belt is at least second generation and commonly has associated foliation-parallel leucosomes. This is overprinted by the Storø shear zone fabric and associated major fold structures. The shear zone fabric is defined by sillimanite-bearing assemblages in the garnet-mica schists.

Amphibolites

Sermitsiaq and Bjørneøen

Amphibolites examined from near the structural base of the Bjørneøen greenstone belt on Sermitsiaq and Bjørneøen are typically garnet-absent. However, calc-silicate layers containing garnet, diopside, and epidote ± titanite ± calcite are locally present. In some cases mafic amphibolite contains small red garnets dispersed throughout the rock. Three samples of garnet-bearing amphibolites from Sermitsiaq were targeted for the purpose of contraining P-T conditions of formation of equilibrated garnet-bearing schistose hornblende-plagioclase-quartz assemblages. Garnet-bearing mafic amphibolites are typically medium-grained with a moderate foliation defined by hornblende ± biotite. They are commonly quartz-bearing and relatively poor in plagioclase. Medium-grained garnets typically have inclusions of ilmenite, apatite, and quartz. Garnet occurs in equilibrated textures with hornblende, biotite, plagioclase, and quartz ± epidote ± titanite, and accessory ilmenite and apatite. Where calc-silicate lenses are present these are composed of medium- to coarse-grained garnet and diopside. Titanite, epidote, and calcite are also common in calc-silicate layers. Diopside and plagioclase in these layers are in some cases separated by symplectites of epidote and hornblende, consistent with partial retrogression.

Storø and the Nuuk peninsula

Mafic amphibolites examined on Storø and the Nuuk peninsula are typically medium-grained and hold a moderate to strong schistose fabric defined by hornblende ± biotite and typically with equilibrated assemblages of hornblende-quartz-plagioclase ± biotite ± garnet ± epidote with accessory ilmenite. Garnet porphyroblasts are typically inclusion-poor and in many cases have partial plagioclase rims. In some cases they show partial to complete breakdown textures to plagioclase ± hornblende ± biotite ± epidote.

Metasedimentary rocks

Garnet-mica schists were collected from Sermitsiaq and Storø. These preserve an early schistose fabric (in some cases gneissose) defined by medium- to coarse-grained garnet-biotite-plagioclase-quartz ± sillimanite ± cordierite ± muscovite. On Storø these rocks host foliation-parallel leucosomes that often contain garnet and/or cordierite (481255, 481465). Aligned biotite-sillimanite ± muscovite typically wrap garnet porphyroblasts. In two samples from Sermitsiaq (479309, 479317) garnet porphyroblasts contain staurolite, ilmenite, and biotite inclusions. In samples from Storø ilmenite often defines an early foliation discordant to that in the matrix. In some cases cordierite is present as a medium-grained matrix phase in textural equilibrium with garnet-biotite-plagioclase-quartz ± sillimanite ± muscovite (e.g. 481465). In a sample from Storø (481255) matrix biotite shows very fine-grained partial breakdown to cordierite. Also, in some cases garnet porphyroblasts show limited development of fine-grained staurolite, sillimanite, or biotite (465005, 481255). Within the Storø shear zone garnet porphyroblasts in garnet-mica schists typically overgrow an early fabric, consistent with their formation during development of the shear zone fabric. These garnets show optical zonation with inclusion-free cores, surrounded by an inclusion-rich rim, in turn surrounded by an inclusion-poor outer rim. Limited replacement of garnet, biotite, and cordierite by chlorite during retrogression is apparent in samples from Sermitsiaq (479317) and Storø (481465). In some cases chlorite defines a crenulation cleavage.

Mineral chemistry

Quantitative mineral compositions were determined and element maps collected using the University of Copenhagen JEOL Superprobe electron microprobe using standard operating conditions of 25nA, 15kV and a spot size of 3μm. Data were processed using standard ZAF correction procedures. Mineral compositional abbreviations given below are as follows: XAn = Ca/[Ca+Na], XSps = Mn/[Fe^{2+}+Mg+Ca+Mn], XAlm = Fe^{2+}/[Fe^{2+}+Mg+Ca+Mn], XPyp = Mg/[Fe^{2+}+Mg+Ca+Mn], XGrs = Ca/[Fe^{2+}+Mg+Ca+Mn], XMg = Mg/[Fe^{2+}+Mg].

Table 2. *Sample descriptions and THERMOCALC PT data at 1 σ uncertainty.*

Sample	Latitude	Longitude	Location	Lithology	Description	THERMOCALC assemblage	P (kb)	T (C)
479311	64 15.296	-51 28.033	Sermitsiaq	G-bearing amphibolite	Med-grained foliated g-bearing amphibolite with g, hbl, bi, q, and pl in equilibrated textures.	g-bi-hbl-pl-q-H_2O	4.7 1.0	521 43
479334	64 15.914	-51 27.064	Sermitsiaq	G-bearing amphibolite	Equilibrated med-grained g-hbl-bi-pl-q amphibolite. G has inclusions of ilm-ap-qtz. Ilm and ap are also common accessory phases in the matrix.	g-bi-hbl-pl-q-H_2O	5.2 1.1	590 46
479339	64 12.827	-51 31.801	Sermitsiaq	G-bearing amphibolite	G-bearing calc-silicate lense in med-grained amphibolite. Med-grained assemblage of g-cpx-tit-cc-pl-q-ilm-zo-ep. Cpx-pl are separated by ep. Zo is late, overgrowing the foliation defined by hbl.	g-ep-pl-hbl-di-q-H_2O	6.1 0.7	624 28
479318	64 15.36	-50 45.858	Sermitsiaq	G-bi schist	Med-grained g-pl-bi-q schist. G porphyroblasts have st-bi-ilm inclusions. St is not present in the matrix, which consists of g-bi-pl-q-to.			
479057	64 22.546	-51 16.14	Bjørneøen	G-bearing amphibolite	Med-coarse grained g-bearing intermediate composition amphibolite from isoclinal fold hinge in heterogeneous layered supracrustal package. Matrix g-hbl-q-ep-ilm-ap in equilibrated textures. Very little pl.	g-hbl-pl-ep-q-H_2O	6.1 1.0	579 42
479011	64 12.33	-51 25.148	Nuuk peninsula	G-bearing amphibolite	Med-grained g-hbl-pl-q amphibolite with partial pl-q rims on g.	g-bi-hbl-pl-q-H_2O	7.6 1.3	712 58
481235	64 24.202	-51 05.667	Storø	G-bearing amphibolite	Med-grained g-bearing amphibolite with the assemblage g-hbl-q-pl-ilm-bi-ep. Large g porphyroblasts show partial breakdown to pl-bi-ep.	g-hbl-pl-q-H_2O	5.2 1.2	571 52
479309	64 15.296	-51 28.033	Sermitsiaq	G-bi schist	Med-grained g-bi-hbl-pl-q schist. Large g porphyroblasts have st-ilm-ap-q inclusions.			
479315	64 26.36	-51 17.559	Sermitsiaq	G-bi schist	Med-grained g-bi schist with g, bi, mu, and q in equilibrated textures. Also has Zn spinel is equilibrium with matrix assemblage.	g-bi-mu-pl-q-H_2O	5.2 1.0	589 27
479317	64 15.36	-50 45.858	Sermitsiaq	G-bi-sill schist	Med-grained g-pl-sill-q schist with foliation defined by fine-grained bi-sill-mu, which wraps g. G porphyroblasts contain st-ilm-q inclusions with an early fabric defined by ilm inclusions. St is not present in the matrix. Matrix is crenulated with chl developed along a crenulation cleavage.			
481255	64 23.584	-51 07.570	Storø	G-bi-sill gneiss	High-strain med-grained g-bi-sill-pl-q-ilm gneiss. G has inclusions of ru, qtz, zrn. The oxide phases in the matrix are ilm-py. Matrix bi shows partial breakdown to fine-grained cd. Fine-grained st-cd has formed on pl rims adjacent to qtz and bi, and fine-grained st has formed on g rims. G and bi have partial necklaces of ilm.	g-bi-sill-pl-q-H_2O	4.5 1.6	548 101
481465	64 23.672	-51 07.557	Storø	G-bi-sill gneiss	Med-grained g-bi-sill-cd-pl-q gneiss. G porphyroblasts have inclusions of bi-q-zrn-ru. Foliated med-grained matrix g-cd-bi-sill-pl-q in equilibrated textures. Ilm is the matrix oxide phase.	g-bi-sill-pl-q-H_2O	5.1 0.8	620 73
465003	64 24.547	-51 05.666	Storø	G-bi schist	Med-grained g-bi-pl-q schist with bi foliation. G forms large euhedral porphyroblasts with partial breakdown textures to st, sill, bi. G porphyroblasts show zonation: homogeneous core rimmed by inclusion-rich zone (ilm-ap-qtz), rimmed by inclusion-free zone. Ilm inclusions define foliation discordant to matrix bi foliation. Matrix bi-pl-q-sill-to.			
465005	64 24.547	-51 05.687	Storø	G-bi schist	Med-grained g-bi-pl-q-sill-st schist with bi foliation. Matrix pl-bi-qtz. Pl shows undulose extinction and partial recrystallisation. Large g porphyroblasts have poikiloblastic cores surrounded by inclusion-free outer cores, in turn rimmed by a heterogeneous inclusion-rich zone (qtz and ilm), with a homogeneous outer rim. Ilm inclusions define a relict foliation. G rims show partial recrystallisation to sill, st, or bi.			

Abbreviations: ap – apatite; bi – biotite; cc – calcite; cd – cordierite; ep – epidote; g – garnet; hbl – hornblende; ilm – ilmenite; mu – muscovite; pl – plagioclase; py – pyrite; ru – rutile; sill – sillimanite; st – staurolite; tit – titanite; to – tourmaline; qtz – quartz; zrn – zircon; zo – zoisite.

Table 3. *Representative mineral compositions from electron microprobe analysis used in PT calculations.*

	481311				479315			481235					479011					
	hbl	grt rim	pl	bi	pl	bi	mu	grt core	pl(m)	grt	hbl(m)	pl	grt rim	pl	bi(m)	hbl(m)	pl core	pl rim
SiO_2	41.61	37.81	53.65	36.49	60.20	35.25	45.94	37.54	57.48	37.67	43.10	58.34	37.78	57.24	36.50	44.05	62.00	61.60
TiO_2	0.73	0.03	0.02	2.16	0.01	1.39	0.33	0.02	0.02	0.07	0.85	0.00	0.02	0.00	1.72	0.95	0.00	0.02
Al_2O_3	14.15	21.54	29.10	17.80	24.70	18.73	34.86	21.55	26.41	21.50	13.28	26.33	21.74	26.94	17.13	12.68	23.17	23.72
Cr_2O_3	0.00	0.04	0.02	0.00	0.00	0.00	0.02	0.00	0.00	0.01	0.06	0.01	0.04	0.00	0.00	0.02	0.02	0.04
Fe_2O_3	0.00	0.00	0.00	0.00	0.00	0.00	0.00	0.00	0.00	0.00	0.00	0.00	0.00	0.00	0.00	0.00	0.00	0.00
FeO	20.96	30.70	0.12	20.44	0.00	18.98	1.58	28.70	0.06	30.46	19.89	0.18	29.87	0.04	19.26	18.06	0.02	0.02
MnO	0.17	2.87	0.00	0.05	0.00	0.12	0.04	8.60	0.07	3.88	0.22	0.00	2.86	0.00	0.14	0.30	0.00	0.00
MgO	7.92	2.41	0.00	10.38	0.02	9.80	0.63	3.00	0.01	2.01	8.59	0.00	2.36	0.01	11.07	8.84	0.01	0.00
CaO	10.14	6.00	12.04	0.00	6.31	0.01	0.00	1.76	8.56	5.88	10.42	8.14	6.82	9.16	0.00	11.42	4.05	4.80
Na2O	1.18	0.02	4.91	0.23	8.19	0.20	0.76	0.05	6.81	0.02	1.66	7.15	0.00	6.60	0.20	1.37	9.63	9.35
K2O	0.51	0.01	0.05	9.48	0.03	9.47	10.34	0.00	0.03	0.14	0.51	0.05	0.01	0.03	9.27	0.50	0.05	0.05
Total oxides	97.37	101.44	99.91	97.02	99.45	93.95	94.49	101.22	99.45	101.64	98.59	100.20	101.50	100.03	95.29	98.19	98.94	99.60
Ox.	24	12	8	22	8	22	22	12	8	12	24	8	12	8	22	24	8	8
Si	6.607	2.986	2.431	5.477	2.693	5.441	6.176	2.985	2.589	2.981	6.728	2.606	2.977	2.567	5.549	6.848	2.775	2.746
Ti	0.088	0.002	0.001	0.244	0.000	0.162	0.034	0.001	0.001	0.004	0.100	0.000	0.001	0.000	0.197	0.111	0.000	0.001
Al	2.648	2.005	1.554	3.149	1.302	3.407	5.523	2.020	1.402	2.005	2.443	1.386	2.019	1.424	3.069	2.323	1.222	1.246
Cr	0.000	0.003	0.001	0.000	0.000	0.000	0.002	0.000	0.000	0.001	0.008	0.000	0.003	0.000	0.000	0.002	0.001	0.001
Fe^{3+}	0.000	0.000	0.000	0.000	0.000	0.000	0.000	0.000	0.000	0.000	0.000	0.000	0.000	0.000	0.000	0.000	0.000	0.000
Fe^{2+}	2.783	2.027	0.005	2.566	0.000	2.450	0.178	1.909	0.002	2.016	2.596	0.007	1.968	0.002	2.449	2.348	0.001	0.001
Mn	0.022	0.192	0.000	0.006	0.000	0.015	0.004	0.579	0.003	0.260	0.030	0.000	0.191	0.000	0.018	0.040	0.000	0.000
Mg	1.874	0.284	0.000	2.322	0.001	2.255	0.126	0.356	0.000	0.237	1.998	0.000	0.277	0.001	2.509	2.048	0.000	0.000
Ca	1.725	0.508	0.584	0.000	0.302	0.002	0.000	0.150	0.413	0.499	1.743	0.390	0.576	0.440	0.000	1.902	0.194	0.229
Na	0.364	0.004	0.431	0.065	0.710	0.061	0.197	0.007	0.595	0.003	0.502	0.619	0.000	0.574	0.060	0.413	0.836	0.808
K	0.102	0.001	0.003	1.815	0.001	1.865	1.773	0.000	0.002	0.014	0.101	0.003	0.001	0.002	1.798	0.100	0.003	0.003
Total cations	16.214	8.011	5.008	15.645	5.011	15.657	14.013	8.007	5.007	8.020	16.249	5.011	8.012	5.009	15.648	16.135	5.032	5.035

Table 3 continued. *Representative mineral compositions from electron microprobe analysis used in PT calculations.*

	479317				479318					481255					481465				
	st inc	grt rim	bi inc	bi(m)	st inc	bi(m)	bi inc	grt r	grt core	pl inc	pl(m)	cd	grt rim	bi(m)	cd	bi(m)	grt core	grt rim	bi inc
SiO_2	27.19	38.23	36.88	36.60	27.65	36.61	36.68	37.80	37.62	61.30	59.11	48.98	38.31	36.96	49.22	36.37	38.62	37.57	37.72
TiO_2	0.32	0.00	1.63	1.07	0.66	1.42	1.24	0.00	0.00	0.03	0.00	0.00	0.01	1.83	0.00	1.45	0.05	0.03	1.45
Al_2O_3	52.76	21.30	18.37	19.36	53.77	18.80	19.14	21.62	21.62	24.44	25.66	33.40	21.86	18.58	32.93	18.66	22.18	21.66	19.35
Cr_2O_3	0.00	0.00	0.00	0.07	0.00	0.00	0.00	0.03	0.00	0.05	0.02	0.04	0.03	0.08	0.00	0.23	0.00	0.04	0.07
Fe_2O_3	0.00	0.00	0.00	0.00	0.00	0.00	0.00	0.00	0.00	0.00	0.00	0.00	0.00	0.00	0.00	0.00	0.00	0.00	0.00
FeO	11.87	29.93	14.76	17.07	12.72	15.08	14.52	33.75	34.57	0.18	0.00	5.96	33.25	15.38	7.07	17.44	32.19	32.98	14.52
MnO	0.33	6.15	0.06	0.03	0.11	0.00	0.06	1.96	1.86	0.00	0.03	0.07	0.82	0.00	0.03	0.07	0.95	0.80	0.00
MgO	1.68	3.77	14.06	11.98	2.51	13.79	13.78	4.53	4.06	0.01	0.00	9.48	5.37	13.59	9.06	12.18	6.07	4.64	14.47
CaO	0.01	1.90	0.02	0.00	0.01	0.00	0.00	1.36	1.48	5.64	7.44	0.00	1.90	0.00	0.02	0.02	1.86	1.72	0.01
Na_2O	0.28	0.01	0.43	0.44	0.11	0.43	0.44	0.03	0.00	8.56	7.47	0.53	0.03	0.34	0.46	0.34	0.01	0.04	0.47
K_2O	0.01	0.00	9.26	9.17	0.00	9.18	9.13	0.01	0.00	0.04	0.06	0.02	0.01	8.90	0.01	8.70	0.00	0.05	8.72
Total oxides	94.45	101.29	95.46	95.79	97.53	95.30	94.99	101.09	101.21	100.24	99.79	98.48	101.59	95.67	98.80	95.46	101.93	99.52	96.77
Ox.	24	12	22	22	24	22	22	12	12	8	8	18	12	22	18	22	12	12	22
Si	4.050	3.018	5.469	5.458	4.000	5.441	5.451	2.985	2.978	2.718	2.644	4.988	2.987	5.467	5.018	5.448	2.984	2.994	5.472
Ti	0.036	0.000	0.182	0.119	0.071	0.159	0.139	0.000	0.000	0.001	0.000	0.000	0.000	0.204	0.000	0.163	0.003	0.001	0.158
Al	9.262	1.982	3.210	3.402	9.166	3.293	3.352	2.012	2.017	1.277	1.352	4.009	2.009	3.239	3.956	3.294	2.020	2.034	3.308
Cr	0.000	0.000	0.000	0.009	0.000	0.000	0.000	0.002	0.000	0.002	0.001	0.003	0.002	0.010	0.000	0.027	0.000	0.002	0.008
Fe^{3+}	0.000	0.000	0.000	0.000	0.000	0.000	0.000	0.000	0.000	0.000	0.000	0.000	0.000	0.000	0.000	0.000	0.000	0.000	0.000
Fe^{2+}	1.478	1.976	1.830	2.128	1.539	1.874	1.804	2.228	2.288	0.007	0.000	0.508	2.168	1.902	0.603	2.184	2.080	2.197	1.761
Mn	0.042	0.411	0.007	0.004	0.013	0.000	0.007	0.131	0.125	0.000	0.001	0.006	0.054	0.000	0.003	0.008	0.062	0.054	0.000
Mg	0.373	0.444	3.107	2.663	0.541	3.055	3.052	0.533	0.479	0.000	0.000	1.439	0.624	2.996	1.377	2.719	0.699	0.551	3.129
Ca	0.002	0.161	0.003	0.000	0.001	0.000	0.000	0.115	0.126	0.268	0.356	0.000	0.159	0.000	0.002	0.003	0.154	0.147	0.001
Na	0.080	0.001	0.122	0.127	0.031	0.122	0.128	0.004	0.000	0.736	0.648	0.105	0.004	0.099	0.091	0.099	0.001	0.006	0.132
K	0.001	0.000	1.751	1.744	0.000	1.740	1.731	0.001	0.000	0.002	0.003	0.002	0.001	1.679	0.001	1.662	0.000	0.005	1.614
Total cations	15.324	7.992	15.682	15.653	15.362	15.685	15.663	8.011	8.013	5.011	5.005	11.059	8.009	15.594	11.050	15.609	8.003	7.992	15.584

Table 3 continued. *Representative mineral compositions from electron microprobe analysis used in PT calculations.*

	479334				479057				479339					479309				
	grt core	pl(m)	bi(m)	hbl	grt	hbl	pl(m)	ep(m)	cpx	grt	hbl	ep	pl	grt core	grt rim	bi(m)	st inc	pl(m)
SiO_2	37.95	56.52	35.98	42.00	37.61	41.03	46.25	38.21	50.84	38.16	42.82	38.21	46.25	37.63	37.77	35.78	27.85	59.80
TiO_2	0.07	0.04	1.73	0.69	0.09	0.70	0.05	0.07	0.13	0.01	0.66	0.04	0.01	0.55	0.09	1.44	0.58	0.00
Al_2O_3	21.24	27.14	17.61	14.69	21.05	15.00	34.64	27.33	0.83	20.41	12.20	25.97	34.13	21.05	21.52	20.06	53.28	25.22
Cr_2O_3	0.08	0.02	0.18	0.01	0.00	0.00	0.00	0.00	0.02	0.14	0.13	0.00	0.04	0.07	0.06	0.09	0.24	0.08
Fe_2O_3	0.00	0.00	0.00	0.00	0.00	0.00	0.00	8.98	0.00	0.00	0.00	10.05	0.00	0.00	0.00	0.00	0.00	0.00
FeO	32.22	0.15	20.32	20.18	30.57	22.41	0.20	0.00	16.77	22.58	22.95	0.00	0.06	31.22	33.34	18.48	12.59	0.07
MnO	2.06	0.01	0.01	0.34	1.22	0.13	0.03	0.10	0.45	4.03	0.42	0.07	0.00	5.42	2.48	0.00	0.08	0.00
MgO	2.77	0.00	10.56	7.21	2.10	6.30	0.00	0.02	7.95	0.88	6.25	0.02	0.02	2.05	3.32	10.76	1.71	0.00
CaO	5.21	9.33	0.00	10.78	7.99	11.01	17.68	23.96	23.01	14.32	11.77	23.44	17.19	3.59	2.76	0.00	0.00	7.06
Na_2O	0.01	6.20	0.16	1.43	0.00	1.79	1.37	0.00	0.20	0.01	1.32	0.00	1.68	0.05	0.00	0.28	0.12	7.85
K_2O	0.00	0.04	9.12	0.54	0.01	0.55	0.03	0.01	0.00	0.00	0.20	0.00	0.00	0.01	0.00	9.18	0.00	0.04
Total oxides	101.60	99.45	95.66	97.87	100.64	98.92	100.25	98.67	100.21	100.53	98.72	97.81	99.37	101.64	101.34	96.07	96.46	100.12
Ox.	12	8	22	24	12	24	8	12.5	6	12	24	12.5	8	12	12	22	24	8
Si	2.995	2.551	5.474	6.623	2.992	6.489	2.123	2.971	1.975	3.022	6.795	3.005	2.139	2.990	2.988	5.358	4.068	2.665
Ti	0.004	0.001	0.198	0.082	0.006	0.083	0.002	0.004	0.004	0.000	0.079	0.003	0.000	0.033	0.005	0.162	0.063	0.000
Al	1.976	1.444	3.157	2.730	1.973	2.796	1.874	2.504	0.038	1.905	2.282	2.407	1.860	1.971	2.006	3.540	9.171	1.324
Cr	0.005	0.001	0.021	0.001	0.000	0.000	0.000	0.000	0.000	0.009	0.016	0.000	0.001	0.004	0.004	0.011	0.028	0.003
Fe^{3+}	0.000	0.000	0.000	0.000	0.000	0.000	0.000	0.525	0.000	0.000	0.000	0.595	0.000	0.000	0.000	0.000	0.000	0.000
Fe^{2+}	2.126	0.006	2.585	2.661	2.033	2.964	0.008	0.000	0.545	1.495	3.045	0.000	0.002	2.074	2.206	2.314	1.538	0.003
Mn	0.138	0.000	0.001	0.045	0.082	0.017	0.001	0.006	0.015	0.270	0.057	0.005	0.000	0.365	0.166	0.000	0.010	0.000
Mg	0.326	0.000	2.395	1.694	0.249	1.485	0.000	0.002	0.460	0.104	1.478	0.003	0.001	0.243	0.391	2.402	0.372	0.000
Ca	0.441	0.451	0.000	1.821	0.681	1.866	0.869	1.996	0.958	1.215	2.001	1.975	0.852	0.306	0.234	0.000	0.000	0.337
Na	0.001	0.542	0.047	0.437	0.000	0.549	0.122	0.000	0.015	0.001	0.406	0.000	0.151	0.008	0.000	0.082	0.035	0.678
K	0.000	0.002	1.770	0.109	0.001	0.112	0.001	0.000	0.000	0.000	0.040	0.000	0.000	0.001	0.000	1.754	0.001	0.002
Total cations	8.011	4.998	15.647	16.203	8.017	16.360	5.000	8.010	4.010	8.021	16.200	7.992	5.006	7.994	8.001	15.622	15.287	5.012

Amphibolites

Sermitsiaq (479311, 479334) Storø (481235), Bjørneøen (479057), and Nuuk peninsula (479011, 479339)

Amphiboles are all calcic. Those defining the main fabric-forming schistosity in two samples from Sermitsiaq (479311, 479334) are edenitic to hornblenditic ([Na+K] = 0.47–0.56 and 6.61–6.70 Si) with little variation in composition between or within grains. In the calc-silicate lens analysed from the Nuuk peninsula (479339) they are compositionally homogeneous hornblenditic grains ([Na+K] = 0.41–0.51 and 6.78–6.86 Si). From Storø (481235), matrix amphiboles defining the fabric-forming schistosity and those in partial replacement textures around garnet are edenitic ([Na+K] = 0.57–0.63 and 6.65–6.78 Si), with no observed compositional difference between the different textural associations. From the Nuuk peninsula (479011), matrix amphiboles defining the fabric-forming schistosity are hornblenditic with [Na+K] = 0.48–0.54 and 6.82–6.89 Si. In sample 479057, from an amphibolite forming an isoclinal fold hinge in a heterogeneous layered supracrustal rocks on south-east Bjørneøen, matrix amphiboles defining the fabric-forming schistosity are more pargasitic with [Na+K] = 0.61–0.66 and 6.49–6.55 Si.

Plagioclase composition in the mafic amphibolites from Sermitsiaq (479311, 479334) is variable but generally rather anorthitic with XAn 0.42–0.63. In a calc-silicate layer in host mafic amphibolite from the Nuuk peninsula (479339) it is very anorthitic (XAn 0.80–0.88). Plagioclase in mafic amphibolites from Storø and the Nuuk peninsula (481235, 479011) is albitic (XAn 0.36–0.48), and plagioclase forming rims around garnet in partial replacement textures falls in the same compositional range. From an amphibolite forming an isoclinal fold hinge in a heterogeneous layered supracrustal rocks on south-east Bjørneøen (479057) plagioclase is close to the anorthite endmember (XAn 0.86–0.90).

Chemical traverses of *garnet* porphyroblasts in the mafic amphibolites from Sermitsiaq (479311, 479334) reveal that these are typically fairly homogeneous (little or no core-rim zonation) with compositions in the range XSps 0.03–0.07, XAlm = 0.60–0.72, XPyp = 0.03–0.12, XGrs = 0.15–0.22. In a calc-silicate layer (479339) garnet is – not surprisingly – much more grossular-rich with XSps 0.06–0.11, XAlm = 0.48–0.57, XPyp = 0.03–0.05, XGrs = 0.32–0.39. Despite the presence of partial breakdown textures around garnet in samples from Storø and the Nuuk peninsula, garnet is fairly homogeneous with compositions XSps 0.05–0.08, XAlm = 0.58–0.67, XPyp = 0.08–0.12, XGrs = 0.17–0.25 (479235, 481465, 479011). From the amphibolite on south-east Bjørneøen (479057) garnet is slightly more Fe-rich with XSps 0.02–0.04, XAlm = 0.66–0.70, XPyp = 0.08–0.09, XGrs = 0.19–0.22.

Biotite in samples from Sermitsiaq (479311, 479334) has XMg = 0.47–0.49 and 1.73–2.16 wt% TiO_2. In a sample from Storø with biotite in partial replacement textures around garnet (481235) has XMg = 0.45–0.48 and 1.65–1.81 wt% TiO_2. Biotite defining the fabric-forming schistosity in a sample from the Nuuk peninsula (479011) has XMg = 0.50–0.51 and 1.71–1.80 wt% TiO_2.

The amphibolite from south-east Bjørneøen (479057) also has pistacitic *epidote* (0.48–0.53 Fe^{3+}), as does the calc-silicate lens from Sermitsiaq (479334) (0.51–0.60 Fe^{3+}).

Diopsidic clinopyroxene in the calc-silicate lens from Sermitsiaq (479334) has XMg = 0.43–0.48.

Metasedimentary rocks

Sermitsiaq (479309, 479315, 479317, 479318) and Storø (481255, 481465, 465003, 465005)
Large *plagioclase* grains in the matrix of 479317 (Sermitsiaq) are zoned with albitic cores (XAn = 0.18–0.19) and more Ca-rich rims (XAn = 0.22–0.23). Plagioclase inclusions in garnet porpyroblasts from sample 479318 (Sermitsiaq) have XAn = 0.27 – no plagioclase was found in the matrix. Plagioclase in the matrix of samples 479315 and 479309 from Sermitsiaq has XAn = 0.30–0.36. Matrix plagioclase from samples 481255 and 481465 on Storø are slightly more calcic (XAn = 0.33–0.45).

Garnet from most samples are rather homogeneous but a few chemical traverses – particularly of the larger porphyroblasts – reveal minor core-rim zonation in samples 479318, 481255, 481465, 479309, 465003, and 465005. For most samples garnet porphyroblasts and small garnets in equilibrated textures with matrix minerals fall in the compositional range XSps 0.01–0.11, XAlm = 0.63–0.78, XPyp = 0.08–0.25, XGrs = 0.03–0.15, typically with smaller ranges within a single grain. Exceptions are small garnets in equilibrated textures with biotite-muscovite-quartz from sample 479315 and garnet porphyroblasts with staurolite inclusions from sample 479317, which have higher XSps of 0.13–0.22, and garnet porphyroblasts from two samples from two biotite-plagioclase-quartz-sillimanite schists from the Storø shear zone (465003 and 465005), which have higher XAlm of 0.73–0.87 and corresponding lower XPyp of 0.03–0.11. The samples that show core-rim zonation typically show cores enriched in XSps and XAlm and poor in XPyp (and rarely also in XGrs). Garnet element maps for samples 465003 and 465005 from the Storø shear zone are shown in Figure 80 and 81 and illustrate the core-rim zonation described above.

Matrix *biotite* from sample 479315 (Sermitsiaq) has XMg = 0.48–0.52 and 1.06–1.73 wt% TiO_2. Biotite inclusions in garnet porpyroblasts from sample 379317 (Sermitsiaq) have XMg = 0.62–0.63 and 1.19–1.63 wt% TiO_2, while matrix biotite have lower XMg = 0.55–0.56 and 0.89–1.12 wt% TiO_2. Biotite inclusions in garnet porphyroblasts from sample 379318 (Sermitsiaq) have XMg = 0.62–0.65 and 0.85–1.29 wt% TiO_2, while matrix biotite have lower XMg = 0.57–0.62 and 1.32–1.42 wt% TiO_2. Matrix biotite from sample 481255 (Storø) has XMg = 0.60–0.64 and 1.60–2.08 wt% TiO_2. Biotite inclusions in garnet porphyroblasts from sample 481465 (Storø) have XMg = 0.64–0.65 and 1.28–1.45 wt% TiO_2, while matrix biotite have lower XMg = 0.54–0.62 and 1.37–1.69 wt% TiO_2. Matrix biotite from sample 479309 (Sermitsiaq) has XMg = 0.50–0.53 and 1.44–1.63 wt% TiO_2.

Staurolite inclusions in garnet porphyroblasts in samples from Sermitsiaq (479317, 479318, 479309) have XMg = 0.19–0.26.

Matrix *muscovite* in sample 479315 from Sermitsiaq has XMg 0.38–0.43.

Fine-grained *cordierite* in partial replacement textures on biotite in sample 481255 from Storø has XMg = 0.73–0.76 whereas medium- to coarse-grained cordierite in equilibrated textures with garnet-biotite-sillimanite-plagioclase-quartz in sample 481465 (Storø) has slightly lower XMg = 0.70–0.71.

Minor *spinel* in sample 479315 (pale blue in thin section) from Sermitsiaq is a Zn-rich variety (gahnite) with considerable Fe (0.29–0.35 cations) and lesser Mg (0.06–0.07 cations) substitution for Zn.

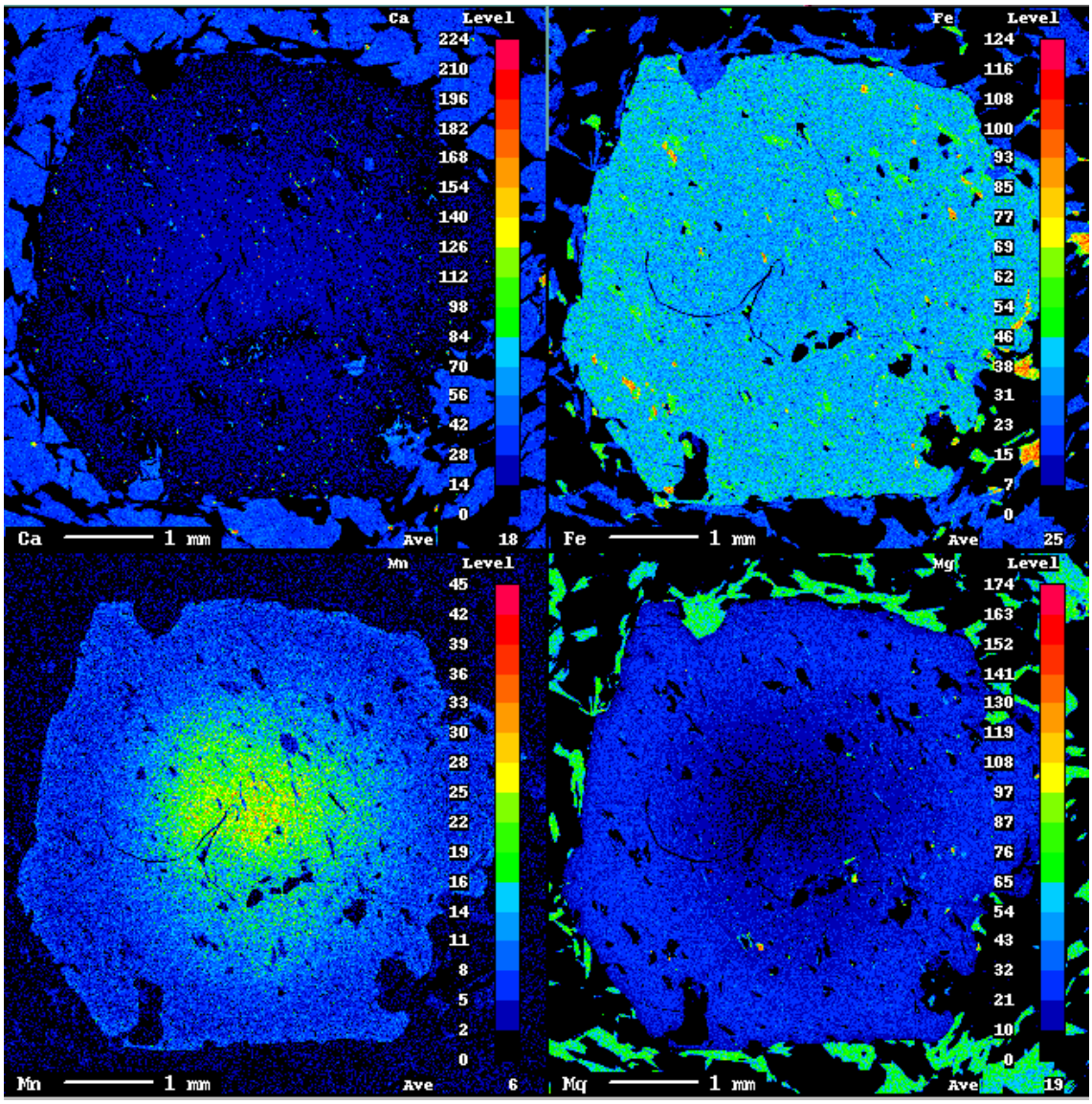

Figure 80. *Element maps of a garnet porphyroblast from sample 465003 from the Storø shear zone, showing core-rim growth zonation in Ca, Fe, Mn, and Mg.*

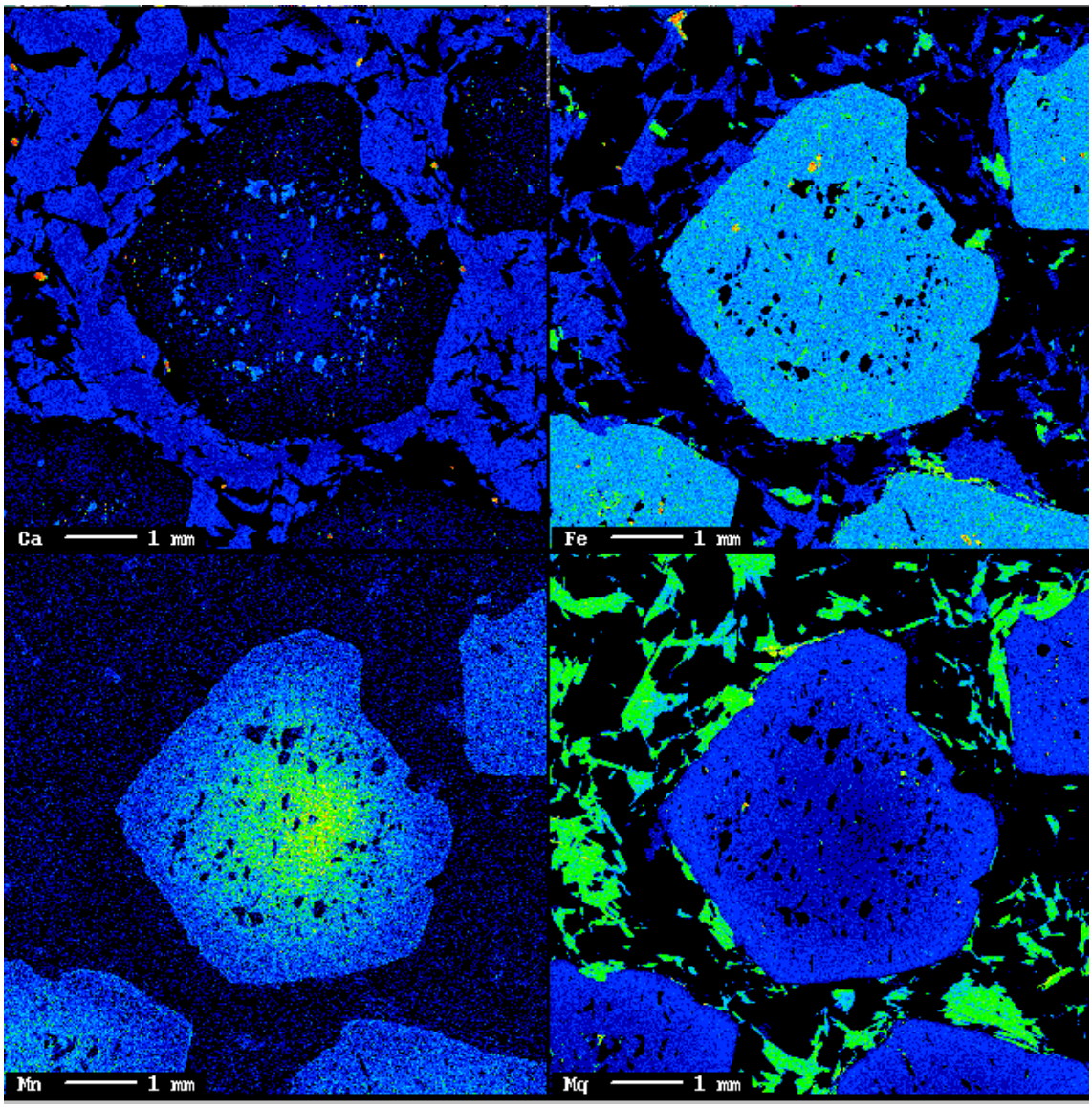

Figure 81. *Element maps of a garnet porphyroblast from sample 465005 from the Storø shear zone, showing core-rim growth zonation in Ca, Fe, Mn, and Mg and partial resorption (top right).*

Thermobarometry

Pressure-temperature (PT) calculations were made using the internally consistent mineral thermodynamic dataset and computer program THERMOCALC v.3.23 (2003 update of Holland and Powell 1998), using mineral endmember activities calculated from representative electron microprobe data using the computer program AX written by Dr Tim Holland, University of Cambridge (http://www.esc.cam.ac.uk/astaff/holland/ax.html). This approach allows calculation of an internally consistent set of mineral reactions appropriate to the observed mineral assemblages with error propagation.

PT calculations were made for six garnet-bearing amphibolites from Sermitsiaq, Bjørneøen, Storø, and the Nuuk peninsula, and for three garnet-mica schists from Sermitsiaq and Storø. The results are shown in Table 2.

Amphibolites

Mineral assemblages defining regional foliations in the garnet-bearing amphibolites from Sermitsiaq, Bjørneøen, and Storø all give PTs in the range 4.7–6.1 kbar at 521–624 C. The lack of chemical zonation in garnet from the Storø sample (481235) – which shows partial garnet breakdown textures – is probably a consequence of retrograde chemical reequilibration. The garnet amphibolite sample from the Nuuk peninsula (479011) gives higher PT conditions of 7.6 kbar at 712°C. Garnet in this sample has plagioclase rims interpreted as formed during decompression. The higher PT conditions recorded for this sample may indicate that rocks on the Nuuk peninsula reached higher PT conditions than on Storø, Sermitsiaq or Bjørneøen, or alternatively may indicate that retrograde reequilibration was not as significant here.

Garnet-mica schists

Two samples of medium-grained matrix assemblages defining foliation in garnet-mica schists from Storø give PT estimates of 4.5–5.1 kbar at 548–620°C. These fall in the same range as estimates from the garnet-bearing amphibolites (above), excluding the one higher PT samples from the Nuuk peninsula. Note that in the case of samples 479309, 479317, and 479318 from Sermitsiaq, insufficient reactions were found for PT calculations based on the mineral assemblages, and thus no PT estimates are given in Table 2.

Main findings

All samples of garnet amphibolites and garnet-mica schists from Sermitsiaq, Bjørneøen, and Storø give a similar range in PT estimates for medium-grained matrix assemblages defining the dominant foliations, i.e. 521–624°C and 4.5–6.1 kbar. This suggests that all of these rocks experienced similar metamorphic conditions, relating to formation of garnet-hornblende-plagioclase-quartz ± biotite ± epidote ± diopside in mafic rocks, and garnet-plagioclase-quartz ± biotite ± muscovite ± sillimanite in aluminous metasedimentary rocks.

In light of the new geochronology data, which support a model of tectonic interleaving of mid and late Archaean supracrustal rocks, it is possible that all of these rocks form part of the tectonically dismembered late Archaean Storø greenstone belt. All samples from Sermitsiaq and Bjørneøen were collected from close to the structural base of the supracrustal package, which is now though to be dominated by a tectonic panel of late Archaean supracrustal rocks of the Storø greenstone belt. This would go some way to explaining the similarity in PT estimates. However it is also possible that the mid Archaean rocks of the Bjørneøen greenstone belt also experienced similar metamorphic conditions, either in the mid Archaean, or during terrane amalgamation in the late Archaean.

The presence of staurolite inclusions in garnet in two samples of garnet-mica schists from Sermitsiaq records earlier, slightly lower T conditions, on the prograde path. The absence of staurolite from the matrix in these two samples is consistent with T estimates from Sermitsiaq of 521–624°C (probably beyond the upper T stability limit of staurolite in these rocks). Partial breakdown of biotite to cordierite in a garnet-mica gneiss from Storø (481255), and medium- to coarse-grained cordierite in a sillimanite-bearing assemblage in another sample from Storø (481465) also indicates peak metamorphic conditions beyond the T stability range of staurolite. Subsequent formation of fine-grained staurolite on garnet in garnet-mica gneiss samples from Storø (481255, 465003, 465005), is interpreted as formed on the retrograde path.

The higher PT estimate of 712°C and 7.6 kbar from a garnet amphibolite with decompression textures from the Nuuk peninsula is more difficult to interpret. Plagioclase rims on garnet – interpreted as decompression textures – are observed in many parts of the Storø greenstone belt. Polat (this volume) also describes the presence of early kyanite (partially replaced by biotite) in one metasedimentary sample from Storø, suggestive of early higher P. It is difficult to say whether (a) all late Archaean rocks in the region experienced early higher P and the evidence for this has been largely erased by retrograde reequilibration, or (b) some high P rocks were and tectonically interleaved with late Archaean supracrustal rocks at a higher crustal level during late Archaean thrusting and metamorphism.

Given the small number of samples analysed it is difficult to draw many conclusions regarding regional metamorphic conditions. However it appears that a large region of central Godthåbsfjord experienced amphibolite facies metamorphism at c. 520–620°C and c. 4.5–6 kbar along a heating path, probably with some associated burial. This likely relates to widespread metamorphic ages of c. 2700 and/or c. 2630 Ma during amalgamation of different crustal blocks in this period.

Chemical signature of tourmaline in Archaean metasedimentary and metavolcanic rocks from Sermitsiaq

[1]Mikkel Vognsen & [2]Julie A. Hollis
[1]University of Copenhagen
[2]Geological Survey of Denmark and Greenland

A representative selection of tourmaline-bearing rocks from the greenstone belt on Sermitsiaq were investigated to address the (1) relative timing of tourmaline growth and recrystallisation, and (2) what the chemical signature of tourmaline can tell us about the fluid regime.

In geological environments in which the fluid phase is highly reactive and changeable, any pre-existing tourmaline may be susceptible to destabilisation, breakdown and/or result in dissolution-reprecipitation processes (e.g. Putnis 2002). The primary controlling factor for tourmaline stability and growth rates is the composition of the fluid phase with which it interacts. This fluid phase may range from being rock-buffered to be externally-controlled. Tourmaline is the main host for boron in crustal rocks and often plays a significant role in the behaviour of boron during metamorphism. During metamorphism the tourmalines may have been broken up, fractured and undergone dissolution processes, followed by sealing of fractures, healing and growth by reprecipitation of boron-rich metamorphic fluids.

The metamorphic rocks from the eastern leg of Sermitsiaq are dominated by heterogeneous layered supracrustal rocks interpreted as metamorphosed mafic volcanics. A representative selection of four different lithologies within the supracrustal belt have been analysed. These are tourmaline ± garnet bearing amphibolite, tourmalinite-quartzite, tourmaline-hornblende-garnet mica schist and tourmaline bearing quartzofeldspatic mica schist. Electron microprobe and scanning electron microscope (SEM) were used to analyse and characterise the four different tourmaline-bearing rocks. Detailed quantitative electron microprobe traverses were made on tourmaline clasts and associated minerals.

Tourmaline mineralogy and chemistry

Tourmaline is relatively abundant in the metasedimentary units, but also occurs in the metavolcanic units. It occurs as a black, fine-to-coarse grained crystals (< 2 cm), both as isolated crystals and some tourmalinite layers, in places showing preferred orientation consistent with the amphibole and mica mineral-lineation observed. This indicates that at least some tourmaline crystals have formed under strain induced metamorphism. In thin section, most tourmaline crystals are optically zoned, showing a general bluish dark inner core. In back-scattered electron images, many tourmalines display a zonation characterised by irregular cellular, spongy cores and lighter outer rims.

Homogeneous tourmaline

Back scattered electron (BSE) images of tourmaline in the amphibolite (479328) and hornblende-garnet mica schist (479306) are generally homogeneous. The lack of zonation may be a product of chemical homogenisation during metamorphism. Traverses across tourmaline grains show little or no compositional variation in major or minor elements. These tourmalines show higher Cr and distinct lower Mg compared with those from quartzite and quartzofeldspathic mica schist. The homogenised tourmaline crystals tend be sub- to euhedral < 2 cm elongate black prismatic crystals. In general the pleochroism is colourless/slightly pinkish to a dusty olive-green. Small, often elongate, fluid inclusions forming trails in the tourmaline grains.

Zoned tourmaline

Optically zoned tourmalines from the quartzite (479302) and quartzofeldspatic mica schist (479053) display a wide display of pleochroism. Often these have a bright bluish inner core, light bluish olive-green outer rim, which again is surrounded by an even darker bluish olive-green rim. All zones are either patchy or irregular. Nearly all grains have a significant number of fluid inclusions, frequently occurring in trails. BSE images of the tourmalines show irregular zonation, interpreted as the product of dissolution-reprecipitation processes. It is likely that at least some of the B required for new tourmaline growth was provided by dissolution of the destabilised tourmaline crystals.

Gradational changes within the some of the zones suggests crystal growth has occurred under changing P-T conditions and/or fluid composition and that crystal growth is not related to general mineralogical kinetics of crystal formation.

Early microfractures have been used as pathways for entering metamorphic fluids – generally enriched in Ca, Fe and Na – and now seen as thin light semi- to non-systematic seams in the tourmaline crystals. Late microfractures in the tourmaline crystals have not been used by perculating metamorphic fluids and seem to have developed after fluid alteration of the crystals. No sub-to-euhedral cores have been detected. Some tourmaline crystals show corroded outer rims (Fig. 83). The zonation of the tourmalines varies between a few near-concentric zonation zones (Fig. 82) to highly irregular zonation patterns (Fig. 83).

As seen in Figure 84 several compositional zones have been identified in tourmaline from these rock types. The dark zone 1 tourmaline is characterised by a relatively high content of Li and Ca. Zone 2 is relatively enriched in Ca, Ti and to a lesser degree Fe and Na (Fig. 85). The patchy appearance of zone 2 is mainly the product of variation in Ca content. The broad concentric light zone 3 is characterised by generally higher intensities of Ca, Fe, Na, Ti and Li, along with Si and Al. Throughout all three identified zones Mg tends to follow the same pattern as Fe and Ca. Al and Si vary inverse proportionally to Na and Fe. There is only a minor difference in composition between different tourmaline grains within each sample.

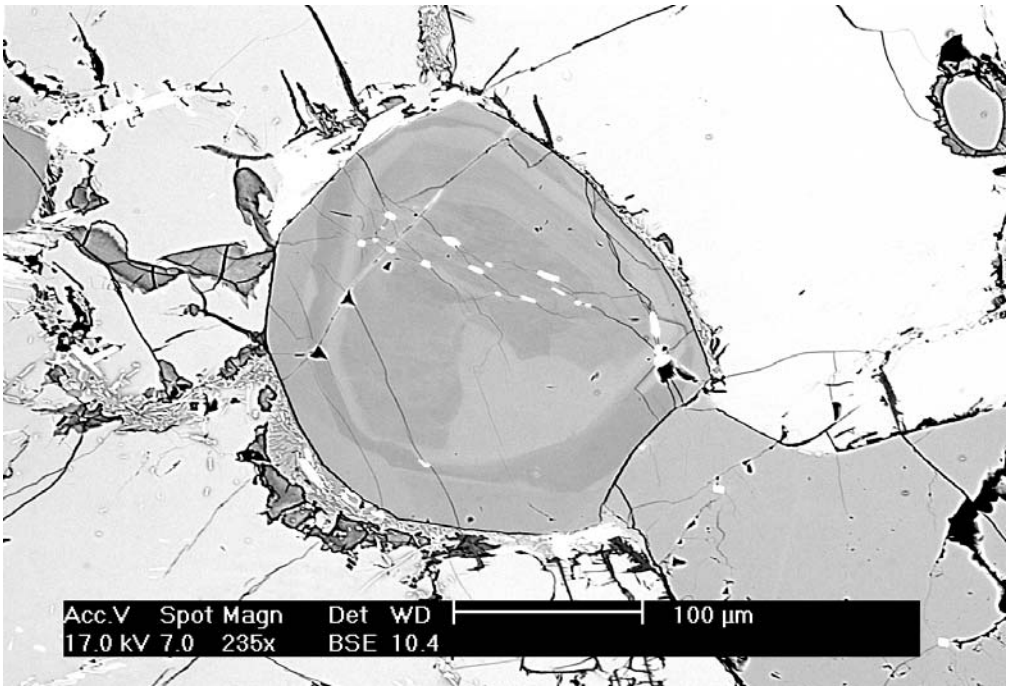

Figure 82. *Tourmaline crystal showing clear optical compositional differences between the different zones (479306). The tourmaline crystal shows semi-regular outer zones, but an irregular patchy inner area. Late microfractures have been used by fluid resulting in precipitation of zircon (small bright spots).*

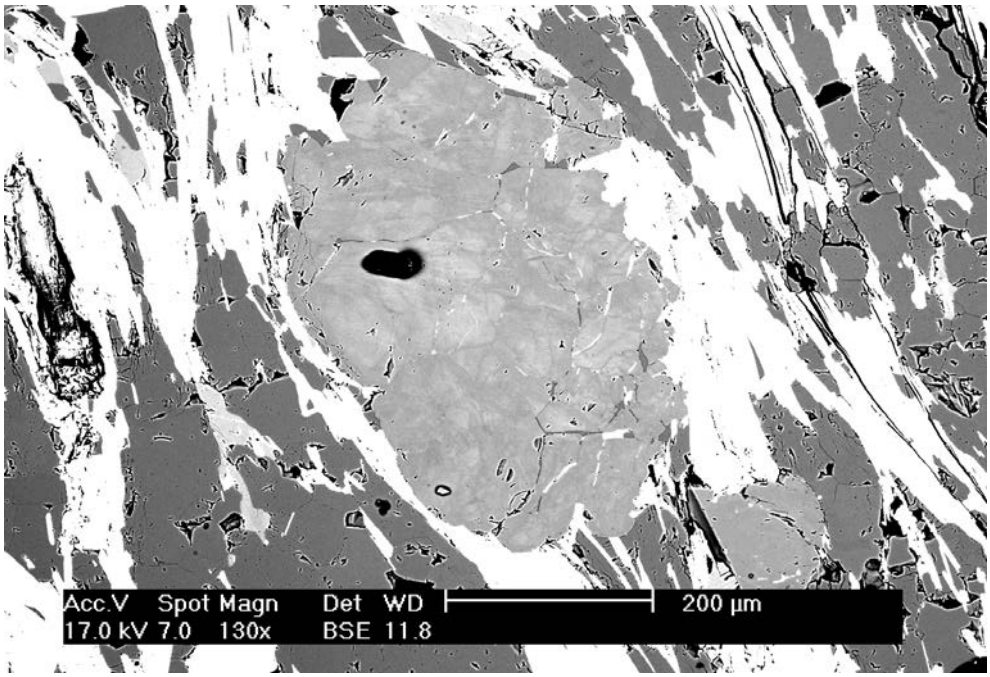

Figure 83. *Tourmaline grained that has undergone complete dissolution-reprecipitation resulting in a distinct irregular patchy/cellular looking texture (479053).*

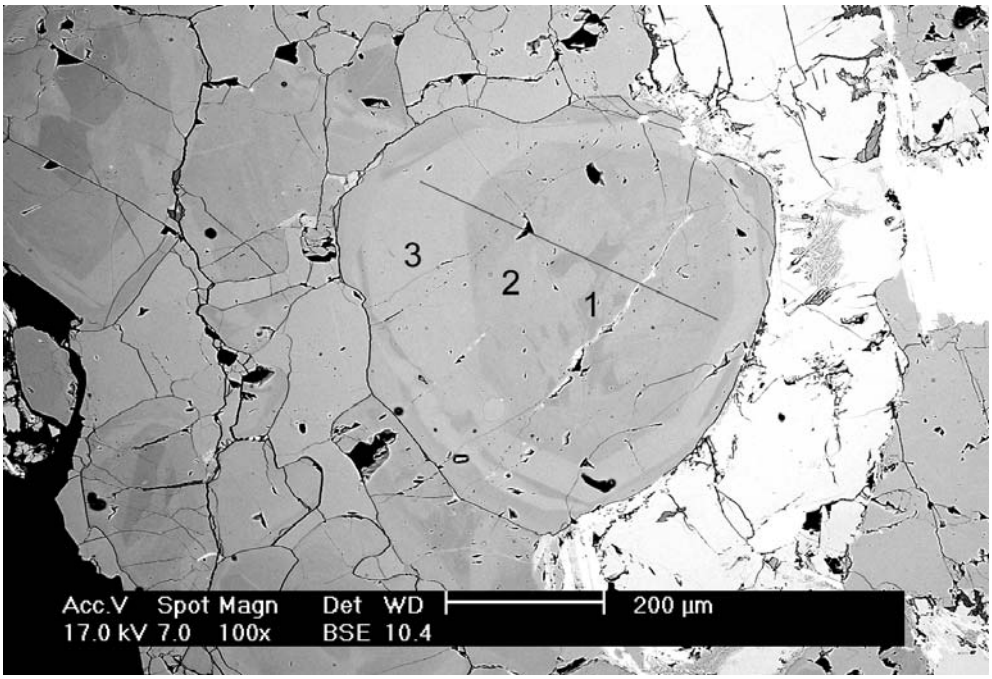

Figure 84. *Line represents the electron microprobe traverse path (479306).*

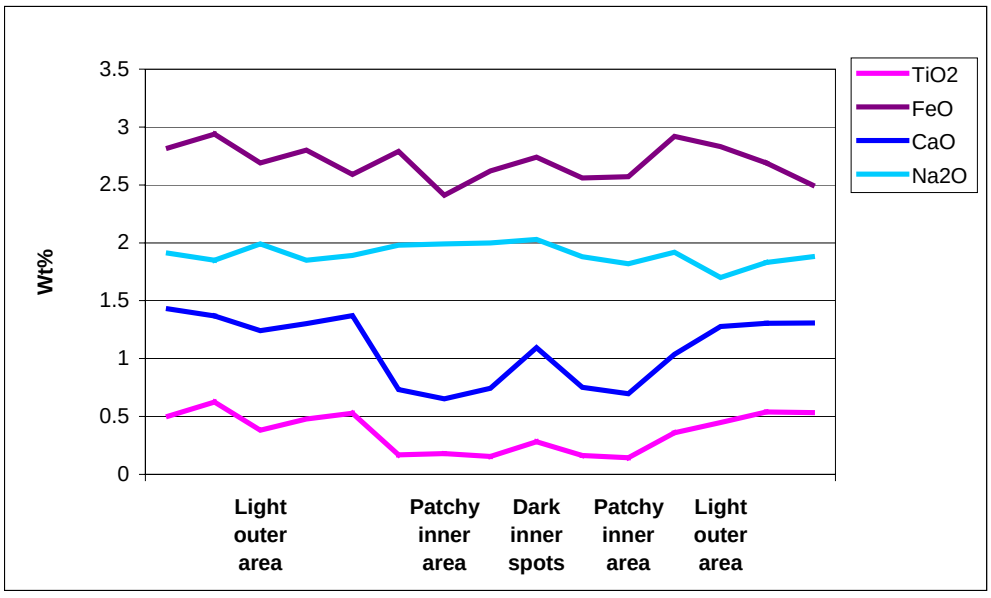

Figure 85. *Compositional plot from electron microprobe traverse showing compositional differences along the path shown in Figure 84. Si and Al (not shown) have a positive correlation with Na and Fe and a negative correlation with Ca, Mg (not shown) and Ti. Li (not shown) is detectable but at low intensities.*

Findings

The general compositional trends in the tourmaline zones are consistent with progressive fractionation of the reacting fluids, becoming successively enriched in Ca, Fe and Mg. Ele-

mental leaching of other minerals (e.g. plagioclase, hornblende) could have contributed significantly to this enrichment.

The major element analyses reveal that the different tourmalines have chemical compositions distinctly different from granite and pegmatite related tourmalines. Tourmaline from all four samples range from Mg-poor to Mg-rich (Mg/[Mg+Fe] = 0.595–0.860). Based on detailed mapping of the area, mineral chemical data, and known scheelite occurrences in the area, this is consistent with a submarine-exhalative origin combined with a distinct metamorphic fluid generation history.

Further work involving fluid inclusion and detailed electron microprobe work could be used to constrain the evolution of metamorphic fluids in these rocks, which are likely influenced by dissolution-reprecipitation processes, and to further investigate the origin and genesis of the tourmaline.

Acknowledgements

This project was financially supported by the Bureau of Minerals and Petroleum (BMP), Nuuk. The topographic base was produced by GEUS in 2004, financed by BMP. The following people are acknowledged for involvement in analytical work and discussion of results: Louise Josefine Nielsen, Peter Venslev, Daniel Weilandt (University of Copenhagen), Lev Ilyinsky, Bodil Kajrup, Martin Whitehouse (Swedish Natural History Museum), Peter Appel, Margareta Christoffersen, Carsten Guvad, Karen Merete Henriksen, Jørgen Kystol, Hanne Lamberts, Annette Thorning Hindø, Eric A. Nielsen, Ingerlise Nørgaard, Frands Schjøth, Henrik Stendal (GEUS). Samples used in this study were collected by the authors and Steven Grimes (Memorial University), Nigel Kelly (University of Edinburgh), Mark T. Hutchison, Peter Roll Jakobsen, and Stig Schack Pedersen (GEUS).

References

Aftalion, M., Bowes, D.R. & Vrana, S. 1989: Early Carboniferous U-Pb zircon age for garnetiferous, perpotassic granulites, Blansky les massif, Czechoslovakia. Neues Jahrbuch fuer Mineralogie. Monatshefte 4, 145-152.

Alt, J.C. 1999: Hydrothermal alteration and mineralization of oceanic crust: Mineralogy, geochemistry, and processes. In: Barrie, C.T. & Hannington, M.D. (eds.): Volcanic-Associated Massive Sulphide Deposits: Processes and Examples in Modern and Ancient Settings. Reviews in Economic Geology 8, 133-155.

Appel, P.W.U. 1990: Gold occurrences in supracrustal rocks of the Nuuk region, West Greenland. Rapport Grønlands Geologiske Undersøgelse Open File Series 90/9, 28 pp.

Appel, P.W.U. 1994: Stratabound scheelite in alteredArchean komatiites, West Greenland. Mineralium Deposita 29, 341-352.

Appel, P.W.U 1997: High bromine and low Cl/Br ratios in hydrothermally altered Archean komatiitic rocks, West Greenland. Precambrian Research 82, 177-189.

Appel, P.W.U., Bliss, I.C., Coller, D.W., Grahl-Madsen, L. & Pedersen, J.S. 2000: Recent gold discoveries in Archean rocks of central West Greenland. Transactions of the Institution of Mining and Metallurgy 109, B34-B41.

Appel, P.W.U., Garde, A.A., Jørgensen, M.S., Moberg, E., Rasmussen, T.M., Schjøth, F. & Steenfelt, A. 2003: Preliminary evaluation of the economic potential of the greenstone belts in the Nuuk region. Danmarks og Grønlands Geologike Undersøgelse Rapport 2003/94, 147 pp., 1 DVD.

Appel, P.W.U., Coller, D.W., Coller, V., Heijlen, W., Moberg, E.D., Polat, A., Raith, J., Schjøth, F., Stendal, H. & Thomassen, B. 2005: Is there a gold province in the Nuuk region? Report from field work carried out in 2004. Danmarks og Grønlands Geologiske Undersøgelse Rapport 2005/27, 79 pp.

Banerjee, N.R., Gillis, K.M. & Muenlenbachs, K., 2000: Discovery of epidosites in a modern oceanic setting, Tonga forearc. Geology 28, 151-154.

Brewer, M.A., Chadwick, B., Coe, K. & Park, J.F.W. 1984: Further field investigations in the Ivisârtoq region of southern West Greenland. Rapport Grønlands Geologiske Undersøgelse 120, 55-67.

Cawthorn, R.G., McIlver, J.R., McCarthy, T.S., Wyatt, B.A., Ferguson, J., & Barnes S.J. 1979: Possible liquid immiscibility textures in high magnesia basalts from the ventersdorp Supergroup, South African Journal of Geology 87, 105-113.

Chadwick, B. 1985: Contrasting styles of tectonism and magmatism in the late Archean crustal evolution of the northeastern part of the Ivisârtoq region, inner Godthåbsfjord, southern West Greenland. Precambrian Research 27, 215-236.

Chadwick, B. 1986: Malene stratigraphy and late Archean structure: new data from Ivisârtoq, inner Godthåbsfjord, southern West Greenland. Grønlands Geologiske Undersøgelse Rapport 130, 74-85.

Chadwick, B. 1990: The stratigraphy of a sheet of supracrustal rocks within high-grade orthogneisses and its bearing on late Archean structure in southern West Greenland. Journal of the Geological Society, London 147, 639-652.

Chadwick, B. and Coe, K. 1988: Geological map of Greenland, 1:100 000, Ivisârtoq, sheet 64 V.2 Nord. Copenhagen: Grønlands Geologiske Undersøgelse.

Coltorti, M., Giradi, V.A.V. & Schorscher, J.H.D. 1987: Liquid immiscibility in the Archean greenstone belt of Piumhi (Minais Gerais, Brazil). Lithos 20, 77-91.

de Wit, M.J. 1998: On Archean granites, greenstones, cratons, and tectonics: does the evidence demand a verdict? Precambrian Research 91, 181-226.

de Wit, M.J., Jones, M.G. & Buchanan, D.L. 1992. The geology and tectonic evolution of the Pietersburg greenstone belt, South Africa. Precambrian Research 55, 123-153.

Escher, J.C. & Pulvertaft, T.C.R. 1995: Geological map of Greenland, 1:2 500 000. Copenhagen: Grønlands Geologiske Undersøgelse.

Friend, C.R.L., Hall, R.P. & Hughes, D.J. 1981: The geochemistry of the Malene (mid-Archean) ultramafic-mafic amphibolite suite, southern West Greenland. In: Glover , J.E., Groves, D.E. (eds.): Archean Geology, Special Publication of the Geological Society of Australia 7, 301-312.

Friend, C. R. L. & Nutman, A.P. 2005: New pieces to the Archean jigsaw puzzle in the Nuuk region, southern West Greenland: steps in transforming a simple insight into a complex regional tectonothermal model. Journal of the Geological Society, London 162, 147-162.

Garde, A. A. 1989: Geological map of Greenland, 1:100 000, Fiskefjord, sheet 64 V.1 Nord. Copenhagen: Grønlands Geologiske Undersøgelse.

Garde, A.A., Friend, C.R.L., Nutman, A.P. & Marker, M. 2000: Rapid maturation and stabilisation of middle Archaean continental crust: the Akia terrane, southern West Greenland. Bulletin of the Geological Society of Denmark 47, 1-27.

Gélinas, L., Brooks, C. & Trzcienski, W.E. 1976: Archean variolites-quenched immiscible liquids. Canadian Journal of Earth Sciences 13, 210-230.

Gillis, K.M. & Robinson, P.T. 1990: Patterns and processes of alteration in the lavas and dykes of the Troodos ophiolite, Cyprus. Journal of Geophysical Research 95, 21523-21548.

Harper, G.D., Brown, J.R. & Kuhns, R. 1988: A field chemical and stable isotope study of subseafloor metamorphism of the Josephine ophiolite, California-Oregon. Journal of Geophysical Research 93, 4625-4656.

Harper, G.D., Bowman, J.R. & Kuhns, R. 1988: A field, chemical, and stable isotope study of sub-seafloor metamorphism of the Josephine ophiolite, California-Oregon. Journal of Geophysical Research 97, 4625-4656.

Hawkesworth, C.J. Gallanger, K., Hergt, J.M. & McDermott, F. 1993: Mantle and slab contributions in arc magmas. Annual Reviews Earth and Planetary Science Letters 21, 175-204.

Hofmann, A.W. 1988: Chemical differentiation of the Earth: the relationships between mantle, continental crust, and oceanic crust. Earth and Planetary Science Letters 90, 297-314.

Holland, T.J.B & Powell, R. 1998: An internally consistent thermodynamic data set for phases of petrological interest. Journal of Metamorphic Geology 16, 309-343.

Hollis, J.A., van Gool, J.A.M., Steenfelt, A. & Garde, A.A. 2004: Greenstone belts in the central Godthåbsfjord region, southern West Greenland. Danmarks og Grønlands Geologiske Undersøgelse Rapport 2004/110, 110 pp., 1 DVD.

Humphris S.E., Alt J.A., Teagle A.H. & Honnorez J.J. 1998: Geochemical changes during hydrothermal alteration of basement in the stockwork beneath the active TAG hydrothermal mound. In: Herzig, P.M., Humphris, S.E., Miller, D.J. & Zierenberg, R.A. (eds.): Proceedings of the Ocean Drilling Program Scientific Results 158, 255-276.

Jackson, S.E., Pearson, N.J., Griffin, W.L. & Belousova, E.A. 2004: The application of laser ablation-inductively coupled plasma-mass spectrometry to in situ U/ Pb zircon geochronology. Chemical Geology 211/1-2, 47-69.

Jenner, G.A., Longerich, H.P., Jackson, S.E. & Fryer, B.J. 1990: ICP-MS- a powerful tool for high precision trace element analysis in earth sciences: evidence from analysis of selected U.S.G.S. Reference samples. Chemical Geology 83, 133-148.

Ludwig, K.R. 2003: IsoPlot/Ex version 3.0: A geochronological toolkit for Microsoft Excel. Berkeley Geochronological Center, Berkeley.

McGregor, V.R. 1984: Geological map of Greenland, 1:100 000, Qôrqut, sheet 64 V.1 Syd. Copenhagen: Grønlands Geologiske Undersøgelse.

McGregor, V. R. 1993: Qôrqut 74 V.1 Syd, Descriptive Text. Geological map of Greenland 1:100 000. Copenhagen: Grønlands Geologiske Undersøgelse.

McGregor, V. R., Friend, C.R.L. & Nutman, A.P. 1991: The late Archaean mobile belt through Godthåbsfjord, southern West Greenland: a continent-continent collision zone? Bulletin of the Geological Society of Denmark 39, 179-197.

Nehling, P., Juteau, T., Bendel, V. & Cotton, J. 1994: The root zone of oceanic hydrothermal systems: constraints from the Semail ophiolite (Oman). Journal of Geophysical Research 99, 4703-4713.

Nutman, A.P., Friend, C.R.L., Baadsgaard, H. & McGregor, V.R. 1989: Evolution and assembly of Archean gneiss terranes in the Godthåbsfjord region, southern West Greenland: structural, metamorphic, and isotopic evidence. Tectonics 8, 573-589.

Nutman, A.P., Friend, C.R.L., Barker, S.L.L. & McGregor, V.R. 2004. Inventory and assessment of Palaeoarchaean gneiss terrains and detrital zircons in southern West Greenland. In: Mojzsis, S.J. (ed.): The first billion years; selected papers presented at the 13th V. M. Goldschmidt conference. Precambrian Research 135/4, 281-314.

Pearce, J.A. & Peate, D.W. 1995: Tectonic implications of the composition of volcanic arc magmas. Annual Reviews, Earth and Planetary Science Letters 23, 251-285.

Polat, A., Kerrich, R. & Wyman, D.A. 1998: The late Archean Schreiber-Hemlo and White River-Dayohessarah greenstone belts, Superior Province: Collages of oceanic plateaus, Oceanic island arcs, and subduction-accretion complexes. Tectonophysics 289, 295-326.

Polat, A., Hofmann, A.W. & Rosing, M.T. 2002: Boninite-like volcanic rocks in the 3.7-3.8 Ga Isua greenstone belt, West Greenland: Geochemical evidence for intra-oceanic subduction zone processes in the early Earth. Chemical Geology 184, 231-254.

Putnis, A. 2002: Mineral replacement reactions: from macroscopic observations to microscopic mechanisms. Mineralogical Magazine 66/5, 689-708.

Richardson, C.J., Cann, J.R., Richards, H.G. & Cowan, J.G. 1987: Metal depleted root zones of the Troodos ore-forming hydrothermal systems, Cyprus. Earth and Planetary Science Letters 84, 243-253.

Saunders A.D., Norry, M.J. & Tarney, J. 1991: Fluid influence on the trace element compositions of subduction zone magmas: Philosophical Transactions of Royal Society of London A. 335, 377-392.

Schiffman, P., Smith, B.M., Varga, J.R. & Moores, E.M. 1987: Geometry, conditions and timing of off-axis hydrothermal metamorphism and ore deposition in the Solea graben. Nature 325, 423-425.

Schiøtte, L., Compston, W. & Bridgwater, D. 1988: Late Archaean ages for the deposition of clastic sediments belonging to the Malene supracrustals, southern West Greenland:

evidence from an ion probe U-Pb zircon study. Earth and Planetary Science Letters 87, 45-58.

Sun S.S. & McDonough, W.F. 1989: Chemical and isotopic systematics of oceanic basalts: implications for mantle composition and processes. In: Saunders A.D., Norry, M. J. (eds.): Magmatism in the Ocean Basins. Geological Society of London Special Publication 42, 313-345.

Taylor, S.R. & McLennan, S.M. 1985: The Continental Crust: Its Composition and Evolution, Blackwell, Oxford, pp. 312.

Taylor, S.R. & McLennan, S.M. 1995: The geochemical evolution of the continental crust. Reviews in Geophysics 33, 241-265.

Whitehouse, M.J., Claesson, S., Sunde, T. & Vestin, J. 1997: Ion microprobe U-Pb zircon geochronology and correlation of Archaean gneisses from the Lewisian Complex of Gruinard Bay, northwestern Scotland. Geochimica et Cosmochimica Acta 61/20: 4429-4438

Wiedenbeck, M., Alle, P., Corfu, F., Griffin, W.L., Meier, M., Oberli, F., Von Quadt, A., Roddick, J.C. & Spiegel, W. 1995: Three natural zircon standards for U-Th-Pb, Lu-Hf, trace element and REE analyses. Geostandards Newsletter 19/1: 1-23.

Appendix 1: Explanatory notes to the DVD

This DVD contains digital data accompanying GEUS report 2005/42, 'Greenstone belts in the central Godthåbsfjord region, southern West Greenland: Geochemistry, geochronology and petrography arising from 2004 field work, and digital map data'. The DVD is basically an update of the DVD from GEUS report 2004/110, 'Greenstone belts in the central Godthåbsfjord region, southern West Greenland: preliminary results from field work in 2004'. All data on this DVD are copyright of GEUS (2005). The DVD contains the full report and compiled field maps in PDF format, as well as an ArcView© project file containing georeferenced compiled field data including localities, geological descriptions, sample localities, structural data, geochronology, and references to digital photographs (see below). It also contains reduced resolution digital photographs in JPEG format from the 2004 fieldwork. Descriptions of the views in the ArcView-project, maps, geochemistry and geochronology data, and photographs stored on the DVD can be found in the Explanatory_notes.pdf file on the DVD. An installation kit for Acrobat Reader© version 6.0 is included on this DVD. After installation, PDF-files can be open from within the reader, or just by double-clicking the files.

Directory structure

The DVD contains the following directories and main files:

Directories:
AcrobatReader6
Field_maps
Geochemistry
Geochemistry_spreadsheets
Geology
Photographs
Topography

Files in the root directory:
Explanatory_notes.pdf
Frontispiece.jpg
GEUS2005R42.pdf
Godthaabsfjord2004.apr
Terms_of_Delivery.pdf

Note that all files on the DVD use spelling without special letters to avoid problems reading files.

Use of the DVD

1. Place the DVD into DVD reader.
2. Read the Explanatory_notes.pdf file. This provides explanations of the contents of the DVD.
3. Run ArcView© 3.2 on your computer.
4. Open the ArcView© file.
5. The file Godthaabsfjord2004.apr will open on a cover view. When this cover view is closed, a list of available views will become visible. Choose the desired view to begin exploring the data.

ArcView© project

The ArcView© project (constructed in ArcView© version 3.2) contains the geo-referenced data collected during the 2004 field work, as well as new geochemical and geochronology data and pre-existing 1:100 000 geological maps, both in the original old version and new updated and enlarged version. The data are placed in separate views and can be explored and combined within the program. The ArcView© project, Godthaabsfjord2004.apr, is contained within the root directory of the DVD and refers to the Frontispiece.jpg file within the root directory and to files within the folders Geochemistry, Geology, and Topography.

The following is a list of the views within the ArcView© project file (Godthaabsfjord2004.apr), containing different types of digital data sets.

0.1 Frontispiece
1.1 Index map - Location of the Godthåbsfjord region
1.2 Topographic map
1.3 Digital geological map 1:100 000
1.4 Digital geological maps 1:100 000 (old version)
1.5 Scanned geological maps 1:100 000 (old version)
2.1 Visited outcrop localities
2.2 Geological observations
2.3 Samples collected in 2004
2.4 Structures
2.5 Geochronology
2.6 Photographs
3.1 Rock geochemistry
3.2 Geochemistry, 2005
3.3 Stream sediment chemistry

Appendix 2: Tabulated LA-SF-ICPMS zircon U-Pb age data

Zircon U-Pb age data were collected using a NewWave Research/Merchantek UP213 laser and Element2 sector-field inductively coupled plasma mass spectrometer at GEUS. Back-scattered electron images of the grains analysed are not included in this report owing to the large number (> 500) of grains analysed.

Sample/	U	Pb	Th/U	^{207}Pb	± 1s	^{207}Pb	± 1s	^{206}Pb	± 1s	^{207}Pb age	± 1s	^{206}Pb age	± 1s	^{207}Pb age	± 1s
analysis	ppm	ppm	meas	^{206}Pb	%	^{235}U	%	^{238}U	%	^{235}U	Ma	^{238}PbU	Ma	^{206}Pb	Ma
461526															
39	70	33	0.026	0.1745	0.3	10.9484	1.8	0.4549	1.7	2519	45	2417	42	2602	6
50	51	23	0.010	0.1753	0.7	10.4924	1.7	0.4341	1.6	2479	43	2324	37	2609	11
30	130	65	0.019	0.1758	0.5	11.8123	2.3	0.4873	2.3	2590	60	2559	58	2614	8
49	84	41	0.023	0.1760	0.6	11.4215	1.6	0.4706	1.5	2558	41	2486	37	2616	10
24	106	48	0.037	0.1761	0.4	10.7913	1.6	0.4444	1.6	2505	41	2370	38	2617	6
25	177	89	0.017	0.1763	0.6	11.8739	1.2	0.4884	1.0	2595	31	2564	27	2619	10
43	109	49	0.051	0.1764	0.5	10.5434	1.9	0.4336	1.9	2484	48	2322	44	2619	8
46	158	79	0.027	0.1764	0.4	11.8574	1.1	0.4874	1.0	2593	29	2560	26	2620	7
45	114	58	0.031	0.1765	0.4	12.0993	1.0	0.4972	1.0	2612	27	2602	25	2620	6
47	180	88	0.015	0.1767	0.3	11.6827	1.0	0.4796	1.0	2579	27	2526	25	2622	5
34	45	21	0.031	0.1767	0.9	11.1847	1.8	0.4591	1.5	2539	45	2436	37	2622	15
35	146	71	0.019	0.1767	0.3	11.6250	1.0	0.4771	0.9	2575	26	2515	24	2622	6
48	177	83	0.018	0.1768	0.4	11.1389	1.8	0.4570	1.8	2535	46	2426	43	2623	7
33	142	72	0.012	0.1768	0.4	12.0475	1.3	0.4943	1.2	2608	34	2589	32	2623	7
38	48	24	0.038	0.1768	0.6	11.9174	1.4	0.4888	1.3	2598	37	2566	33	2623	10
22	84	39	0.040	0.1771	0.5	11.0241	2.1	0.4515	2.0	2525	52	2402	48	2626	8
51	107	49	0.031	0.1773	0.5	10.9156	1.9	0.4465	1.8	2516	47	2380	43	2628	8
21	138	59	0.021	0.1774	0.4	10.2015	2.9	0.4172	2.9	2453	71	2248	64	2628	7
44	120	56	0.016	0.1776	0.3	11.0364	2.1	0.4507	2.1	2526	53	2398	50	2630	5
23	198	97	0.015	0.1776	0.3	11.7445	1.0	0.4796	1.0	2584	27	2526	26	2631	4
52	123	62	0.015	0.1781	0.4	12.0781	1.1	0.4919	1.0	2610	29	2579	27	2635	6
32	335	128	0.241	0.1856	0.7	9.0445	1.6	0.3535	1.4	2343	37	1951	28	2703	11
479008															
26	228	122	0.017	0.1863	0.4	13.2923	2.3	0.5174	2.2	2701	61	2688	60	2710	7
25	107	66	0.537	0.1969	1.1	14.9545	2.2	0.5508	2.0	2812	63	2829	55	2801	18
9	67	41	0.370	0.1997	0.7	14.7131	2.7	0.5343	2.6	2797	76	2760	72	2824	11
33	86	57	0.906	0.2023	0.9	15.7472	2.1	0.5647	1.9	2862	60	2886	55	2845	15
8	68	44	0.557	0.2026	0.6	15.3016	2.0	0.5477	1.9	2834	56	2815	53	2848	10
12	81	55	0.860	0.2035	0.6	15.7739	2.0	0.5622	1.9	2863	57	2876	54	2854	10
5	55	36	0.692	0.2039	0.7	15.2966	2.0	0.5441	1.9	2834	57	2801	52	2858	12
34	86	51	0.666	0.2054	0.6	14.6700	2.1	0.5180	2.0	2794	60	2691	55	2870	10
38	72	45	0.622	0.2070	0.5	15.3611	2.4	0.5381	2.3	2838	67	2775	64	2883	9
20	48	33	0.695	0.2072	0.6	16.6952	2.0	0.5844	1.9	2917	58	2966	56	2884	9
4	50	33	0.526	0.2074	0.6	15.9879	2.3	0.5591	2.3	2876	67	2863	65	2885	10
11	32	24	1.353	0.2074	0.6	16.2661	2.0	0.5687	1.9	2893	58	2903	55	2886	10
31	76	49	0.798	0.2075	0.6	15.5689	2.2	0.5442	2.2	2851	64	2801	61	2886	9
10	40	27	0.583	0.2076	0.7	16.2878	2.0	0.5690	1.9	2894	59	2904	55	2887	12
35	101	67	0.734	0.2078	1.0	16.5335	2.2	0.5772	2.0	2908	63	2937	57	2888	15
19	64	42	0.713	0.2078	0.8	16.0145	2.1	0.5590	1.9	2878	60	2862	55	2888	12
22	100	61	0.435	0.2081	0.7	15.7337	2.9	0.5483	2.8	2861	84	2818	80	2891	11
24	40	29	1.095	0.2084	0.6	17.0121	2.3	0.5920	2.2	2936	68	2997	67	2893	10
23	65	50	1.978	0.2089	0.5	15.5719	2.0	0.5407	1.9	2851	56	2786	53	2897	8
18	30	22	1.148	0.2092	1.0	16.9340	2.3	0.5870	2.0	2931	66	2977	61	2900	15
7	46	31	0.729	0.2093	0.6	15.9697	2.0	0.5533	1.9	2875	59	2839	55	2900	10
32	57	37	0.848	0.2096	0.6	15.8889	2.1	0.5497	2.0	2870	60	2824	57	2903	10
36	25	17	0.880	0.2098	1.0	16.4101	2.5	0.5674	2.3	2901	72	2897	66	2904	16
30	89	59	0.292	0.2118	0.8	17.6673	2.6	0.6050	2.4	2972	76	3050	74	2919	13
21	135	109	0.936	0.2611	0.5	22.9916	2.0	0.6386	1.9	3227	63	3184	61	3253	7
37	45	43	0.707	0.3305	0.7	34.2784	2.0	0.7523	1.9	3618	74	3616	70	3619	10
13	11	11	0.799	0.3311	0.8	35.0891	2.5	0.7686	2.4	3641	92	3676	87	3622	13
479014															
19	148	73	0.474	0.1807	0.5	10.5982	1.9	0.4254	1.8	2489	93	2285	83	2659	8
34	111	65	0.723	0.1848	0.5	12.3485	1.8	0.4845	1.7	2631	95	2547	88	2697	9
4	79	45	0.536	0.1849	0.6	12.4942	1.8	0.4900	1.7	2642	96	2571	89	2698	10
36	105	63	0.810	0.1853	0.6	12.4067	2.4	0.4857	2.4	2636	128	2552	120	2701	9
37	141	65	0.655	0.1853	0.3	9.5054	1.9	0.3720	1.9	2388	93	2039	78	2701	6
30	366	138	0.221	0.1853	0.7	8.8634	2.1	0.3469	2.0	2324	99	1920	77	2701	11
35	95	49	0.687	0.1853	0.5	10.7141	2.4	0.4193	2.3	2499	119	2257	105	2701	9
21	39	22	0.479	0.1862	0.7	12.5200	2.6	0.4878	2.5	2644	138	2561	128	2708	12
33	102	60	0.630	0.1862	0.4	12.8363	1.8	0.4999	1.8	2668	98	2613	93	2709	7
38	71	42	0.687	0.1864	0.6	12.1944	1.9	0.4744	1.8	2619	100	2503	92	2711	9
32	106	26	0.925	0.1868	0.6	4.8554	3.0	0.1885	2.9	1795	108	1113	66	2714	10
25	251	126	0.235	0.1871	1.0	11.3296	2.2	0.4392	1.9	2551	110	2347	89	2717	17

Sample/ analysis	U ppm	Pb ppm	Th/U meas	$^{207}Pb/^{206}Pb$	± 1s %	$^{207}Pb/^{235}U$	± 1s %	$^{206}Pb/^{238}U$	± 1s %	^{207}Pb age ^{235}U	± 1s Ma	^{206}Pb age ^{238}PbU	± 1s Ma	^{207}Pb age ^{206}Pb	± 1s Ma
18	87	47	0.560	0.1872	0.6	11.8078	1.8	0.4574	1.7	2589	94	2428	84	2718	9
6	118	65	0.755	0.1876	0.4	11.6122	2.6	0.4490	2.6	2574	136	2391	125	2721	6
22	46	28	0.550	0.1921	0.9	13.5953	1.9	0.5132	1.7	2722	106	2670	91	2760	15
20	115	49	0.439	0.1948	0.8	9.4442	2.1	0.3517	2.0	2382	102	1943	77	2783	13
24	176	42	0.222	0.2277	1.9	5.8038	4.6	0.1849	4.3	1947	181	1093	93	3036	30
23	130	104	1.503	0.2279	0.5	17.8653	2.0	0.5687	1.9	2983	117	2902	110	3037	9
7	380	211	0.445	0.3066	0.8	18.7338	4.2	0.4431	4.1	3028	252	2365	193	3504	12
8	295	113	0.315	0.3162	0.4	12.9309	4.5	0.2966	4.5	2675	241	1675	150	3551	6
479036															
13	201	180	0.330	0.3381	0.6	33.5162	2.9	0.7189	2.8	3596	103	3492	97	3654	10
22	38	42	0.579	0.3405	0.7	40.1398	2.3	0.8550	2.1	3774	85	3983	85	3665	11
37	95	85	0.189	0.3416	0.7	33.7371	3.0	0.7163	2.9	3602	108	3482	102	3670	11
12	126	118	0.422	0.3436	0.8	33.0990	2.2	0.6986	2.0	3584	78	3415	70	3679	12
5	73	68	0.372	0.3437	0.8	32.7842	2.6	0.6919	2.4	3574	91	3390	82	3679	13
8	59	43	0.437	0.3449	0.5	25.8658	3.4	0.5439	3.4	3341	114	2800	94	3685	7
10	41	40	0.381	0.3450	0.4	37.1622	2.1	0.7813	2.0	3698	77	3722	76	3685	6
30	101	89	0.671	0.3486	0.3	30.6559	2.1	0.6378	2.0	3508	73	3180	65	3701	5
38	161	165	0.600	0.3589	0.5	37.1184	2.2	0.7501	2.1	3697	80	3608	75	3745	8
25	21	24	0.956	0.3656	0.5	41.3162	2.1	0.8196	2.1	3803	81	3859	79	3773	8
17	27	30	0.679	0.3697	0.7	41.0714	2.2	0.8057	2.1	3797	83	3810	80	3790	10
4	175	157	0.195	0.3735	0.8	35.9034	2.4	0.6971	2.3	3664	88	3410	77	3806	12
24	25	28	1.161	0.3746	0.4	38.2382	2.2	0.7404	2.2	3726	84	3572	79	3810	7
11	79	77	0.236	0.3782	0.9	37.3497	2.2	0.7162	2.0	3703	82	3482	71	3825	13
23	84	82	0.148	0.3786	0.4	40.4071	2.1	0.7741	2.0	3781	78	3696	75	3826	5
19	43	45	0.654	0.3796	0.6	39.0762	2.4	0.7466	2.3	3748	89	3595	83	3830	8
479049															
31	164	91	1.718	0.2067	0.5	13.3619	2.8	0.4689	2.8	2706	76	2479	68	2880	8
9	284	187	0.446	0.2113	0.8	16.6547	1.9	0.5717	1.7	2915	54	2915	49	2915	13
8	88	59	0.304	0.2166	1.3	17.7494	2.3	0.5943	1.9	2976	68	3007	56	2956	21
26	118	71	0.515	0.2245	0.5	15.7127	2.4	0.5077	2.3	2859	67	2647	61	3013	7
20	195	138	0.572	0.2255	0.5	18.2891	1.8	0.5881	1.7	3005	53	2982	51	3021	8
35	216	140	0.374	0.2263	0.5	17.4338	1.8	0.5587	1.8	2959	54	2861	51	3026	8
33	126	78	0.426	0.2266	0.4	16.3539	1.9	0.5235	1.9	2898	55	2714	50	3028	7
21	221	150	0.391	0.2268	0.5	18.3334	2.0	0.5864	1.9	3007	59	2975	56	3029	8
10	189	125	0.492	0.2268	0.8	17.3886	2.0	0.5561	1.8	2957	59	2850	51	3030	13
22	140	90	0.430	0.2270	0.5	17.2937	1.8	0.5526	1.7	2951	53	2836	49	3031	7
37	170	116	0.496	0.2273	0.8	18.0151	2.0	0.5749	1.9	2991	60	2928	55	3033	12
13	267	183	0.652	0.2278	0.4	17.7138	1.7	0.5639	1.7	2974	52	2883	49	3037	6
5	90	61	0.488	0.2280	0.5	18.0044	1.9	0.5726	1.8	2990	56	2919	53	3038	8
24	143	101	0.540	0.2280	0.6	18.7592	1.8	0.5967	1.7	3030	55	3016	51	3038	10
25	291	208	0.519	0.2281	0.4	19.0253	1.8	0.6048	1.8	3043	55	3049	54	3039	7
6	286	201	0.499	0.2282	0.5	18.9305	2.1	0.6016	2.0	3038	63	3036	62	3040	8
34	174	121	0.619	0.2286	0.5	18.0552	2.0	0.5728	1.9	2993	59	2919	55	3042	8
11	111	76	0.579	0.2289	0.8	18.2174	1.9	0.5772	1.7	3001	56	2937	49	3045	14
23	230	171	0.667	0.2290	0.4	19.0825	1.7	0.6045	1.7	3046	52	3048	51	3045	6
17	215	159	0.814	0.2290	0.6	18.9675	1.8	0.6008	1.7	3040	54	3033	51	3045	9
30	66	48	0.501	0.2291	0.7	19.6963	1.8	0.6235	1.7	3077	56	3124	52	3046	11
18	71	51	0.446	0.2292	0.6	19.4059	2.0	0.6141	1.9	3062	62	3087	60	3046	9
38	257	185	0.593	0.2294	0.5	18.7616	1.9	0.5933	1.8	3030	56	3003	54	3048	8
12	199	140	0.582	0.2294	0.4	18.2814	2.1	0.5779	2.1	3005	64	2940	62	3048	7
7	285	201	0.608	0.2295	0.6	18.5525	1.8	0.5862	1.7	3019	53	2974	49	3049	10
19	101	69	0.474	0.2302	0.6	18.2838	1.9	0.5761	1.8	3005	56	2933	52	3053	10
4	89	58	0.420	0.2314	0.9	17.9783	2.0	0.5634	1.8	2989	60	2881	52	3062	14
36	350	248	0.675	0.2316	0.6	18.4826	1.7	0.5788	1.6	3015	53	2944	49	3063	9
32	40	28	0.434	0.2325	0.6	19.4492	1.8	0.6068	1.8	3064	57	3057	54	3069	9
39	358	224	0.581	0.2339	0.8	16.6802	1.9	0.5173	1.7	2917	55	2688	46	3079	13
479301															
24	227	155	0.195	0.1986	0.6	17.2194	3.8	0.6287	3.8	2947	113	3144	119	2815	10
34	108	74	0.379	0.1989	0.7	16.6679	3.6	0.6077	3.5	2916	105	3061	108	2817	12
6	116	74	0.480	0.1997	0.8	15.0655	3.6	0.5473	3.5	2819	102	2814	100	2823	12
8	145	73	0.353	0.2003	0.5	12.2219	3.5	0.4426	3.5	2622	93	2362	83	2829	8
13	83	47	0.380	0.2004	0.5	13.4350	3.6	0.4863	3.5	2711	97	2555	91	2829	8
5	110	71	0.332	0.2010	0.5	15.9456	4.0	0.5755	4.0	2874	115	2930	116	2834	9

Sample/ analysis	U ppm	Pb ppm	Th/U meas	$^{207}Pb/^{206}Pb$	± 1s %	$^{207}Pb/^{235}U$	± 1s %	$^{206}Pb/^{238}U$	± 1s %	^{207}Pb age ^{235}U	± 1s Ma	^{206}Pb age ^{238}PbU	± 1s Ma	^{207}Pb age ^{206}Pb	± 1s Ma
22	97	65	0.408	0.2010	0.5	16.1666	3.5	0.5834	3.5	2887	102	2963	104	2834	8
20	132	78	0.314	0.2011	0.4	14.4358	3.6	0.5206	3.5	2779	99	2702	96	2835	7
10	86	58	0.379	0.2011	0.8	16.1892	3.8	0.5837	3.7	2888	108	2964	109	2835	13
38	109	59	0.303	0.2012	0.5	13.1010	3.5	0.4723	3.5	2687	95	2493	87	2836	8
12	75	51	0.328	0.2013	0.5	16.6389	3.8	0.5994	3.8	2914	111	3028	114	2837	9
36	178	104	0.402	0.2013	0.4	13.9919	4.0	0.5040	3.9	2749	109	2631	104	2837	7
23	153	85	0.403	0.2014	0.5	13.1516	3.6	0.4735	3.5	2691	96	2499	88	2838	9
17	91	58	0.323	0.2017	0.5	15.9723	3.5	0.5743	3.5	2875	101	2925	102	2840	8
32	81	55	0.392	0.2018	0.5	16.2053	3.6	0.5825	3.6	2889	104	2959	105	2841	8
19	225	120	0.251	0.2019	0.6	13.3492	5.3	0.4795	5.3	2705	144	2525	134	2842	10
37	111	71	0.381	0.2020	0.5	15.5247	3.8	0.5573	3.7	2848	107	2855	107	2843	8
31	138	86	0.358	0.2027	0.5	15.2052	3.6	0.5440	3.6	2828	102	2800	100	2848	8
39	110	77	0.456	0.2030	0.5	16.8603	3.8	0.6023	3.8	2927	111	3039	115	2851	8
4	87	49	0.303	0.2031	0.5	13.9078	3.8	0.4968	3.7	2743	103	2600	97	2851	8
35	113	74	0.362	0.2040	0.5	15.9691	3.5	0.5678	3.5	2875	102	2899	102	2858	8
11	195	90	0.331	0.2046	0.4	11.2528	4.3	0.3989	4.3	2544	111	2164	93	2863	7
479326															
12	32	17	0.075	0.1750	1.1	12.7275	2.1	0.5274	1.8	2660	56	2730	49	2606	19
32	53	31	0.190	0.1905	0.8	14.1457	2.0	0.5385	1.8	2760	56	2777	51	2747	13
30	16	11	0.345	0.2022	0.9	15.7726	2.3	0.5657	2.1	2863	67	2890	62	2844	15
4	30	15	0.182	0.2025	1.1	12.8447	2.7	0.4600	2.4	2668	72	2440	60	2846	18
39	26	18	0.732	0.2037	1.0	16.2570	2.1	0.5788	1.9	2892	62	2944	56	2856	16
6	14	10	0.509	0.2047	0.8	16.0121	2.0	0.5673	1.8	2878	57	2897	53	2864	12
22	21	13	0.450	0.2047	0.7	14.8645	2.0	0.5266	1.8	2807	55	2727	50	2864	12
33	25	17	0.372	0.2049	0.5	16.5543	1.8	0.5861	1.8	2909	53	2974	53	2865	8
5	19	13	0.371	0.2054	0.6	16.1790	2.1	0.5713	2.0	2887	59	2913	57	2869	10
36	11	7	0.357	0.2059	1.1	15.9172	3.2	0.5608	3.0	2872	91	2870	86	2873	17
7	17	12	0.704	0.2061	0.6	16.7346	2.2	0.5889	2.1	2920	64	2985	64	2875	9
11	17	11	0.374	0.2062	0.6	16.3527	1.9	0.5752	1.8	2898	54	2929	52	2876	10
19	16	11	0.384	0.2062	0.9	16.7774	2.0	0.5901	1.8	2922	58	2990	53	2876	15
9	22	14	0.378	0.2065	0.6	16.0854	1.9	0.5649	1.8	2882	54	2887	51	2879	10
26	29	20	1.021	0.2068	0.5	15.2155	1.9	0.5337	1.8	2829	54	2757	50	2880	9
10	17	12	0.398	0.2068	0.6	16.6151	2.0	0.5828	1.9	2913	58	2960	55	2880	11
38	23	16	0.814	0.2068	0.7	15.8659	1.9	0.5565	1.8	2869	55	2852	51	2880	11
23	26	18	0.527	0.2071	0.7	16.5421	1.9	0.5793	1.8	2909	56	2946	53	2883	11
24	18	12	0.398	0.2072	0.7	16.6367	2.2	0.5823	2.1	2914	64	2958	61	2884	12
13	15	9	0.402	0.2072	0.9	15.8410	2.1	0.5544	1.9	2867	61	2843	55	2884	15
34	18	13	0.400	0.2073	0.8	17.3562	2.0	0.6074	1.8	2955	59	3059	55	2884	14
37	18	12	0.432	0.2074	0.8	16.0387	2.0	0.5609	1.8	2879	58	2870	53	2885	13
25	22	15	0.714	0.2077	0.5	15.6787	2.0	0.5474	1.9	2857	57	2814	55	2888	8
31	15	10	0.423	0.2078	0.8	16.5235	2.0	0.5768	1.8	2908	58	2936	54	2888	13
17	18	12	0.426	0.2078	0.6	16.2925	2.0	0.5686	1.9	2894	57	2902	54	2888	10
8	14	10	0.392	0.2082	0.8	16.4252	1.9	0.5723	1.7	2902	55	2917	51	2891	12
18	30	19	0.384	0.2083	0.5	16.2326	1.9	0.5652	1.8	2891	55	2888	52	2892	9
20	22	15	0.705	0.2084	0.6	16.4808	2.0	0.5734	1.9	2905	57	2922	54	2894	10
35	13	9	0.524	0.2127	1.3	16.9624	2.2	0.5783	1.8	2933	66	2942	54	2926	21
21	19	13	0.528	0.2145	0.6	17.0187	2.0	0.5756	1.9	2936	58	2931	55	2940	10
479606															
37	61	41	0.547	0.2279	0.9	18.2135	2.4	0.5797	2.2	3101	71	3166	71	3037	14
31	100	68	0.527	0.2299	0.5	17.8886	2.3	0.5643	2.2	2565	77	1967	49	3051	8
22	66	47	0.419	0.2300	0.5	18.8725	2.3	0.5950	2.3	3010	77	2930	73	3052	8
7	139	95	0.420	0.2302	0.6	18.5576	2.3	0.5847	2.2	3019	69	2968	65	3053	9
24	106	71	0.448	0.2304	0.4	18.3629	2.3	0.5782	2.2	3012	74	2935	70	3054	7
12	204	152	0.533	0.2305	0.7	19.9319	2.4	0.6272	2.3	2990	70	2873	66	3055	12
35	130	84	0.551	0.2307	0.5	16.8947	2.3	0.5312	2.3	3211	75	3417	75	3057	8
23	71	52	0.395	0.2309	0.6	19.3233	2.3	0.6070	2.3	3088	74	3139	71	3058	9
39	38	27	0.473	0.2309	0.6	18.3435	2.3	0.5762	2.2	3037	70	2982	68	3058	10
33	121	81	0.589	0.2310	0.5	17.8833	2.6	0.5614	2.5	3026	69	2968	65	3059	8
4	143	109	0.442	0.2311	0.5	20.2099	2.3	0.6341	2.3	3038	72	2980	68	3060	7
8	136	93	0.643	0.2316	0.5	18.4147	2.4	0.5767	2.4	2979	68	2843	63	3063	8
25	108	75	0.448	0.2317	0.4	18.9522	2.4	0.5932	2.3	3048	71	3020	68	3064	6
32	63	43	0.569	0.2318	0.8	17.9078	3.5	0.5604	3.4	3035	71	3010	69	3064	13
17	33	23	0.568	0.2318	0.6	18.6844	2.3	0.5846	2.2	3058	72	3058	69	3064	10
6	80	54	0.434	0.2318	0.6	18.3919	2.6	0.5754	2.5	3009	68	2941	65	3065	9
21	104	73	0.469	0.2321	0.6	19.1205	2.3	0.5975	2.3	3039	71	3002	70	3066	10

Sample/ analysis		U ppm	Pb ppm	Th/U meas	$^{207}Pb/^{206}Pb$	± 1s %	$^{207}Pb/^{235}U$	± 1s %	$^{206}Pb/^{238}U$	± 1s %	^{207}Pb age ^{235}U	± 1s Ma	^{206}Pb age ^{238}PbU	± 1s Ma	^{207}Pb age ^{206}Pb	± 1s Ma
9		72	49	0.498	0.2325	0.5	18.0011	2.3	0.5616	2.3	3074	71	3075	69	3069	8
34		39	29	0.506	0.2328	0.7	19.5769	2.6	0.6099	2.5	3024	68	2950	65	3071	11
19		44	30	0.609	0.2329	0.6	17.8024	2.3	0.5544	2.2	2984	68	2884	64	3072	10
38		42	31	0.652	0.2330	0.7	20.3792	2.6	0.6344	2.5	2985	105	2868	98	3073	11
30		99	69	0.514	0.2330	0.4	18.6450	2.2	0.5802	2.2	2983	77	2873	73	3073	7
26		66	48	0.556	0.2331	0.5	19.6470	2.3	0.6113	2.2	3071	80	3070	77	3073	8
13		77	54	0.620	0.2331	0.4	18.9062	2.3	0.5882	2.3	2929	68	2747	62	3073	6
18		99	68	0.515	0.2335	0.6	18.9171	2.4	0.5876	2.3	2961	72	2790	63	3076	10
5		323	137	0.428	0.2339	1.7	11.5034	3.0	0.3567	2.5	3001	71	2948	65	3079	27
36		16	11	0.498	0.2339	0.9	17.4668	2.4	0.5415	2.3	3110	82	3167	80	3079	15
11		51	42	0.729	0.2348	0.9	22.6352	2.3	0.6992	2.2	3008	70	2933	66	3085	14
479665																
4		167	88	0.498	0.2249	0.6	20.6524	1.6	0.7102	1.2	2771	46	2424	36	3035	11
6		30	21	0.468	0.2252	0.5	27.1554	1.7	0.9382	0.8	3041	40	3048	37	3037	9
17		118	74	0.417	0.2258	0.5	23.3817	1.7	0.8363	1.9	2944	63	2804	58	3040	8
13		64	45	0.517	0.2268	0.4	26.0349	1.2	0.9176	0.8	3034	39	3012	36	3048	7
18		91	62	0.419	0.2269	0.4	26.4081	1.2	0.9108	0.8	3032	38	3006	35	3048	7
8		82	47	0.141	0.2270	0.3	22.8433	2.8	0.8129	3.6	2913	108	2720	101	3049	5
7		95	65	0.643	0.2270	0.5	26.1101	1.6	0.8881	1.9	2997	65	2919	62	3049	8
5		78	50	0.353	0.2274	0.5	26.1668	1.5	0.8791	0.8	2987	40	2891	35	3052	9
19		57	37	0.447	0.2279	0.8	23.8009	1.7	0.8364	1.1	2955	48	2809	40	3055	13
12		87	53	0.477	0.2281	0.4	24.6572	2.6	0.8121	2.1	2920	69	2726	63	3057	7
10		93	63	0.497	0.2285	0.4	26.1962	1.5	0.8900	0.7	3008	37	2931	33	3060	7
9		152	102	0.474	0.2296	0.5	27.1482	0.7	0.8925	1.1	3014	44	2936	40	3067	8
11		393	281	0.296	0.2306	0.5	28.4822	1.0	0.9816	1.0	3112	43	3172	42	3074	8
479681																
18		157	127	1.242	0.2272	0.5	18.7554	2.2	0.5986	2.1	3029	66	3024	64	3033	7
17		177	149	0.915	0.2303	0.4	20.9218	2.1	0.6589	2.0	3135	65	3263	67	3054	6
36		125	87	0.919	0.2312	0.3	17.3480	2.3	0.5443	2.3	2954	68	2801	64	3060	5
8		125	103	1.017	0.2315	0.3	20.7621	2.3	0.6506	2.2	3128	70	3230	72	3062	5
30	c	138	97	0.955	0.2316	0.4	17.2007	2.6	0.5386	2.6	2946	78	2778	72	3063	6
32	c	159	112	0.889	0.2317	0.5	17.1319	2.3	0.5362	2.3	2942	68	2767	63	3064	8
24		144	107	1.131	0.2323	0.4	18.0766	2.2	0.5645	2.1	2994	65	2885	61	3068	7
21	r	136	100	1.142	0.2323	0.4	17.8372	2.2	0.5568	2.2	2981	66	2853	63	3068	6
39		180	120	0.922	0.2324	0.5	16.7367	2.6	0.5223	2.5	2920	75	2709	68	3069	8
11		166	119	0.886	0.2325	0.4	17.7450	2.1	0.5536	2.1	2976	64	2840	60	3069	6
38	c	206	113	0.918	0.2326	0.4	13.5307	2.6	0.4219	2.6	2717	70	2269	58	3070	6
19		118	81	0.873	0.2326	0.5	17.3731	2.3	0.5416	2.2	2956	67	2790	62	3070	8
5		116	77	0.900	0.2330	0.5	17.4005	2.2	0.5415	2.1	2957	65	2790	60	3073	8
13		165	122	0.822	0.2332	0.3	18.8160	2.1	0.5853	2.0	3032	63	2970	60	3074	5
37		113	87	0.932	0.2332	0.3	19.2590	2.0	0.5990	2.0	3055	62	3026	61	3074	5
35	c	156	112	1.043	0.2332	0.4	18.2236	2.1	0.5668	2.0	3002	62	2895	59	3074	7
7		162	113	1.225	0.2336	0.5	17.1414	2.4	0.5322	2.4	2943	71	2751	65	3077	8
25		152	104	1.330	0.2338	0.4	16.2960	2.2	0.5055	2.1	2894	63	2637	56	3078	6
26		127	87	0.898	0.2341	0.4	17.1195	2.2	0.5303	2.2	2942	65	2743	60	3081	6
20		195	138	0.995	0.2346	0.4	17.2033	2.4	0.5318	2.3	2946	70	2749	64	3084	7
9		210	142	0.899	0.2347	0.9	16.7604	2.6	0.5179	2.4	2921	75	2690	65	3085	15
4		171	122	0.799	0.2355	0.5	18.0821	2.4	0.5568	2.3	2994	71	2854	66	3090	8
23		161	120	1.084	0.2355	2.0	18.4948	2.9	0.5695	2.2	3016	89	2906	63	3090	32
479703																
13		50	31	0.444	0.1963	0.6	14.4087	1.8	0.5324	1.7	2777	50	2752	47	2796	9
38		138	85	0.977	0.1972	0.4	13.2746	1.7	0.4882	1.6	2699	46	2563	42	2803	6
5		77	50	0.510	0.1976	0.6	14.9160	1.6	0.5474	1.5	2810	46	2814	43	2807	10
6		79	50	0.540	0.1979	0.5	14.6272	1.6	0.5360	1.5	2791	45	2767	42	2809	9
26		74	43	0.431	0.1986	0.7	14.0837	1.8	0.5143	1.7	2755	51	2675	45	2815	12
21		57	35	0.577	0.1989	0.5	14.4117	1.6	0.5256	1.6	2777	46	2723	43	2817	9
35		75	42	0.482	0.1991	0.5	13.3557	2.9	0.4866	2.8	2705	78	2556	73	2819	8
19		143	86	0.632	0.2002	0.4	13.6808	1.8	0.4956	1.7	2728	49	2595	45	2828	7
9		201	119	0.255	0.2003	0.5	14.9309	1.6	0.5407	1.6	2811	46	2786	44	2828	7
12		163	109	0.909	0.2005	0.3	14.4449	1.5	0.5226	1.5	2779	43	2710	41	2830	5
18		120	79	0.730	0.2005	0.3	14.9659	1.5	0.5414	1.5	2813	43	2789	42	2830	5
30		183	119	0.866	0.2011	0.3	14.3784	1.5	0.5186	1.5	2775	43	2693	41	2835	6
10		86	55	0.615	0.2012	0.4	14.6459	1.6	0.5280	1.6	2793	45	2733	43	2836	6
17		84	53	0.599	0.2012	0.4	14.6227	1.6	0.5271	1.5	2791	43	2729	41	2836	6
23		104	61	0.636	0.2013	0.6	13.3732	2.7	0.4819	2.6	2706	73	2536	67	2836	9

Sample/ analysis	U ppm	Pb ppm	Th/U meas	$^{207}Pb/^{206}Pb$	± 1s %	$^{207}Pb/^{235}U$	± 1s %	$^{206}Pb/^{238}U$	± 1s %	^{207}Pb age ^{235}U	± 1s Ma	^{206}Pb age ^{238}PbU	± 1s Ma	^{207}Pb age ^{206}Pb	± 1s Ma
11	109	70	0.671	0.2016	0.4	14.6006	1.6	0.5252	1.5	2790	44	2721	41	2839	7
33	89	57	0.747	0.2017	0.4	14.5809	1.6	0.5242	1.5	2788	44	2717	41	2840	6
36	57	36	0.635	0.2022	0.5	14.9127	1.6	0.5348	1.5	2810	45	2762	41	2844	9
24	89	56	0.704	0.2024	0.6	14.3400	1.6	0.5137	1.5	2772	46	2673	41	2846	9
20	147	95	0.789	0.2025	0.5	14.4448	1.6	0.5174	1.6	2779	46	2688	42	2846	8
31	86	54	0.609	0.2025	0.5	14.8089	1.6	0.5304	1.5	2803	45	2743	42	2846	8
7	55	34	0.477	0.2030	0.5	14.8458	2.5	0.5303	2.4	2805	69	2743	66	2851	8
25	48	29	0.525	0.2031	0.6	14.6860	1.6	0.5245	1.5	2795	46	2718	42	2851	9
39	74	48	0.745	0.2032	0.4	15.2264	1.6	0.5434	1.5	2830	45	2798	43	2852	7
22	75	38	0.212	0.2034	0.9	13.0505	2.8	0.4654	2.7	2683	75	2464	65	2853	14
37	29	19	0.628	0.2034	0.5	15.1944	1.6	0.5418	1.6	2828	46	2791	43	2854	9
8	51	34	0.687	0.2034	0.8	14.6922	2.6	0.5239	2.5	2796	72	2716	67	2854	12
4	62	42	0.592	0.2034	0.5	15.8168	1.7	0.5640	1.6	2866	49	2883	47	2854	8
34	129	83	0.794	0.2035	0.6	14.5482	1.6	0.5185	1.5	2786	46	2693	42	2855	9
479704															
22	67	36	0.102	0.1839	1.1	23.8243	1.4	0.9437	1.1	2692	53	2659	46	2718	16
39	109	57	0.091	0.1849	1.3	24.2188	0.8	0.9135	0.7	2675	53	2612	39	2723	21
9	81	45	0.097	0.1862	0.5	24.4634	0.6	0.9785	0.5	2728	42	2720	39	2733	8
12	73	39	0.102	0.1859	0.4	23.8776	2.0	0.9136	2.2	2680	71	2575	67	2761	8
7	66	32	0.098	0.1842	0.9	21.0645	1.8	0.8422	2.4	2602	74	2401	65	2762	12
32	91	50	0.086	0.1897	1.0	26.0105	0.6	0.9455	0.7	2731	50	2677	40	2771	17
33	124	69	0.094	0.1924	1.1	26.5614	1.2	0.9565	1.8	2758	68	2704	60	2798	18
4	47	26	0.115	0.1937	1.1	25.5916	4.0	0.9700	2.0	2757	72	2694	65	2803	18
5	49	43	0.118	0.3076	0.6	49.8498	1.6	1.3487	0.6	3524	54	3503	52	3535	7
24	101	99	0.414	0.3311	0.6	61.7951	0.9	1.4211	1.0	3659	67	3680	62	3648	10
19	71	73	0.611	0.3324	0.7	65.0808	1.2	1.4657	0.6	3688	61	3758	56	3650	11
6	117	102	0.431	0.3404	0.9	59.6184	1.3	1.2460	1.1	3543	68	3295	57	3686	13
479745															
36	105	78	0.167	0.1900	1.0	18.3666	3.6	0.7009	3.5	3009	109	3424	120	2743	17
18	240	136	0.031	0.1938	0.3	14.5461	3.4	0.5445	3.3	2786	93	2802	94	2774	5
35	194	122	0.435	0.1984	0.7	15.0840	3.4	0.5513	3.3	2821	97	2831	95	2813	12
4	101	64	0.347	0.1985	0.5	15.4727	3.4	0.5653	3.3	2845	96	2888	97	2814	8
7	200	138	0.281	0.1991	0.4	17.2514	3.4	0.6285	3.4	2949	100	3144	106	2819	7
38	128	79	0.388	0.1992	0.6	14.9088	3.5	0.5428	3.5	2809	98	2795	96	2820	9
23	196	125	0.518	0.1994	0.4	15.1516	3.5	0.5511	3.5	2825	99	2830	98	2821	6
11	152	92	0.374	0.1994	0.4	14.6033	3.4	0.5312	3.3	2790	94	2746	92	2821	6
6	215	139	0.277	0.1997	0.5	16.1290	3.4	0.5859	3.4	2884	98	2973	100	2823	8
5	172	105	0.436	0.2000	0.4	14.8162	3.4	0.5372	3.3	2804	95	2772	93	2826	7
24	353	215	0.154	0.2002	1.3	15.5919	3.6	0.5648	3.4	2852	103	2887	97	2828	21
32	206	114	0.373	0.2003	0.6	13.4668	3.4	0.4876	3.4	2713	93	2560	87	2829	9
30	193	109	0.379	0.2005	0.3	13.7298	3.4	0.4967	3.4	2731	92	2600	87	2830	5
17	187	141	0.369	0.2023	0.5	18.7140	3.4	0.6708	3.4	3027	103	3309	112	2845	7
10	330	183	0.276	0.2033	0.7	14.0032	3.4	0.4996	3.4	2750	94	2612	88	2853	11
20	81	50	0.299	0.2034	0.4	15.6289	3.4	0.5572	3.3	2854	96	2855	96	2854	6
19	284	172	0.548	0.2041	1.0	14.3556	3.5	0.5100	3.4	2773	98	2657	90	2860	17
26	324	212	0.220	0.2042	1.3	16.9170	3.7	0.6007	3.5	2930	109	3033	106	2860	21
39	233	146	0.489	0.2044	0.7	15.1394	3.5	0.5373	3.5	2824	100	2772	96	2861	11
9	323	186	0.344	0.2046	0.8	14.3255	3.5	0.5079	3.4	2772	97	2647	90	2863	13
8	116	76	0.513	0.2056	0.5	15.6780	3.4	0.5530	3.4	2857	97	2838	95	2871	8
25	268	190	0.614	0.2071	1.5	16.8519	3.7	0.5901	3.4	2926	109	2990	102	2883	25
37	322	182	0.138	0.2087	1.2	15.1051	3.6	0.5249	3.4	2822	101	2720	92	2896	20
33	286	176	0.545	0.2103	1.2	15.1455	3.8	0.5223	3.6	2824	107	2709	98	2908	19
479813															
19	335	214	0.026	0.2199	0.4	18.1967	1.4	0.6001	1.3	3000	42	3030	41	2980	7
17	213	137	0.072	0.2205	0.4	18.2497	1.4	0.6004	1.4	3003	43	3031	41	2984	7
5	151	94	0.088	0.2206	0.4	17.5802	1.4	0.5779	1.3	2967	41	2940	39	2985	6
23	315	193	0.055	0.2208	0.4	17.3539	1.4	0.5700	1.3	2955	41	2908	39	2987	6
24	199	126	0.078	0.2209	0.4	17.8694	1.4	0.5866	1.3	2983	41	2976	39	2988	7
31	370	220	0.040	0.2212	0.5	16.9314	1.6	0.5552	1.5	2931	47	2847	43	2989	9
12	147	94	0.049	0.2213	0.5	18.2568	1.4	0.5984	1.4	3003	43	3023	41	2990	8
25	140	89	0.104	0.2217	0.4	17.9117	1.4	0.5860	1.3	2985	42	2973	40	2993	7
36	211	122	0.045	0.2223	0.5	16.5591	2.4	0.5403	2.4	2910	70	2785	66	2997	8
6	345	214	0.058	0.2223	0.4	17.7612	1.4	0.5794	1.4	2977	43	2946	40	2998	7
39	256	172	0.057	0.2225	0.8	19.1903	1.6	0.6254	1.4	3051	49	3131	43	2999	13
7	189	124	0.157	0.2228	0.5	18.3739	1.5	0.5981	1.4	3010	46	3022	43	3001	9

Sample/ analysis	U ppm	Pb ppm	Th/U meas	$^{207}Pb/^{206}Pb$	± 1s %	$^{207}Pb/^{235}U$	± 1s %	$^{206}Pb/^{238}U$	± 1s %	^{207}Pb age ^{235}U	± 1s Ma	^{206}Pb age ^{238}PbU	± 1s Ma	^{207}Pb age ^{206}Pb	± 1s Ma
11	241	152	0.056	0.2232	0.6	17.9592	1.5	0.5835	1.4	2988	44	2963	41	3004	9
35	189	118	0.064	0.2234	1.6	17.6519	2.1	0.5731	1.3	2971	62	2921	39	3005	25
21	775	483	0.034	0.2237	1.1	17.9594	1.8	0.5824	1.5	2988	55	2958	43	3007	17
23	400	241	0.062	0.2162	0.6	16.7753	13.4	0.5628	13.2	2922	393	2878	380	2952	10
4	163	92	0.072	0.2174	0.7	15.7288	5.0	0.5247	4.8	2860	144	2719	132	2962	12
37	465	284	0.087	0.2182	0.4	17.0755	24.4	0.5675	24.2	2939	718	2898	702	2968	7
30	491	295	0.119	0.2187	0.4	16.6619	17.4	0.5526	17.2	2916	508	2836	488	2971	6
39	501	297	0.081	0.2189	0.3	16.6327	26.4	0.5511	26.2	2914	770	2830	742	2973	5
22	471	282	0.044	0.2194	0.4	16.9595	12.4	0.5605	12.2	2933	365	2869	350	2977	7
34	392	230	0.043	0.2196	0.4	16.6322	21.4	0.5494	21.2	2914	625	2823	599	2978	6
36	476	284	0.084	0.2197	0.4	16.7513	23.4	0.5530	23.2	2921	685	2838	659	2978	6
8	387	247	0.073	0.2198	0.4	18.0657	4.2	0.5962	4.2	2993	127	3014	125	2979	7
33	549	339	0.078	0.2200	0.4	17.4342	20.4	0.5748	20.2	2959	605	2927	592	2981	6
35	400	250	0.012	0.2202	0.5	17.9379	22.4	0.5908	22.2	2986	670	2993	665	2982	8
25	284	171	0.040	0.2205	0.4	17.1444	15.4	0.5639	15.2	2943	454	2883	439	2984	7
5	250	155	0.040	0.2205	0.5	17.6659	3.0	0.5810	2.8	2972	88	2953	82	2985	9
19	431	261	0.036	0.2213	0.4	17.3150	9.4	0.5675	9.2	2952	279	2897	267	2990	7
32	528	306	0.090	0.2213	0.6	16.3956	19.4	0.5373	19.2	2900	564	2772	533	2990	10
11	229	146	0.014	0.2215	0.5	18.4161	4.4	0.6030	4.2	3012	134	3042	128	2992	8
21	220	145	0.035	0.2218	0.5	18.9485	11.4	0.6196	11.2	3039	348	3108	349	2994	8
38	324	209	0.039	0.2219	0.4	18.5511	25.4	0.6064	25.2	3019	768	3055	770	2994	7
31	348	221	0.055	0.2220	0.7	18.0857	18.4	0.5909	18.2	2994	552	2993	545	2995	12
9	198	133	0.013	0.2220	0.5	19.3072	2.4	0.6307	2.2	3057	75	3152	70	2995	8
20	528	312	0.025	0.2224	0.4	17.0171	10.4	0.5549	10.2	2936	306	2846	291	2998	6
7	427	259	0.076	0.2224	0.6	17.2403	3.3	0.5621	3.1	2948	98	2875	90	2998	9
18	272	168	0.042	0.2226	0.5	17.7309	8.4	0.5778	8.2	2975	251	2940	241	2999	7
12	417	262	0.039	0.2236	0.8	18.1095	5.4	0.5874	5.2	2996	163	2979	155	3007	12
6	599	355	0.042	0.2312	1.2	17.5608	3.9	0.5510	3.0	2966	114	2829	84	3060	20
10	619	360	0.012	0.2421	2.1	17.9954	3.4	0.5392	3.2	2989	103	2780	89	3134	34
481201															
19	40	29	0.704	0.2190	0.6	17.9311	1.8	0.5938	1.6	2986	52	3005	49	2973	10
7	62	43	0.722	0.2243	0.5	17.4995	1.7	0.5659	1.6	2963	49	2891	46	3012	8
8	40	27	0.725	0.2285	0.8	17.5620	2.1	0.5573	2.0	2966	64	2856	57	3042	12
5	37	24	0.428	0.2300	1.3	17.2136	3.2	0.5427	3.0	2947	96	2795	83	3052	21
13	28	19	0.518	0.2302	0.6	18.3364	1.8	0.5777	1.6	3008	53	2939	48	3053	10
34	53	37	0.635	0.2303	0.6	18.0142	2.5	0.5674	2.4	2990	74	2897	69	3054	10
12	38	29	0.911	0.2313	0.6	18.5637	1.8	0.5822	1.7	3019	55	2958	50	3061	10
33	29	21	0.640	0.2315	0.7	19.1193	1.8	0.5990	1.7	3048	54	3026	50	3062	11
10	30	21	0.531	0.2316	0.7	18.4722	1.8	0.5785	1.7	3015	54	2943	49	3063	11
6	41	31	0.751	0.2320	0.5	19.1053	1.7	0.5972	1.6	3047	52	3019	49	3066	9
37	38	28	0.730	0.2321	0.6	18.8941	1.8	0.5905	1.7	3036	54	2991	50	3066	10
18	65	49	0.776	0.2322	0.4	19.1895	1.7	0.5994	1.7	3051	52	3027	50	3067	6
23	49	37	0.630	0.2322	0.6	19.8700	1.8	0.6206	1.7	3085	55	3113	52	3067	10
17	57	41	0.678	0.2322	0.5	18.8280	1.7	0.5880	1.6	3033	51	2981	48	3067	8
9	48	33	0.585	0.2328	0.5	18.2030	2.3	0.5672	2.2	3001	69	2896	65	3071	8
32	36	27	0.979	0.2331	0.6	18.5951	1.8	0.5785	1.7	3021	54	2943	49	3074	10
26	65	50	0.999	0.2331	0.5	19.0074	1.9	0.5913	1.8	3042	57	2995	54	3074	8
20	51	37	0.600	0.2332	0.5	18.8931	1.7	0.5876	1.6	3036	51	2980	48	3074	8
22	34	25	0.559	0.2333	0.8	19.2398	1.8	0.5981	1.7	3054	56	3022	50	3075	12
4	16	11	0.514	0.2333	1.4	18.3985	4.1	0.5719	3.9	3011	124	2916	113	3075	22
21	57	42	0.594	0.2336	0.5	19.2671	1.7	0.5982	1.6	3055	51	3023	48	3077	8
25	68	48	0.437	0.2336	0.5	19.6612	1.7	0.6104	1.7	3075	53	3072	51	3077	7
31	46	38	1.252	0.2337	0.5	19.4532	1.7	0.6036	1.6	3065	53	3044	50	3078	8
39	41	31	0.862	0.2340	0.6	19.1708	1.7	0.5942	1.6	3050	53	3006	50	3080	9
36	29	20	0.569	0.2341	0.6	19.2440	1.8	0.5963	1.7	3054	55	3015	51	3080	10
38	38	27	0.769	0.2342	0.6	19.1616	2.1	0.5933	2.0	3050	63	3003	59	3081	10
24	42	31	0.621	0.2351	0.7	19.7649	1.8	0.6098	1.7	3080	56	3069	52	3087	10
11	41	30	0.605	0.2353	0.6	19.6825	1.8	0.6066	1.7	3076	55	3056	52	3089	9
30	32	25	0.688	0.2486	1.5	21.0138	2.3	0.6131	1.7	3139	71	3082	52	3176	24

Sample/ analysis	U ppm	Pb ppm	Th/U meas	$^{207}Pb/^{206}Pb$	± 1s %	$^{207}Pb/^{235}U$	± 1s %	$^{206}Pb/^{238}U$	± 1s %	^{207}Pb age ^{235}U	± 1s Ma	^{206}Pb age ^{238}PbU	± 1s Ma	^{207}Pb age ^{206}Pb	± 1s Ma
481217															
19	1750	737	0.048	0.1835	0.3	10.1393	1.5	0.4008	1.5	2448	38	2173	33	2684	4
6	2613	1126	0.036	0.1840	0.4	10.5154	1.8	0.4144	1.8	2481	46	2235	40	2690	6
22	474	255	0.055	0.1893	0.2	13.3898	1.4	0.5131	1.4	2708	38	2670	37	2736	4
8	707	395	0.061	0.1893	0.3	13.8349	1.3	0.5301	1.3	2738	37	2742	36	2736	5
39	489	269	0.053	0.1895	0.2	13.7448	1.3	0.5259	1.3	2732	36	2724	36	2738	4
9	328	170	0.048	0.1897	0.3	12.9373	1.4	0.4946	1.4	2675	38	2591	36	2740	5
4	495	264	0.045	0.1901	0.4	13.3205	1.4	0.5081	1.3	2703	37	2649	36	2743	6
32	463	246	0.046	0.1902	0.3	13.2727	1.4	0.5061	1.4	2699	38	2640	36	2744	4
18	542	293	0.056	0.1906	0.2	13.5224	1.4	0.5146	1.4	2717	38	2676	37	2747	4
21	379	205	0.048	0.1906	0.2	13.5410	2.0	0.5152	2.0	2718	56	2679	54	2747	4
26	440	238	0.056	0.1909	0.2	13.5590	1.4	0.5152	1.3	2719	37	2679	36	2750	4
5	548	288	0.062	0.1910	0.3	13.1410	1.5	0.4989	1.4	2690	39	2609	37	2751	5
33	640	349	0.042	0.1915	0.3	13.6750	1.4	0.5180	1.4	2727	38	2691	36	2755	5
10	574	308	0.059	0.1915	0.3	13.3993	1.4	0.5075	1.3	2708	37	2646	35	2755	6
17	314	172	0.030	0.1921	0.3	13.8473	1.3	0.5228	1.3	2739	37	2711	36	2760	4
38	661	343	0.044	0.1943	0.5	13.1041	1.5	0.4891	1.4	2687	39	2567	35	2779	8
23	705	388	0.041	0.1954	0.4	14.0486	1.4	0.5215	1.4	2753	39	2705	38	2788	6
36	###	1376	0.039	0.1987	0.3	15.3860	1.4	0.5615	1.3	2839	39	2873	38	2816	4
25	467	254	0.039	0.1992	0.2	13.8912	1.5	0.5058	1.5	2742	42	2639	40	2820	4
12	492	273	0.052	0.2037	0.4	14.2291	1.4	0.5065	1.3	2765	38	2642	35	2856	7
481227															
19	86	55	0.252	0.2149	0.4	16.9298	1.6	0.5713	1.5	2931	46	2913	44	2943	7
5	100	69	0.369	0.2183	0.5	18.1855	1.6	0.6042	1.6	3000	49	3047	48	2968	8
34	87	55	0.270	0.2186	0.6	16.9101	1.7	0.5610	1.5	2930	48	2871	44	2971	10
10	139	93	0.370	0.2231	0.7	17.7889	2.1	0.5783	2.0	2978	64	2942	59	3003	12
11	56	39	0.289	0.2254	0.6	19.5536	1.8	0.6293	1.7	3070	55	3147	54	3019	9
24	111	75	0.411	0.2255	0.4	18.2600	1.6	0.5872	1.5	3004	48	2978	46	3021	6
18	95	63	0.367	0.2261	0.2	17.9762	1.5	0.5767	1.5	2988	45	2935	44	3024	4
35	71	47	0.431	0.2265	0.4	17.5478	1.6	0.5620	1.5	2965	47	2875	44	3027	6
21	64	42	0.375	0.2267	0.3	17.8188	1.6	0.5702	1.5	2980	47	2909	45	3029	4
37	59	39	0.350	0.2271	0.5	17.7644	1.7	0.5673	1.6	2977	49	2897	45	3032	9
4	83	59	0.347	0.2281	0.3	19.3721	1.6	0.6159	1.5	3061	48	3094	47	3039	5
20	92	65	0.345	0.2282	0.3	19.5527	1.6	0.6214	1.5	3069	48	3116	48	3039	5
8	100	69	0.430	0.2284	0.4	18.5553	1.7	0.5892	1.7	3019	52	2986	50	3041	6
31	76	53	0.346	0.2286	0.4	19.0237	1.7	0.6037	1.6	3043	51	3045	50	3042	7
17	96	66	0.318	0.2289	0.5	18.8597	1.6	0.5976	1.5	3035	49	3020	46	3044	8
36	77	53	0.400	0.2292	0.6	18.9797	1.7	0.6007	1.6	3041	52	3033	48	3046	10
22	169	115	0.462	0.2294	0.9	18.3265	2.3	0.5795	2.1	3007	69	2947	61	3048	15
32	53	34	0.312	0.2297	0.3	17.9162	1.7	0.5656	1.7	2985	50	2890	48	3050	5
12	89	58	0.363	0.2298	0.4	17.9181	2.3	0.5654	2.3	2985	69	2889	66	3051	7
23	69	43	0.377	0.2300	0.4	17.2047	2.0	0.5425	2.0	2946	59	2794	55	3052	7
38	77	55	0.408	0.2308	0.5	19.3259	1.6	0.6072	1.5	3058	50	3059	47	3058	8
7	95	64	0.316	0.2316	1.3	18.6609	2.0	0.5844	1.5	3024	60	2967	44	3063	21
9	146	102	0.548	0.2316	0.7	18.6032	1.8	0.5826	1.6	3021	54	2959	49	3063	11
33	70	47	0.311	0.2322	0.7	18.5974	1.9	0.5809	1.7	3021	57	2952	51	3067	12
481311															
22	163	93	0.385	0.1996	0.7	14.0996	10.4	0.5122	10.2	2756	288	2666	272	2823	11
24	116	84	0.313	0.2105	0.6	18.6196	12.4	0.6414	12.2	3022	376	3194	390	2910	10
19	74	51	0.262	0.2153	1.4	18.6075	9.4	0.6269	9.2	3022	285	3137	289	2946	22
18	74	52	0.262	0.2209	0.7	19.2807	8.4	0.6332	8.2	3056	258	3162	260	2987	11
33	99	64	0.242	0.2232	0.8	17.9959	16.4	0.5848	16.2	2990	491	2968	481	3004	13
13	125	83	0.160	0.2234	0.7	18.6642	6.4	0.6060	6.2	3025	195	3054	190	3005	11
38	56	47	0.524	0.2244	1.4	22.5787	21.4	0.7297	21.2	3209	688	3532	749	3013	23
31	57	35	0.343	0.2265	0.6	16.7986	14.4	0.5379	14.2	2923	422	2775	394	3027	10
36	95	67	0.448	0.2268	0.7	18.7108	19.4	0.5983	19.2	3027	588	3023	581	3030	11
17	235	155	0.396	0.2270	0.5	17.8429	7.4	0.5700	7.2	2981	222	2908	210	3031	8
34	81	51	0.166	0.2271	0.9	18.1738	17.4	0.5803	17.2	2999	523	2950	508	3032	14
35	37	25	0.420	0.2273	1.3	17.9781	18.4	0.5737	18.2	2989	551	2923	532	3033	21
30	89	61	0.222	0.2283	0.6	19.2433	13.4	0.6114	13.2	3054	410	3076	406	3040	10
11	222	158	0.422	0.2286	0.3	19.3862	4.4	0.6150	4.2	3061	136	3090	130	3042	5
8	106	69	0.374	0.2287	0.7	17.6255	4.2	0.5590	4.2	2970	126	2862	119	3043	10
32	82	59	0.345	0.2288	0.5	20.1631	15.4	0.6390	15.2	3099	478	3185	485	3044	8
23	84	56	0.307	0.2292	0.5	18.5115	11.4	0.5858	11.2	3017	345	2972	333	3046	8

Sample/ analysis		U ppm	Pb ppm	Th/U meas	$^{207}Pb/^{206}Pb$	± 1s %	$^{207}Pb/^{235}U$	± 1s %	$^{206}Pb/^{238}U$	± 1s %	^{207}Pb age ^{235}U	± 1s Ma	^{206}Pb age ^{238}PbU	± 1s Ma	^{207}Pb age ^{206}Pb	± 1s Ma
23		84	56	0.307	0.2292	0.5	18.5115	11.4	0.5858	11.2	3017	345	2972	333	3046	8
5		65	43	0.311	0.2295	0.4	18.7020	3.0	0.5910	2.8	3027	90	2993	83	3049	7
6		149	103	0.317	0.2302	0.5	19.6665	3.9	0.6196	3.0	3075	119	3108	92	3053	8
9		139	98	0.460	0.2306	0.4	19.1690	2.4	0.6029	2.2	3050	74	3041	67	3056	7
10		139	99	0.460	0.2306	0.4	19.2040	3.4	0.6040	3.2	3052	105	3046	98	3056	7
37		66	45	0.252	0.2309	0.7	19.4431	20.4	0.6107	20.2	3064	626	3073	621	3058	12
39		78	50	0.227	0.2322	0.5	18.1276	22.4	0.5661	22.2	2997	672	2892	642	3068	9
4		241	172	0.492	0.2327	0.8	19.2827	5.0	0.6010	4.8	3056	154	3034	147	3071	13
7		202	154	0.561	0.2333	1.3	20.7592	3.3	0.6453	3.1	3127	104	3210	101	3075	21
12		207	145	0.420	0.2337	0.9	19.4414	5.4	0.6035	5.2	3064	167	3044	159	3077	15
481461																
8		121	61	0.003	0.1819	0.9	12.3579	6.7	0.4927	6.7	2632	177	2582	173	2670	15
5		440	221	0.003	0.1834	0.3	12.3982	6.5	0.4904	6.5	2635	172	2572	168	2684	5
24		447	234	0.002	0.1840	0.5	12.9655	6.5	0.5110	6.5	2677	175	2661	173	2689	9
34		334	188	0.004	0.1843	0.3	13.9481	6.5	0.5489	6.5	2746	179	2821	183	2692	5
36		529	300	0.003	0.1843	0.3	14.0615	6.5	0.5532	6.5	2754	179	2839	185	2692	5
20		52	25	0.006	0.1844	1.8	11.7830	6.9	0.4635	6.7	2587	179	2455	164	2693	29
37		232	126	0.003	0.1845	0.4	13.4791	6.6	0.5298	6.6	2714	180	2741	181	2694	6
30		1057	538	0.002	0.1849	0.3	12.6078	6.5	0.4946	6.5	2651	172	2590	168	2697	4
4		261	132	0.011	0.1849	0.5	12.4818	6.9	0.4896	6.8	2641	181	2569	176	2697	8
11		413	193	0.002	0.1851	0.5	11.6171	6.8	0.4552	6.8	2574	175	2418	164	2699	8
23		375	182	0.003	0.1852	0.4	12.0440	6.5	0.4716	6.5	2608	170	2491	162	2700	7
38		630	370	0.003	0.1855	0.4	14.6090	6.5	0.5713	6.5	2790	182	2913	190	2702	6
19		371	183	0.003	0.1855	0.6	12.2725	6.6	0.4799	6.5	2625	172	2527	165	2703	10
26		358	197	0.004	0.1857	0.9	13.7108	6.6	0.5355	6.5	2730	180	2765	181	2704	14
9	c	220	111	0.020	0.1861	0.8	12.4591	6.6	0.4856	6.5	2640	173	2552	166	2708	14
32		578	318	0.002	0.1862	0.3	13.7517	6.5	0.5356	6.5	2733	178	2765	180	2709	5
22		580	294	0.003	0.1869	0.2	12.7016	6.5	0.4928	6.5	2658	173	2583	168	2715	4
31		663	356	0.003	0.1869	0.4	13.4538	6.5	0.5220	6.5	2712	177	2708	176	2715	7
7		228	105	0.003	0.1870	0.3	11.5487	6.7	0.4480	6.7	2569	173	2386	160	2716	4
39		534	306	0.003	0.1889	0.5	14.4806	6.5	0.5558	6.5	2782	182	2849	185	2733	8
35	c	343	208	0.017	0.1890	0.4	15.2677	6.5	0.5858	6.5	2832	185	2972	193	2734	7
25	c	192	113	0.140	0.1947	0.7	14.6953	6.6	0.5475	6.6	2796	185	2815	185	2782	12
33	c	323	196	0.080	0.1954	1.0	15.4236	6.6	0.5725	6.5	2842	187	2918	190	2788	16
18	c	247	138	0.035	0.2028	0.8	14.8325	6.6	0.5305	6.5	2805	184	2744	178	2849	13
13	c	252	146	0.132	0.2043	0.8	15.0833	6.6	0.5354	6.5	2821	185	2764	180	2861	13
21	c	230	124	0.117	0.2115	0.5	14.4135	6.5	0.4943	6.5	2777	181	2589	168	2917	9
17	c	206	115	0.228	0.2125	0.7	14.4794	6.5	0.4943	6.5	2782	182	2589	169	2924	12
481465																
38		156	94	0.320	0.2071	0.4	15.4847	2.1	0.5424	2.1	2846	59	2793	57	2883	6
52		158	99	0.449	0.2073	0.5	15.7289	2.1	0.5503	2.1	2860	60	2827	58	2884	8
8		54	32	0.679	0.2073	0.7	13.9357	2.2	0.4875	2.1	2745	61	2560	54	2885	11
25		72	42	0.394	0.2075	0.7	14.7820	2.2	0.5168	2.1	2801	61	2685	56	2886	11
32		67	44	0.604	0.2076	0.5	15.8038	2.1	0.5522	2.0	2865	59	2834	57	2887	8
43		90	57	0.571	0.2076	0.5	15.4664	2.1	0.5403	2.1	2844	61	2785	58	2887	7
70		34	21	0.383	0.2086	0.9	15.8440	2.8	0.5509	2.7	2867	82	2829	76	2895	14
62		37	29	0.359	0.2088	0.9	20.1341	2.2	0.6993	2.0	3098	68	3418	69	2896	15
56		77	52	0.600	0.2094	0.4	16.4832	2.2	0.5710	2.2	2905	64	2912	63	2901	7
19		69	45	0.604	0.2096	0.5	15.6994	2.1	0.5433	2.0	2859	60	2797	57	2902	8
35		69	46	0.749	0.2097	0.7	16.1005	2.2	0.5570	2.1	2883	63	2854	60	2903	11
10		30	20	0.671	0.2098	1.1	16.2429	3.2	0.5616	3.0	2891	92	2873	85	2904	18
49		85	57	0.747	0.2098	0.5	15.8928	2.0	0.5494	2.0	2870	59	2823	56	2904	9
20		269	168	0.416	0.2098	0.5	15.8060	2.0	0.5463	2.0	2865	59	2810	56	2904	8
61		74	44	0.872	0.2115	0.6	13.4558	2.2	0.4615	2.1	2712	61	2446	53	2917	10
77		40	29	0.902	0.2115	0.7	16.6844	2.1	0.5722	2.0	2917	62	2917	59	2917	11
31		45	29	0.447	0.2115	0.9	16.7369	2.2	0.5740	2.0	2920	65	2924	59	2917	15

Sample/ analysis	U ppm	Pb ppm	Th/U meas	$^{207}Pb/^{206}Pb$	± 1s %	$^{207}Pb/^{235}U$	± 1s %	$^{206}Pb/^{238}U$	± 1s %	^{207}Pb age ^{235}U	± 1s Ma	^{206}Pb age ^{238}PbU	± 1s Ma	^{207}Pb age ^{206}Pb	± 1s Ma
60	39	26	0.671	0.2115	0.8	16.1769	2.2	0.5547	2.1	2887	64	2845	59	2917	12
9	87	51	0.303	0.2119	1.1	15.3464	2.4	0.5253	2.2	2837	68	2722	59	2920	18
58	41	30	0.861	0.2127	0.6	17.1991	2.1	0.5864	2.1	2946	63	2975	61	2926	9
37	28	19	0.613	0.2127	1.9	16.3869	2.8	0.5587	2.0	2900	81	2861	58	2927	31
48	32	21	0.653	0.2128	0.9	15.9184	2.3	0.5425	2.1	2872	66	2794	59	2927	15
36	51	33	0.481	0.2138	0.8	16.5664	2.2	0.5621	2.1	2910	64	2875	59	2934	12
18	15	10	0.600	0.2186	0.8	17.4889	2.2	0.5803	2.1	2962	66	2950	61	2970	13
51	38	27	0.817	0.2208	0.6	17.6145	2.1	0.5786	2.0	2969	62	2943	59	2987	9
64	180	116	0.116	0.2344	0.6	18.8605	2.4	0.5835	2.3	3035	72	2963	67	3083	10
481496															
30	135	201	0.186	0.3041	1.9	29.3898	4.6	0.7008	4.1	3467	317	3424	284	3491	30
12	139	213	0.155	0.3178	0.6	27.9209	4.2	0.6371	4.1	3416	286	3178	263	3559	10
36	85	156	0.307	0.3238	0.3	36.4358	4.2	0.8160	4.1	3678	305	3846	319	3588	5
9	115	108	0.175	0.3296	0.6	30.2259	4.2	0.6650	4.1	3494	291	3287	271	3615	10
24	124	176	0.137	0.3346	1.3	32.7770	4.6	0.7105	4.4	3574	331	3460	307	3638	20
5	184	89	0.223	0.3362	0.8	29.8351	4.2	0.6437	4.2	3481	294	3203	266	3645	12
35	218	87	0.175	0.3374	4.5	29.3398	6.3	0.6307	4.4	3465	437	3152	278	3651	69
37	170	214	0.205	0.3388	0.8	34.4889	4.3	0.7383	4.2	3624	309	3564	299	3657	12
17	228	21	0.327	0.3414	1.7	29.6844	4.6	0.6306	4.3	3476	322	3152	272	3669	26
21	136	185	0.596	0.3415	0.6	32.4229	4.2	0.6886	4.1	3563	298	3377	280	3669	9
8	85	92	0.200	0.3447	1.0	34.5798	4.3	0.7276	4.2	3627	315	3525	297	3684	16
10	122	187	0.429	0.3464	0.6	31.9009	4.2	0.6680	4.2	3547	298	3298	274	3691	9
6	77	166	0.688	0.3530	0.9	39.2786	4.3	0.8069	4.2	3753	320	3814	317	3720	14
20	24	127	0.463	0.3564	1.2	31.5979	4.3	0.6429	4.1	3538	302	3201	263	3735	18
23	234	115	0.273	0.3590	3.0	29.7740	5.3	0.6016	4.4	3479	371	3036	266	3745	46
26	170	115	0.761	0.3597	1.0	35.0705	4.2	0.7071	4.1	3641	308	3447	283	3749	15
34	244	172	0.507	0.3744	1.1	31.9708	4.4	0.6193	4.3	3549	315	3107	268	3809	16
31	241	235	0.128	0.3777	1.9	32.9928	5.0	0.6335	4.6	3580	354	3164	288	3823	29
7	175	82	0.526	0.3839	1.8	34.2226	5.1	0.6465	4.8	3616	368	3214	307	3847	26
38	237	-	0.248	0.4192	2.5	36.0788	5.3	0.6242	4.7	3669	388	3127	292	3979	37

Appendix 3: Tabulated SIMS zircon U-Pb age data

Zircon U-Pb age data were collected using the CAMECA IMS 1270 secondary ion mass spectrometer at the NORDSIM laboratory, Swedish Museum of Natural History, Stockholm. Back-scattered electron images of the grains analysed, and the position of analyses on these grains, are given in PDF format (Supplementary_data_zircon_images.pdf) on the DVD. Abbreviations given in the table are as follows: c - core, r - rim, h - homogeneous, lU - low uranium, t - tip.

Sample/ analysis	[U] ppm	[Th] ppm	Th/U meas	f206%	$^{207}Pb/^{206}Pb$	± 1s %	$^{207}Pb/^{235}U$	± 1s %	$^{206}Pb/^{238}U$	±s %	^{207}Pb age ^{206}Pb	± 1s Ma	Disc. % conv.
465048													
s2_3	6613	412	0.062	4.20	0.1597	0.24	7.1609	1.41	0.3252	1.39	2453	4	-29.8
s2_4	4910	177	0.036	5.51	0.1632	1.22	8.5286	2.33	0.3790	1.98	2489	20	-19.6
s1_12	5772	361	0.063	0.04	0.1676	0.19	9.9879	1.86	0.4323	1.85	2533	3	-10.2
s1_8	5831	341	0.059	0.14	0.1722	0.07	9.4907	1.72	0.3998	1.72	2579	1	-18.7
s1_9	5493	379	0.069	0.12	0.1735	0.45	12.4567	1.79	0.5208	1.73	2591	8	5.3
s2_1	5532	320	0.058	3.25	0.1746	0.18	10.9897	1.50	0.4565	1.49	2602	3	-8.2
s1_1	3558	137	0.039	0.01	0.1758	0.41	12.8206	1.80	0.5291	1.75	2613	7	5.8
s1_20	3455	178	0.052	0.00	0.1767	0.07	12.6492	1.70	0.5192	1.70	2622	1	3.4
s1_19	4044	275	0.068	0.00	0.1769	0.07	12.8417	1.71	0.5266	1.71	2624	1	4.8
s1_3	3059	244	0.080	0.01	0.1771	0.09	12.7670	1.70	0.5229	1.70	2626	1	4.0
s2_7	8243	800	0.097	0.00	0.1773	0.05	12.8538	1.39	0.5258	1.39	2628	1	4.5
s1_2	11880	1070	0.090	0.00	0.1773	0.04	13.9009	1.70	0.5686	1.70	2628	1	13.0
s1_5	4656	267	0.057	0.00	0.1773	0.06	13.0019	1.71	0.5317	1.71	2628	1	5.6
s1_18	8470	634	0.075	0.00	0.1774	0.05	14.0805	1.70	0.5756	1.70	2629	1	14.3
s1_6	10014	710	0.071	0.00	0.1775	0.06	13.6600	1.70	0.5583	1.70	2629	1	10.9
s2_5	1921	56	0.029	0.01	0.1775	0.10	12.4143	1.39	0.5072	1.39	2630	2	0.7
s1_10	8681	662	0.076	0.01	0.1775	0.07	13.0415	1.70	0.5328	1.70	2630	1	5.8
s1_17	4580	255	0.056	0.00	0.1779	0.10	12.9099	1.74	0.5263	1.74	2633	2	4.3
s2_12	4894	192	0.039	0.01	0.1779	0.07	12.3951	1.39	0.5053	1.39	2634	1	0.1
s1_7	2290	82	0.036	0.01	0.1780	0.09	12.5145	1.71	0.5099	1.70	2634	1	1.0
s1_15	4765	181	0.038	0.00	0.1782	0.08	12.9199	1.70	0.5258	1.70	2636	1	4.1
s1_4	4087	156	0.038	0.00	0.1782	0.08	12.8163	1.70	0.5216	1.70	2636	1	3.2
s1_16	2725	96	0.035	0.00	0.1783	0.08	12.8068	1.70	0.5211	1.70	2637	1	3.1
s1_14	1938	57	0.029	0.01	0.1783	0.10	12.5929	1.71	0.5123	1.71	2637	2	1.4
s2_6	4876	179	0.037	0.01	0.1783	0.06	12.5841	1.39	0.5119	1.39	2637	1	1.3
s1_13	2805	92	0.033	0.01	0.1783	0.08	12.6442	1.71	0.5143	1.70	2637	1	1.8
s2_10	6630	432	0.065	0.82	0.1784	0.15	13.9781	1.44	0.5683	1.43	2638	2	12.4
s2_11	3755	125	0.033	0.00	0.1784	0.07	12.5905	1.39	0.5118	1.39	2638	1	1.2
s2_12	7638	342	0.045	0.53	0.1785	0.15	14.1438	1.44	0.5747	1.43	2639	3	13.6
s2_13	3320	104	0.031	0.00	0.1787	0.12	12.4401	1.39	0.5050	1.39	2641	2	-0.3
s1_11	7492	208	0.028	0.00	0.1788	0.06	13.5560	1.70	0.5500	1.70	2642	1	8.6
s2_14	4025	290	0.072	0.17	0.1794	0.08	13.5810	1.45	0.5490	1.45	2647	1	8.1
465049													
5	9923	364	0.037	0.21	0.1710	0.07	20.9577	1.70	0.8887	1.70	2568	1	81.6
4	2444	59	0.024	0.02	0.1723	0.07	13.1994	1.70	0.5555	1.70	2580	1	12.9
12	14828	656	0.044	0.06	0.1744	0.13	13.2755	1.71	0.5520	1.71	2601	2	11.1
2	15734	739	0.047	0.03	0.1756	0.05	12.0243	1.75	0.4965	1.75	2612	1	-0.6
11	1857	41	0.022	0.01	0.1771	0.09	12.2697	1.70	0.5024	1.70	2626	1	-0.1
1	13086	503	0.038	0.15	0.1793	0.04	11.8183	1.74	0.4781	1.74	2646	1	-5.8
3	5525	207	0.037	0.05	0.1807	0.07	17.4376	1.70	0.7000	1.70	2659	1	37.1
6	7592	335	0.044	0.06	0.1818	0.05	15.5761	1.70	0.6214	1.70	2669	1	21.1
7	8903	305	0.034	0.57	0.1889	0.15	18.7719	1.75	0.7208	1.74	2732	3	36.6
465054													
12	4414	290	0.066	25.29	0.1580	0.62	9.6156	1.52	0.4413	1.39	2435	10	-3.9
9	9489	410	0.043	0.56	0.1633	0.19	8.4558	1.48	0.3755	1.47	2490	3	-20.4
1	2150	112	0.052	3.50	0.1722	2.21	9.6670	2.66	0.4071	1.48	2579	37	-17.3
11	5664	211	0.037	0.04	0.1738	0.26	8.6897	1.64	0.3626	1.62	2595	4	-26.8
10	7183	312	0.043	5.86	0.1741	0.27	11.6235	1.42	0.4841	1.40	2598	5	-2.4
2	5597	277	0.049	1.45	0.1756	0.26	11.7315	1.49	0.4846	1.46	2611	4	-3.0
4	2063	137	0.066	0.01	0.1769	0.09	12.1167	1.39	0.4968	1.39	2624	2	-1.1
6	5344	2026	0.379	0.11	0.1772	0.14	12.8440	1.40	0.5258	1.39	2627	2	4.5
14	4242	168	0.040	0.03	0.1776	0.07	12.0698	1.39	0.4928	1.39	2631	1	-2.2
3	2536	133	0.053	0.01	0.1777	0.09	12.3182	1.40	0.5027	1.40	2632	2	-0.3
13	5479	453	0.083	0.01	0.1780	0.08	11.6783	1.41	0.4758	1.41	2634	1	-5.7
8	4866	294	0.060	1.16	0.1835	0.45	15.4674	1.72	0.6112	1.66	2685	7	18.3
7	5097	359	0.070	0.44	0.1939	0.06	25.7178	1.39	0.9619	1.39	2776	1	78.8

Sample/ analysis	[U] ppm	[Th] ppm	Th/U meas	f206%	$^{207}Pb/^{206}Pb$	± 1s %	$^{207}Pb/^{235}U$	± 1s %	$^{206}Pb/^{238}U$	±s %	^{207}Pb age ^{206}Pb	± 1s Ma	Disc. % conv.
477307													
8	33	12	0.374	0.15	0.2196	0.72	17.3943	2.28	0.5744	2.16	2978	11	-2.2
7	127	60	0.474	0.02	0.2225	0.36	17.7821	2.17	0.5795	2.14	2999	6	-2.2
4	33	13	0.382	0.17	0.2225	0.73	17.3403	2.29	0.5651	2.17	2999	12	-4.6
6	26	11	0.433	0.14	0.2226	0.80	17.7883	2.29	0.5797	2.14	2999	13	-2.2
9	45	17	0.385	{0.05}	0.2237	0.60	17.6712	2.24	0.5729	2.16	3007	10	-3.6
5	104	47	0.454	{0.02}	0.2239	0.41	17.0606	2.19	0.5527	2.15	3009	7	-7.1
3	28	13	0.452	0.13	0.2240	0.76	17.8947	2.40	0.5794	2.27	3010	12	-2.6
1	40	16	0.390	0.07	0.2242	0.64	18.0038	2.23	0.5823	2.14	3011	10	-2.2
2	48	27	0.554	{0.01}	0.2258	0.58	18.1430	2.22	0.5828	2.14	3022	9	-2.6
477318													
15	260	8	0.031	0.16	0.1679	0.38	10.6820	1.74	0.4615	1.70	2536	6	-4.3
8	870	327	0.376	0.04	0.2132	0.17	16.4522	1.71	0.5596	1.70	2930	3	-2.8
9	1319	53	0.040	0.01	0.2141	0.11	16.4963	1.71	0.5589	1.70	2936	2	-3.1
13	1292	650	0.504	0.01	0.2186	0.15	16.9774	1.71	0.5632	1.70	2971	2	-3.8
7	79	45	0.571	0.05	0.2199	0.47	16.8292	1.77	0.5549	1.70	2980	8	-5.6
3	122	146	1.201	0.06	0.2200	0.37	17.4154	2.20	0.5741	2.17	2981	6	-2.3
10	3079	3295	1.070	0.00	0.2205	0.10	18.0830	1.70	0.5948	1.70	2984	2	1.0
11	944	445	0.471	0.01	0.2205	0.15	17.5848	1.71	0.5784	1.70	2984	2	-1.8
6	302	18	0.059	0.03	0.2212	0.25	17.2996	1.72	0.5673	1.70	2989	4	-3.8
12	632	222	0.351	0.03	0.2212	0.16	18.2331	1.71	0.5977	1.70	2990	3	1.3
1	856	383	0.448	0.01	0.2212	0.16	17.2042	2.14	0.5640	2.13	2990	3	-4.4
14	78	64	0.819	0.05	0.2215	0.52	17.4221	1.78	0.5705	1.70	2991	8	-3.4
4	381	88	0.232	0.02	0.2217	0.21	17.2833	2.15	0.5654	2.14	2993	3	-4.3
2	2538	2345	0.924	0.00	0.2222	0.08	17.8213	2.13	0.5816	2.13	2997	1	-1.7
5	67	51	0.765	0.07	0.2249	0.49	17.9060	1.78	0.5775	1.71	3016	8	-3.2
477320													
3	670	373	0.557	0.01	0.2210	0.18	17.8113	1.71	0.5844	1.70	2988	3	-0.9
9	381	204	0.535	0.06	0.2213	0.23	16.9816	1.72	0.5566	1.70	2990	4	-5.7
8	475	247	0.519	0.03	0.2216	0.24	18.2107	1.72	0.5961	1.70	2992	4	0.9
7	452	275	0.609	0.02	0.2217	0.19	18.0722	1.71	0.5913	1.70	2993	3	0.1
1	726	443	0.610	0.02	0.2217	0.15	17.4822	1.71	0.5720	1.70	2993	2	-3.2
5	503	320	0.635	0.03	0.2222	0.18	18.2284	1.71	0.5951	1.70	2996	3	0.6
10	555	307	0.554	0.04	0.2227	0.17	18.1654	1.71	0.5916	1.70	3000	3	-0.2
4	791	519	0.656	0.02	0.2235	0.16	18.2098	1.71	0.5910	1.70	3006	3	-0.5
6	475	317	0.668	0.03	0.2236	0.22	17.9796	1.72	0.5831	1.70	3007	4	-1.9
2	554	288	0.520	0.02	0.2238	0.17	18.1016	1.71	0.5867	1.70	3008	3	-1.3
477321													
9	477	267	0.560	23.74	0.2202	3.56	15.8212	4.02	0.5212	1.85	2982	56	-11.4
8	6561	2182	0.333	0.59	0.2246	0.12	21.0523	1.71	0.6798	1.70	3014	2	14.0
1	107	45	0.425	0.19	0.2267	0.58	19.4814	1.81	0.6231	1.71	3029	9	3.9
5	328	132	0.403	0.07	0.2278	0.30	19.4918	1.73	0.6205	1.70	3037	5	3.1
13	5838	759	0.130	0.01	0.2279	0.09	19.9261	1.70	0.6342	1.70	3037	1	5.4
12	330	148	0.450	0.18	0.2280	0.29	18.4080	1.73	0.5855	1.70	3038	5	-2.8
16	140	34	0.241	0.04	0.2287	0.33	19.0137	1.74	0.6029	1.70	3043	5	-0.1
10	1991	516	0.259	1.59	0.2291	0.21	16.5258	1.95	0.5231	1.94	3046	3	-13.4
15	225	126	0.559	1.11	0.2292	0.32	18.3185	1.73	0.5797	1.70	3046	5	-4.0
14	441	265	0.600	0.01	0.2292	0.21	18.9363	1.71	0.5991	1.70	3047	3	-0.8
3	78	31	0.395	0.14	0.2296	0.70	19.7872	1.87	0.6251	1.74	3049	11	3.3
2	1271	104	0.082	0.07	0.2304	0.16	20.1657	1.71	0.6347	1.70	3055	3	4.7
4	362	204	0.562	0.13	0.2304	0.29	19.9515	1.73	0.6280	1.70	3055	5	3.6
7	606	576	0.952	0.05	0.2304	0.22	19.2553	1.72	0.6060	1.70	3055	4	0.0
6	415	340	0.819	0.04	0.2307	0.26	19.3654	1.72	0.6087	1.70	3057	4	0.3
11	368	253	0.687	0.46	0.2311	0.26	18.9353	1.72	0.5943	1.70	3060	4	-2.2

Sample/		[U]	[Th]	Th/U	f206%	^{207}Pb	± 1s	^{207}Pb	± 1s	^{206}Pb	±s	^{207}Pb age	± 1s	Disc. %
analysis		ppm	ppm	meas		^{206}Pb	%	^{235}U	%	^{238}U	%	^{206}Pb	Ma	conv.
477352														
7	t	3331	86	0.026	0.03	0.1946	0.08	14.2887	1.70	0.5325	1.70	2782	1	-1.3
11	c	3116	47	0.015	0.01	0.1981	0.46	16.0648	2.45	0.5883	2.41	2810	8	7.7
6	c	3231	40	0.013	0.03	0.1988	0.26	16.2874	1.79	0.5943	1.77	2816	4	8.5
15	c	3395	71	0.021	0.01	0.2136	0.19	18.0574	1.74	0.6130	1.73	2933	3	6.4
17	c	1746	9	0.005	0.01	0.2172	0.17	17.8555	1.71	0.5961	1.71	2960	3	2.3
5	t	2742	44	0.016	0.01	0.2184	0.15	17.9770	1.73	0.5970	1.72	2969	2	2.1
4	t	1361	29	0.021	0.01	0.2186	0.12	17.3256	1.71	0.5747	1.70	2971	2	-1.8
18	t	1489	28	0.018	0.01	0.2190	0.13	18.1607	1.71	0.6013	1.70	2974	2	2.6
8	c	1467	5	0.004	0.01	0.2194	0.13	17.8354	1.71	0.5895	1.70	2976	2	0.5
2	t	1253	20	0.016	0.01	0.2197	0.11	17.4237	1.71	0.5751	1.70	2979	2	-2.1
10	t	1277	32	0.025	0.01	0.2202	0.11	17.7092	1.70	0.5833	1.70	2982	2	-0.8
12	lU	58	59	1.029	0.11	0.2202	0.52	17.9473	1.78	0.5911	1.71	2982	8	0.5
19	t	1289	45	0.035	0.02	0.2204	0.12	18.3551	1.71	0.6039	1.70	2984	2	2.6
20	t	1901	41	0.021	0.01	0.2205	0.09	18.7429	1.70	0.6166	1.70	2984	2	4.7
3	t	1681	33	0.020	0.01	0.2205	0.10	18.2532	1.70	0.6004	1.70	2984	2	2.0
9	t	2142	54	0.025	0.01	0.2205	0.08	18.0361	1.70	0.5932	1.70	2984	1	0.8
14	t	1588	35	0.022	0.02	0.2208	0.09	18.3965	1.70	0.6042	1.70	2987	2	2.5
21	lU	40	31	0.773	0.10	0.2217	0.62	18.2381	1.82	0.5967	1.71	2993	10	1.0
16	t	2113	32	0.015	0.00	0.2218	0.08	18.9190	1.70	0.6186	1.70	2994	1	4.6
1	lU	43	40	0.920	0.10	0.2229	0.60	18.3016	1.81	0.5956	1.71	3001	10	0.4
13	lU	95	91	0.963	0.06	0.2242	0.39	18.3548	1.75	0.5936	1.70	3011	6	-0.3
477367														
3		984	84	0.085	0.47	0.2150	0.19	16.7340	1.41	0.5645	1.40	2944	3	-2.5
1		1955	206	0.106	0.00	0.2174	0.08	17.3543	1.39	0.5790	1.39	2962	1	-0.7
5		1327	184	0.139	0.01	0.2182	0.12	17.4864	1.40	0.5813	1.39	2967	2	-0.6
14		1322	146	0.110	0.01	0.2184	0.12	17.4627	1.40	0.5800	1.39	2969	2	-0.8
10		1020	115	0.112	0.03	0.2186	0.15	17.6331	1.40	0.5851	1.40	2970	2	0.0
18		828	71	0.086	0.01	0.2191	0.12	17.3112	1.40	0.5732	1.39	2974	2	-2.2
7		946	69	0.073	0.01	0.2192	0.11	17.6656	1.40	0.5845	1.40	2975	2	-0.3
6		905	79	0.088	0.01	0.2194	0.16	17.6657	1.41	0.5840	1.40	2976	3	-0.5
2		1191	186	0.156	0.01	0.2195	0.11	17.5974	1.40	0.5816	1.40	2977	2	-0.9
13		969	84	0.087	0.01	0.2198	0.13	17.6969	1.40	0.5840	1.39	2979	2	-0.6
12		1706	186	0.109	0.01	0.2201	0.08	17.6312	1.40	0.5810	1.40	2981	1	-1.2
9		882	43	0.049	0.01	0.2202	0.12	17.8673	1.39	0.5886	1.39	2982	2	0.1
4		1710	212	0.124	0.01	0.2206	0.15	17.7717	1.41	0.5842	1.40	2985	2	-0.8
15		862	45	0.052	0.01	0.2212	0.14	18.0385	1.40	0.5913	1.39	2990	2	0.2
8		631	48	0.076	0.02	0.2219	0.20	18.2819	1.40	0.5974	1.39	2995	3	1.0
11		521	127	0.244	0.03	0.2278	0.18	18.5226	1.41	0.5897	1.39	3037	3	-2.0
16		267	72	0.271	0.02	0.2301	0.22	19.9013	1.43	0.6272	1.41	3053	4	3.5
17		339	158	0.466	0.02	0.2323	0.18	19.4251	1.40	0.6066	1.39	3068	3	-0.5

Sample/		[U]	[Th]	Th/U	f206%	^{207}Pb	± 1s	^{207}Pb	± 1s	^{206}Pb	±s	^{207}Pb age	± 1s	Disc. %
analysis		ppm	ppm	meas		^{206}Pb	%	^{235}U	%	^{238}U	%	^{206}Pb	Ma	conv.
477385														
2		158	151	0.954	{3.25}	0.2080	0.28	17.9522	1.43	0.6259	1.40	2890	5	10.6
6		1067	65	0.061	0.01	0.2159	0.19	16.9660	1.41	0.5699	1.39	2951	3	-1.8
14		1275	69	0.054	0.01	0.2191	0.09	17.8148	1.42	0.5896	1.42	2974	2	0.6
4		1943	83	0.043	0.00	0.2194	0.08	17.6476	1.40	0.5833	1.40	2977	1	-0.6
3		1923	56	0.029	0.00	0.2195	0.12	17.6746	1.44	0.5840	1.43	2977	2	-0.5
15		2326	64	0.028	0.01	0.2198	0.11	17.7851	1.39	0.5868	1.39	2979	2	-0.1
1		2218	70	0.031	0.00	0.2199	0.07	17.5449	1.41	0.5788	1.40	2980	1	-1.5
9		857	43	0.050	0.03	0.2205	0.20	19.0759	1.44	0.6275	1.42	2984	3	6.6
8		2228	76	0.034	0.00	0.2205	0.09	17.7727	1.40	0.5845	1.39	2985	1	-0.7
11		1847	96	0.052	0.00	0.2208	0.08	17.7529	1.39	0.5831	1.39	2987	1	-1.1
10		1356	42	0.031	0.01	0.2211	0.09	17.8641	1.39	0.5860	1.39	2989	1	-0.6
12		1259	88	0.070	0.01	0.2213	0.12	18.1142	1.43	0.5937	1.42	2990	2	0.6
17		1371	183	0.133	0.01	0.2215	0.09	18.2579	1.39	0.5979	1.39	2991	1	1.3
16		1679	73	0.044	0.01	0.2215	0.10	17.9477	1.39	0.5876	1.39	2992	2	-0.5
7		639	32	0.050	0.01	0.2216	0.14	17.6779	1.40	0.5787	1.39	2992	2	-2.0
5		1992	81	0.041	0.00	0.2222	0.13	17.8571	1.39	0.5830	1.39	2996	2	-1.5
13		233	86	0.370	0.13	0.2279	0.39	17.7093	1.54	0.5635	1.49	3038	6	-6.4
479010														
10	r	515	2	0.004	0.97	0.1828	0.24	12.3103	2.15	0.4884	2.13	2678	4	-5.2
11	r	813	0	0.001	0.01	0.1848	0.16	12.9768	2.14	0.5093	2.14	2697	3	-1.9
7		502	3	0.005	0.04	0.1849	0.20	12.8876	2.14	0.5056	2.14	2697	3	-2.7
2	h	1721	5	0.003	0.01	0.1849	0.10	13.2704	2.14	0.5206	2.14	2697	2	0.2
6		507	2	0.005	0.01	0.1852	0.28	13.0435	2.15	0.5108	2.14	2700	5	-1.8
3		919	4	0.004	0.01	0.1853	0.13	13.3146	2.14	0.5211	2.14	2701	2	0.1
5		490	3	0.007	0.02	0.1855	0.21	13.1634	2.15	0.5146	2.14	2703	3	-1.2
8		558	4	0.006	0.13	0.1856	0.19	13.0957	2.14	0.5117	2.13	2704	3	-1.8
9		546	3	0.005	0.05	0.1857	0.19	13.1473	2.15	0.5136	2.14	2704	3	-1.5
1	c	520	3	0.005	0.02	0.1858	0.19	13.2960	2.14	0.5191	2.13	2705	3	-0.4
4		470	2	0.005	0.02	0.1861	0.19	13.2156	2.15	0.5149	2.14	2708	3	-1.4
12		559	3	0.006	0.01	0.1862	0.27	13.0386	2.15	0.5080	2.13	2709	4	-2.7
479014														
9		348	7	0.020	0.02	0.1748	0.23	11.7992	1.43	0.4895	1.41	2604	4	-1.7
3		559	154	0.275	9.81	0.1774	3.24	6.1713	3.62	0.2523	1.62	2628	53	-49.9
20		335	7	0.022	0.04	0.1777	0.23	12.1089	1.41	0.4942	1.39	2632	4	-2.0
12		3785	1686	0.445	0.93	0.1791	0.21	5.3473	1.64	0.2166	1.62	2644	4	-57.3
16		745	334	0.449	0.33	0.1796	0.53	5.5443	8.03	0.2239	8.02	2649	9	-56.0
13		213	145	0.680	0.14	0.1818	0.30	12.5738	1.42	0.5017	1.39	2669	5	-2.2
14		181	114	0.629	0.04	0.1833	0.31	13.0361	1.43	0.5157	1.39	2683	5	-0.1
18		147	84	0.570	0.13	0.1836	0.39	9.9785	1.61	0.3942	1.56	2685	6	-23.7
6		227	158	0.699	0.10	0.1837	0.30	12.8163	1.44	0.5061	1.40	2686	5	-2.1
1		116	75	0.641	1.37	0.1838	1.08	12.6441	1.76	0.4989	1.39	2688	18	-3.6
8		150	95	0.636	0.79	0.1847	0.39	11.9063	1.48	0.4675	1.42	2696	6	-10.0
19		290	215	0.742	0.18	0.1847	0.25	12.4391	1.41	0.4883	1.39	2696	4	-5.9
17		293	247	0.842	0.03	0.1848	0.21	13.2345	1.42	0.5194	1.40	2696	4	0.0
2		228	167	0.732	0.13	0.1849	0.35	12.8880	1.43	0.5056	1.39	2697	6	-2.7
7		330	251	0.759	0.03	0.1849	0.23	12.9226	1.42	0.5068	1.40	2698	4	-2.5
10		123	70	0.571	0.05	0.1855	0.38	12.8871	1.44	0.5039	1.39	2702	6	-3.2
11		60	26	0.429	0.08	0.1856	0.54	12.9063	1.50	0.5043	1.40	2704	9	-3.2
15		90	47	0.519	0.06	0.1862	0.45	12.8616	1.46	0.5011	1.39	2709	7	-4.1
5		190	97	0.511	0.53	0.2218	1.04	15.9407	1.84	0.5213	1.51	2994	17	-11.8

Sample/		[U]	[Th]	Th/U	f206%	^{207}Pb	± 1s	^{207}Pb	± 1s	^{206}Pb	±s	^{207}Pb age	± 1s	Disc.
analysis		ppm	ppm	meas		^{206}Pb	%	^{235}U	%	^{238}U	%	^{206}Pb	Ma	% conv.
479040														
3		205	68	0.334	0.06	0.1965	0.41	14.3138	1.75	0.5283	1.70	2797	7	-2.8
4		128	51	0.401	0.04	0.2070	0.48	15.8141	1.77	0.5542	1.70	2882	8	-1.7
1		659	258	0.391	0.04	0.2079	0.18	15.9920	1.71	0.5578	1.70	2890	3	-1.4
8		297	213	0.718	0.02	0.2080	0.32	15.6118	1.73	0.5443	1.70	2890	5	-3.8
7	h	2649	1814	0.685	0.01	0.2083	0.08	16.5090	1.70	0.5748	1.70	2892	1	1.5
9		738	424	0.575	0.02	0.2083	0.19	16.2273	1.71	0.5649	1.70	2893	3	-0.2
6	h	2458	1621	0.660	0.01	0.2083	0.09	16.5052	1.70	0.5746	1.70	2893	2	1.5
2	h	2104	791	0.376	0.01	0.2086	0.12	16.5438	1.71	0.5751	1.70	2895	2	1.5
5	h	3107	1934	0.623	0.01	0.2090	0.07	16.7593	1.70	0.5816	1.70	2898	1	2.5
10		183	106	0.580	0.04	0.2299	0.29	18.3119	1.73	0.5777	1.70	3051	5	-4.6
479052														
2		122	66	0.540	0.13	0.1993	0.41	14.5134	1.75	0.5283	1.70	2820	7	-3.7
1		273	208	0.764	0.15	0.2003	0.24	14.5477	1.72	0.5266	1.70	2829	4	-4.4
4		207	107	0.518	0.04	0.2005	0.28	14.9447	1.73	0.5406	1.71	2830	5	-1.9
6		317	196	0.621	0.07	0.2006	0.20	15.8471	1.72	0.5730	1.71	2831	3	3.9
3		355	200	0.563	0.01	0.2008	0.20	15.0014	1.71	0.5417	1.70	2833	3	-1.8
10		157	88	0.558	0.03	0.2010	0.37	14.8095	1.74	0.5343	1.70	2835	6	-3.3
9		181	117	0.647	0.06	0.2011	0.27	14.9572	1.72	0.5395	1.70	2835	4	-2.3
5		223	153	0.689	0.05	0.2011	0.32	14.7145	1.73	0.5307	1.70	2835	5	-3.9
8		418	253	0.607	0.01	0.2013	0.17	15.2378	1.71	0.5490	1.70	2837	3	-0.7
7		303	251	0.827	0.03	0.2021	0.20	15.3119	1.72	0.5495	1.71	2843	3	-0.9
479060														
10		1306	4	0.003	0.01	0.1776	0.11	12.2575	1.40	0.5007	1.39	2630	2	-0.6
9		483	4	0.008	0.27	0.1780	0.24	11.6769	1.42	0.4759	1.40	2634	4	-5.7
12		579	2	0.003	0.05	0.1789	0.17	13.9811	1.41	0.5668	1.40	2643	3	11.9
7		359	170	0.473	0.12	0.1950	0.23	14.4958	1.41	0.5391	1.39	2785	4	-0.2
11		142	92	0.652	0.08	0.2112	0.35	16.5847	1.44	0.5696	1.39	2915	6	-0.4
15		330	228	0.691	0.03	0.2190	0.24	17.4265	1.41	0.5771	1.39	2973	4	-1.5
1		378	100	0.266	0.23	0.2258	0.23	16.1271	1.41	0.5179	1.39	3023	4	-13.4
14		283	53	0.186	0.05	0.2275	0.21	18.5968	1.41	0.5930	1.39	3034	3	-1.4
8		415	106	0.256	0.10	0.2286	0.25	16.0789	1.51	0.5101	1.49	3042	4	-15.4
4		280	103	0.369	0.05	0.2288	0.26	16.9347	1.42	0.5368	1.40	3044	4	-11.0
2		326	118	0.361	0.03	0.2291	0.18	19.0681	1.42	0.6037	1.41	3046	3	0.0
6		501	191	0.380	0.20	0.2294	0.25	18.4012	1.42	0.5817	1.40	3048	4	-3.8
13		390	136	0.349	0.03	0.2299	0.24	19.1427	1.43	0.6039	1.41	3051	4	-0.2
5		440	63	0.143	0.01	0.2300	0.16	19.4029	1.41	0.6119	1.40	3052	3	1.1
16		127	46	0.359	0.16	0.2305	0.48	18.1589	1.47	0.5713	1.39	3056	8	-5.8
3		321	89	0.278	0.02	0.2311	0.19	20.0649	1.41	0.6297	1.40	3060	3	3.7
479745														
12		1594	154	0.096	0.04	0.1900	0.30	10.0759	3.68	0.3847	3.66	2742	5	0.0
14		404	119	0.295	0.47	0.1958	0.28	13.7646	1.50	0.5100	1.47	2791	5	0.5
11		233	63	0.269	0.14	0.1975	0.34	14.6008	1.91	0.5360	1.88	2806	6	0.1
5		348	69	0.197	0.20	0.1979	0.22	14.3807	1.48	0.5270	1.46	2809	4	0.2
16		1885	526	0.279	0.37	0.1982	0.32	12.8154	1.62	0.4690	1.59	2811	5	0.4
6		607	212	0.350	0.06	0.1983	0.15	15.5518	1.40	0.5687	1.39	2812	2	0.1
9		621	232	0.374	0.02	0.1990	0.15	15.2612	1.40	0.5563	1.39	2818	2	0.0
15		370	84	0.227	0.05	0.1993	0.21	15.1163	1.41	0.5500	1.39	2821	3	0.1
1		470	108	0.229	0.67	0.1994	0.24	14.5854	1.41	0.5304	1.39	2822	4	0.7
8		695	213	0.307	0.03	0.1995	0.16	15.5509	1.40	0.5654	1.39	2822	3	0.0
7		571	226	0.396	0.03	0.1996	0.16	15.1289	1.43	0.5498	1.42	2823	3	0.0
10		261	68	0.259	0.09	0.1997	0.33	14.7553	1.43	0.5360	1.40	2823	5	0.1
4		505	144	0.284	0.08	0.1998	0.26	15.1980	1.41	0.5518	1.39	2824	4	0.1
3		468	239	0.511	0.11	0.1999	0.18	14.9574	1.43	0.5428	1.41	2825	3	0.1
2		307	100	0.324	0.09	0.2001	0.26	14.7980	1.42	0.5364	1.39	2827	4	0.1
13		515	171	0.332	0.05	0.2002	0.18	15.0637	1.41	0.5457	1.40	2828	3	0.1

Sample/ analysis	[U] ppm	[Th] ppm	Th/U meas	f206%	^{207}Pb / ^{206}Pb	± 1s %	^{207}Pb / ^{235}U	± 1s %	^{206}Pb / ^{238}U	±s %	^{207}Pb age / ^{206}Pb	± 1s Ma	Disc. % conv.
479825													
4	698	168	0.240	0.04	0.2153	0.16	15.7674	1.71	0.5311	1.70	2946	3	-8.3
8	626	60	0.096	0.04	0.2219	0.20	16.7256	1.71	0.5466	1.70	2995	3	-7.5
2	273	60	0.220	0.05	0.2219	0.30	17.5100	1.73	0.5722	1.70	2995	5	-3.2
7	497	10	0.021	0.05	0.2225	0.20	16.6436	1.71	0.5426	1.70	2999	3	-8.4
9	609	92	0.152	0.04	0.2229	0.21	16.0563	1.72	0.5225	1.70	3002	3	-11.9
14	251	35	0.138	0.07	0.2235	0.32	17.1982	1.73	0.5581	1.70	3006	5	-6.0
12	292	279	0.956	0.05	0.2273	0.28	18.0828	1.72	0.5771	1.70	3033	4	-3.9
6	53	31	0.584	0.25	0.2298	1.11	17.6680	2.03	0.5575	1.70	3051	18	-7.9
11	180	111	0.618	0.33	0.2301	0.42	18.4414	1.75	0.5812	1.70	3053	7	-4.1
15	92	53	0.581	0.14	0.2303	0.45	18.0416	1.76	0.5683	1.70	3054	7	-6.2
10	166	129	0.777	0.08	0.2314	0.35	17.5572	1.74	0.5503	1.70	3062	6	-9.5
13	63	42	0.662	0.10	0.2319	0.52	18.4334	1.78	0.5765	1.70	3065	8	-5.3
3	286	218	0.763	0.03	0.2321	0.24	18.6597	1.72	0.5830	1.70	3067	4	-4.3
1	77	42	0.552	0.05	0.2325	0.46	18.9199	1.76	0.5902	1.70	3069	7	-3.2
5	302	295	0.978	0.02	0.2327	0.25	18.3812	1.72	0.5730	1.70	3070	4	-6.1
479827													
8	57	20	0.353	0.07	0.2235	0.45	17.8532	1.93	0.5793	1.88	3006	7	-2.5
17	1009	1024	1.015	0.01	0.2255	0.15	18.7116	1.71	0.6017	1.70	3021	2	0.7
21	912	716	0.785	0.01	0.2307	0.85	23.2489	7.04	0.7310	6.99	3057	13	20.5
5	153	93	0.610	0.05	0.2309	0.29	18.2927	1.73	0.5746	1.70	3058	5	-5.4
16	858	367	0.427	0.01	0.2310	0.11	19.3921	1.71	0.6090	1.70	3059	2	0.3
6	1251	525	0.419	0.01	0.2311	0.10	19.1580	1.70	0.6013	1.70	3059	2	-1.0
4	1663	1060	0.638	0.01	0.2325	0.09	19.7122	1.71	0.6150	1.70	3069	2	0.9
1	1086	818	0.753	0.01	0.2325	0.11	19.2473	1.70	0.6005	1.70	3069	2	-1.5
15	1444	937	0.649	0.01	0.2325	0.09	19.1497	1.70	0.5973	1.70	3069	2	-2.1
14	1388	596	0.430	0.01	0.2325	0.09	19.6554	1.70	0.6130	1.70	3070	2	0.5
11	1310	851	0.649	0.01	0.2327	0.11	19.0902	1.71	0.5950	1.70	3071	2	-2.5
2	1944	1316	0.677	0.01	0.2327	0.08	19.3763	1.71	0.6039	1.71	3071	1	-1.0
7	2265	2660	1.174	0.01	0.2327	0.07	19.8037	1.70	0.6172	1.70	3071	1	1.2
9	2611	1710	0.655	0.01	0.2327	0.08	19.8169	1.70	0.6175	1.70	3071	1	1.2
3	623	408	0.655	0.02	0.2328	0.14	19.0185	1.71	0.5925	1.70	3071	2	-2.9
20	1301	997	0.767	0.01	0.2329	0.10	19.5165	1.71	0.6079	1.71	3072	2	-0.4
10	895	554	0.619	0.01	0.2329	0.14	19.4382	1.71	0.6054	1.70	3072	2	-0.8
13	1182	936	0.792	0.01	0.2329	0.11	19.3873	1.70	0.6038	1.70	3072	2	-1.1
18	2860	1401	0.490	0.00	0.2330	0.06	20.7254	1.70	0.6451	1.70	3073	1	5.6
12	1790	1278	0.714	0.01	0.2330	0.08	19.7773	1.70	0.6155	1.70	3073	1	0.8
19	2224	4980	2.240	0.01	0.2331	0.07	19.6563	1.71	0.6117	1.70	3073	1	0.2
481246													
4	5974	397	0.066	1.87	0.1425	0.07	21.6110	2.13	1.0997	2.13	2258	1	162.1
2	22606	1125	0.050	0.15	0.1459	0.46	8.6330	5.38	0.4290	5.36	2299	8	0.1
11	3096	120	0.039	1.10	0.1541	0.14	43.1797	2.15	2.0329	2.14	2391	2	352.6
10	4658	123	0.026	1.23	0.1549	0.07	21.4081	2.15	1.0023	2.15	2401	1	122.1
3	16933	612	0.036	0.05	0.1566	0.03	29.4971	2.14	1.3660	2.14	2419	1	199.9
1	25569	1375	0.054	0.11	0.1577	0.11	15.7618	2.72	0.7247	2.72	2432	2	58.2
9	3743	108	0.029	0.14	0.1659	0.28	35.1263	2.27	1.5360	2.25	2516	5	221.7
6	2220	64	0.029	0.09	0.1665	0.10	11.8080	2.14	0.5142	2.14	2523	2	7.3
5	1777	57	0.032	0.25	0.1672	0.20	11.7600	2.15	0.5101	2.14	2530	3	6.1
7	20002	906	0.045	0.01	0.1733	0.04	14.0651	2.13	0.5885	2.13	2590	1	19.0
8	4159	138	0.033	0.02	0.1942	0.12	30.0951	2.29	1.1241	2.28	2778	2	108.7

Sample/ analysis	[U] ppm	[Th] ppm	Th/U meas	f206%	^{207}Pb / ^{206}Pb	± 1s %	^{207}Pb / ^{235}U	± 1s %	^{206}Pb / ^{238}U	±s %	^{207}Pb age ^{206}Pb	± 1s Ma	Disc. % conv.
481271													
3	63	21	0.328	{0.04}	0.2282	0.51	18.2390	1.78	0.5796	1.70	3040	8	-3.8
7	189	86	0.455	0.03	0.2287	0.29	18.8187	1.73	0.5967	1.70	3043	5	-1.1
6	154	64	0.418	0.03	0.2293	0.32	18.8823	1.73	0.5971	1.70	3047	5	-1.2
8	178	90	0.503	0.05	0.2296	0.30	18.7870	1.73	0.5934	1.70	3049	5	-1.9
5	173	77	0.449	0.03	0.2302	0.31	18.5857	1.74	0.5856	1.71	3053	5	-3.3
9	260	198	0.760	0.02	0.2304	0.32	18.8802	1.73	0.5944	1.70	3055	5	-1.9
4	209	104	0.497	0.05	0.2307	0.27	19.3508	1.73	0.6084	1.71	3057	4	0.3
1	191	83	0.437	0.03	0.2308	0.41	18.6197	1.75	0.5852	1.70	3057	7	-3.6
2	224	101	0.452	0.03	0.2315	0.27	18.0705	1.72	0.5661	1.70	3062	4	-6.9
481293													
4	2727	422	0.155	2.65	0.1539	3.45	7.5256	4.09	0.3546	2.19	2390	58	-21.0
9	2954	280	0.095	4.17	0.1571	0.24	4.6548	2.24	0.2148	2.22	2425	4	-53.0
2	4397	210	0.048	2.28	0.1579	0.24	7.8550	2.20	0.3608	2.19	2433	4	-21.3
6 r	3012	163	0.054	1.22	0.1630	0.16	7.9535	2.14	0.3538	2.14	2487	3	-24.9
11	1225	33	0.027	0.02	0.1708	0.14	11.3426	2.14	0.4818	2.14	2565	2	-1.4
12	1867	63	0.034	0.14	0.1710	0.12	11.2458	2.14	0.4771	2.13	2567	2	-2.5
15 c	732	251	0.342	0.02	0.1711	0.18	11.2030	2.14	0.4748	2.13	2569	3	-3.0
1	536	140	0.262	0.04	0.1712	0.21	11.2451	2.15	0.4765	2.14	2569	4	-2.7
14 r	2816	108	0.038	0.99	0.1712	0.20	12.5232	2.18	0.5306	2.17	2569	3	8.4
16	330	146	0.443	0.05	0.1712	0.31	11.2836	2.16	0.4780	2.14	2570	5	-2.4
5	612	155	0.253	0.02	0.1717	0.20	11.1736	2.14	0.4720	2.14	2574	3	-3.8
8 r	1825	56	0.031	0.68	0.1737	0.22	12.5151	2.15	0.5226	2.14	2593	4	5.5
7 c	255	15	0.059	0.41	0.1754	0.36	11.7554	2.17	0.4861	2.14	2610	6	-2.6
10 c	633	103	0.163	0.04	0.1762	0.19	11.8779	2.14	0.4890	2.14	2617	3	-2.4
13 c	720	109	0.152	0.10	0.1762	0.19	11.8825	2.15	0.4890	2.14	2618	3	-2.4
3 c	365	179	0.491	3.11	0.2123	0.54	15.9380	2.20	0.5446	2.13	2923	9	-5.1
481461													
5	1281	4	0.003	0.01	0.1757	0.12	12.2494	1.41	0.5055	1.40	2613	2	1.1
7	731	3	0.004	0.01	0.1760	0.15	12.2120	1.41	0.5034	1.40	2615	3	0.6
12	802	3	0.004	0.03	0.1761	0.17	12.0575	1.47	0.4965	1.46	2617	3	-0.8
1	959	4	0.004	0.01	0.1766	0.14	12.2318	1.40	0.5024	1.39	2621	2	0.2
14	1042	4	0.004	0.01	0.1769	0.14	12.3364	1.41	0.5058	1.40	2624	2	0.7
8	1023	3	0.003	0.01	0.1771	0.13	12.4212	1.41	0.5086	1.41	2626	2	1.1
13	965	4	0.004	0.01	0.1776	0.18	12.4860	1.41	0.5100	1.40	2630	3	1.2
9	891	3	0.003	0.05	0.1776	0.18	12.4116	1.42	0.5068	1.40	2631	3	0.6
3	1562	5	0.003	0.01	0.1777	0.11	12.3836	1.42	0.5055	1.42	2631	2	0.3
11	783	3	0.004	0.02	0.1777	0.15	12.4119	1.40	0.5065	1.39	2632	3	0.5
10	1077	3	0.003	0.01	0.1779	0.14	12.5058	1.42	0.5098	1.41	2633	2	1.0
2	1875	6	0.003	0.01	0.1779	0.10	12.6137	1.43	0.5141	1.43	2634	2	1.9
6	1413	4	0.003	0.01	0.1780	0.13	12.6479	1.41	0.5153	1.40	2635	2	2.1
4	881	169	0.192	0.01	0.1838	1.45	13.4878	2.76	0.5321	2.35	2688	24	2.9
481465													
11	590	3	0.005	0.12	0.1777	0.21	12.3550	1.50	0.5043	1.48	2631	4	0.0
3	617	3	0.005	0.03	0.1781	0.25	12.0959	1.43	0.4927	1.41	2635	4	-2.4
2	657	3	0.004	0.01	0.1785	0.16	12.3605	1.40	0.5022	1.39	2639	3	-0.7
10	1170	4	0.003	0.01	0.1795	0.13	12.6106	1.41	0.5095	1.40	2648	2	0.3
9	923	3	0.003	0.04	0.1809	0.14	12.3752	1.42	0.4962	1.42	2661	2	-2.9
4	897	3	0.004	0.01	0.1811	0.14	12.6850	1.40	0.5080	1.39	2663	2	-0.7
13	1021	3	0.003	0.02	0.1820	0.14	12.9557	1.41	0.5164	1.40	2671	2	0.6
8	940	2	0.002	0.02	0.1838	0.14	13.5354	1.43	0.5340	1.42	2688	2	3.2
12	504	1	0.003	0.02	0.1846	0.23	14.4775	1.45	0.5687	1.43	2695	4	9.6
5	1198	4	0.004	0.01	0.1851	0.11	13.2257	1.40	0.5182	1.39	2699	2	-0.3
1	705	61	0.086	0.02	0.1945	0.33	14.4943	1.44	0.5404	1.40	2781	5	0.2
7	689	281	0.407	0.02	0.2065	0.24	17.6052	1.45	0.6183	1.43	2878	4	9.9

Appendix 4: Tabulated geochemical data

	SY-3 Measured	SY-3 Recommended	W-2 Measured	W-2 Recommended	BIR-1 Measured	BIR-1 Recommended
SiO_2	59.62	59.62	52.37	52.44	47.53	47.77
Al_2O_3	11.52	11.75	15.24	15.35	15.31	15.35
Fe_2O_3	6.44	6.49	10.67	10.74	11.26	11.26
MnO	0.320	0.32	0.163	0.163	0.169	0.171
MgO	2.56	2.67	6.34	6.37	9.67	9.68
CaO	8.25	8.26	10.81	10.87	13.22	13.24
Na_2O	4.11	4.12	2.25	2.14	1.83	1.75
K_2O	4.23	4.23	0.61	0.627	0.03	0.027
TiO_2	0.150	0.15	1.064	1.06	0.955	0.96
P_2O_5	0.53	0.54	0.13	0.131	0.03	0.05
Ba	443	450	173	182	8	7.7
Sr	302	302	192	194	107	108
Y	718	718	22	24	16	16
Sc	7	6.8	34	35	44	44
Zr	322	320	85	94	15	22
Be	21	20	1	1.3	-1	0.58
V	50	50	263	262	322	313

USGS: United States geological Survey. SY-3: Syenite; W-2: Diabase; BIR-1: Basalt

Table A4.1. *Measured and recommended concentrations of major (wt.%) and trace (ppm) analyses of USGS standards by ICP*.*

	BHVO-2 (n=10) Measured	BHVO-2 Recommended	AGV-2 (n=6) Measured	AGV-2 Recommended	BHVO-1 (n=10)* Measured	BHVO-1 Recommended
Li	3.9	5.0	11.7	11.0		
V	331	317	130	120		
Cr	286	280	17	17		
Co	44	45	17	16		
Ni	116	119	21	19		
Cu	133	127	58	53		
Zn	102	103	91	86		
Rb	9.0	9.8	65.1	68.6		
Sr	393	389	719	658		
Y	24.1	26.0	18.7	20.0	24.1	28
Zr	163	172	236	230	166.2	179
Nb	14.79	18.00	11.48	15.00	14.1	19
Cs	0.10		1.19	1.16	0.10	0.13
Ba	131	130	1210	1140	127.1	139
La	15	15	38	38	14.7	16
Ce	38	38	72	68	37.2	39
Pr	5.38		8.53	8.30	5.17	5.4
Nd	24.7	25.0	32.2	30.0	23.6	25
Sm	6.19	6.20	5.87	5.70	5.99	6.4
Eu	2.03		1.49	1.54	1.97	2.06
Gd	6.39	6.30	4.27	4.69	6.21	6.4
Tb	0.95	0.90	0.59	0.64	0.90	0.96
Dy	5.36		3.47		5.13	5.2
Ho	0.98	1.04	0.67	0.71	0.94	0.99
Er	2.64		2.02	1.79	2.49	
Tm	0.33		0.28	0.26	0.32	0.33
Yb	1.99	2.00	1.83	1.60	1.91	2.00
Lu	0.27	0.28	0.28	0.25	0.27	0.29
Hf	4.39	4.10	5.85	5.08	3.91	4.4
Ta	1.01	1.40	0.78	0.89	0.88	1.2
Pb	1.77		14.25	13.00	1.85	2.6
Th	1.47	1.20	7.98	6.10	1.36	1.1
U	0.36		1.89	1.88	0.27	

*Sinter analyses. USGS: United States Geological Survey. BHVO-1: Basalt; BHVO-2: basalt; AGV-2: Andesite

Table A4.2. *Measured and recommended values for the USGS standards BHVO-1, BHVO-2, and AGV-2.*

	Group 1			Group 2			Group 3			Group 4		
Samples	485401	485407	485411	485402	485403	485406	485404	485405	485409	485410	485412	485413
SiO_2	42.88	48.09			52.73		50.04	51.25	50.62			
TiO_2	1.14	0.61			1.42		1.61	1.04	1.59			
Al_2O_3	12.74	13.45			13.49		13.87	14.60	13.98			
Fe_2O_3	20.54	14.53			10.21		15.62	12.03	14.85			
MnO	0.15	0.13			0.13		0.23	0.19	0.22			
MgO	8.76	6.77			10.25		6.62	8.14	5.67			
CaO	12.88	14.50			7.96		9.41	10.12	9.53			
K_2O	0.01	0.13			0.35		0.26	0.08	0.33			
Na_2O	0.90	1.77			3.45		2.15	2.36	2.95			
P_2O_5	0.01	0.02			0.01		0.19	0.19	0.26			
LOI	0.74	0.81			1.64		0.62	0.80	0.36			
Mg#	0.46	0.48			0.67		0.46	0.57	0.43			
Cr	110	221	109	189	172	286	196	362	152	588	2	34
Co	57	48	15	36	35	45	42	41	38	42	4	15
Ni	85	88	62	63	62	64	64	81	59	107	1	30
Rb	3	3	6	52	49	3	8	1	6	4	52	81
Sr	119	127	112	52	54	34	93	129	118	152	121	116
Cs	0.92	0.67	11.58	7.21	6.80	3.19	2.35	0.04	0.37	0.07	0.97	2.89
Ba	3.1	19.7	17.8	60.0	56.9	13.6	113.0	17.4	47.5	190.3	435.8	643.6
Sc	35.3	24.2			45.7		42.3	35.3	43.2			
V	284	228	62	204	189	93	237	143	182	207	1	51
Ta	0.02	0.10	0.03	0.09	0.10	0.18	0.22	0.14	0.16	0.16	0.51	0.32
Nb	0.13	1.08	0.17	1.00	0.97	2.18	3.67	2.45	2.46	2.64	4.26	5.17
Zr	42.3	68.5		9.3	79.3	8.1	90.6	94.7	76.3			137.5
Hf	0.53	0.66	0.44	0.38	0.43	0.43	1.17	0.67	1.22	0.95	2.11	3.43
Th	0.05	0.44	0.21	0.05	0.04	0.20	0.82	0.60	0.68	1.98	5.24	4.69
U	0.04	0.22	0.02	0.02	0.02	0.03	0.19	0.13	0.17	0.50	1.32	0.90
Y	34.8	31.0	19.1	6.2	6.9	7.7	27.8	25.4	32.3	20.8	1.5	8.1
Cu	7	102	4	13	9	10	66	30	12	5	4	5
Zn	91	73	50	86	89	87	158	111	164	144	54	134
Mo	0.08	0.40	0.24	0.04	0.24	0.07	0.17	0.40	0.19	0.31	0.39	0.31
Ga	45	40	22	41	38	30	55	40	49	58	102	133
Pb	1.4	4.3	3.6	1.7	1.7	1.4	3.7	2.0	6.5	12.6	22.2	15.6
La	1.15	2.25	0.65	1.48	1.76	2.39	3.93	4.09	5.86	11.72	15.09	26.38
Ce	4.18	6.87	2.98	2.60	3.38	4.99	11.80	12.05	15.56	24.51	31.74	50.70
Pr	0.83	1.29	0.70	0.29	0.39	0.58	1.92	1.90	2.30	3.32	3.48	5.73
Nd	5.48	8.02	4.41	1.18	1.63	2.42	9.94	9.82	11.45	14.73	12.53	21.13
Sm	2.54	3.38	1.90	0.31	0.43	0.59	3.26	3.14	3.57	3.70	2.27	3.59
Eu	0.61	0.76	0.30	0.29	0.33	0.45	1.17	1.24	1.35	1.15	0.50	0.90
Gd	4.50	4.85	2.75	0.47	0.64	0.81	4.59	4.23	5.12	4.21	1.48	3.13
Tb	0.85	0.85	0.50	0.09	0.10	0.14	0.76	0.71	0.88	0.63	0.13	0.38
Dy	6.02	5.77	3.45	0.77	0.93	1.07	5.12	4.68	5.83	4.03	0.44	1.87
Ho	1.33	1.25	0.75	0.22	0.25	0.28	1.09	1.01	1.29	0.81	0.06	0.34
Er	4.03	3.63	2.30	0.84	0.91	1.03	3.22	2.98	3.84	2.40	0.15	0.88
Tm	0.57	0.50	0.34	0.16	0.17	0.18	0.47	0.42	0.54	0.34	0.01	0.11
Yb	3.76	3.12	2.21	1.34	1.51	1.49	3.11	2.83	3.56	2.24	0.08	0.69
Lu	0.55	0.44	0.33	0.25	0.27	0.27	0.45	0.42	0.53	0.32	0.00	0.10
$(La/Yb)_{cn}$	0.22	0.52	0.21	0.79	0.84	1.15	0.91	1.04	1.18	3.74	136.94	27.30
$(La/Sm)_{cn}$	0.29	0.43	0.22	3.09	2.66	2.62	0.78	0.84	1.06	2.05	4.29	4.74
$(Gd/Yb)_{cn}$	0.99	1.28	1.03	0.29	0.35	0.45	1.22	1.24	1.19	1.55	15.47	3.73
$(Eu/Eu^*)_{cn}$	0.55	0.57	0.40	2.29	1.93	1.97	0.93	1.04	0.96	0.89	0.83	0.82
$(Ce/Ce^*)_{cn}$	1.04	0.99	1.09	0.98	0.99	1.04	1.05	1.06	1.04	0.96	1.07	1.01
Al_2O_3/TiO_2	11.22	22.22			9.47		8.64	14.05	8.78			
Nb/Ta	5.78	11.33	5.49	10.61	10.02	12.18	16.85	17.06	15.80	16.52	8.42	15.99
Zr/Y	1.22	2.21		1.50	11.55	1.06	3.26	3.73	2.36			17.05
Ti/Zr	160.84	52.94			107.63		106.32	65.73	125.08			
Nb/Nb*	0.20	0.39	0.17	1.37	1.38	1.15	0.74	0.56	0.45	0.20	0.17	0.17
Zr/Zr*	0.79	0.92		1.07	6.61	0.48	1.11	1.19	0.83			1.10
Ti/Ti*	0.83	0.37			6.70		1.02	0.70	0.92			

Table A4.3. *Major (wt.%) and trace (ppm) element concentrations and significant element ratios for the lower amphibolites of the Ivisaartoq belt.*

	Inner pillow cores							Outer pillow cores					
Sample	485441	485443	485444	485445	485446	485447	485448	485449	485450	485451	485453	485454	485455
SiO_2	50.46	53.53	49.16	55.21	50.07	55.72	51.97	58.27	58.20	51.33	51.39	56.61	58.42
TiO_2	0.57	0.47	0.55	0.53	0.52	0.51	0.47	0.57	0.52	0.56	0.58	0.54	0.48
Al_2O_3	15.36	13.01	14.66	13.89	14.61	13.59	12.39	15.25	13.72	14.02	14.57	14.89	14.36
Fe_2O_3	7.87	8.45	8.68	7.25	9.38	6.91	9.96	6.25	8.78	10.20	10.83	8.19	6.22
MnO	0.21	0.22	0.22	0.19	0.21	0.19	0.24	0.17	0.16	0.22	0.20	0.16	0.17
MgO	4.39	4.51	5.89	4.70	4.29	4.02	4.25	5.34	5.58	7.86	8.24	5.88	5.79
CaO	20.76	19.26	19.74	17.40	20.45	18.69	20.52	12.01	11.52	14.16	11.41	11.68	13.60
K_2O	-0.01	0.02	0.01	0.03	0.01	0.01	0.01	0.11	0.10	0.11	0.18	0.18	0.11
Na_2O	0.34	0.48	1.07	0.75	0.41	0.31	0.15	1.99	1.37	1.50	2.56	1.82	0.81
P_2O_5	0.04	0.05	0.03	0.03	0.05	0.04	0.04	0.03	0.04	0.04	0.02	0.05	0.03
LOI	1.24	0.72	0.30	0.30	1.02	1.77	0.81	0.74	0.68	3.76	0.80	0.56	0.49
Mg#	0.52	0.51	0.57	0.56	0.48	0.54	0.46	0.63	0.56	0.60	0.60	0.59	0.65
Cr	735	582	665	605	627	645	546	649	603	634	688	620	584
Co	63	54	64	70	52	41	56	38	45	52	63	58	39
Ni	403	369	366	383	329	267	294	175	182	253	319	257	212
Rb	4.2	2.5	2.0	2.0	4.6	2.0	2.0	2.7	2.2	2.1	2.0	2.6	2.7
Sr	77	72	98	88	110	75	109	76	64	138	76	85	87
Ba	21	15	27	28	36	8	9	53	30	39	57	55	41
Sc	47	37	46	44	43	43	38	46	42	47	46	43	39
V	233	223	186	193	221	214	232	226	206	243	251	225	208
Nb	2.21	1.32	1.33	1.37	1.25	1.24	1.26	1.33	1.18	1.29	1.29	1.28	1.06
Zr	32.5	27.3	30.0	31.6	29.3	31.4	27.1	30.7	29.3	32.8	34.1	32.6	29.0
Hf	1.14	0.96	1.06	1.10	1.05	1.11	0.92	1.09	0.93	1.13	1.18	1.02	0.95
Th	0.72	0.51	0.59	0.56	0.57	0.53	0.44	0.56	0.55	0.64	0.61	0.55	0.54
U	0.21	0.19	0.14	0.15	0.55	0.15	0.14	0.15	0.16	0.21	0.20	0.17	0.15
Y	14.6	12.4	15.1	14.8	13.3	13.6	14.8	16.6	14.2	15.8	17.0	14.9	13.8
Zn	87.6	40.7	35.2	43.6	34.6	30.5	45.6	30	57	88	712	57	35
Ga	18.2	16.7	13.9	16.8	19.5	16.4	16.3	11.0	12.4	13.6	12.0	15.0	13.8
Pb	5.7	6.2	5.0	5.3	13.6	7.8	8.1	5.0	5.0	9.0	39.5	5.0	5.3
La	3.26	3.40	3.19	3.83	3.28	3.14	2.53	3.41	2.50	3.57	3.05	3.63	3.19
Ce	7.25	6.85	7.20	8.07	7.20	6.76	5.81	7.98	6.31	8.08	7.35	7.94	6.95
Pr	0.86	0.79	0.89	0.93	0.86	0.82	0.71	0.96	0.80	0.97	0.92	0.89	0.82
Nd	4.64	4.03	4.63	4.94	4.34	4.11	3.73	5.06	4.38	5.07	4.84	4.61	4.22
Sm	1.45	1.28	1.50	1.55	1.41	1.30	1.23	1.56	1.39	1.65	1.54	1.40	1.34
Eu	0.50	0.51	0.56	0.55	0.56	0.53	0.44	0.54	0.49	0.55	0.53	0.57	0.48
Gd	1.91	1.64	2.00	2.01	1.85	1.73	1.65	2.15	1.78	2.06	2.09	1.83	1.72
Tb	0.36	0.31	0.38	0.38	0.34	0.32	0.31	0.40	0.34	0.40	0.39	0.36	0.33
Dy	2.40	2.00	2.49	2.48	2.23	2.22	2.15	2.60	2.24	2.56	2.60	2.36	2.22
Ho	0.52	0.43	0.54	0.54	0.48	0.48	0.49	0.56	0.50	0.57	0.59	0.52	0.48
Er	1.58	1.32	1.69	1.64	1.47	1.47	1.55	1.76	1.56	1.84	1.84	1.58	1.51
Tm	0.23	0.20	0.25	0.24	0.22	0.22	0.24	0.27	0.24	0.28	0.27	0.24	0.23
Yb	1.40	1.23	1.56	1.51	1.34	1.40	1.55	1.70	1.48	1.76	1.74	1.49	1.45
Lu	0.20	0.18	0.23	0.22	0.20	0.21	0.23	0.26	0.21	0.26	0.26	0.22	0.21
$(La/Yb)_{cn}$	1.66	1.97	1.47	1.82	1.76	1.61	1.17	1.44	1.21	1.45	1.26	1.75	1.58
$(La/Sm)_{cn}$	1.45	1.71	1.37	1.59	1.51	1.56	1.33	1.42	1.16	1.40	1.28	1.67	1.54
$(Gd/Yb)_{cn}$	1.12	1.10	1.06	1.10	1.15	1.02	0.88	1.05	0.99	0.97	0.99	1.02	0.98
$(Eu/Eu^*)_{cn}$	0.92	1.08	0.98	0.95	1.07	1.09	0.94	0.90	0.96	0.92	0.91	1.08	0.97
$(Ce/Ce^*)_{cn}$	1.06	1.03	1.05	1.05	1.05	1.03	1.06	1.08	1.09	1.07	1.08	1.08	1.05
Al_2O_3/TiO_2	26.9	27.8	26.7	26.0	28.1	26.7	26.4	26.6	26.6	25.0	25.0	27.5	29.9
Zr/Y	2.2	2.2	2.0	2.1	2.2	2.3	1.8	1.8	2.1	2.1	2.0	2.2	2.1
Ti/Zr	105	103	109	101	106	97	104	112	105	102	102	99	99
Nb/Nb*	0.52	0.36	0.35	0.34	0.33	0.35	0.43	0.35	0.37	0.31	0.34	0.33	0.29
Zr/Zr*	0.88	0.84	0.79	0.80	0.83	0.95	0.88	0.76	0.83	0.79	0.87	0.89	0.85
Ti/Ti*	0.85	0.79	0.78	0.74	0.79	0.83	0.81	0.77	0.81	0.75	0.80	0.83	0.78

Table A4.4. *Major (wt.%) and trace (ppm) element concentrations and significant element ratios for pillow basalts of the Ivisaartoq belt.*

	Pillow rims								
Sample	485457	485458	485459	485460	485461	485462	485464	485465	485466
SiO_2	49.48	48.52	51.97	47.44	47.47	50.32	51.12	48.22	49.89
TiO_2	0.56	0.57	0.53	0.56	0.56	0.55	0.54	0.57	0.50
Al_2O_3	14.55	14.16	13.28	14.85	14.74	12.23	14.72	13.15	13.36
Fe_2O_3	11.57	12.09	11.19	12.70	12.85	12.34	10.65	12.82	11.82
MnO	0.23	0.22	0.22	0.24	0.24	0.24	0.19	0.26	0.21
MgO	8.65	9.45	8.59	9.38	9.40	10.32	8.21	10.40	9.80
CaO	12.89	13.18	12.08	12.98	12.90	11.83	11.71	13.06	12.35
K_2O	0.15	0.16	0.15	0.19	0.21	0.25	0.18	0.15	0.16
Na_2O	1.89	1.62	1.94	1.63	1.61	1.86	2.63	1.33	1.86
P_2O_5	0.04	0.04	0.04	0.03	0.03	0.04	0.05	0.03	0.05
LOI	0.82	0.89	0.95	1.00	0.93	1.00	0.76	1.01	0.87
Mg#	0.60	0.61	0.60	0.59	0.59	0.62	0.60	0.62	0.62
Cr	670	642	592	631	623	604	631	640	603
Co	69	60	61	63	63	62	49	68	51
Ni	315	255	314	271	265	207	264	228	248
Rb	3.1	2.5	2.3	7.9	6.7	3.0	2.0	3.9	2.8
Sr	88	93	79	67	66	59	96	89	114
Ba	50	47	42	70	68	60	77	54	48
Sc	46	46	42	44	45	45	44	45	41
V	251	220	231	227	225	229	217	218	204
Nb	1.46	1.28	1.22	1.05	1.06	1.22	1.21	1.01	1.11
Zr	35.0	34.1	32.6	32.8	32.5	33.1	32.3	34.3	30.7
Hf	1.15	1.16	1.05	1.07	1.13	1.14	1.13	1.10	1.04
Th	0.59	0.58	0.52	0.51	0.54	0.51	0.47	0.55	0.52
U	0.18	0.15	0.16	-0.10	-0.10	0.12	0.16	0.12	0.13
Y	19.3	16.8	15.5	15.8	15.8	14.7	15.9	15.1	15.1
Zn	99	83	88	67	78	84	61	81	85
Ga	13.3	12.2	11.8	12.6	12.5	11.5	13.6	11.4	11.9
Pb	6.7	5.0	9.1	5.1	5.0	10.9	5.0	5.1	5.0
La	3.33	2.86	2.74	2.14	2.12	2.37	2.09	1.70	2.59
Ce	7.88	6.87	6.43	5.70	5.61	6.05	6.01	4.79	6.27
Pr	0.97	0.86	0.77	0.73	0.72	0.76	0.77	0.63	0.77
Nd	5.09	4.64	4.24	4.04	3.97	4.24	4.26	3.69	4.25
Sm	1.71	1.53	1.44	1.31	1.31	1.44	1.44	1.25	1.37
Eu	0.59	0.44	0.48	0.50	0.49	0.50	0.52	0.44	0.48
Gd	2.32	2.04	1.93	1.87	1.85	1.93	1.94	1.68	1.78
Tb	0.45	0.39	0.37	0.36	0.34	0.36	0.37	0.34	0.34
Dy	2.98	2.65	2.40	2.45	2.34	2.35	2.50	2.37	2.26
Ho	0.67	0.58	0.53	0.55	0.54	0.52	0.55	0.53	0.50
Er	2.05	1.78	1.67	1.70	1.65	1.62	1.70	1.68	1.58
Tm	0.32	0.26	0.25	0.25	0.25	0.24	0.26	0.25	0.24
Yb	1.98	1.63	1.57	1.62	1.55	1.56	1.65	1.66	1.49
Lu	0.30	0.24	0.23	0.24	0.24	0.24	0.25	0.26	0.22
$(La/Yb)_{cn}$	1.20	1.26	1.25	0.95	0.98	1.09	0.91	0.74	1.24
$(La/Sm)_{cn}$	1.25	1.20	1.23	1.05	1.05	1.06	0.94	0.88	1.22
$(Gd/Yb)_{cn}$	0.97	1.04	1.01	0.95	0.98	1.02	0.97	0.84	0.98
$(Eu/Eu^*)_{cn}$	0.91	0.76	0.88	0.97	0.96	0.92	0.95	0.92	0.93
$(Ce/Ce^*)_{cn}$	1.08	1.08	1.09	1.12	1.12	1.11	1.17	1.14	1.09
Al_2O_3/TiO_2	26.0	24.8	25.2	26.4	26.3	22.2	27.3	23.2	26.7
Zr/Y	1.8	2.0	2.1	2.1	2.1	2.2	2.0	2.3	2.0
Ti/Zr	96	100	97	103	103	100	100	99	98
Nb/Nb*	0.38	0.36	0.37	0.36	0.36	0.40	0.44	0.38	0.35
Zr/Zr*	0.83	0.89	0.92	0.99	1.00	0.93	0.91	1.12	0.89
Ti/Ti*	0.69	0.79	0.78	0.88	0.89	0.81	0.80	0.96	0.79

Table A4.4 continued. *Major (wt.%) and trace (ppm) element concentrations and significant element ratios for pillow basalts of the Ivisaartoq belt.*

	Group 1			Group 2					Group 3				
Samples	493109	493114	493126	485489	485491	485497	493108	493125	485490	485493	485494	493110	493111
SiO_2	48.75	52.97	52.22	50.86	49.15		47.61		49.83	43.12	49.06	52.48	51.47
TiO_2	1.76	1.37	0.59	1.71	0.78		1.92		1.87	2.52	2.30	1.80	1.15
Al_2O_3	13.65	13.31	13.66	13.18	15.55		14.12		14.28	15.35	14.22	13.61	15.46
Fe_2O_3	16.13	14.76	12.03	14.68	12.89		16.36		14.23	19.73	15.10	12.54	12.17
MnO	0.23	0.21	0.19	0.18	0.20		0.23		0.19	0.29	0.21	0.22	0.19
MgO	6.67	5.81	8.45	6.77	7.93		5.85		7.74	7.75	5.58	5.61	6.84
CaO	10.16	9.09	10.26	9.29	11.76		11.09		8.68	8.15	10.11	10.71	9.84
K_2O	0.14	0.27	0.19	0.14	0.12		0.20		0.29	0.46	0.51	0.18	0.21
Na_2O	2.24	1.97	2.37	2.97	1.55		2.33		2.66	2.31	2.58	2.69	2.47
P_2O_5	0.26	0.24	0.05	0.22	0.07		0.28		0.22	0.31	0.32	0.16	0.19
LOI	0.12	0.34	0.53	0.19	0.62		0.18		0.45	0.28	0.18	0.22	0.65
Mg#	0.45	0.44	0.58	0.48	0.55		0.41		0.52	0.44	0.42	0.47	0.53
Cr	191	97	121	187	262	490	167	319	184	194	61	196	345
Co	48	34	49	43	54	58	51	44	48	53	38	46	36
Ni	80	49	72	60	130	156	92	88	75	75	48	67	77
Rb	2.2	4.5	2.6	1.2	1.3	14.2	2.6	0.6	9.4	17.3	4.5	2.1	2.7
Sr	188	72	77	57	113	60	117	80	103	69	121	91	109
Cs	0.03	0.04	0.04	0.07	0.21	0.64	0.04	0.03	1.49	2.71	0.38	0.02	0.07
Ba	32	20	20	17	4	124	21	7	99	49	175	25	40
Sc	41	42	53	41	43		40		41	59	37	42	34
V	238	174	212	278	216	144	243	177	264	339	261	262	143
Ta	0.26	0.24	0.03	0.26	0.08	0.06	0.30	0.09	0.28	0.37	0.40	0.27	0.14
Nb	4.18	4.00	0.52	3.96	1.15	0.98	4.60	1.35	4.23	5.53	6.23	4.59	2.31
Zr	114	101	30	99	43		129		118	148	149	106	60
Th	0.87	1.58	0.14	1.06	0.45	2.77	0.99	0.37	1.20	1.43	1.39	1.04	0.58
U	0.36	0.47	0.12	0.22	0.09	0.48	1.48	0.21	0.54	0.94	1.81	0.40	0.48
Y	30.4	59.6	17.9	31.4	18.3	13.0	33.0	15.8	34.1	44.1	41.7	33.8	28.0
Cu	25.1	22.5	35.3	7.8	74.0	17.4	13.8	59.2	42.8	22.3	18.5	9.6	43.5
Zn	159.4	111.8	119.2	165.1	118.2	322.9	282.5	105.9	153.3	194.4	166.8	170.3	148.4
Mo	0.32	0.40	0.13	0.31	0.21	0.18	0.37	0.28	0.31	0.26	0.31	0.58	0.92
Ga	43.7	47.4	33.5	44.1	35.2	51.6	46.0	31.6	58.0	56.9	75.8	44.5	45.5
Pb	5.3	3.8	1.2	2.4	1.9	3.1	18.2	3.2	4.2	3.1	3.4	4.2	5.5
La	3.64	7.13	0.92	5.46	2.50	2.46	6.62	2.70	8.17	10.45	10.62	7.87	5.72
Ce	11.80	23.25	2.82	14.80	6.32	6.68	18.55	7.11	22.53	26.48	28.92	21.46	13.97
Pr	2.03	3.56	0.47	2.27	0.97	1.02	2.76	1.03	3.11	3.84	4.09	2.85	2.14
Nd	10.85	18.75	2.76	11.68	4.99	5.21	13.60	5.32	14.55	19.08	19.43	13.73	10.41
Sm	3.69	6.34	1.23	3.67	1.73	1.59	4.18	1.69	4.37	5.51	5.71	4.07	3.20
Eu	1.25	1.36	0.45	1.32	0.67	0.73	1.58	0.64	1.10	1.69	1.87	1.42	1.20
Gd	5.03	8.91	2.06	4.87	2.63	2.31	5.55	2.40	5.75	7.35	7.39	5.34	4.34
Tb	0.85	1.52	0.43	0.88	0.47	0.35	0.95	0.42	0.98	1.32	1.23	0.92	0.75
Dy	5.67	10.57	2.94	5.66	3.37	2.42	6.17	2.80	6.43	8.42	7.88	6.20	5.12
Ho	1.16	2.25	0.68	1.21	0.72	0.53	1.30	0.59	1.34	1.75	1.67	1.29	1.09
Er	3.49	7.02	2.16	3.71	2.18	1.55	3.86	1.82	3.96	5.26	4.96	3.86	3.21
Tm	0.50	0.99	0.33	0.52	0.32	0.21	0.54	0.26	0.59	0.75	0.71	0.55	0.47
Yb	3.17	6.70	2.14	3.61	2.10	1.47	3.67	1.72	3.81	4.95	4.62	3.58	3.11
Lu	0.48	0.97	0.32	0.54	0.32	0.23	0.53	0.25	0.59	0.73	0.69	0.54	0.49
$(La/Yb)_{cn}$	0.82	0.76	0.31	1.09	0.85	1.20	1.29	1.13	1.54	1.51	1.65	1.58	1.32
$(La/Sm)_{cn}$	0.64	0.73	0.49	0.96	0.93	1.00	1.02	1.03	1.21	1.22	1.20	1.25	1.15
$(Gd/Yb)_{cn}$	1.31	1.10	0.79	1.12	1.04	1.30	1.25	1.15	1.25	1.23	1.32	1.23	1.15
$(Eu/Eu^*)_{cn}$	0.89	0.55	0.87	0.95	0.97	1.17	1.00	0.97	0.67	0.81	0.88	0.93	0.99
$(Ce/Ce^*)_{cn}$	1.06	1.13	1.05	1.03	0.99	1.03	1.06	1.04	1.10	1.02	1.08	1.11	0.98
Al_2O_3/TiO_2	7.8	9.7	23.0	7.7	19.9		7.4		7.6	6.1	6.2	7.6	13.5
Nb/Ta	15.8	16.7	15.4	15.2	14.6	16.0	15.3	15.1	15.0	15.1	15.7	16.9	16.0
Zr/Y	3.8	1.7	1.7	3.2	2.4		3.9		3.4	3.4	3.6	3.1	2.2
Ti/Zr	92	81	118	104	108		89		95	102	92	102	114
Nb/Nb*	0.85	0.43	0.53	0.60	0.40	0.14	0.65	0.48	0.49	0.52	0.59	0.58	0.46
Zr/Zr*	1.26	0.65	1.14	1.06	1.03		1.20		1.03	1.01	0.99	0.99	0.73
Ti/Ti*	1.00	0.45	0.92	1.00	0.90		0.98		0.92	0.97	0.87	0.95	0.76

Table A4.5. *Major (wt.%) and trace (ppm) element concentrations and significant element ratios for metavolcanic rocks in the Storø greenstone belt.*

	Group 3							Calc-silicate
Samples	493112	493113	493115	493127	493118	493119	493120	485492
SiO_2	47.21				49.81	50.67	53.76	82.90
TiO_2	0.92				1.26	1.25	1.67	0.12
Al_2O_3	9.85				15.99	16.08	13.66	5.80
Fe_2O_3	17.79				12.81	13.54	11.96	3.60
MnO	0.25				0.20	0.26	0.34	0.06
MgO	14.14				6.39	5.42	4.74	1.67
CaO	8.30				9.71	10.84	12.95	4.80
K_2O	0.26				0.79	0.33	0.07	0.01
Na_2O	1.09				2.88	1.46	0.62	0.99
P_2O_5	0.18				0.17	0.14	0.23	0.04
LOI	1.06				0.64	0.51	0.27	0.37
Mg#	0.61				0.50	0.44	0.44	0.48
Cr	303	261	178	53	180	108	130	21
Co	80	29	38	22	41	59	46	10
Ni	217	54	78	54	94	100	64	8
Rb	15.0	4.6	9.0	10.0	24.0	4.3	1.1	1.8
Sr	17	139	100	317	122	131	100	65
Cs	1.77	0.17	0.14	1.03	1.24	0.15	0.05	0.52
Ba	19	30	58	110	136	65	17	13.29
Sc	32				28	42	37	4.01
V	152	102	172	64	159	189	213	59.92
Ta	0.08	0.05	0.16	0.42	0.26	0.17	0.36	0.02
Nb	1.24	0.58	2.65	6.67	3.89	2.69	5.89	0.40
Zr	40				79	81	149	5.02
Th	0.44	0.29	0.11	2.78	0.36	0.68	1.54	0.07
U	0.30	0.34	0.32	0.54	0.35	0.87	0.39	2.27
Y	16.8	7.3	31.8	15.7	23.0	20.2	40.2	2.9
Cu	34.8	37.4	28.2	8.3	11.5	108.4	56.3	34.3
Zn	140.3	103.5	152.0	126.3	191.3	325.5	154.0	79.1
Mo	0.43	0.15	0.68	0.75	0.47	0.49	0.47	0.14
Ga	30.3	42.8	51.9	57.2	59.7	49.4	40.6	16.28
Pb	2.0	6.1	3.7	7.1	18.9	33.7	3.7	14.21
La	4.89	1.66	7.33	16.74	7.20	5.69	11.31	2.16
Ce	10.59	3.74	16.87	41.23	20.61	13.34	27.17	3.11
Pr	1.45	0.54	2.44	4.80	3.04	1.87	3.84	0.36
Nd	6.90	2.66	12.30	19.19	14.00	8.61	17.65	1.35
Sm	2.08	0.82	3.81	3.97	3.45	2.32	5.02	0.28
Eu	0.82	0.47	1.48	1.08	1.61	0.96	1.63	0.35
Gd	2.71	1.13	5.51	3.88	4.12	3.06	6.69	0.40
Tb	0.48	0.20	0.92	0.52	0.63	0.52	1.11	0.07
Dy	3.21	1.30	5.85	3.04	4.11	3.45	7.13	0.43
Ho	0.65	0.29	1.27	0.60	0.86	0.74	1.51	0.09
Er	2.10	0.87	3.69	1.73	2.57	2.36	4.47	0.33
Tm	0.27	0.12	0.51	0.23	0.37	0.34	0.63	0.05
Yb	1.82	0.78	3.34	1.55	2.53	2.21	4.14	0.35
Lu	0.28	0.13	0.51	0.22	0.38	0.33	0.63	0.06
$(La/Yb)_{cn}$	1.92	1.52	1.57	7.74	2.04	1.85	1.96	4.46
$(La/Sm)_{cn}$	1.52	1.31	1.24	2.72	1.35	1.58	1.46	4.94
$(Gd/Yb)_{cn}$	1.23	1.19	1.36	2.07	1.35	1.15	1.34	0.95
$(Eu/Eu^*)_{cn}$	1.06	1.48	0.99	0.84	1.31	1.10	0.86	3.19
$(Ce/Ce^*)_{cn}$	0.97	0.97	0.98	1.13	1.08	1.00	1.01	0.86
Al_2O_3/TiO_2	10.7				12.7	12.9	8.2	46.7
Nb/Ta	16.1	11.4	16.3	15.9	14.9	16.3	16.2	16.7
Zr/Y	2.4				3.4	4.0	3.7	1.7
Ti/Zr	136				96	92	67	148
Nb/Nb*	0.30	0.30	1.06	0.35	0.88	0.49	0.51	0.36
Zr/Zr*	0.75				0.79	1.27	1.11	0.57
Ti/Ti*	0.96				0.82	1.15	0.71	0.91

Table A4.5 continued. *Major (wt.%) and trace (ppm) element concentrations and significant element ratios for metavolcanic rocks in the Storø greenstone belt.*

Samples	485495	485499	493101	493103	493104	493105	493106	493107	493116	493117	493121	493122	493123
SiO_2	55.33	87.41		42.55	82.53	51.76	52.15		50.34	60.55	55.31		66.99
TiO_2	2.32	0.22		0.20	0.45	0.92	0.85		1.62	1.02	0.99		0.82
Al_2O_3	20.46	6.27		4.61	8.60	21.32	21.77		16.49	15.92	18.52		14.89
Fe_2O_3	11.49	2.45		49.46	4.74	10.62	10.53		16.75	9.16	15.50		5.67
MnO	0.18	0.03		0.04	0.07	0.11	0.10		0.24	0.16	0.16		0.11
MgO	2.42	0.68		2.04	1.19	4.32	4.41		4.68	3.77	2.70		1.96
CaO	3.80	1.01		0.97	0.85	2.41	2.71		4.90	4.71	2.33		4.49
K_2O	1.04	1.27		0.01	0.84	4.30	3.43		4.08	3.53	0.94		1.31
Na_2O	2.83	0.62		0.01	0.69	4.16	3.98		0.67	0.95	3.48		3.55
P_2O_5	0.15	0.04		0.10	0.04	0.08	0.06		0.24	0.23	0.06		0.19
LOI	0.13	0.46		1.96	0.61	1.15	0.80		0.81	0.87	0.65		0.27
Mg#	0.29	0.35		0.08	0.33	0.45	0.45		0.36	0.45	0.26		0.41
Cr		63	81	39	121	240		183	53	33	97	100	5
Co		5	17	10	7	45		31	31	21	20	21	15
Ni		8	41	25	12	120		60	41	33	42	52	22
Rb		36	52	2	30	303		196	162	140	37	100	62
Sr	92	41	91	1	87	142	266	115	68	78	161	41	205
Cs		2.23	2.74	0.25	2.41	28.51		23.22	7.27	4.72	1.98	4.72	4.33
Ba	222	277	444	13	208	265	436	321	534	831	198	569	292
Sc	48	5		9	12	32	33		25	18	27		13
V	391	29	28	42	62	166	203	321	179	75	107	136	52
Ta		0.11	0.17	0.07	0.13	0.44		0.56	0.44	0.62	0.47	0.56	0.68
Nb		1.50	1.73	0.61	1.95	5.37		8.35	7.25	9.83	7.48	11.04	11.09
Zr	157	60		23	71	113	100	133	145	249	181		248
Hf		1.17	1.26	0.71	1.56	2.47		3.52	0.00	0.00	0.00		0.00
Th		2.09	1.03	1.86	4.46	0.00		2.64	3.15	4.87	4.94	6.59	3.82
U		4.38	0.34	0.57	2.24	0.00		4.48	0.57	0.85	0.98	1.58	1.69
Y	44	4	4	9	11	6	24	21	23	29	32	13	23
Cu		6	31	9	36	12		55	47	8	33	24	22
Zn		68	80	63	86	183		245	144	173	107	159	119
Mo		0.36	0.20	0.70	0.61	0.32		1.24	0.72	0.14	0.81	1.75	0.43
Ga		61.4	89.6	16.1	55.1	93.3		113.4	135.7	188.2	62.3	138.1	83.5
Pb		5.0	18.6	0.4	8.2	20.4		19.3	8.5	8.8	19.3	8.5	6.6
La		9.70	9.06	1.15	11.61	21.70		14.50	17.11	39.52	22.81	27.13	23.82
Ce		19.63	19.73	3.07	23.96	47.73		35.33	41.70	83.26	49.76	60.50	62.19
Pr		2.27	2.31	0.43	2.85	5.73		4.50	5.06	10.38	5.98	7.25	7.02
Nd		8.43	8.91	1.98	11.32	22.71		19.94	20.21	41.43	23.49	28.33	27.31
Sm		1.61	1.80	0.88	2.21	4.68		4.92	4.08	7.68	4.70	5.81	5.73
Eu		0.47	0.55	0.35	0.56	1.22		1.77	1.24	1.74	1.98	0.94	1.29
Gd		1.47	1.64	1.58	2.35	4.08		5.08	4.30	7.39	5.54	4.83	5.34
Tb		0.16	0.21	0.26	0.32	0.41		0.74	0.67	1.04	0.97	0.59	0.74
Dy		0.84	1.04	1.60	2.05	1.81		4.42	4.28	5.83	6.03	3.02	4.34
Ho		0.18	0.16	0.32	0.44	0.30		0.89	0.89	1.10	1.22	0.57	0.85
Er		0.55	0.38	0.99	1.28	0.82		2.65	2.60	3.11	3.38	1.83	2.50
Tm		0.07	0.04	0.14	0.18	0.11		0.40	0.37	0.41	0.48	0.28	0.36
Yb		0.48	0.24	0.94	1.23	0.83		2.62	2.44	2.51	3.06	2.08	2.26
Lu		0.08	0.03	0.13	0.19	0.13		0.39	0.35	0.35	0.43	0.32	0.33
$(La/Yb)_{cn}$		14.58	26.55	0.88	6.75	18.74		3.98	5.04	11.31	5.34	9.37	7.54
$(La/Sm)_{cn}$		3.89	3.26	0.85	3.39	2.99		1.90	2.71	3.32	3.13	3.02	2.69
$(Gd/Yb)_{cn}$		2.55	5.53	1.39	1.58	4.07		1.61	1.46	2.44	1.50	1.92	1.95
$(Eu/Eu^*)_{cn}$		0.94	0.99	0.91	0.75	0.85		1.08	0.90	0.71	1.18	0.54	0.71
$(Ce/Ce^*)_{cn}$		1.03	1.06	1.06	1.02	1.05		1.07	1.10	1.01	1.04	1.06	1.18
Al_2O_3/TiO_2	8.8	27.9		22.8	19.2	23.1	25.7		10.2	15.6	18.8		18.2
Nb/Ta		13.6	10.0	8.9	15.4	12.2		15.0	16.5	15.9	15.8	19.6	16.4
Zr/Y	3.6	13.9		2.7	6.3	17.6	4.2	6.2	6.4	8.6	5.6		10.8
Ti/Zr	88	22		52	38	49	51		67	25	33		20
Nb/Nb*		0.12	0.20	0.15	0.10			0.49	0.36	0.26	0.25	0.30	0.42
Zr/Zr*		1.14		1.24	1.00	0.77		0.94	1.12	0.97	1.20		1.38
Ti/Ti*		0.36		0.42	0.48	0.52			0.95	0.33	0.48		0.36

Table A4.6. *Major (wt.%) and trace (ppm) element concentrations and significant element ratios for metasedimentary rocks in the Storø greenstone belt.*

	Au (ppm)	Mass (gr)
485489	20	10.00
485490	51	10.00
485491	11	10.00
485492	8	10.00
485493	12	10.00
485494	17	10.00
485495	14	10.00
485496	19	6.80
485497	11	6.19
485498	11	10.00
485499	12	10.00
493101	18	6.26
493102	18	6.75
493103	15	10.00
493104	10	10.00
493105	10	9.26
493106	23	10.00
493107	24	6.37
493108	18	10.00
493109	15	10.00
493110	1730	10.00
493111	12	10.00
493112	10	10.00
493113	18	6.40
493114	9	10.00
BLANK	-1	10.00
STD UMT-1	55	2.00
STD WMG-1	99	2.00
STD LOW PGM	143	10.00
STD HI PGM	316	10.00
UMT-1 Cert	48	
WMG-1 Cert	110	
STD LOW PGM Cert	145	
STD HI PGM Cert	270	

Table A4.7. *Gold concentrations in the Ivisaartoq metavolcanic and metasedimentary rocks.*

Appendix 5: A mid-Archaean island arc complex with gold mineralisation at Qussuk, Akia terrane, southern West Greenland

Draft manuscript for submission to the Journal of the Geological Society, London

A mid-Archaean island arc complex with gold mineralisation at Qussuk, Akia terrane, southern West Greenland

Adam A. Garde
Geological Survey of Denmark and Greenland
Øster Voldgade 10, 1350 Copenhagen K, Denmark

Manuscript to be submitted to the
Journal of the Geological Society, London, July 2005

Abstract: Remnants of a c. 3070 Ma oceanic island arc complex in the eastern Akia terrane north of Nuuk, southern West Greenland, provide a genetic link between amphibolite of ocean floor affinity and the regional grey gneisses, and may represent a regional source of gold. The island arc complex now forms steep, isoclinally folded panels east of Qussuk in northern Godthåbsfjord and on adjacent Bjørneøen. Predominant andesitic amphibolite with volcaniclastic texture is intercalated with layered schists of andesite-like composition and opx-rich cumulates and intruded by c. 3005–2980 Ma tonalite and granite. Associated tholeiitic metabasalts may be older than the island arc complex itself. Thin horizons with disseminated pyrrhotite within the andesitic amphibolite are associated with exhalative quartz-, garnet- and tourmaline-rich rocks and locally contain gold in the ppm range, and epidote+diopside-rich boudins of altered volcaniclastic rocks without metal anomalies are interpreted as metamorphosed, supra-subduction zone epidosites representing hydrothermal feeders to the gold mineralised horizons.

A volcanic U-Pb zircon age of 3071 ± 1 Ma at Bjørneøen is the first deposition age obtained from Akia supracrustal rocks; a minimum deformation age of 2984 ± 2 Ma was determined east of Qussuk. Other new age data indicates peak metamorphic recrystallisation of zircon at 2995–2975 Ma. The Qussuk area was not affected by the late Archaean thermal and structural reworking that was associated with the inferred terrane assembly at c. 2700 Ma in other parts of the Nuuk region.

Keywords: Archaean, Akia terrane, andesite, gold, metamorphic zircon

Introduction

The Nuuk region of southern West Greenland is renowned both for its early Archaean Isua greenstone belt and Amîtsoq gneisses, and for the application of the so-called terrane model to Archaean rocks, according to which the grey gneisses in the Nuuk region form a collage of individual tectono-stratigraphic terranes. The Nuuk region also contains several greenstone belts of middle to late Archaean age, which are dominated by upper amphibolite facies basic metavolcanic rocks (references). The terrane model implies that each of these belts may have unique ages and primary geotectonic settings, but the depositional ages, lithological components and tectono-thermal histories of most of them are only imperfectly known. Several gold occurrences have previously been found within the greenstone belts, and the economic potential of one of them, on Storø east of Bjørneøen, is currently being assessed by a private company. However, the genesis of the gold deposits remains poorly understood, and it has not yet been established if a common regional process of gold mineralisation has been active.

This paper describes the intensely deformed and metamorphosed, but still identifiable remnants of a large, mid-Archaean island arc complex that occurs close to the south-eastern edge of the Akia terrane on Bjørneøen and the peninsula east of Qussuk (Fig. 1; in the following called the Qussuk peninsula). The Akia terrane is the largest and most northerly of several previously identified tectono-stratigraphic terranes in the Nuuk region (Friend & Nutman 2005).

The island arc complex provides a hitherto missing link between basic amphibolites and layered complexes of ocean floor affinity in the greenstone belts, and the grey, continental crustal tonalite-trondhjemite-granodiorite (TTG) orthogneiss precursors that intruded them. The tectonic setting of the island arc complex and its relationship with the surrounding grey gneisses are described, and new geochemical data from the island arc complex and recently discovered gold anomalies within it are presented. In addition, new zircon U-Pb ion probe geochronology from the Qussuk peninsula and Bjørneøen provides the first precise age of deposition of supracrustal rocks from the Akia terrane and a minimum age of their deformation, and confirms that the entire Qussuk area was unaffected by the thermal and structural reworking that occurred in other parts of the Nuuk region during the subsequent late Archaean terrane assembly.

Previous work

The Archaean accretion and tectonothermal evolution of the Akia terrane have previously been studied by e.g. Berthelsen (1960), Lauerma (1964), Taylor et al. (1980), Wells (1980), Dymek (1984), Garde et al. (1986, 2000), Nutman & Garde (1989),, Riciputi et al. (1990), McGregor et al. (1991) and Garde (1997).

The Akia terrane has undergone a complex history of plutonic igneous activity, deformation and metamorphism. As currently known, the terrane contains two continental crustal complexes of

different age. An older dioritic gneiss dated at 3221 ± 13 Ma (Garde 1997) with fragments of amphibolite and a dismembered anorthosite-leucogabbro complex forms the central and southern parts of the Akia peninsula (Fig. 1). These rocks form the core of a larger block of 3.05–2.97 Ga grey gneiss between Fiskefjord and Godthåbsfjord (Garde et al. 2000). The bulk of the grey gneiss in this region consist of diorite and tonalite, besides younger plutons in the south-east such as the 2982 ± 7 Ma Taserssuaq tonalite complex and Qugssuk granite (Garde 1990, 1997). The grey gneisses were emplaced into supracrustal rocks and associated mafic intrusive complexes. Only little detailed work has previously been carried out on Bjørneøen apart from regional mapping (McGregor 1993); Baadsgaard & McGregor (1981) reported apparent emplacement ages < 3065 Ma of parent magmas to grey gneisses but disturbed zircon U-Th-Pb systematics, and Taylor et al. (1980) likewise suggested postmagmatic resetting of mid-Archaean Pb-Pb ages.

Although The the supracrustal sequences in the grey gneiss block between inner Fiskefjord and Godthåbsfjord (Fig. 1) are older than 3.05 Ga (Garde et al. 2000), their actual age (s) of deposition have not previously been established. The supracrustal sequences in the grey gneiss block between inner Fiskefjord and Godthåbsfjord (Fig. 1) are older than 3.05 Ga, which is the age of the oldest zircon populations in the tonalitic grey gneiss that intrude them (Garde et al. 2000), but their age of deposition has not previously been established. The supracrustal sequences consist of heterogeneous, compositionally banded metavolcanic amphibolite and pelitic metasediment, associated with voluminous metagabbro and ultrabasic rocks derived from disrupted layered intrusive complexes and possibly lumps of the uppermost mantle (Garde 1997). The latter author tentatively interpreted the bulk of the supracrustal rocks as representing remnants of oceanic crust, into which the precursors of the grey gneisses were intruded in a convergent plate-tectonic scenario. Also grey, leucocratic amphibolite of intermediate composition and andesitic chemical affinity was recognised locally in the easternmost part of the Akia terrane.

Early magmatic accretion of the 3.05–2.97 Ga grey gneiss precursors and intercalation of supra- and infracrustal rocks by thrusting was followed by continued intrusion of tonalite, trondhjemite and granodiorite, 2–3 phases of recumbent folding, upright folding, and finally emplacement of granitic rocks derived from mobilisation of grey gneiss (Garde et al. 1987; Garde 1997). The terrane is also intensely deformed by localised steep, narrow N- to NE-trending shear zones that are broadly contemporaneous with the Qugssuk granite(2975 ± 5 Ma). These granites are locally weakly deformed, but they predate a series of undeformed post-kinematic dioritic plugs of almost the same age (Garde 1991; Garde et al. 2000).

Most of the Akia terrane underwent thermal granulite facies metamorphism at 2981 ± 8 Ma, the age of metamorphic zircons in granulite facies gneisses (Garde et al. 2000). Immediately thereafter the north-eastern part of the granulite facies terrain underwent static hydrous retrogression under declining amphibolite facies facies P-T conditions. Only the easternmost parts of the Akia terrane north and east of Qussuk and on Bjørneøen do not display direct field evidence of former granulite facies metamorphism or high-grade static retrogression, instead preserving peak, amphibo-

lite facies assemblages. Previous work has indicated that the central and eastern parts of the Qussuk peninsula itself is underlain by relatively young components of the grey gneiss complex such as the above mentioned Qugssuk granite and the Taserssuaq tonalite complex. The Qugssuk granite has also previously yielded a Rb-Sr whole-rock age of 2969 ± 32 Ma (MSWD = 1, Garde et al., 1986), and ten samples of amphibolite facies grey gneiss from the eastern coast of Qussuk yielded a Rb-Sr yielded an errorchron of 2954 ± 120 Ma (MSWD = 6.85, Garde 1997). The area north and east of Qussuk thus appears to be slightly younger than the rest of the Akia terrane and underwent a simpler structural history than its central part (Garde 1997).

The relict island arc complex on the Qussuk peninsula

The supracrustal units on the Qussuk peninsula form two steep, isoclinally folded panels up to 15 km long and 2 km wide, with several thinner panels, intruded by voluminous sheets of tonalite and granite (Figs 2 and 5). The supracrustal rocks are dominanted by grey, intermediate amphibolites and schists of various types, including rocks with fragmental primary textures (see below), as well as localized trains of highly altered ultramafic rocks. The fragmental amphibolite is of andesitic composition (see section on geochemistry), and corresponds to small occurrences of 'leuco-amphibolite' and 'grey amphibolite' previously reported by several authors from the Archaean of southern West Greenland (references).

Field relationships with host orthogneisses and discordant granitic veins

The external contacts between the supracrustal panels and the tonalitic to granitic orthogneisses which underlie most of the Qussuk peninsula are straight and strongly deformed and, viewed in isolation, might be considered purely tectonic. However, the map patterns in the south-western part of the peninsula display branching and interfingering relationships between the two groups at a scale of hundreds of metres and larger (Fig. 2) that cannot be explained entirely by folding and thrusting. These outcrop patterns suggest that the contacts were originally magmatic. This interpretation is confirmed by xenoliths of supracrustal amphibolite with a previous tectonic fabric that are commonly embedded in the generally less intensely deformed orthogneisses (Fig. 3). Furthermore, numerous sheets of tonalite and granite are clearly intrusive into the amphibolite panels (Fig. 4).

The supracrustal lithologies

The predominant rocks interpreted as volcaniclastic are composed of elongate, closely packed, angular, fine-grained clasts, up to about 10-15 cm long and set in a fine-grained matrix (Figs 6–7). The clasts consist of fine-grained plagioclase, hornblende and accessory titanite, and commonly also minor biotite, diopsidic clinopyroxene and/or quartz, with slight variations in colour index and grain

size. The matrix has a similar or slightly more leucocratic composition. The rocks are mostly highly deformed, with strongly elongate or more rarely pancake-shaped clasts depending on the strain intensity and local components of constriction versus flattening, but occasionally the original shapes of the clasts are well preserved (Figs 6–7). The fragmental texture is also well preserved in zones that seem to have undergone hydrothermal alteration and cementation prior to the most intense penetrative deformation (described below) and were therefore more competent than the adjacent unaltered rocks. In these places it can be ascertained that adjacent individual clasts, although angular, do not fit together like pieces in a jigsaw puzzle. They are therefore not autoclastic but are interpreted to be genuine volcanic clasts that were transported by water, air or in rock slides to their final loci of deposition. A detailed field map from the central Qussuk area, shows traverses where this texture has been noted, although in a very variable state of preservation (Fig. 5).

The fragmental amphibolite contains trains of c. 5–10 m (rarely up to 50 m) wide lenses of coarse-grained, pale brown weathering ultramafic rocks with closely packed, 2–5 cm large pseudomorphs of orthopyroxene (Fig. 8). The lenses now largely consist of pale, Mg-rich amphibole with a radiating, poikiloblastic texture, deep green chlorite, and occasionally fine-grained magnetite. These rocks are interpreted as hydrated and tectonically dismembered orthopyroxene-rich cumulate rocks, in which the primary textures have survived the regional deformation.

Rare units up to a few metres thick of more mafic, heterogeneous, but not fragmental amphibolite s.s. occur within the fragmental amphibolite but without clear timing relationships. The heterogeneous amphibolite s.s. contains irregular, flattened networks of thin (cm-scale), pale, diopside and calcic plagioclase - rich veins in a homogeneous, fine-to medium-grained groundmass of hornblende and plagioclase. These rocks may represent former pillow lavas and/or autoclastic volcanic rocks. Adjacent are sheets of homogeneous amphibolite s.s. up to about 10 m thick without such networks. The homogeneous amphibolite locally displays indistinct rhythmic layering at a scale of 5-10 cm, outlined by variations in the proportions of hornblende and plagioclase, and interpreted to be of magmatic origin. The homogeneous amphibolite may reflect hypabyssal sill complexes, which together with the net-veined amphibolite may represent the basement to the fragmental amphibolite. Alternatively the sill complexes may also have been intruded into the fragmental amphibolite.

In all of its outcrop areas the fragmental amphibolite is closely associated with schistose, relatively fine-grained rocks of intermediate composition, which in addition to a generally strong planar fabric also possess a distinct millimetre- to centimetre-scale compositional layering, defined by variations in the relative contents of plagioclase, biotite, quartz, and sometimes hornblende. They occur intimately intercalated with the fragmental amphibolite, and are characterised by persistent thin, lateral compositional layering. Moreover, they commonly contain hornblende but never alumino-silicate. The assemblage perserved in the intermediate schist, and the absence of quartz-rich rocks, suggest that these deposits are not of purely detrital origin but more likely tuffs or tuffites.

Sheets of variably discordant, massive, fine-grained diorite, up to a couple of metres thick, occasionally occur within the fragmental amphibolite and associated metasediment. These sheets are

interpreted as feeder dykes that have been rotated towards parallelism with their hosts during deformation, or as hypabyssal sills emplaced into previously deformed pyroclastic rocks.

Epidote- and diopside-rich alteration zones interpreted as metamorphosed epidosites

In the central part of the western panel of supracrustal rocks on the Qussuk peninsula, are lenses of fragmental surpracrustal rocks that have a dark yellowish green matrix consisting of medium-grained assemblage primarily consisting of diopside, zoisite, titanite, and garnet. The largest lens is about 350 m long and more than 50 m wide; others form strings of tectonic boudins only a few metres large. The assemblage in the matrix is interpreted to have formed through metamorphism of hydrothermally altered material. In these rocks, the volcanic clasts themselves are only weakly altered. The appearance of the hydrothermally altered rocks as tectonic boudins with relatively weak internal deformation, suggests that the alteration occurred prior to the intense regional deformation. Furthermore, since the alteration is largely confined to the matrix between the volcanic clasts, it is considered likely that the alteration took place soon after deposition while the matrix was more porous and permeable than the clasts, i.e., before the rocks were fully compacted and recrystallised.

The epidote- and diopside-rich lenses are interpreted as metamorphosed epidosites, low-temperature hydrothermal duct systems rich in epidote but depleted in metals, common to modern supra-subduction zones below exhalative metalliferous vents (Richardson et a., 1987; Schliffman et al. 1987; Banerjee et al. 2000). The hydrothermal fluids associated with the epidote alteration are generally thought to be mixtures of sea water and magmatic fluids released from the underlying subduction systems. Epidote alteration has also been reported from the Ivisârtoq greenstone belt at inner Godthåbsfjord but in a different setting (Polat 2005), as well as from ancient arc settings such as at Kangerluluk in the forearc of the Palaeoproterozoic Ketilidian orogen in South Greenland. At Kangerluluk, flat-lying andesitic pillow breccias and tuffs contain irregular, subvertical alteration zones many metres wide rich in epidote, which are closely associated with sulphidic exhalative rocks and gold deposits hosted in quartz veins (Stendal & Frei 2000; Stendal et al. 2001).

Pyrrhotite-bearing horizons and associated rocks of possible volcanogenic-exhalative origin

Several horizons within the fragmental amphibolite, about 1 m thick and up to 3 km long and recognised by their rusty weathering colours, contain fine-grained (<1 mm), disseminated iron sulphides (mainly pyrrhotite). Under the microscope the pyrrhotite is seen to form evenly distributed grains in textural equilibrium with the amphibolite facies silicate assemblage. The pyrrhotite-mineralised horizons are conformable with lithological variations in the fragmental rocks and therefore appear to follow certain stratigraphic levels (Fig. 5). Moreover, they are repeated by the isoclinal folds and are not associated with late shear zones or faults. This suggests that the disseminated pyrrhotite horizons are not related to late shear zones, but are interpreted to be either synvolcanic-

exhalative or formed during early diagenetic hydrothermal processes prior to the regional deformation and metamorphism.

Layers up to a few metres thick of coarse-grained, garnet-, quartz-, and locally tourmaline-rich rocks occur sporadically within the amphibolite adjacent to the pyrrhotite-bearing horizons. Some of these rocks contain up to about 50 % garnet, and resemble quartz-garnet rocks reported e.g. by McGregor & Mason (1977) from the early Archaean Akilia association south of outer Godthåbsfjord. In an occurrence at the head of Qussuk discordant quartz-garnet veins up to c. 10 cm thick protrude into the adjacent amphibolite. It is considered that the majority of garnet-, quartz-, and locally tourmaline-rich rocks in the Qussuk area are of volcanogenic-exhalative or hydrothermal origin.

Gold mineralisation

Fifty-seven rock and 15 soil samples from the above described lithologies on Qussuk, and 41 rock samples from Bjørneøen were analysed for gold (Fig. 9). A quartz-tourmaline rock at the head of Qussuk contains 2.2 ppm Au, and a nearby coarse-grained garnet-quartz rock 0.2 ppm Au. A layer with disseminated pyrrhotite in fragmental amphibolite the south-western Qussuk peninsula contains 1.4 ppm Au, and a nearby sample of rust-coloured residual soil as much as 14 ppm Au. Although the layer with disseminated pyrrhotite is cut by a narrow Palaeoproterozoic fracture zone, it is devoid of sulphide minerals and seems unrelated to the gold occurrence. Several other rock and soil samples from these or geologically similar localities within the fragmental amphibolite panels contain anomalous gold in the low ppb range.

Gold occurrences on Bjørneøen, hosted in amphibolite of intermediate to mafic composition and associated intermediate schist and in some cases associated with disseminated iron sulphides, were first discovered by Nunaoil A/S (Skyseth 1998; Smith 1998).

Summary: field evidence for an island arc complex

The ubiquitous, slight heterogeneity of the clasts, where they are present, and the lack of jigsaw-puzzle fits between them, show that the fragmental amphibolite is generally not autoclastic but consists of pyroclastic and perhaps resedimented deposits. Lithological, structural and geochemical evidence of synvolcanic exhalative activity and early diagenetic alteration processes is also preserved (see below). However, the isoclinal folding, the almost ubiquitous high strain, and the regional metamorphism at amphibolite facies have destroyed most of the primary lithological details. Moreover, it has not been possible to identify individual volcanic edifices or unravel further diagnostic primary relationships between their components.

A few general inferences can nevertheless be made. First of all, no basement to the fragmental amphibolite has been identified, although the mafic amphibolite and metagabbro inside the supra-

crustal panels may have acted as such. Field observations of the contacts between the tonalitic to granitic orthogneisses and the fragmental amphibolite show that these are either tectonic or intrusive. Secondly, volcanism was explosive in nature. The intimate mixture of the coarse, fragmental metavolcanic rocks with finely layered rocks of likely tuffaceous origin, combined with the occasional presence of rocks interpreted as pillow lavas, show that the volcanism was probably shallow subaqueous and possibly in part subaerial.

Since the predominance of explosive volcanism points to a shallow-water or in part subaerial volcanic environment and there is no identifiable continental crustal basement to the volcanic rocks, the lithologies and their field relationships neither correspond to a sea floor setting nor to a continental arc. On the other hand, several of the essential primary features are present that one would expect to find in an island arc setting.

Geochemistry

Representative major and trace element compositions of two main associations of supracrustal rocks, arranged in five lithological groups, are presented in Table 1 and Figs 10–15. These are metavolcanic amphibolite s.s. and associated metagabbro (groups 1–2), and fragmental amphibolite, fragmental amphibolite with disseminated pyrrhotite, and schistose intermediate metasediment intercalated with the fragmental amphibolite (groups 3–5).

The amphibolite-metagabbro association

The amphibolite-metagabbro association (groups 1-2) has chemical compositions not unlike modern MORB, with c. 46.5–49.5 wt% SiO_2, 15-17 % Al_2O_3, 7–13 % MgO, 10–12 % FeO (total), and moderate contents of alkali elements (Table 1). TiO_2 is somewhat lower than in N-MORB for a given Mg# (Hofmann 1988)).

The chondrite-normalised rare earth element (REE) patterns are flat, with less than 10 x enrichment, relative depletion of LREE, and a small positive Eu anomaly in the metagabbros (Figs 10–11). The element distributions normalised to primitive mantle and N-MORB are likewise flat, but they are more irregular than the chondrite-normalised REE patterns, and there are negative Nb and P anomalies. As commonly seen in Archaean basic rocks interpreted as ocean floor basalts, Ni and Cr are both relatively high compared to modern MORB.

The large-ion lithophile (LIL) elements, including Pb and U, are strongly enriched, but the patterns of these elements are very variable. The present LIL contents are unlikely to represent the original compositions and are tentatively ascribed to alteration during the c. 2980 Ma thermal event that has previously been documented in the Akia terrane; the rocks were metamorphosed at upper amphibolite facies, and although the most of the area studied here does not contain visible field or microscopic signs of alteration, it is nevertheless likely that they have received LIL elements related

to thermal dehydration of underlying granulite facies rocks and granite emplacement during the peak of thermal metamorphism (see Garde 1997 and Garde et al. 2000 for further discussion).

Small geochemical differences between the rocks interpreted in the field as in- and extrusive support this field distinction. The metagabbro samples have slightly lower REE and higher field strength elements, and the small positive Eu anomaly points to the presence of cumulus plagioclase. A Harker diagram of MgO vs. SiO2 (Fig. 12a) shows that the amphibolite-metagabbro association plots in a small, well-defined field. Some metagabbros have higher MgO, probably due to cumulate orthopyroxene. In Fig. 12b the amphibolites s.s. plot on the Mg-rich side of modern MORB glasses and arc lavas, whereas the associated metagabbros, which are unlikely to represent pure melt compositions, show a larger spread. Figure 12c, an AFM diagram, corroborates that no clear differentiation trend, such as iron or silica enrichment, is evident within the amphibolite-metagabbro association.

In conclusion, the geochemical signature of the amphibolite-metagabbro association in broad terms points to basic lavas not unlike MORB that formed in a spreading environment, either in a passive continental margin or mid-ocean ridge setting.

The fragmental amphibolite association

The fragmental amphibolite (group 3) is of overall andesitic composition (Table 1). This group is quite evolved compared to the amphibolite-metagabbro association, with 54.5–66.5 wt% SiO2, only 1.7–5 wt% MgO and 5.5–8.5 wt% FeO (total), and a clear negative correlation between MgO and SiO2 (Fig. 12a). Furthermore, iron expressed as FeO (total), is low at a given Mg# when compared to modern MORB and plot within or close to the field of modern arc lavas (Fig. 12b). There no trend of iron enrichment on the FeO-Mg# and AFM diagrams (Figs 12b-c), indicating a calc-alkaline rather than tholeiitic affinity. The Al2O3 content ($\leq$ 17.74 wt%) is not particularly high, which is expected in relatively evolved rocks if plagioclase has been a main fractionating phase.

The multi-element geochemical patterns of the fragmental amphibolite (Fig. 13) are distinct from the amphibolite-metagabbro association. The fragmental amphibolite has clear negative Nb, Ta, P and Ti anomalies compared to primitive mantle. It is enriched in LREE and Zr (with a small negative Eu anomaly in some samples), and more enriched in LIL elements and U, Th, Pb than the amphibolite-metagabbro association relative to both primitive mantle and N-MORB. Furthermore, the fragmental amphibolite association does not display the same scatter in these elements as the former association. It is speculated that primary hydrous mineral phases such as hornblende or biotite in the igneous precursor of the fragmental amphibolite, if present, would enable a stronger whole-rock control of the LIL elements during diagenesis and metamorphism than observed in the amphibolite-metagabbro association.

The horizons with disseminated pyrrhotite and anomalous gold within the fragmental amphibolite have compositions that are almost identical to the normal fragmental amphibolite (Fig. 14).

The four samples of schistose, intermediate metasediment have compositions which are very similar to the fragmental amphibolite and exhibit a general igneous-like composition (Table 1, Fig. 15). These rocks contain a little more SiO2 (c. 61.5–72.0 wt%) and K2O (1–2.3 wt%) and a little less MgO, FeO (total), Cr, Ni, Co and V than the fragmental amphibolite. They also display a larger range of intermediate and heavy REE than the fragmental amphibolite. Despite these small differences the geochemical data from the intermediate schists are fully compatible with the field interpretation that these rocks are metamorphosed tuffs or tuffites. The different compositions compared with the fragmental amphibolite itself may either suggest that their source was a little more evolved, or that the proportions of detrital mineral phases have been modified by sedimentary processes.

In conclusion, the fragmental amphibolite (including the variety with disseminated pyrrhotite) and the associated metasediment possess well-defined, general geochemical characteristics of evolved andesitic volcanic rocks such as are typically formed in primary convergent environments. Not surprisingly, the geochemistry of the fragmental amphibolite also resembles that of amphibolite facies dioritic gneiss from the Qussuk peninsula (Garde 1997).

Geochronology

Previous systematic mapping and published zircon U-Pb age data from north of Qussuk (Taserssuaq tonalite complex, 2982 ± 7 Ma; Qugssuk granite, 2975 ± 5 Ma, see previous work) indicate that the easternmost, tonalitic to granitic continental crustal members of the Akia terrane are relatively young compared to the bulk of the Akia terrane, and that the area north and east of Qussuk experienced a simpler structural and metamorphic history than the rest of the Akia terrane (Garde 1989, 1997; Garde et al. 2000). However, no zircon U-Pb geochronology from the peninsula itself has previously been reported.

The following sections present new zircon U-Pb ion probe age data from three samples of fragmental amphibolite and volcanogenic metasediment from the Qussuk peninsula and Bjørneøen, and from three late granites from the Qussuk peninsula (Table 2, Figs 16–21). One of these granites cuts the fragmental amphibolite and thus provides a minimum age of the supracrustal package. The age data were obtained in May-June 2005 with the Cameca 1270 ion probe at the NORDSIM laboratory, Naturhistoriska Riksmuseet in Stockholm, Sweden (see Whitehouse et al. 1997 for analytical details). All ages reported here are mean or individual 207Pb/206Pb ages as appropriate, quoted with 2 sigma errors. Error ellipses shown on Figures are at 1 sigma level. Isoplot/EX (Ludwig 2003) was used for age calculations and data presentation.

The volcanogenic metasediment from Bjørneøen (479827) yields a very precise age of 3071 ± 1 Ma which is interpreted as the eruption age of the volcanic precursor (see below), whereas most of the analysed zircons in all of the remaining samples yield ages of 2995–2970 Ma, coinciding with the thermal maximum in the Akia terrane previously dated at around 2980 Ma (Garde et al. 2000). Based on field relationships, zircon morphology and internal textures, distribution of apparent ages,

and zircon U and Th contents it is argued in the following that the zircon in the remaining samples from the Qussuk peninsula has been variably, and in some cases thoroughly affected by metamorphic recrystallisation during the thermal maximum that affected most of the Akia terrane.

Age data from Bjørneøen

Sample **479827** comprises a fine-grained layer of homogeneous intermediate schist intercalated with intermediate metavolcanic rocks. Central Bjørneøen (Fig. 1). Volcanic and probable deposition age: 3071 ± 1 Ma.

The sample contains a homogeneous population of very small (c. 100-150 microns), equant to stubby prismatic zircons displaying concentric zoning on backscatter electron (BSE) images, sometimes with relatively bright, prismatic cores and slightly darker rims (Fig. 16). The zircons are generally somewhat pitted or cracked, especially the narrow rims. Most grains have relatively high U and Th contents (c. 850–2250 and 500–1500 ppm, respectively).

Twenty-one spots in 20 grains were analysed. Sixteen grains yield a very precise age of 3071 ± 1 Ma (MSWD = 1.6, n = 16), in accord with the field interpretation that this rock is of volcaniclastic origin. This age is interpreted as the eruption age of the volcanic precursor. Three other grains (5, 6 and 21) yield ages of 3057–3059 Ma. If these represent a second, well-defined source they would decrease the age of final deposition to 3058 Ma, but they could also be slightly reset. The two remaining spots (#8 from the rim of a large grain, and #17) with apparent ages of 3006 and 3021 Ma are unexplained but not considered sufficient evidence to propose a much lower age of deposition.

Age data from the Qussuk peninsula

477385. Fragmental metavolcanic rock, intensely deformed, with a strung-out, pancake-like lensoid structure. Within the western panel of fragmental amphibolite on the Qussuk peninsula (Fig. 1). Metamorphic age c. 2995–2975 Ma.

The zircons are small, typically 50–100 microns in length – with aspect ratios of 1:1 to 1:2, and commonly fairly rounded (Fig. 17). The majority are homogeneous in appearance when imaged in BSE. A few contain relict darker cores, suggesting that homogeneous rims and whole grains may be metamorphic in origin.

Sixteen spots in 15 grains were analysed (Fig. 17). A dark core gives the oldest age – 3038 ± 12 Ma – and the highest Th/U of 0.37. Thirteen analyses of homogeneous grains and rims fall between 2996 and 2974 Ma, with significant spread outside the error of individual analyses (a mean age calculation of 2984 ± 4 Ma has an unacceptable MSWD = 19). These spots have high U concentrations of 640–2330 ppm and low Th/U (typically 0.03 to 0.09). A single, still younger zircon at 2951 ± 6 Ma also has low Th/U (0.06).

Given the homogeneous nature of the bulk of the grains (n = 14), their very low Th/U, and the

spread in apparent ages, the zircons in this fragmental amphibolite are interpreted as originally igneous zircon that have been recrystallised during amphibolite facies metamorphism in the period c. 2995–2975 Ma. It is well established that metamorphic zircon in metabasalts and metagabbros may form following release of Zr during breakdown of igneous pyroxenes (reference). However, this sample contains 64.76 wt% SiO2 and 222 ppm Zr (Table 1), and it is therefore considered unlikely that its magmatic precursor did not contain any zircon. The single core yielding 3038 ± 12 Ma may be detrital or inherited from the volcanic precursor, but in view of the nature of the entire data set from this sample and other age data reported here, it is considered likely that even this grain has been partially reset. The age of the youngest grain may reflect early lead loss.

477367. Fine-grained, garnet-bearing intermediate amphibolite. Within the western panel of fragmental amphibolite on the Qussuk peninsula (Fig. 1). Metamorphic age c. 2995–2975 Ma. Three older cores ≤ 3068 Ma.

The zircons are small, typically 50–150 microns long and commonly rounded, with aspect ratios typically less than 1:2. The majority are homogeneous (Fig. 18). A few contain relict darker cores when imaged by BSE, suggesting that homogeneous rims and whole grains may be recrystallised or reflect new zircon growth.

Seventeen spots in 17 grains were analysed (Fig. 18). Three analyses of dark cores with moderate U concentrations (267–521 ppm) give the oldest ages – 3068 ± 6, 3053 ± 8, and 3037 ± 6 Ma – and the highest Th/U of 0.24–0.47. These are interpreted as derived from the volcanic precursor and/or from detritus included at the time of deposition. Fourteen analyses of homogeneous grains fall between 2995 and 2962 Ma, like in sample 477385 with significant spread outside the error of individual analyses (a mean apparent age of 2975 ± 5 Ma has an unacceptable MSWD of 23). All these analyses have high U concentrations of 631–1955 ppm and fairly low Th/U (typically 0.05–0.16), consistent with a growth or recrystallisation during metamorphism. It is quite possible that the ages of the oldest grains have also been partially reset. A single younger zircon at 2944 ± 6 Ma also has low Th/U (0.09) and probably also reflects recrystallisation or early lead loss.

Although sample 477367 is a little less evolved than 477385 (61.23 wt% SiO2 and 135 ppm Zr; Table 1), it is considered unlikely that its magmatic precursor did not contain zircon. The oldest, 3068 ± 6 Ma zircon core is within error identical to the age of 3071 ± 1 Ma of sample 479827 from Bjørneøen, and may represent the age of volcanism (implying that the two other > 3000 Ma cores have been partially reset). Given the homogeneous nature of the remainder of the grains (n = 15), their low Th/U, and the spread in 207Pb/206Pb ages, these are interpreted as recrystallised during amphibolite facies metamorphism shortly after c. 2990 Ma.

477352. Granite vein cutting grey amphibolite, central Qussuk peninsula. Age 2984 ± 2 Ma (six grains). Four inherited zircons (c. 3000 Ma) and a tail of younger apparent ages from 11 high-U grains

Two different zircon populations with different shapes and very different U contents are present in this granite. The first group is stubby grains 250–350 microns long with low U contents (40–95 ppm) and narrow, metamict, high-U rims. The second group consists of smaller, slender prismatic zircons 150–250 microns long with U contents above 1250 ppm; both groups contain less than 100 ppm Th. Most zircons in the second group have strongly pitted cores with occasional small, BSE-bright inclusions (probably monazite), and up to 40 microns long, more homogeneous growth zones at their tips, in which fine oscillatory zoning may be visible.

21 spots in 19 grains were analysed (Fig. 19). Four grains in the first, low-U group (#1, 12, 13, 21) yield a poorly defined common age of 3000 ± 22 Ma (MSWD = 2.8). These zircons are interpreted as inherited. In the second group of 15 grains, most analyses were made in the well-preserved broad tips with fine oscillatory zoning, but also dark cores with weak oscillatory zoning. A few brighter, less homogeneous cores were also analysed. Six of the broad, high-U tips yield a very precise age of 2984.4 ± 1.3 Ma (MSWD = 0.83), while the remaining 11 spots in high-U, pitted cores and homogeneous tips yield younger ages ranging between 2978–2810 Ma. Given that all of these younger ages are from high-U zircons and and that some of them were obtained from cores, they are interpreted as due to metamorphic recrystallisation or, perhaps more likely, early lead loss, and are discarded.

The age of 2984 ± 2 Ma from six broad tips of high-U zircons with oscillatory zoning is interpreted as the magmatic emplacement age. The granite is part of a larger system of granite veins that cut strongly deformed panels of amphibolite, and which are themselves folded within the regional, steeply S-plunging fold system, less tightly than their hosts. The age of 2984 ± 2 Ma is thus also a minimum age of deformation of the island arc complex.

477320. Deformed granite vein in high-strain zone, south-eastern coast of the Qussuk peninsula. Intrudes intensely deformed host and marks the syn- or lower age limit of the NE-trending high-strain zone. Age 2992 ± 3 Ma. Age of inherited grains: 3005 ± 3 Ma.

The zircons are all small, equant to stubby prismatic, and around 150 microns long (Fig. 20). A weak concentric zonation is just visible on BSE images, besides metamict rims just a few microns wide. In some grains a small core is visible. The zircons contain c. 400–800 ppm U and 200–500 ppm Th and are quite well preserved and thus not suspected to have been thoroughly recrystallised.

The 10 analysed spots all yield concordant results in a cluster around 3000 Ma, but two different, well defined, concordant age populations can be detected without excluding any single analysis. Grains #2, 4, 6, and 10 yield 3005 ± 3 Ma (MSWD = 1.5), and the remaining six grains 2992 ± 3 Ma (MSWD = 0.92). The latter age is interpreted as the emplacement age of the granite vein.

Like sample 477318 below, also sample 477320 shows that a major part of the intense deformation in the south-eastern part of the Qussuk peninsula occurred close to 3000 Ma and not during terrane amalgamation.

477318. Granite vein, south-eastern coast of the Qussuk peninsula.
Cuts an intense LS fabric in metagabbro of the Taserssuaq complex and is itself weakly deformed. Constrains the age of a high-strain zone in the south-eastern boundary region of the Akia terrane.
Age 2990 ± 4 Ma (five spots omitted).

The zircons are pale pinkish, stubby prisms 200–500 microns long (Fig. 21). Most grains display wide, indistinct concentric zones on BSE images, and a few have well-defined cores surrounded by rims c. 25 microns wide. Other grains appear homogeneous, or have large homogeneous parts, suggesting partial recrystallisation. Occasional outer rims only are only a few microns wide. The U and Th contents are very variable, from c. 70–3080 and 10–3300 ppm, respectively. Many of the BSE-bright, U-rich grains are internally pitted and cracked, and a few are heavily altered.

Fifteen spots in 14 different grains were analysed. Ten of these yield an approximate common age of 2990 ± 4 Ma (MSWD = 5.3) interpreted as the emplacement age of the granite. The relatively high MSWD-value may suggest that the analytical precision is overestimated in this sample, or that the ages of some grains have been lowered by metamorphic recrystallisation soon after the magmatic emplacement. Five grains are omitted from the calculation: one low-U grain at 3016 Ma (#5) is presumably inherited, and lower ages of 2970–2930 Ma (#8, 9, 13) are attributed to early lead loss. It cannot be excluded that grain 15 with an apparent age of only 2536 Ma is a contaminant from another sample.

Discussion

Recrystallisation of zircon, mobility of LIL elements in the eastern Akia terrane, and origin of the gold anomalies

Is it conceivable that much of the zircon from the Qussuk peninsula (especially most of the small zircons in fragmental amphibolite 477367 and 477385) is metamorphic? It is generally accepted that Zr release from pyroxene breakdown in ordinary basaltic amphibolites may lead to growth of metamorphic zircon. However, the evolved major element and Zr compositions of the fragmental amphibolite suggest that its igneous precursors contained cognate zircon, and metamorphic recrystallisation of igneous zircon is thought to be very uncommon in most settings. It was nevertheless shown above that the smooth spread of declining ages within individual samples combined with the BSE textures and U and Th compositions of the zircons in question, are all in favour of this interpretation.

There is other, independent evidence of metamorphic fluid-rock interaction from the eastern Akia terrane, which is generally considered a necessary prerequisite for metamorphic zircon growth. The Qussuk area lies within a NE-trending high U, Th, K zone that was discovered by airborne gamma spectrometry already in the 1970s (Steenfelt et al. 1990). Both Taylor et al. (1980), Baadsgaard & McGregor (1981) and Garde (1990, 1997) presented evidence for LIL element mobility

associated with metamorphic fluids, or fluids released from crystallisation of late granitic rocks at around 2980 Ma, and Baadsgaard & McGregor (1981) interpreted their conventional zircon data as influenced by diffusion and episodic lead loss. As previously mentioned, also the multi-element diagrams of Figs 10–15 point to strong mobility and metamorphic enrichment of LIL elements, especially Pb. An important implication of these considerations is that the enrichment of LIL elements in the Qussuk area is not a late Archaean phenomenon, and is therefore unrelated to the c. 2700 Ma terrane assembly (Friend et al. 1996), or to the subsequent emplacement of the Qôrqut granite complex.

Are the gold anomalies in the Qussuk area remnants of synvolcanic mineralisation or was the gold introduced by metamorphic fluids during the c. 2980 Ma thermal event, and what is the relationship between the gold mineralisation at Qussuk and gold occurrences in other parts of the Nuuk region? It follows from the above that the anomalous gold in the Qussuk area is likely to be either residual from original synvolcanic occurrences, or it was introduced by metamorphic fluids at around 2980 Ma from an unknown source. In the former scenario the gold at Qussuk represents a type category of arc-related, volcanogenic-exhalative gold that may have sourced epigenetic, late Archaean gold occurrences in the Nuuk region. If the latter scenario is true, the gold at Qussuk is probably unrelated to most other gold occurrences in the Nuuk region except in the Akia terrane itself. The observation of hydrothermal plumbing systems within the fragmental amphibolite next to the mineralised horizons, and the local field relationships of the auriferous rocks, both seem to favour the first scenario. Further work on the gold occurrences at Qussuk is under way to qualify this preliminary conclusion.

Conclusions

New field work, geochemistry and geochronology data show that a previously scarcely recognised, c. 3070 Ma volcanic island arc complex is embedded within c. 3000 Ma TTG gneisses and granites in the Qussuk area. The island arc system in the Qussuk area provides a petrogenetic and tectonic link in the Akia terrane (and in the entire Nuuk region) between the mafic amphibolites of ocean floor affinity and related layered complexes which form the bulk of the supracrustal rocks, and the voluminous grey gneisses, and strongly supports previous suggestions by various authors that plate-tectonic processes were operative in the Nuuk region in the middle Archaean. The relatively deep, amphibolite to granulite facies exposure of the Archaean crust in most of the Nuuk region itself, and in southern West Greenland in general, may account for the apparent scarcity of identifiable island arc complexes.

Previously reported evidence of fluid movement associated with c. 2980 Ma granulite facies metamorphism in the central Akia terrane is supported by strong metamorphic LIL element enrichment in the supracrustal rocks from the Qussuk area as well as extensive recrystallisation of zircon between 2995–2975 Ma.

The gold mineralisation at Qussuk has several characteristics of more recent volcanogenic-exhalative gold deposits and may represent a primary, regional, arc-related source of gold in the Nuuk region. Relict, now telescoped components of a primary hydrothermal plumbing system are present, such as meta-epidosite and disseminated iron sulphides and associated alumina-rich, garnet-rich, and quartz-tourmaline varieties that could represent leached rocks and chemical precipitates. Alternatively the gold was introduced by metamorphic fluids from an unknown source during the thermal maximum at c. 2980 Ma.

Acknowledgements

This study was supported by the Bureau of Minerals and Petroleum, Nuuk, Greenland, and is published with permission from the Geological Survey of Denmark and Greenland. Help with interpretation of data, sample collection and preparation, analytical work and discussion during preparation of this manuscript from Nigel Kelly, University of Edinburgh, U.K., Tobias Hermansson, Lund University, Sweden, and staff and students at the Geological Survey of Denmark and Greenland including Stefan Bernstein, Julie A. Hollis, Mac Persson, Agnete Steenfelt and Mikkel Vognsen is gratefully acknowledged, but the author remains responsible for all errors and shortcomings. The staff at the NORDSIM laboratory, Naturhistoriska Riksmuseet, Sweden, is thanked for technical support and discussion of the interpretation of the ion probe data.

References

Baadsgaard, H. & McGregor, V.R. 1981: The U-Th-Pb systematics of zircons from type Nûk gneisses, Godthåbsfjord, West Greenland. Geochimica et Cosmochimica Acta, **45**, 1099–1109.

Banerjee, N.R., Gillis, K.M. & Muehlenbachs, K. 2000. Discovery of epidosites in a modern oceanic setting, the Tonga forearc. *Geology*, 28, 151–154.

Berthelsen, A. 1960. Structural studies in the pre-Cambrian of western Greenland. II. Geology of Tovqussap nunâ. *Bulletin Grønlands Geologiske Undersøgelse*, **25**, 223 pp. (Also *Meddelelser om Grønland* **135**(6)).

Dymek, R. F. 1984. Supracrustal rocks, polymetamorphism, and evolution of the SW Greenland Archaean gneiss complex. *In* Holland, H. D. & Trendall, A. F. (ed.) *Patterns of change in Earth evolution,* 313–343. Berlin: Springer-Verlag.

Friend, C.R.L. & Nutman, A.P. 2005. New pieces to the Archaean terrane jigsaw puzzle in the Nuuk region, southern West Greenland: Steps in transforming a simple insight into a complex regional

tectonothermal model. *Journal of the Geological Society, London,* **162**, 147–162.

Friend, C. R. L., Nutman, A. P., Baadsgaard, H., Kinny, P. D. & McGregor, V. R. 1996: Timing of late Archaean terrane assembly, crustal thickening and granite emplacement in the Nuuk region, southern West Greenland. *Earth and Planetary Science Letters* **142**, 353–365.

Garde, A.A. 1989. Geological map of Greenland, 1:100 000, Fiskefjord 64 V.1 Nord. Copenhagen: Geological Survey of Greenland.

Garde, A.A. 1990. Thermal granulite-facies metamorphism with diffuse retrogression in Archaean orthogneisses, Fiskefjord, southern West Greenland. *Journal of Metamorphic Geology*, **8**, 663–682.

Garde, A. A. 1991. Post-kinematic diorite intrusions in Archaean basement rocks around outer Fiskefjord, southern West Greenland. *Bulletin* of the *Geological Society of Denmark*, **39**, 167–177.

Garde, A.A. 1997. Accretion and evolution of an Archaean high-grade grey gneiss-amphibolite complex: the Fiskefjord area, southern West Greenland. *Geology of Greenland Survey Bulletin*, **177**, 114 pp.

Garde, A. A., Larsen, O. & Nutman, A. P. 1986. Dating of late Archaean crustal mobilisation north of Qugssuk, Godthåbsfjord, southern West Greenland. *Rapport Grønlands Geologiske Undersøgelse*, **128**, 23–36.

Garde, A. A., Jensen, S. B. & Marker, M. 1987. Field work in the Fiskefjord area, southern West Greenland. *Rapport Grønlands Geologiske Undersøgelse,* **135**, 36–42.

Garde, A.A., Friend, C.R.L., Nutman, A.P. & Marker, M. 2000. Rapid maturation and stabilisation of middle Archaean continental crust: the Akia terrane, southern West Greenland. *Bulletin of the Geological Society of Denmark*, **47**, 1–27.

Hofmann, A.W. 1988. Chemical differentiation of the Earth: the *relationships between mantle, continental crust, and oceanic crust. Earth and Planetary Science Letters*, **90**, 297–314.

Hollis, J.A., van Gool, J.A.M., Steenfelt, A. & Garde, A.A. 2004. Greenstone belts in the central Godthåbsfjord region, southern West Greenland: Preliminary results from field work in 2004. *Danmarks og Grønlands Geologiske Undersøgelse Rapport* **2004/110**.

Kelemen, P.B., Hanghøj, K. & Greene, A.R. 2003. One View of the Geochemistry of Subduction-

related Magmatic Arcs, with Emphasis on Primitive Andesite and Lower Crust. In Rudnick, R.L. (ed.) *Treatise on geochemistry*, Volume **3**: The crust, 593–659.

Lauerma, R. 1964. On the structure and petrography of the Ipernat dome, western Greenland. *Bulletin de la Commission géologique de la Finlande*, **215**, 1–88 (Also *Bulletin Grønlands Geologiske Undersøgelse* **46**, 88 pp).

Ludwig, K.R. 2003. Isoplot/Ex version 3.00: A geochronological toolkit for Microsoft Excel. Berkeley Geochronological Center, Berkeley, U.S.A.

McGregor, V. R. 1993. Geological map of Greenland, 1:100 000, Qôrqut 64 V. 1 Syd. Descriptive text. Copenhagen: Geological Survey of Greenland, 40 pp.

McGregor, V.R. & Mason, B. 1977. Petrogenesis and geochemistry of metabasaltic and metasedimentary enclaves in the Amîtsoq gneisses. *American Mineralogist*, 62, 887–904.

McGregor, V. R., Friend, C. R. L. & Nutman, A. P. 1991. The late Archaean mobile belt through Godthåbsfjord, southern West Greenland: a continent-continent collision zone? *Bulletin of the Geological Society of Denmark*, **39**, 179–197.

Nutman, A. P. & Garde, A. A. 1989. Fluid control on emplacement of sialic magmas during Archaean crustal accretion. *In* Bridgwater, D. (ed.) *Fluid movements – element transport and the composition of the deep crust*, 235–243. Dordrecht: Kluwer.

Polat, A. 2005. A progress report on the geochemical and petrographic characteristics of the Ivisârtoq and Storø greenstone belts, southern West Greenland. In: Hollis, J. (ed.) Greenstone belts in the central Godthåbsfjord region, southern West Greenland: geochemistry and geochronology arising from 2004 field work, and digital map data. Danmarks og Grønlands Geologiske Undersøgelse Rapport **2005/42** (this volume).

Richardson, C.J., Cann, J.R., Richards, H.G. & Cowan, J.G. 1987. Metal-depleted root zones of the Troodos ore-forming hydrothermal systems, Cyprus. *Earth and Planetary Science Letters*, **84**, 243–253.

Riciputi, L. R., Valley, J. W. & McGregor, V. R. 1990. Conditions of Archean granulite metamorphism in the Godthaab–Fiskenaesset region, southern West Greenland. *Journal of Metamorphic Geology*, **8**, 171–190.

Schliffman, P., Smith, B.M., Varga, R.J. & Moores, E.M. 1987. Geometry, conditions and timing of off-axis hydrothermal metamorphism and ore deposition in the Solea graben. *Nature*, **325**, 423–425.

Skyseth, T. 1998. Gold exploration on Storø 1997, South West Greenland. Internal report, Nunaoil A/S. 25 pp., 5 appendices, 3 plates (in archives of the Geological Survey of Denmark and Greenland, GEUS Report file 21601).

Smith, G.M. 1998. Report on the structure and geometry of the gold mineralization at Qingaq Storø, Nuukfjord, South West Greenland. Internal report, Nunaoil A/S. 13 pp., 14 plates (in archives of the Geological Survey of Denmark and Greenland, GEUS Report file 21602).

Steenfelt, A., Thorning, L. & Tukiainen, T. (eds) 1990. Regional compilations of geoscience data from the Nuuk–Maniitsoq area, southern West Greenland. *Thematic Map Series Grønlands Geologiske Undersøgelse*, **90/1**, 9 pp., 57 maps with legends.

Stendal, H., and Frei, R. 2000. Gold occurrences and Pb isotopes in the Ketilidian mobile belt, South Greenland. *Transactions of the Institution of Mining and Metallurgy*, Section **B**: *Applied Earth Sciences*, **109**: B6–B13.

Stendal, H., Frei, R., Hamilton, M.A. & Mueller, W.U. 2001. The Palaeoproterozoic Kangerluluk gold-copper mineralization (southeast Greenland): Pb and Nd isotopic constraints on its timing and genesis. *Mineralium Deposita*, **36**, 177–188.

Sun, S.-S. & McDonough, W. F. 1989. Chemical and isotopic systematics of oceanic basalts; implication for mantle composition and processes. *In* Saunders, A. D. & Norry, M. J. (ed.) Magmatism in the ocean basins. *Geological Society of London Special Publication* **42**, 313–345.

Taylor, S. R. & McLennan, S. M. 1985. *The continental crust: its composition and evolution*. Oxford: Blackwell, 312 pp.

Taylor, P. N., Moorbath, S., Goodwin, R. & Petrykowski, A. C. 1980. Crustal contamination as an indication of the extent of early Archaean continental crust: Pb isotopic evidence from the late Archaean gneisses of West Greenland. *Geochimica et Cosmochimica Acta*, **44**, 1437–1453.

Wells, P. R. A. 1980. Thermal models for the magmatic accretion and subsequent metamorphism of continental crust. *Earth and Planetary Science Letters* **46**, 253–265.

Whitehouse, M.J., Claesson, S., Sunde, T. & Vestin, J. 1997. Ion microprobe U-Pb zircon geochro-

nology and correlation of Archaean gneisses from the Lewisian Complex at Gruinard Bay, north-western Scotland. *Geochimica et Cosmochimica Acta*, *61*, 4429–4438.

Tables

Table 1. Compositions of metavolcanic and associated rocks from the Qussuk area.

Table 2. Ion probe zircon U-Pb geochronological data from Bjørneøen and the Qussuk area.

Text to Figures

Fig. 1. Simplified geological map of the south-eastern Akia terrane between Fiskefjord and Godthåbsfjord with positions of geochronology samples. Index map shows location in Greenland.

Fig. 2. The central and western part of the Qussuk peninsula with
the relict island arc complex in black. The white frame shows the position of the detail map, Fig. 5.

Fig. 3. Polyphase, tonalitic to granitic orthogneiss with numerous enclaves of leucocratic amphibolite. Western fragmental amphibolite panel, Qussuk peninsula.. Locality shown on Fig. 5.

Fig. 4. Folded granitic vein cutting a much more intensely deformed host of fragmental amphibolite. The granite was dated at 2984 ± 2 Ma (sample 477352). Locality shown on Fig. 2.

Fig. 5. Part of the relict island arc complex east of Qussuk (see Fig. 2 for location). Fragmental texture indicated within the main lithology where observed along traverses.

Fig. 6. Primary, angular volcanic clasts in a weakly deformed fragmental amphibolite. Locality shown on Fig. 5.

Fig. 7. Folded volcanic clasts in a fold hinge of the fragmental amphibolite. Locality shown on Fig. 2.

Fig. 8. Ultramafic lens with closely packed pseudomorphs of orthopyroxene, now consisting of poikiloblastic, Mg-rich amphibole, deep green, cm-sized chlorite, and fine-grained magnetite. The mushroom is 7 cm long. Locality shown on Fig. 2.

Fig. 9. Gold content of rocks and soil samples from Bjørneøen and the Qussuk peninsula. The shaded areas are supracrustal and associated rocks (see Fig. 1). Modified from Hollis et al. (2004,

fig. 44).

Fig. 10. Multi-element diagrams of amphibolite s.s. normalised to chondrite, primitive mantle and MORB. Normalisation factors from Taylor & McLennan (1985), Sun & McDonough (1989) and Hofmann (1988).

Fig. 11. Multi-element diagrams of metagabbroic amphibolite normalised to chondrite, primitive mantle and MORB as for Fig. 10.

Fig. 12. Variation and triangular diagrams for supracrustal rocks from Qussuk, displaying the homogeneous composition of the the amphibolite-metagabbro association and more evolved nature of and fragmental amphibolite association. (**a**) MgO-SiO2. (**b**) FeO (total) - molar Mg#, compared with compositions of modern MORB glasses and arc lavas from Keleman et al. (2003). See the main text for explanation. (**c**) AFM diagram.

Fig. 13. Multi-element diagrams of fragmental amphibolite normalised to chondrite, primitive mantle and MORB as for Fig. 10.

Fig. 14. Multi-element diagrams of fragmental amphibolite with disseminated pyrrhotite, normalised to chondrite, primitive mantle and MORB as for Fig. 10.

Fig. 15. Multi-element diagrams of schistose, intermediate metasediment intercalated with fragmental amphibolite, normalised to chondrite, primitive mantle and MORB as for Fig. 10.

Fig. 16. Geochronology data for sample 479827.
Fig. 17. Geochronology data for sample 477385.
Fig. 18. Geochronology data for sample 477367.
Fig. 19. Geochronology data for sample 477352.
Fig. 20. Geochronology data for sample 477320.
Fig. 21. Geochronology data for sample 477318.

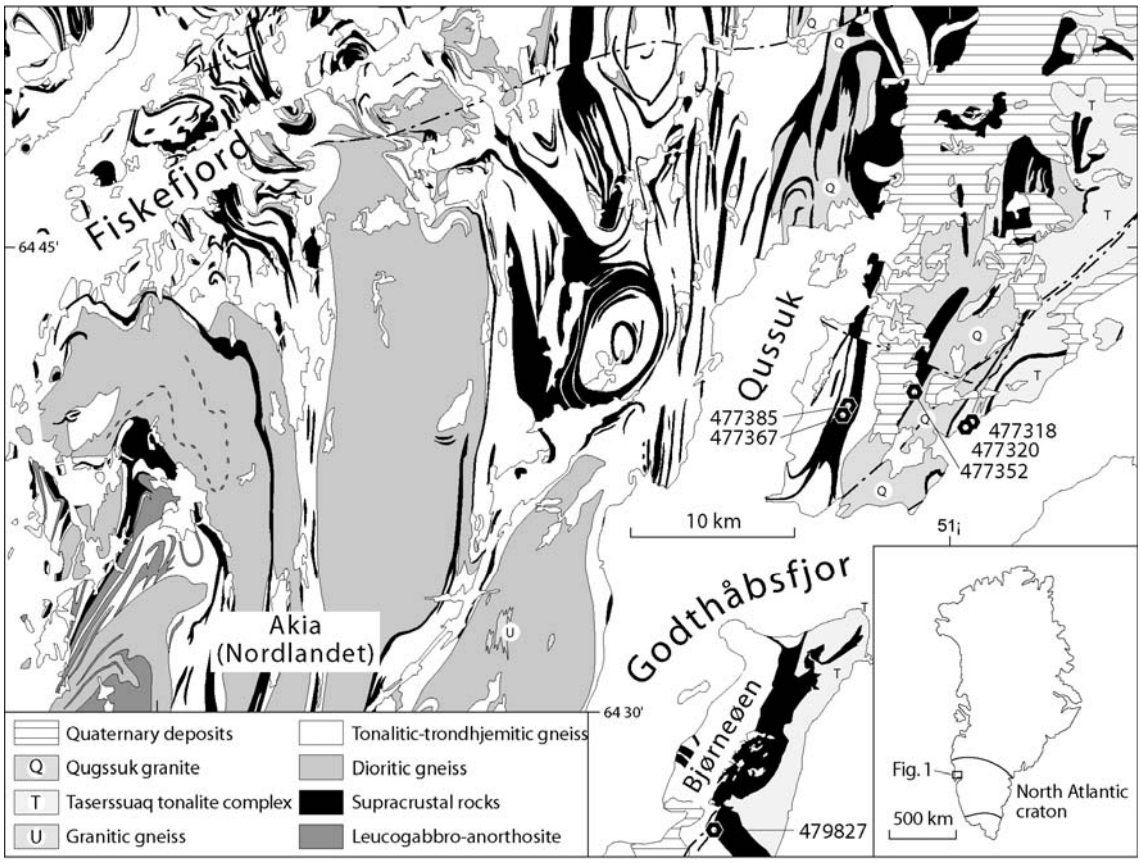

Fig. 1. Simplified geological map of the south-eastern Akia terrane between Fiskefjord and Godthåbsfjord with positions of geochronology samples. Index map shows location in Greenland.

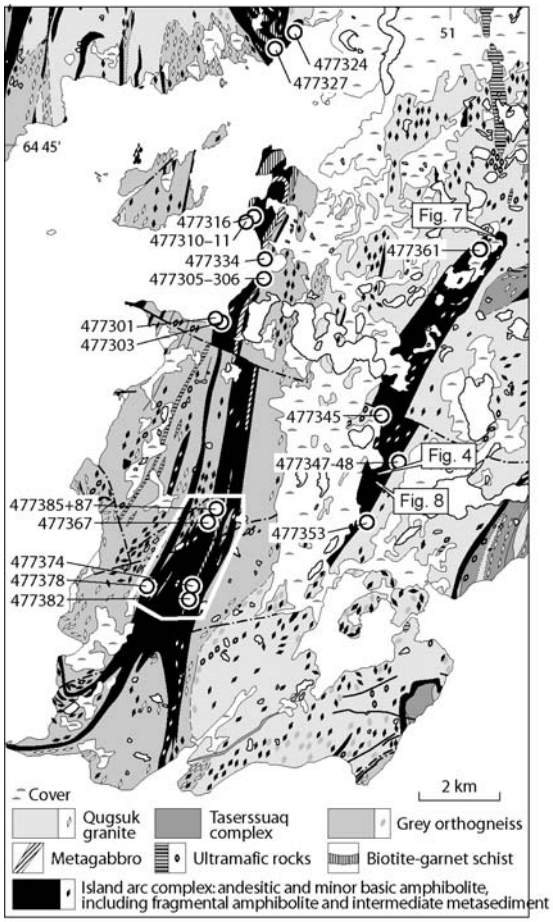

Fig. 2. The central and western part of the Qussuk peninsula with the relict island arc complex in black. The white frame shows the position of the detail map, Fig. 5.

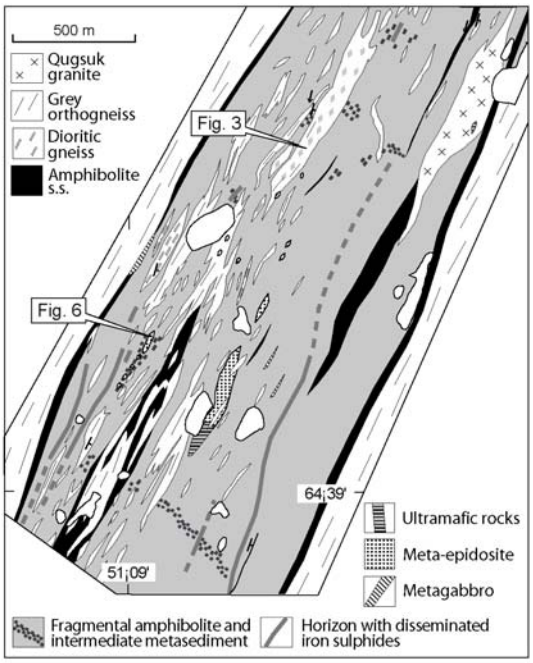

Fig. 5. Part of the relict island arc complex east of Qussuk (see Fig. 2 for location). Fragmental texture within the main lithology is indicated by small squares where observed along traverses.

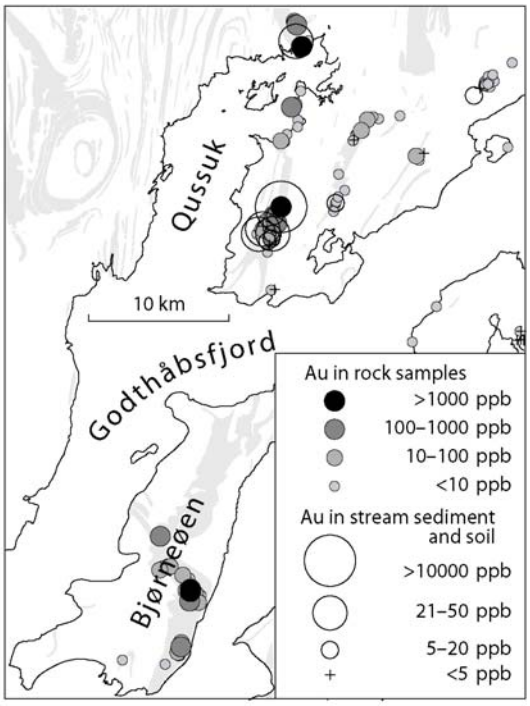

Fig. 9. Gold content of rocks and soil samples from Bjørneøen and the Qussuk peninsula. The shaded areas are supracrustal and associated rocks (see Fig. 1). Modified from Hollis et al. (2004, fig. 44).

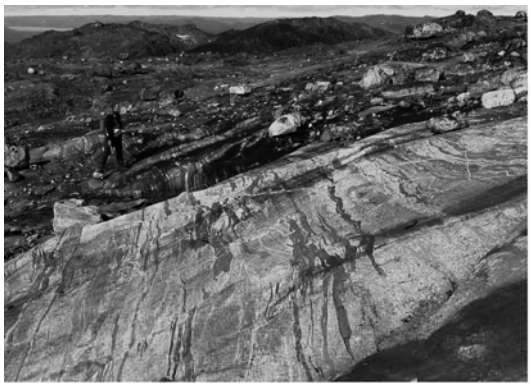

Fig. 3. Polyphase, tonalitic to granitic orthogneiss with numerous enclaves of leucocratic amphibolite. Western fragmental amphibolite panel, Qussuk peninsula.. Locality

Fig. 4. Folded granitic vein cutting a much more intensely deformed host of fragmental amphibolite. The granite was dated at 2984 ± 2 Ma (sample 477352). Locality shown on Fig. 2.

Fig. 6. Primary, angular volcanic clasts in a weakly deformed fragmental amphibolite. Locality shown on Fig. 5.

Fig. 7. Folded volcanic clasts in a fold hinge of the fragmental amphibolite. Locality shown on Fig. 2.

Fig. 8. Ultramafic lens with closely packed pseudomorphs of orthopyroxene, now consisting of poikiloblastic, Mg-rich amphibole, deep green, cm-sized chlorite, and fine-grained magnetite. The mushroom is 7 cm long. Locality shown on Fig.

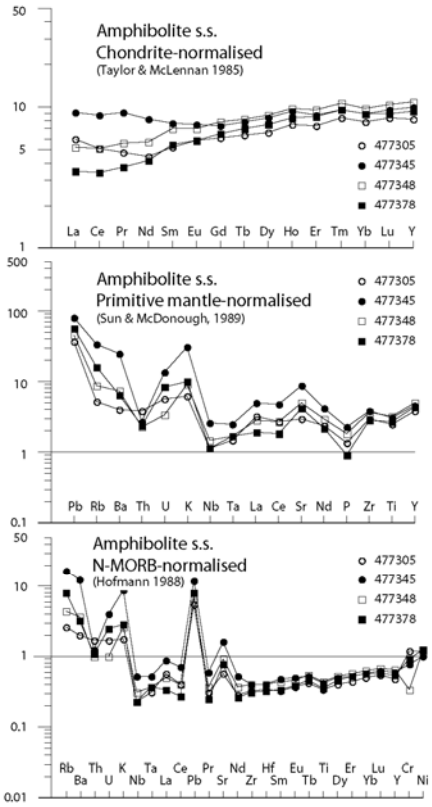

Fig. 10. Multi-element diagrams of amphibolite s.s. normalised to chondrite, primitive mantle and MORB. Normalisation factors from Taylor & McLennan (1985), Sun & McDonough (1989) and Hofmann (1988), supplemented by Cr from Bevins et al. (1984).

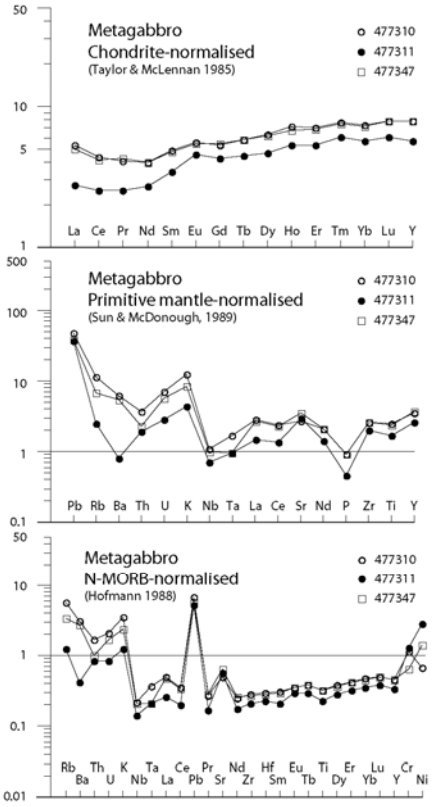

Fig. 11. Multi-element diagrams of metagabbroic amphibolite normalised to chondrite, primitive mantle and MORB as for Fig. 10.

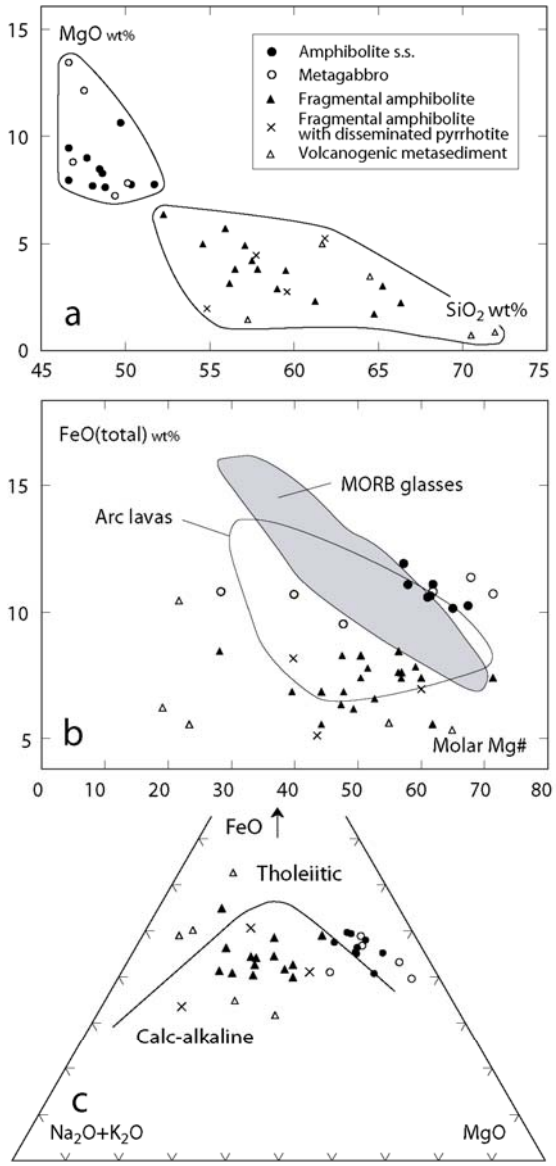

Fig. 12. Variation and triangular diagrams for supracrustal rocks from Qussuk, displaying the homogeneous composition of the the amphibolite-metagabbro association and more evolved nature of and fragmental amphibolite association. (**a**) MgO-SiO2 Harker diagram. (**b**) FeO (total) - molar Mg#, compared with compositions of modern MORB glasses and arc lavas from Keleman et al. (2003). See the main text for explanation. (**c**) AFM diagram.

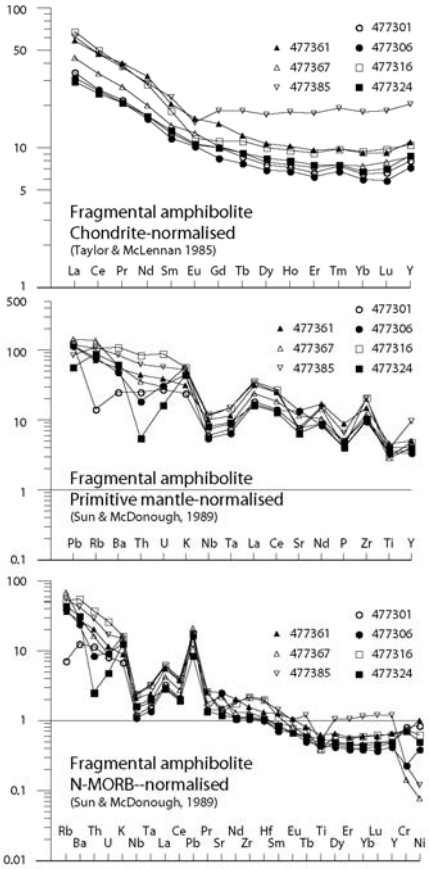

Fig. 13. Multi-element diagrams of fragmental amphibolite normalised to chondrite, primitive mantle and MORB as for Fig. 10.

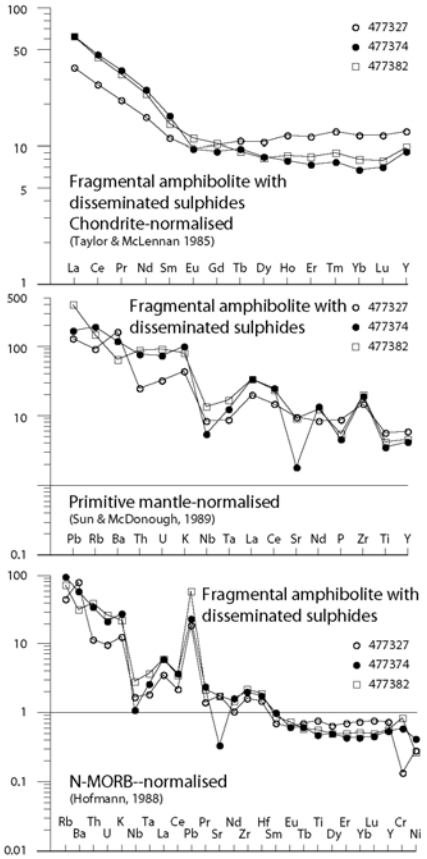

Fig. 14. Multi-element diagrams of fragmental amphibolite with disseminateed sulphides, normalised to chondrite, primitive mantle and MORB as for Fig. 10.

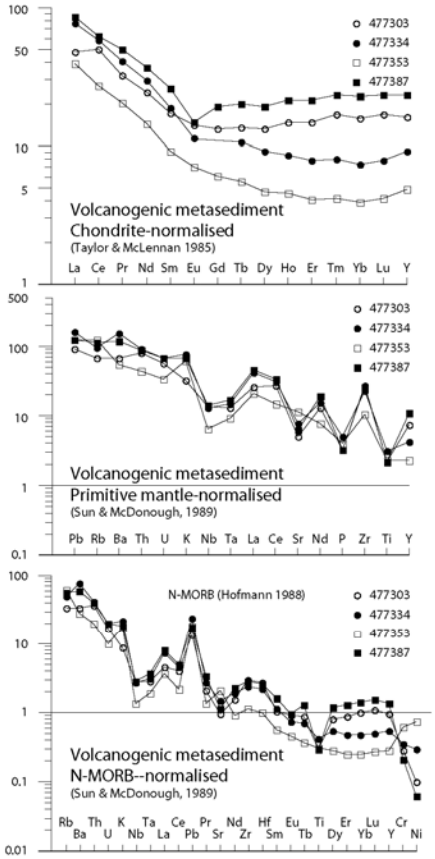

Fig. 15. Multi-element diagrams of schistose, intermediate metasediment intercalated with fragmental amphibolite. Normalised to chondrite, primitive mantle and MORB as for Fig. 10.

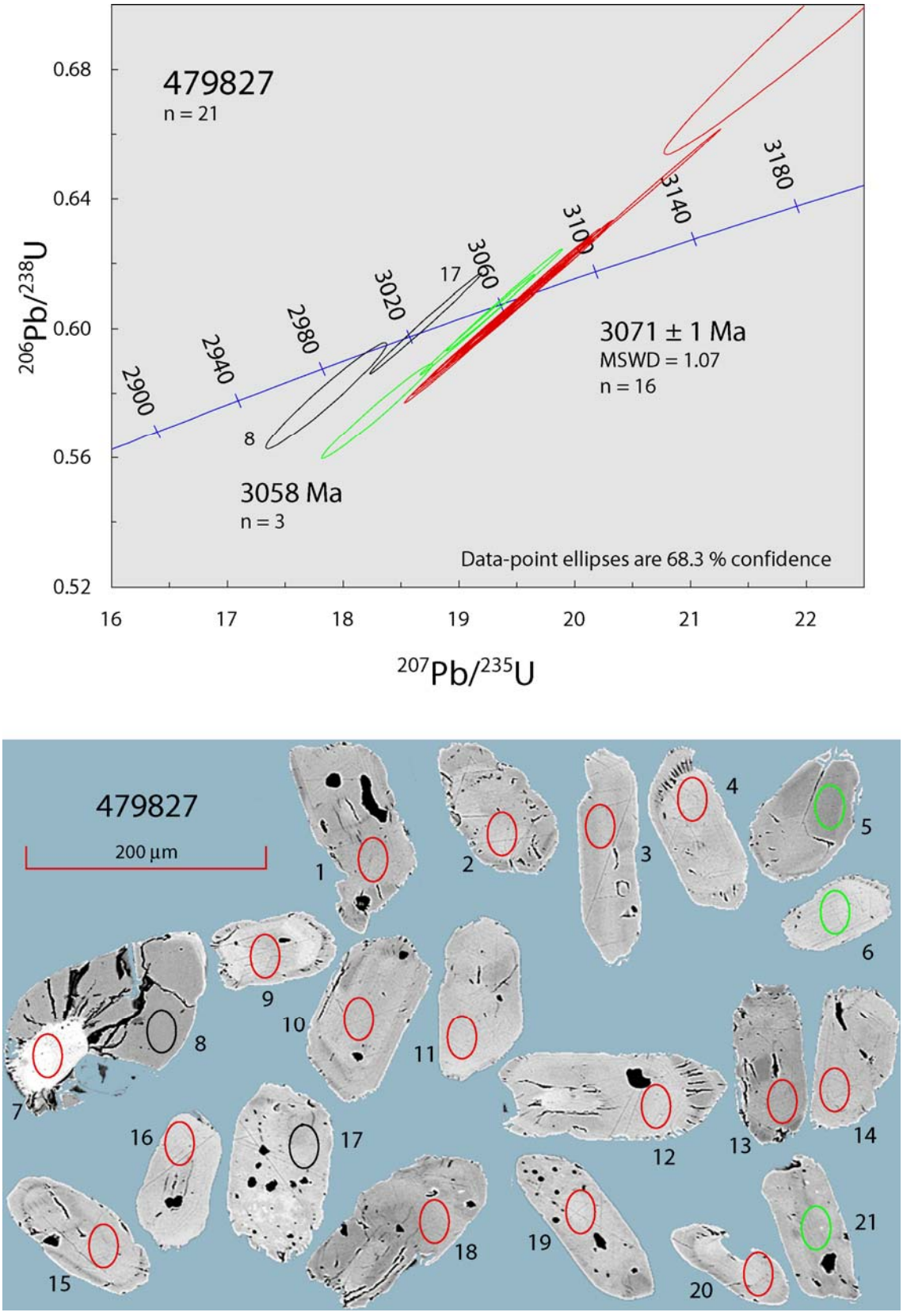

Fig. 16. Geochronology data for sample 479827.

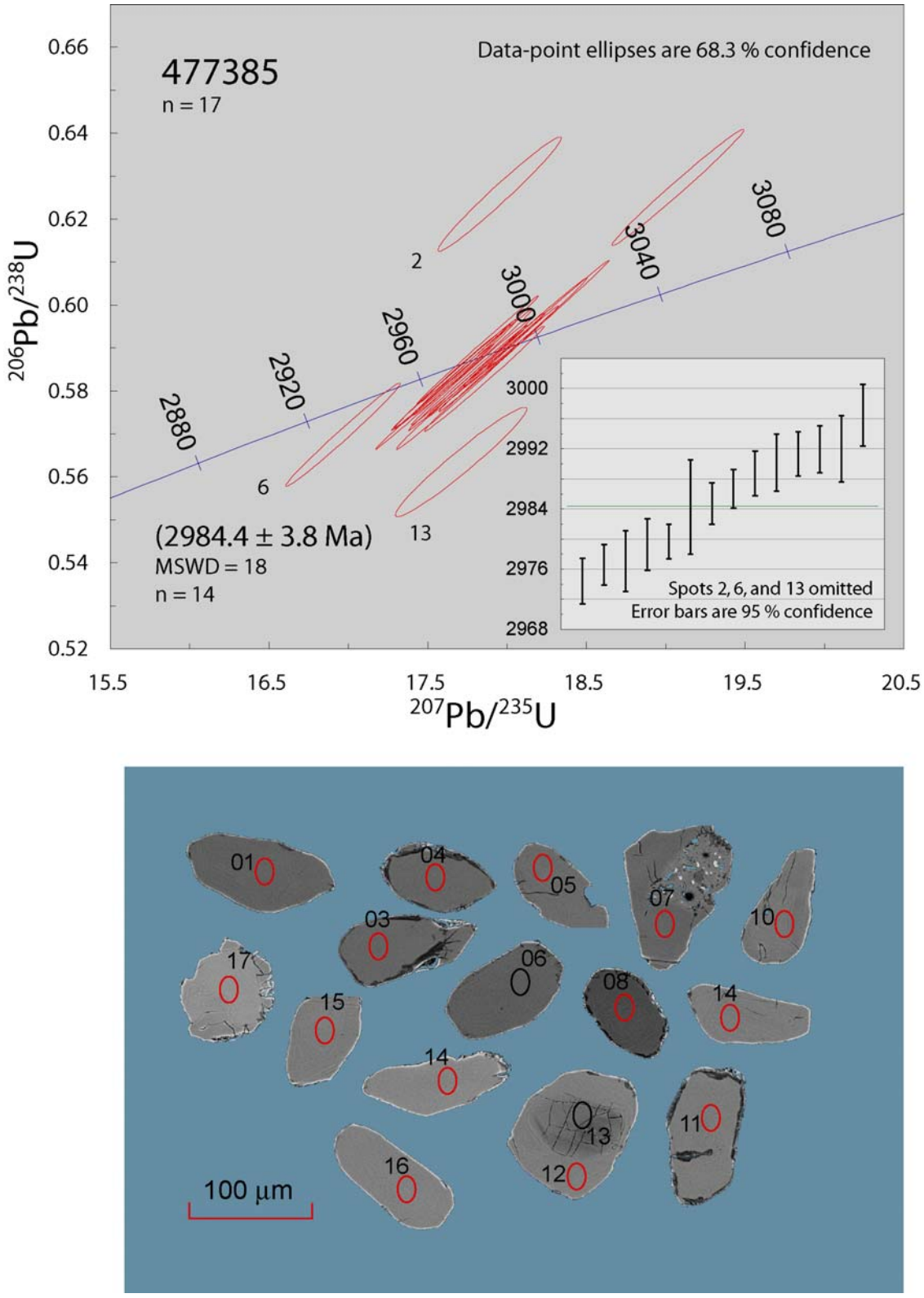

Fig. 17. Geochronology data for sample 477385.

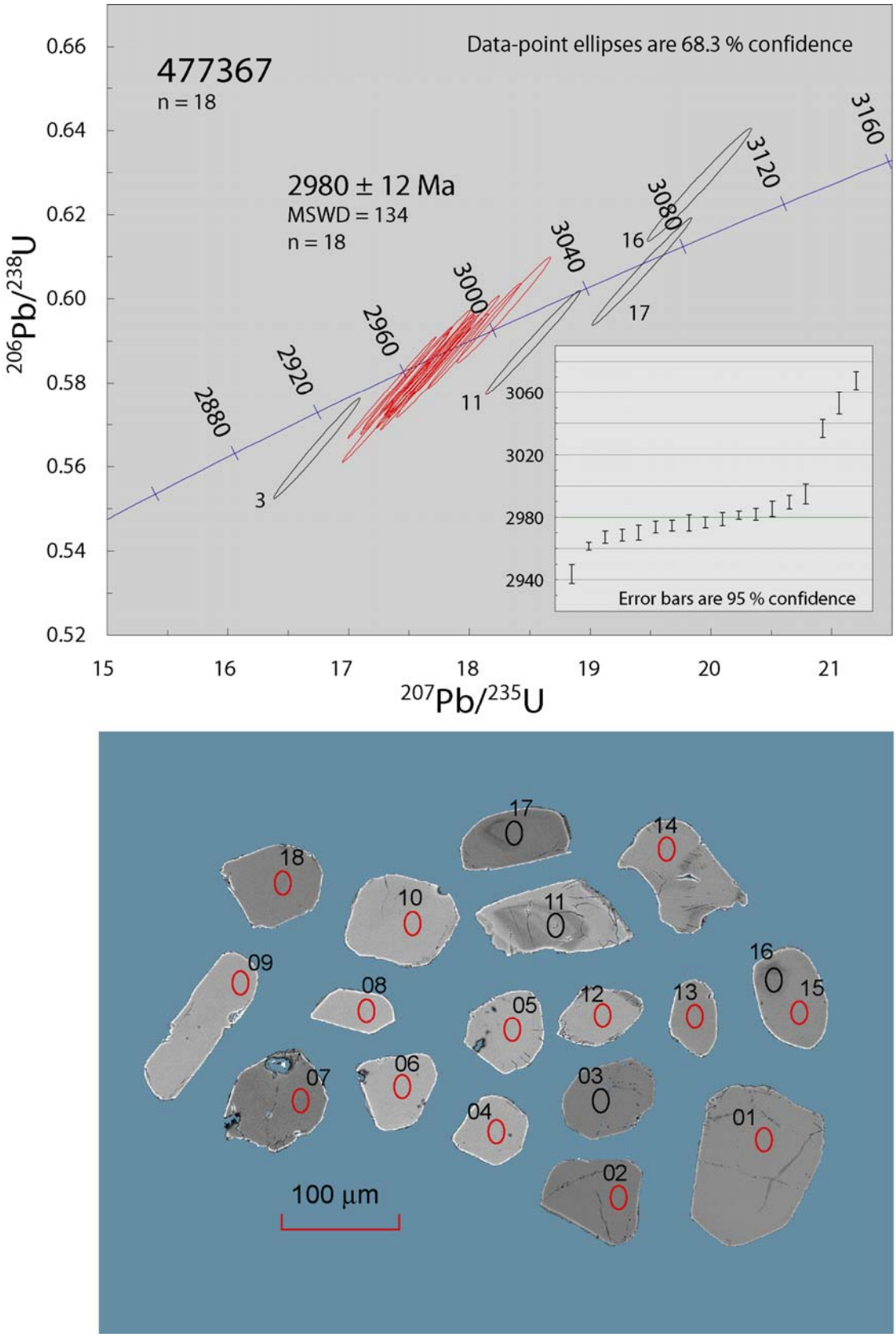

Fig. 18. Geochronology data for sample 477367.

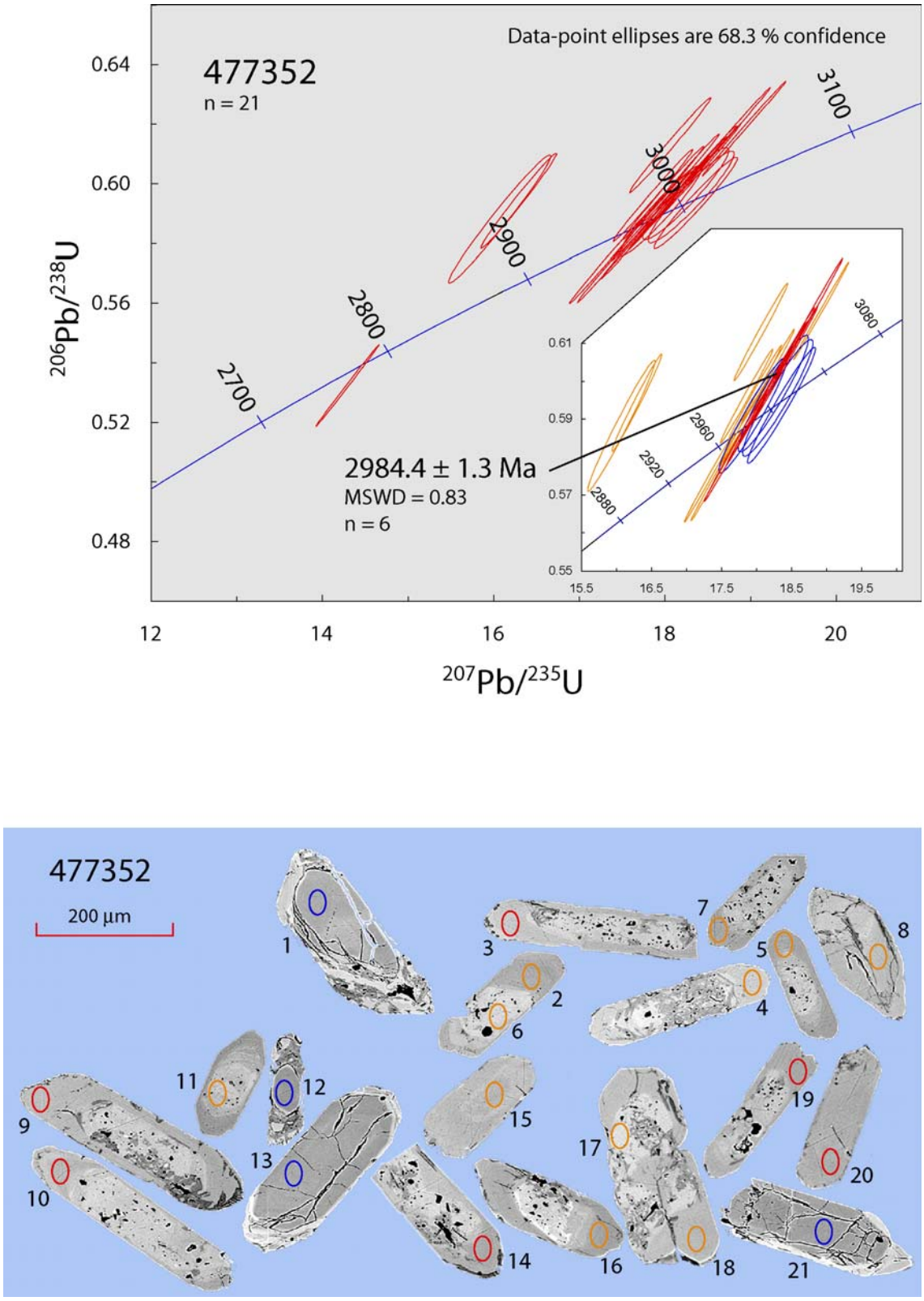

Fig. 19. Geochronology data for sample 477352.

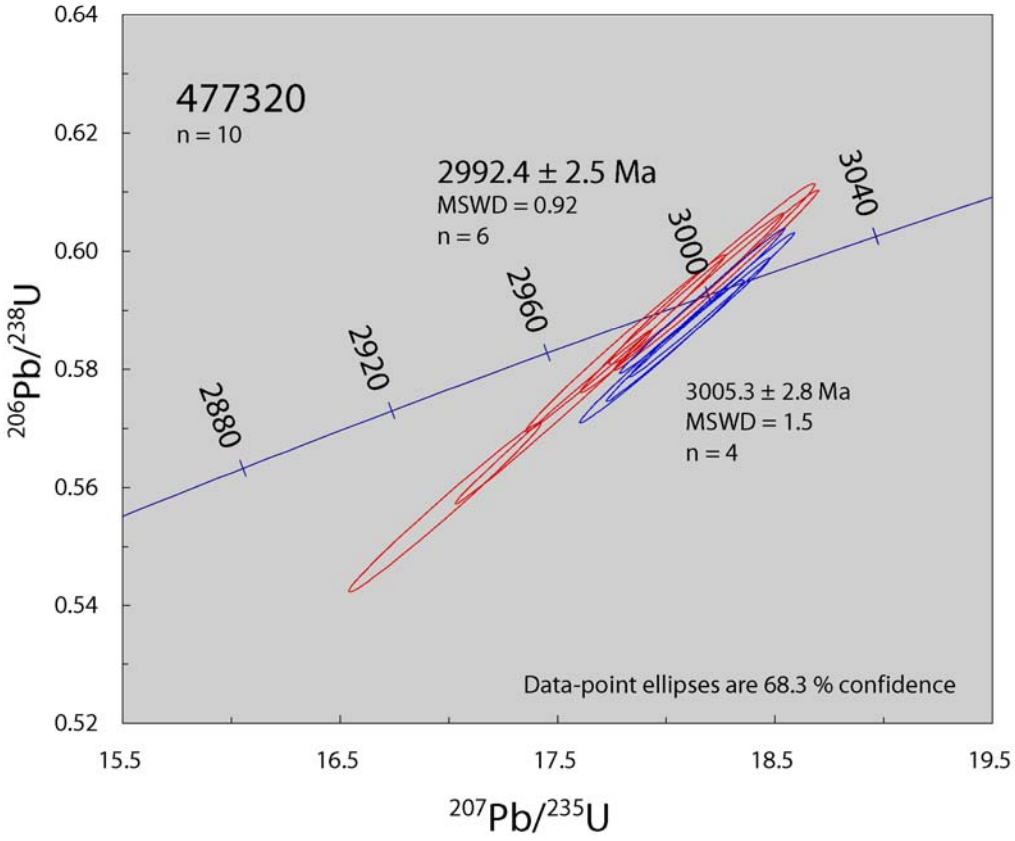

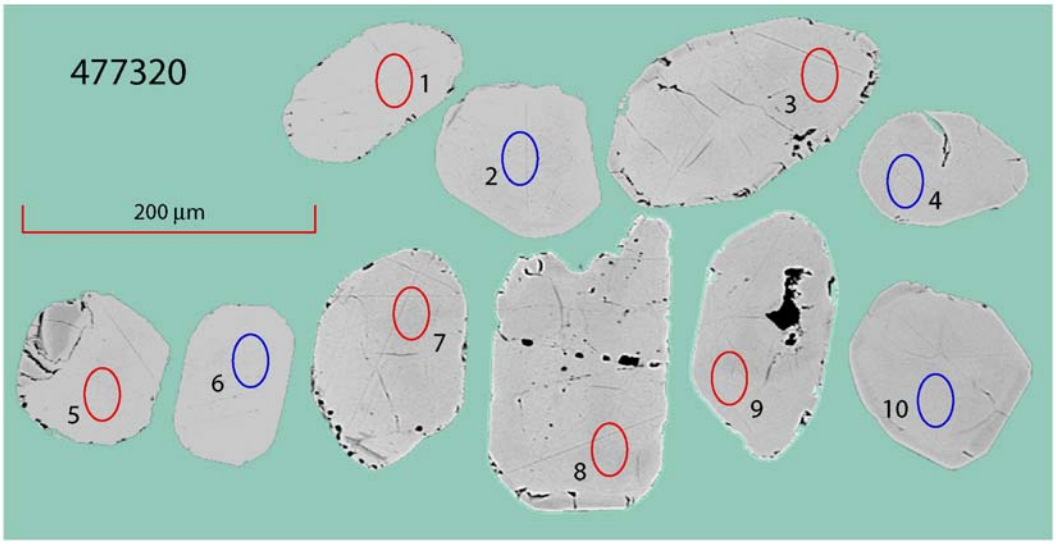

Fig. 20. Geochronology data for sample 477320.

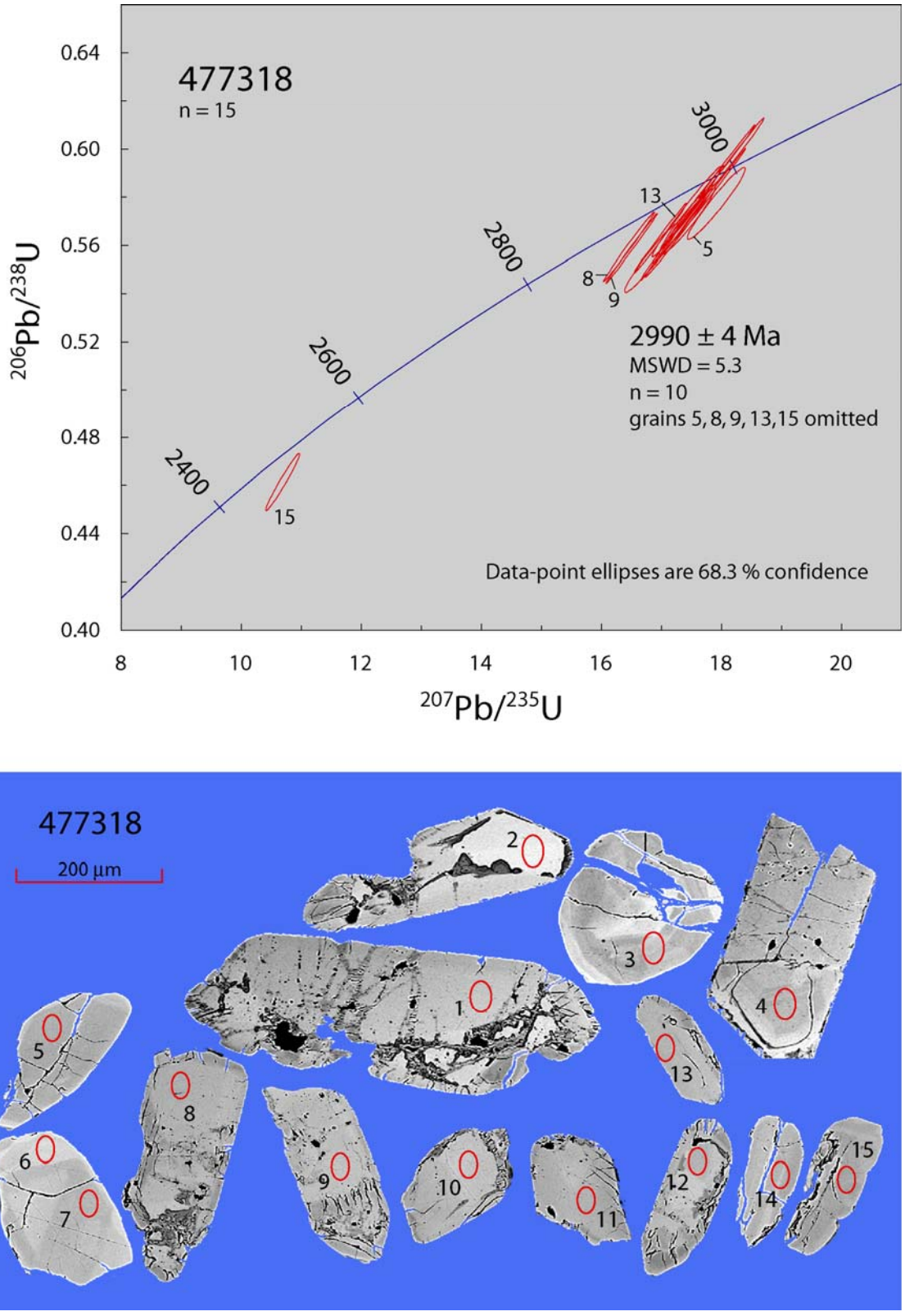

Fig. 21. Geochronology data for sample 477318.

Table 1. Compositions of metavolcanic and associated rocks from the Qussuk area

No	477305	477345	477348	477378	477310	477311	477347	477301	477306	477316	477324	477361	477367	477385	477327	477374	477382	477303	477334	477353
	Amphibolite s.s.				Metagabbro			Fragmental amphibolite							Fragmental amphibolite with disseminated pyrrhotite			Volcanogenic metasediment		
SiO_2	48.58	48.72	46.56	48.46	49.37	46.61	46.83	57.10	57.80	66.36	54.61	56.49	61.23	64.76	59.60	61.83	54.80	71.93	64.50	61.66
TiO_2	0.55	0.67	0.70	0.58	0.53	0.37	0.52	0.76	0.72	0.63	0.88	1.00	0.61	0.82	1.22	0.78	0.92	0.47	0.68	0.49
$Al2O_3$	15.99	15.11	17.38	15.38	16.75	15.23	17.08	15.13	16.50	14.52	17.18	16.35	17.74	13.21	16.62	15.94	21.58	12.91	14.80	15.62
$Fe2O_3$	1.67	2.58	2.10	3.27	1.77	2.21	2.17	1.76	2.15	3.02	1.53	2.07	1.42	2.91	1.88	1.11	3.44	1.93	0.73	1.12
FeO	9.11	8.79	10.03	7.73	7.96	8.76	8.86	5.81	5.48	2.84	6.22	6.41	5.55	5.84	6.49	5.93	1.99	3.84	4.98	4.32
FeO*	10.61	11.11	11.92	10.67	9.55	10.75	10.81	7.39	7.41	5.56	7.60	8.27	6.83	8.46	8.18	6.93	5.09	5.57	5.64	5.33
MnO	0.18	0.20	0.21	0.19	0.17	0.18	0.18	0.13	0.12	0.03	0.15	0.13	0.12	0.14	0.14	0.08	0.06	0.08	0.08	0.07
MgO	8.34	7.69	8.02	8.54	7.27	13.48	8.82	4.91	3.80	2.23	4.99	3.78	2.27	1.68	2.73	5.26	1.99	0.86	3.48	4.97
CaO	11.68	10.31	9.75	10.69	12.54	9.95	10.60	9.26	6.72	3.41	7.69	7.49	5.24	3.76	4.66	0.47	4.55	3.15	2.59	4.73
Na_2O	1.70	2.39	2.43	2.17	1.49	1.24	2.08	3.30	3.86	3.20	3.25	3.15	3.19	3.06	3.04	0.61	4.56	3.14	3.61	3.36
K_2O	0.19	0.94	0.27	0.30	0.38	0.13	0.25	0.72	1.34	1.71	1.31	0.92	1.71	1.55	1.31	3.00	2.45	0.95	2.32	1.90
P_2O_5	0.03	0.05	0.04	0.02	0.02	0.01	0.02	0.09	0.09	0.09	0.11	0.19	0.11	0.14	0.19	0.10	0.12	0.07	0.11	0.09
Volat	1.30	1.66	1.57	1.61	1.31	1.31	1.58	0.89	0.85	1.11	1.06	1.09	1.07	1.17	1.10	3.66	2.36	0.61	0.77	0.87
Sum	99.33	99.12	99.04	98.92	99.56	99.47	98.99	99.85	99.45	99.14	98.98	99.08	100.26	99.03	98.98	98.76	98.83	99.92	98.66	99.20
Mg#	60.9	57.8	57.1	61.3	60.1	71.3	61.8	56.8	50.4	44.3	56.5	47.5	39.7	28.2	39.8	60.0	43.6	23.4	55.0	64.9
Sc	41	40	29	42	45	31	33	27	21	20	32	28	19	26	25	18	22	19	16	20
V	212	200	178	207	207	134	160	136	149	82	148	152	54	77	182	135	160	24	75	88
Cr	341	219	96	261	333	371	189	235	66	217	204	197	42	65	39	173	241	81	104	179
Co	52	51	55	54	44	71	57	33	26	22	31	44	14	14	21	25	18	6	14	25
Ni	180	152	178	188	103	419	213	125	58	92	74	149	12	18	42	62	41	15	44	112
Zn	68	94	105	76	58	68	118	82	72	38	86	103	71	84	52	214	52	83	36	61
Ga	15	16	17	15	15	12	15	18	20	18	21	19	19	18	22	20	25	18	18	17
Pb	2.7	5.8	3.3	4.0	3.4	2.6	2.7	8.7	8.0	8.5	4.1	8.2	10.2	5.8	9.3	11.9	29.0	6.6	11.5	8.9
Th	0.3	0.2	0.2	0.2	0.3	0.2	0.2	2.2	1.6	7.0	0.5	3.8	3.1	5.3	2.1	6.6	7.5	6.8	7.9	3.7
U	0.1	0.3	0.1	0.2	0.2	0.1	0.1	0.6	0.6	1.9	0.3	0.8	0.6	1.2	0.7	1.6	2.0	1.2	1.5	0.7
Rb	3	21	6	10	7	2	4	9	49	66	56	45	87	69	58	122	94	43	62	78
Sr	63	185	106	87	57	63	74	160	281	147	136	281	245	164	199	39	195	107	166	239
Ba	28	171	51	45	44	6	38	174	331	757	430	381	415	588	1119	826	451	463	1065	385
Zr	33	42	41	32	29	22	29	112	109	230	119	163	135	222	166	213	228	309	253	118
Nb	0.8	1.8	1.1	0.8	0.8	0.5	0.7	4.2	3.9	8.3	5.7	7.3	5.2	8.0	5.9	3.9	9.8	9.8	9.3	4.7
Ta	0.06	0.10	0.07	0.07	0.07	0.04	0.04	0.30	0.26	0.61	0.38	0.46	0.36	0.60	0.36	0.51	0.70	0.54	0.60	0.37
Cs	0.03	0.53	0.15	0.10	0.09	0.02	0.06	0.08	2.08	0.73	1.37	2.40	2.22	0.84	1.12	2.77	2.51	0.70	1.65	2.46
La	2.2	3.4	1.9	1.3	2.0	1.0	1.9	12.6	11.7	24.6	11.0	21.3	16.1	22.7	13.6	23.0	22.9	17.6	28.6	14.4
Ce	4.8	8.4	4.9	3.3	4.2	2.4	4.0	24.8	24.4	47.9	23.4	45.0	32.5	44.6	26.5	44.0	42.2	47.5	55.8	26.0
Pr	0.6	1.3	0.8	0.5	0.6	0.4	0.6	3.0	2.8	5.3	2.9	5.5	3.7	5.2	2.9	4.8	4.6	4.4	5.7	2.8
Nd	3.21	5.79	4.08	2.97	2.84	1.95	2.86	12.06	11.53	19.96	11.94	22.73	14.36	20.73	11.59	18.02	16.81	17.31	21.13	10.27
Sm	1.2	1.8	1.6	1.3	1.1	0.8	1.1	2.9	2.7	4.2	3.1	4.7	3.3	5.3	2.7	3.8	3.3	4.0	4.3	2.1
Eu	0.50	0.66	0.62	0.51	0.48	0.40	0.47	0.90	0.89	1.01	0.92	1.39	1.11	1.32	0.83	0.84	1.00	1.24	1.00	0.61
Gd	1.9	2.3	2.4	2.0	1.6	1.3	1.7	3.1	2.6	3.4	3.0	4.5	3.1	5.7	1.7	2.8	3.2	4.0	2.8	1.8
Tb	0.37	0.46	0.48	0.41	0.34	0.26	0.34	0.50	0.45	0.65	0.53	0.70	0.53	1.06	0.63	0.56	0.53	0.78	0.62	0.32
Dy	2.5	3.2	3.3	2.9	2.4	1.8	2.3	2.9	2.7	3.8	3.2	4.0	3.0	6.5	4.1	3.2	3.1	5.1	3.5	1.8
Ho	0.64	0.79	0.83	0.72	0.62	0.45	0.58	0.61	0.57	0.82	0.68	0.87	0.64	1.53	1.02	0.67	0.73	1.26	0.73	0.39
Er	1.8	2.2	2.4	2.1	1.7	1.3	1.7	1.7	1.6	2.3	1.9	2.4	1.8	4.4	2.9	1.8	2.1	3.7	1.9	1.0
Tm	0.30	0.34	0.38	0.34	0.28	0.22	0.27	0.26	0.24	0.35	0.27	0.35	0.27	0.68	0.46	0.28	0.32	0.61	0.29	0.15
Yb	2.0	2.2	2.5	2.2	1.8	1.4	1.8	1.6	1.5	2.3	1.7	2.3	1.8	4.4	2.9	1.7	2.0	3.9	1.8	1.0
Lu	0.32	0.36	0.40	0.34	0.30	0.23	0.30	0.25	0.22	0.37	0.27	0.35	0.30	0.70	0.45	0.27	0.30	0.64	0.30	0.16
Hf	1.0	1.2	1.2	1.0	0.9	0.7	0.8	3.0	2.9	5.9	3.2	3.9	3.3	5.8	4.4	5.2	5.6	8.0	6.4	3.0
Y	17.40	21.10	22.90	19.80	16.40	12.10	16.70	16.90	15.20	22.00	18.30	23.00	18.10	43.50	26.90	19.20	20.70	34.00	19.20	10.20

Mg#: 100 Molar MgO/(MgO + FeO), where FeO = 0.9FeO* to account for magmatic oxidised iron

Table 2. Ion probe zircon U-Pb geochronological data from Bjørneøen and the Qussuk area.

Sarnple/	[U]	[Th]	Th/U	f_{206}%	^{207}Pb	±s	^{207}Pb	±s	^{206}Pb	±s	^{207}Pb age	±s	Disc. %
spot #	ppm	ppm	meas		^{206}Pb	%	^{235}U	%	^{238}U	%	^{206}Pb	Ma	conv.
477367													
3	984	84	0.085	0.47	0.21501	0.19	16.7340	1.41	0.56447	1.40	2943.7	3.1	-2.5
1	1955	206	0.106	0	0.21740	0.08	17.3543	1.39	0.57896	1.39	2961.5	1.2	-0.7
5	1327	184	0.139	0.01	0.21819	0.12	17.4864	1.40	0.58125	1.39	2967.4	2.0	-0.6
14	1322	146	0.110	0.01	0.21836	0.12	17.4627	1.40	0.58001	1.39	2968.6	1.9	-0.8
10	1020	115	0.112	0.03	0.21857	0.15	17.6331	1.40	0.58511	1.40	2970.2	2.4	0.0
18	828	71	0.086	0.01	0.21906	0.12	17.3112	1.40	0.57315	1.39	2973.8	1.9	-2.2
7	946	69	0.073	0.01	0.21919	0.11	17.6656	1.40	0.58453	1.40	2974.8	1.8	-0.3
6	905	79	0.088	0.01	0.21940	0.16	17.6657	1.41	0.58396	1.40	2976.3	2.6	-0.5
2	1191	186	0.156	0.01	0.21946	0.11	17.5974	1.40	0.58157	1.40	2976.7	1.7	-0.9
13	969	84	0.087	0.01	0.21977	0.13	17.6969	1.40	0.58403	1.39	2979.0	2.1	-0.6
12	1706	186	0.109	0.01	0.22007	0.08	17.6312	1.40	0.58105	1.40	2981.2	1.3	-1.2
9	882	43	0.049	0.01	0.22017	0.12	17.8673	1.39	0.58856	1.39	2982.0	1.9	0.1
4	1710	212	0.124	0.01	0.22064	0.15	17.7717	1.41	0.58418	1.40	2985.4	2.5	-0.8
15	862	45	0.052	0.01	0.22125	0.14	18.0385	1.40	0.59132	1.39	2989.8	2.2	0.2
8	631	48	0.076	0.02	0.22194	0.20	18.2819	1.40	0.59742	1.39	2994.8	3.1	1.0
11	521	127	0.244	0.03	0.22782	0.18	18.5226	1.41	0.58968	1.39	3036.8	2.9	-2.0
16	267	72	0.271	0.02	0.23014	0.22	19.9013	1.43	0.62716	1.41	3053.0	3.5	3.5
17	339	158	0.466	0.02	0.23226	0.18	19.4251	1.40	0.60658	1.39	3067.7	2.9	-0.5
477385													
2	158	151	0.954	{3.25}	0.20803	0.28	17.9522	1.43	0.62588	1.40	2890.3	4.6	10.6
6	1067	65	0.061	0.01	0.21592	0.19	16.9660	1.41	0.56987	1.39	2950.5	3.1	-1.8
14	1275	69	0.054	0.01	0.21914	0.09	17.8148	1.42	0.58960	1.42	2974.4	1.5	0.6
4	1943	83	0.043	0	0.21944	0.08	17.6476	1.40	0.58327	1.40	2976.6	1.4	-0.6
3	1923	56	0.029	0	0.21950	0.12	17.6746	1.44	0.58399	1.43	2977.1	2.0	-0.5
15	2326	64	0.028	0.01	0.21981	0.11	17.7851	1.39	0.58683	1.39	2979.3	1.7	-0.1
1	2218	70	0.031	0	0.21986	0.07	17.5449	1.41	0.57877	1.40	2979.6	1.2	-1.5
9	857	43	0.050	0.03	0.22049	0.20	19.0759	1.44	0.62748	1.42	2984.3	3.1	6.6
8	2228	76	0.034	0	0.22055	0.09	17.7727	1.40	0.58445	1.39	2984.7	1.4	-0.7
11	1847	96	0.052	0	0.22082	0.08	17.7529	1.39	0.58308	1.39	2986.7	1.3	-1.1
10	1356	42	0.031	0.01	0.22110	0.09	17.8641	1.39	0.58600	1.39	2988.7	1.5	-0.6
12	1259	88	0.070	0.01	0.22129	0.12	18.1142	1.43	0.59368	1.42	2990.1	1.9	0.6
17	1371	183	0.133	0.01	0.22146	0.09	18.2579	1.39	0.59794	1.39	2991.3	1.5	1.3
16	1679	73	0.044	0.01	0.22154	0.10	17.9477	1.39	0.58757	1.39	2991.9	1.6	-0.5
7	639	32	0.050	0.01	0.22155	0.14	17.6779	1.40	0.57870	1.39	2992.0	2.2	-2.0
5	1992	81	0.041	0	0.22216	0.13	17.8571	1.39	0.58296	1.39	2996.4	2.0	-1.5
13	233	86	0.370	0.13	0.22792	0.39	17.7093	1.54	0.56352	1.49	3037.5	6.2	-6.4
477352													
1 lowU	43	40	0.920	0.1	0.22286	0.60	18.3016	1.81	0.59561	1.71	3001.4	9.6	0.4
2 tip	1253	20	0.016	0.01	0.21973	0.11	17.4237	1.71	0.57512	1.70	2978.7	1.8	-2.1
3 tip	1681	33	0.020	0.01	0.22049	0.10	18.2532	1.70	0.60040	1.70	2984.3	1.5	2.0
4 tip	1361	29	0.021	0.01	0.21865	0.12	17.3256	1.71	0.57470	1.70	2970.8	2.0	-1.8
5 tip	2742	44	0.016	0.01	0.21838	0.15	17.9770	1.73	0.59704	1.72	2968.8	2.3	2.1
6 core	3231	40	0.013	0.03	0.19876	0.26	16.2874	1.79	0.59432	1.77	2816.1	4.2	8.5
7 tip	3331	86	0.026	0.03	0.19462	0.08	14.2887	1.70	0.53248	1.70	2781.6	1.2	-1.3
8 core	1467	5	0.004	0.01	0.21942	0.13	17.8354	1.71	0.58952	1.70	2976.5	2.1	0.5
9 tip	2142	54	0.025	0.01	0.22050	0.08	18.0361	1.70	0.59325	1.70	2984.3	1.4	0.8
10 tip	1277	32	0.025	0.01	0.22019	0.11	17.7092	1.70	0.58331	1.70	2982.1	1.8	-0.8
11 core	3116	47	0.015	0.01	0.19807	0.46	16.0648	2.45	0.58825	2.41	2810.3	7.5	7.7
12 lowU	58	59	1.029	0.11	0.22023	0.52	17.9473	1.78	0.59105	1.71	2982.4	8.3	0.5
13 lowU	95	91	0.963	0.06	0.22424	0.39	18.3548	1.75	0.59365	1.70	3011.4	6.2	-0.3
14 tip	1588	35	0.022	0.02	0.22083	0.09	18.3965	1.70	0.60420	1.70	2986.7	1.5	2.5
15 core	3395	71	0.021	0.01	0.21363	0.19	18.0574	1.74	0.61303	1.73	2933.3	3.1	6.4
16 tip	2113	32	0.015	0	0.22182	0.08	18.9190	1.70	0.61859	1.70	2993.9	1.3	4.6
17 core	1746	9	0.005	0.01	0.21724	0.17	17.8555	1.71	0.59612	1.71	2960.3	2.8	2.3
18 tip	1489	28	0.018	0.01	0.21904	0.13	18.1607	1.71	0.60133	1.70	2973.6	2.0	2.6
19 tip	1289	45	0.035	0.02	0.22043	0.12	18.3551	1.71	0.60392	1.70	2983.9	2.0	2.6
20 tip	1901	41	0.021	0.01	0.22048	0.09	18.7429	1.70	0.61656	1.70	2984.2	1.5	4.7
21 lowU	40	31	0.773	0.1	0.22166	0.62	18.2381	1.82	0.59675	1.71	2992.8	9.9	1.0

Table 2 continued. Ion probe zircon U-Pb geochronological data from Bjørneøen and the Qussuk area.

Sample/	[U]	[Th]	Th/U	f_{206}%	^{207}Pb	±s	^{207}Pb	±s	^{206}Pb	±s	^{207}Pb age	±s	Disc. %
spot #	ppm	ppm	meas		^{206}Pb	%	^{235}U	%	^{238}U	%	^{206}Pb	Ma	conv.
479827													
1	1086	818	0.753	0.01	0.23247	0.1	19.2473	1.7	0.60048	1.7	3069.2	1.7	-1.5
2	1944	1316	0.677	0.01	0.23269	0.1	19.3763	1.7	0.60393	1.7	3070.7	1.3	-1
3	623	408	0.655	0.02	0.23281	0.1	19.0185	1.7	0.59248	1.7	3071.5	2.2	-2.9
4	1663	1060	0.638	0.01	0.23245	0.1	19.7122	1.7	0.61504	1.7	3069	1.5	0.9
5	153	93	0.61	0.05	0.23091	0.3	18.2927	1.7	0.57456	1.7	3058.4	4.6	-5.4
6	1251	525	0.419	0.01	0.23107	0.1	19.158	1.7	0.60132	1.7	3059.5	1.6	-1
7	2265	2660	1.174	0.01	0.2327	0.1	19.8037	1.7	0.61724	1.7	3070.7	1.1	1.2
8	57	20	0.353	0.07	0.22352	0.5	17.8532	1.9	0.57929	1.9	3006.2	7.2	-2.5
9	2611	1710	0.655	0.01	0.23274	0.1	19.8169	1.7	0.61753	1.7	3071	1.2	1.2
10	895	554	0.619	0.01	0.23288	0.1	19.4382	1.7	0.60538	1.7	3071.9	2.2	-0.8
11	1310	851	0.649	0.01	0.23269	0.1	19.0902	1.7	0.59502	1.7	3070.6	1.7	-2.5
12	1790	1278	0.714	0.01	0.23304	0.1	19.7773	1.7	0.61552	1.7	3073	1.3	0.8
13	1182	936	0.792	0.01	0.23289	0.1	19.3873	1.7	0.60376	1.7	3072	1.7	-1.1
14	1388	596	0.43	0.01	0.23254	0.1	19.6554	1.7	0.61302	1.7	3069.6	1.5	0.5
15	1444	937	0.649	0.01	0.23251	0.1	19.1497	1.7	0.59734	1.7	3069.4	1.5	-2.1
16	858	367	0.427	0.01	0.23096	0.1	19.3921	1.7	0.60896	1.7	3058.7	1.8	0.3
17	1009	1024	1.015	0.01	0.22554	0.2	18.7116	1.7	0.6017	1.7	3020.7	2.4	0.7
18	2860	1401	0.49	0	0.23301	0.1	20.7254	1.7	0.64511	1.7	3072.8	1	5.6
19	2224	4980	2.24	0.01	0.23305	0.1	19.6563	1.7	0.61171	1.7	3073.1	1.1	0.2
20	1301	997	0.767	0.01	0.23285	0.1	19.5165	1.7	0.60789	1.7	3071.8	1.6	-0.4
21	912	716	0.785	0.01	0.23066	0.9	23.2489	7	0.731	7	3056.7	14	20.5
477320													
1	726	443	0.610	0.02	0.22168	0.15	17.4822	1.71	0.57196	1.70	2993.0	2.4	-3.2
2	554	288	0.520	0.02	0.22375	0.17	18.1016	1.71	0.58674	1.70	3007.9	2.7	-1.3
3	670	373	0.557	0.01	0.22103	0.18	17.8113	1.71	0.58445	1.70	2988.2	3.0	-0.9
4	791	519	0.656	0.02	0.22349	0.16	18.2098	1.71	0.59096	1.70	3006.0	2.5	-0.5
5	503	320	0.635	0.03	0.22216	0.18	18.2284	1.71	0.59508	1.70	2996.4	2.8	0.6
6	475	317	0.668	0.03	0.22364	0.22	17.9796	1.72	0.58307	1.70	3007.1	3.5	-1.9
7	452	275	0.609	0.02	0.22167	0.19	18.0722	1.71	0.59128	1.70	2992.9	3.0	0.1
8	475	247	0.519	0.03	0.22155	0.24	18.2107	1.72	0.59614	1.70	2992.0	3.9	0.9
9	381	204	0.535	0.06	0.22126	0.23	16.9816	1.72	0.55663	1.70	2989.9	3.7	-5.7
10	555	307	0.554	0.04	0.22271	0.17	18.1654	1.71	0.59157	1.70	3000.4	2.8	-0.2
477318													
1	856	383	0.448	0.01	0.22125	0.16	17.2042	2.14	0.56397	2.13	2989.8	2.6	-4.4
2	2538	2345	0.924	0	0.22222	0.08	17.8213	2.13	0.58164	2.13	2996.8	1.4	-1.7
3	122	146	1.201	0.06	0.22001	0.37	17.4154	2.20	0.57411	2.17	2980.8	5.9	-2.3
4	381	88	0.232	0.02	0.22171	0.21	17.2833	2.15	0.56539	2.14	2993.1	3.3	-4.3
5	67	51	0.765	0.07	0.22488	0.49	17.9060	1.78	0.57749	1.71	3016.0	7.9	-3.2
6	302	18	0.059	0.03	0.22116	0.25	17.2996	1.72	0.56732	1.70	2989.2	4.0	-3.8
7	79	45	0.571	0.05	0.21995	0.47	16.8292	1.77	0.55494	1.70	2980.3	7.5	-5.6
8	870	327	0.376	0.04	0.21323	0.17	16.4522	1.71	0.55958	1.70	2930.3	2.8	-2.8
9	1319	53	0.040	0.01	0.21405	0.11	16.4963	1.71	0.55894	1.70	2936.5	1.8	-3.1
10	3079	3295	1.070	0	0.22050	0.10	18.0830	1.70	0.59479	1.70	2984.3	1.7	1.0
11	944	445	0.471	0.01	0.22050	0.15	17.5848	1.71	0.57840	1.70	2984.4	2.4	-1.8
12	632	222	0.351	0.03	0.22124	0.16	18.2331	1.71	0.59772	1.70	2989.7	2.5	1.3
13	1292	650	0.504	0.01	0.21863	0.15	16.9774	1.71	0.56319	1.70	2970.7	2.4	-3.8
14	78	64	0.819	0.05	0.22148	0.52	17.4221	1.78	0.57051	1.70	2991.5	8.4	-3.4
15	260	8	0.031	0.16	0.16786	0.38	10.6820	1.74	0.46153	1.70	2536.4	6.3	-4.3